DEVELOPMENT AND CHARACTERIZATION OF PEG-B-PCL MICELLES CARRYING ANTICANCER AGENTS

A THESIS SUBMITTED TO
THE GRADUATE SCHOOL OF NATURAL AND APPLIED SCIENCES
OF
MIDDLE EAST TECHNICAL UNIVERSITY

BY

GÜLHAN IŞIK

IN PARTIAL FULFILLMENT OF THE REQUIREMENTS
FOR
THE DEGREE OF DOCTOR OF PHILOSOPHY
IN
BIOTECHNOLOGY

FEBRUARY 2022

Approval of the thesis:

DEVELOPMENT AND CHARACTERIZATION OF PEG-b-PCL MICELLES CARRYING ANTICANCER AGENTS

submitted by **IŞIK GÜLHAN** in partial fulfillment of the requirements for the degree of **Doctor of Philosophy** i**n Biotechnology, Middle East Technical University** by,

Prof. Dr. Halil Kalıpçılar
Dean, Graduate School of **Natural and Applied Sciences** _____

Doç. Dr. Yeşim Soyer
Head of the Department, **Biotechnology** _____

Prof. Dr. Ayşen Tezcaner
Supervisor, **Biotechnology, METU** _____

Prof. Dr. Nesrin Hasırcı
Co-Supervisor, **Chemistry, METU** _____

Examining Committee Members:

Prof. Dr. Dilek Keskin
Engineering Sciences, METU _____

Prof. Dr. Ayşen Tezcaner
Biotechnology, METU _____

Prof. Dr. Pınar Yılgör Huri
Biomedical Engineering, Ankara University _____

Prof. Dr. Cihangir Tanyeli
Chemistry, METU _____

Prof. Dr. Eda Ayşe Aksoy
Basic Pharmaceutical Sciences, Hacettepe University _____

Date: 09.02.2022

I hereby declare that all information in this document has been obtained and presented in accordance with academic rules and ethical conduct. I also declare that, as required by these rules and conduct, I have fully cited and referenced all material and results that are not original to this work.

Name Last name : Işık, Gülhan

Signature :

ABSTRACT

DEVELOPMENT AND CHARACTERIZATION OF PEG-b-PCL MICELLES CARRYING ANTICANCER AGENTS

Işık, Gülhan
Doctor of Philosophy, Biotechnology
Supervisor: Prof. Dr. Ayşen Tezcaner
Co-Supervisor: Prof. Dr. Nesrin Hasırcı

February 2022, 184 pages

Cancer is a disease that decreases the quality of life. Many cancer drugs are either toxic or not effective due to their fast removal by reticuloendothelial system. Therefore, nano-sized drug delivery systems, especially the ones carrying the drugs directly to tumor, gained attention in the last decades. The aim of the study was to prepare nano-sized drug carrying micelles (drug conjugated and drug loaded) from methoxy polyethylene glycol-block-polycaprolactone (mPEG-b-PCL). In order to conjugate drugs, mPEG-b-PCL was activated with hydrazide groups. Doxorubicin (DOX) was conjugated covalently (at 60ºC), and lithocholic acid (LCA) was conjugated ionically (at 60ºC and 25ºC) to obtain micelles (coded as DOX_{conj}-M, LCA_{60}**M and LCA_{25}**M, respectively). Micelles having no conjugation, but loading of DOX (DOX_{ld}-M), and micelles having both drugs together (DL-M) were also prepared. Micelles demonstrated faster drug release in acidic media than the neutral media, which is advantageous for the treatment of cancer since cancer tissue is more acidic than the healthy tissue. Cell culture studies show that micelles having no drugs are not cytotoxic. Internalization of the micelles into MDA-MB-231 cancer cells was determined by using coumarin-6 loaded micelles for LCA containing micelles (LCA_{60}**M and LCA_{25}**M) and DOX for DOX containing micelles

(DOX_{conj}-M, DOX_{ld}-M, and DL-M). All micelles displayed low cell migration and high anti-proliferative effect on MDA-MB-231 cells. Moreover, the ones having LCA (LCA_{60}**M, LCA_{25}**M and DL-M) led a decrease in lipogenic activity, but DOX_{conj}-M and DOX_{ld}-M did not change lipid droplet formation. An increase in the number of apoptotic cells, as well as in apoptotic genes of Bax and p53 expressions, and a significant decrease in anti-apoptotic genes of Bcl-2 and Bcl-xL expressions were observed after the treatment of the cells with DOX_{ld}-M and DL-M. All micelles prepared in this study caused a decrease in the mitochondrial transmembrane potential of the cells, which results in apoptosis, and an increase in ROS generation, which was significantly higher in the cells treated with DOX_{conj}-M, DOX_{ld}-M, and DL-M compared to free DOX applied ones. Micelles having LCA caused a significant decrease in angiogenesis ability of HUVECs. In the future these types of micelles especially immunomicelles targeted to cancer cells will be the candidate carriers in cancer therapy.

Keywords: Lithocholic acid; Doxorubicin; pH sensitive; PEG-b-PCL micelles; MDA-MB-231 cells

ÖZ

ANTİKANSER AJANLAR TAŞIYAN PEG-B-PCL MİSELLERİN GELİŞTİRİLMESİ VE KARAKTERİZASYONU

Işık, Gülhan
Doktora, Biyoteknoloji
Tez Yöneticisi: Prof. Dr. Ayşen Tezcaner
Ortak Tez Yöneticisi: Prof. Dr. Nesrin Hasırcı

Şubat 2022, 184 sayfa

Kanser yaşam kalitesini düşüren bir hastalıktır. Birçok kanser ilacı toksiktir veya retiküloendotelyal sistem tarafından hızla uzaklaştırıldıkları için etkili değildir. Bu nedenle nano boyutlu ilaç taşıyıcı sistemler, özellikle doğrudan tümöre hedefli olanlar dikkat çekmiştir. Çalışmanın amacı, kanser tedavisi için metoksi polietilen glikol-blok-polikaprolakton (mPEG-b-PCL) miseller (ilaç konjuge miseller, tek/çift ilaç yüklü miseller, immünomikeller) hazırlamak ve karakterize etmektir. İlaçları konjuge etmek için önce karboksilasyon ile mPEG-b-PCL aktive edilmiş ve daha sonra hidrazid grupları oluşturulmuştur. Doksorubisin (DOX) kovalent olarak (60°C'de) ve litokolik asit (LCA) iyonik olarak (60°C ve 25°C'de) polimerlere konjuge edilerek miseller (sırasıyla DOX_{conj}-M, LCA_{60}**M ve LCA_{25}**M) elde edilmiştir. DOX ayrıca misellere tek başına veya LCA ile birlikte yüklenmiştir (sırasıyla DOX_{ld}-M, ve DL-M). LCA ve DOX salımlarının, asidik ortamda nötr ortama göre daha hızlı olduğu belirlenmiştir. Hücre kültürü çalışmaları, ilaç içermeyen misellerin sitotoksik olmadığını göstermektedir. Kumarin-6 yüklü LCA_{60}**M, kumarin-6 yüklü LCA_{25}**M, DOX_{conj}-M, DOX_{ld}-M ve DL-M, MDA-MB-231 hücrelerinde etkili hücre internalizasyonuna neden olmuştur. Tüm

misellerin MDA-MB-231 üzerinde düşük hücre göçüne ve yüksek anti-proliferatif etkiye sahip olduğu belirlenmiştir. Ayrıca, LCA içeren miseller (LCA_{60}**M, LCA_{25}**M ve DL-M) lipojenik aktivitede azalmaya neden olurken, DOX_{conj}-M ve DOX_{ld}-M lipojenik aktiviteyi değiştirmemiştir. Hücrelerin, DOX_{ld}-M ve DL-M ile inkübasyonundan sonra apoptotik hücre sayısında ve ayrıca apoptotik gen Bax ve p53 ifadelerinde bir artış ve anti-apoptotik gen Bcl-2 ve Bcl-xL ifadelerinde önemli bir azalma gözlendi. Tüm miseller, hücrelerin mitokondriyal transmembran potansiyelini azalttı ve bu da apoptozun başladığını göstermektedir. Tüm miseller ROS oluşumunu artırmıştır ancak DOX_{conj}-M, DOX_{ld}-M ve DL-M, serbest DOX ile karşılaştırıldığında ROS üretiminde önemli bir artışa sebep olmuştur. LCA içeren miseller, HUVEC'lerin anjiyogenez yeteneğinde önemli bir azalmaya neden oldu. Gelecekte bu tip miseller, özellikle kansere hedefli immünomiseller kanser tedavisinde aday taşıyıcılar olacaktır.

Anahtar Kelimeler: Litokolik asit; Doksorubisin; pH’a duyarlı; PEG-b-PCL miselleri; MDA-MB-231 hücreleri

To my family and my fiancé,

ACKNOWLEDGMENTS

I would like to thank my supervisor Prof. Dr. Ayşen Tezcaner and my co-supervisor Prof. Dr. Nesrin Hasırcı for their guidance, advice, encouragement, and support during all the stages of my thesis. I also would like to thank Prof. Dr. Cihangir Tanyeli for his valuable contribution in the synthesis of copolymers and thesis monitoring committee members Prof. Dr. Dilek Keskin and Prof. Dr. Pınar Yılgör Huri for their criticism and guidance.

I also thank Dr. Aysel Kızıltay, for her continuous guidance, support, and friendship.

I would like to thank METU for the financial support via the project GAP-310-2019-10184.

I would like to thank Scientific and Technological Research Council of Turkey (TUBİTAK) for granting me with 2211/C National Ph.D. Scholarship in the Priority Fields in Science and Technology.

I also would like to thank all BIOMATEN members for their support during the experimental parts of this thesis. I would like to thank to Dr. Senem Büyüksungur for confocal and flow cytometry analysis. I am grateful to Ezgi Bayer Kömüşdoğan for the help in the synthesis of copolymer. I also feel very lucky to have my beloved friends, Sema Akbaba, Ahmet Engin Pazarçeviren, Yasemin Pazarçeviren, Milad Fathi, and Mustafa Bahadır Güner in the lab. I am really grateful for their contributions in my experiments and their friendship.

Finally, and most importantly, I would like to thank my family, Hanife Işık, Nazmi Işık and Gülten Işık, and my fiancé, Kağan Ertop, for all their support, endless love and trust in me.

TABLE OF CONTENTS

LIST OF TABLES

TABLES

LIST OF FIGURES

FIGURES

LIST OF ABBREVIATIONS

ABBREVIATIONS

A549	Non-small cell lung cancer cell line
Abs	Absorbance
ADP	Adenosine diphosphate
AMP	Adenosine monophosphate
Ch:MeOH	Chloroform:methanol
CMC	Critical micelle concentrations
CPB	Citrate-phosphate buffer
DCFDA	2’,7’-Dichlorofluorescin diacetate
DCM	Dichloromethane
DiOC6	3,3’-Dihexyloxacarbocyanine iodide
DL-M	DOX and LCA loaded micelles
DLC	Drug loading capacity
DLL4	Delta-like ligand 4
DMEM	Dulbecco's modified Eagle medium
DMXXAA	dimethylxanthenone-4-acetic acid (DMXAA)
DMSO	Dimethylsulfoxide
DOX	Doxorubicin
DOX_{conj}-M	DOX conjugated micelles
DOX_{ld}-M	DOX loaded micelles

DSC	Differential scanning calorimetry
ε-CL	ε-caprolactone
EC	Endothelial cell
EE	Encapsulation efficiency
EPR	Enhanced permeability and retention effect
ERBC	Estrogen receptor positive breast cancer
FBS	Fetal bovine serum
FT-IR	Fourier transform infrared spectroscopy
GPC	Gel permeation chromatography
GSH	Glutathione
^{1}H-NMR	Nuclear magnetic resonance spectroscopy
HER2-BC	Human epidermal growth factor receptor positive breast cancer
HIFs	Hypoxia-inducible factors
HPMA	N-(2-hydroxypropyl)methacrylamide (HPMA)
HUVECs	Human umbilical vein endothelial cells
IC_{50}	Half maximal inhibitory concentration
LCA	Lithocholic acid
LCA_{25}**M	mPEG-b-PCL-CO-NH-NH_2**LCA micelles at 25ºC
LCA_{60}**M	mPEG-b-PCL-CO-NH-NH_2**LCA micelles at 60ºC
LCST	Lower critical solution temperature
M	mPEG-b-PCL micelles

MDA-MB-231	Triple negative breast cancer cell line
MMPs	Matrix metalloproteinases
Mn	The number average molecular weight
mPEG	Methoxy poly(ethylene glycol)
mPEG-b-PCL	methoxy poly(ethylene glycol)-block-polycaprolactone
MTT	3-(4,5-dimethylthiazol-2-yl)-2,5-diphenyltetrazolium bromide
Mw	The weight average molecular weight
MWCO	Molecular weight cut-off
NHS	N-hydroxysuccinimide
PBS	Phosphate buffered saline
PDI	Polydispersity index
PEG	Poly(ethylene glycol)
PEG-b-PCL	Poly(ethylene glycol)-block-polycaprolactone
PEG-b-P(Glu)	PEG–b-poly(glutamic acid)
PEG-b-PLGA	poly(ethylene glycol)-block-poly(lactide-co-glycolide)
PEG-PEI	Poly(ethylene glycol)-polyethylenimine
PEI	Polyethyleneimine (PEI)
PLLA	Poly(L-lactic acid)
PNIPAAm	Poly(N-isopropylacrylamide)
PRBC	Progesterone receptor positive breast cancer
PVA	Polyvinyl alcohol

qRT-PCR	Quantitative reverse transcription polymerase chain reaction
ROS	Reactive oxygen species
RT	Room temperature
SDS	Sodium dodecyl sulfate
SK-MEL-30	Melanoma cell line
TEM	Transmission electron microscopy
TFA	Trifluoroacetic acid
Tg	Glass transition temperature
THF	Tetrahydrofuran
TILs	Tumor infiltrating lymphocytes
TNBC	Triple negative breast cancer
VEGF	Vascular endothelial growth factor
VNAR	Variable new antigen receptor

CHAPTER 1

INTRODUCTION

In this study, the aim was to produce polymeric micelles to deliver selected bioactive drugs to the cancer cells. In order to do this successfully, it is necessary to have some information about cancer, types of cancer and the properties of cancer cells.

1.1 Cancer

Cancer is uncontrolled cell division of abnormal cells. Cancer cells have some properties like limitless proliferation, tissue invasion and metastasis. Meanwhile, they also have high angiogenesis around the tumour tissue and high production of growth signals. Cancer cells can evade from antigrowth signals by controlling phosphorylation of them or overexpression of the growth signals like TGF-β. Cancer cells can also escape from apoptosis and immune cells. They have genome instability so mutations occur in cancer cells for providing them to live and escape from cell death. They also cause tumor-promoting inflammation and affect the cell's energy metabolism to promote their own survival (Fouad & Aanei, 2017).

Mutations which are mainly caused by some chemicals, infectious agents, radiation, errors in DNA replication, or heredity may cause cancer. Genes that encode cell proliferation and survival are mutated in cancer cells and these genes are termed as 'oncogenes'. Deletion or loss of function in tumor suppressor genes are other reasons for uncontrolled cell proliferation in cancer cells (Pezzella et al., 2019). The most important issue in cancer cells is metastasis, which is the spreading ability of the pathogenic agent's from the initial site to the other parts of the body (brain, bones, liver, etc.) via the bloodstream or lymphatic system.

1.1.1 Cancer Types

It is known that cancer begins when the orderly process of the cell growth is disturbed. The cells grow in an uncontrollable way and form a lump called 'tumor'. There are different types of cancer. The most common ones are breast, lung and skin cancers.

Breast cancer is the most common cancer type in women. Almost 20% of these patients have metastasis. It is the second type of cancer after lung cancer that causes the highest death among cancer types (H. M. Kim et al., 2017). Breast cancer also has different types as estrogen receptor positive breast cancer (ERBC), progesterone receptor positive breast cancer (PRBC), human epidermal growth factor receptor positive breast cancer (HER2-BC) and triple negative breast cancer (TNBC). TNBC is about 15-20% of breast cancers, does not contain a cell surface receptor and is a highly aggressive type of cancer. As the cells do not carry a receptor on the cell surface, cancer-targeted drug delivery systems are not available for this type (Parvani & Jackson, 2017). TNBC is also resistant to radiotherapy and therefore, treatment is quite difficult (W. Chen et al., 2017). In order to develop a targeted drug delivery system for TNBC, researchers are investigating only highly secreted molecules, signaling pathways and mechanisms in cancerous tissues (Garmpis et al., 2017).

Lung cancer is the leading cause of cancer deaths in the United States, among both men and women. There are two types of lung cancer: small-cell lung cancer and non-small-cell lung cancer. Heavy smoking causes small-cell lung cancer, but non-small-cell lung cancer is more common than small-cell lung cancer. Non-small cell lung cancers include squamous cell carcinoma, adenocarcinoma and large cell carcinoma (Couraud et al., 2012; Subramanian & Govindan, 2008).

Skin cancer generally develops on skin exposed to the sun. There are three types of skin cancer: basal cell carcinoma, squamous cell carcinoma (known as nonmelanoma skin cancer) and malignant melanoma. Malignant melanoma has a much higher mortality rate than the other types of skin cancer (Martinez & Otley, 2001).

1.2 Treatment of Cancer

Treatment of cancer is generally carried out as surgery, chemotherapy and radiotherapy. If there is no metastasis, complete removal of the tumor tissue from the body by surgery is done. After the surgery, chemotherapy and/or radiotherapy is applied to the patient in order to kill the remaining cancer cells on the operational site. In radiotherapy, high-energy X-rays or ionizing radiation are being used to destroy the cancer cells. Chemotherapy is the usage of drugs that circulate in the bloodstream and kill cancer cells or interfere with the ability of cancer cells to proliferate. Chemotherapy is also used when metastasis occurs. Antimetabolites, alkylating agents, platinum drugs, topoisomerase inhibitors, mitotic inhibitors, hormone therapy drugs, antibiotics and targeted therapy are being used in chemotherapy. Antimetabolites are molecules that are analogs of some molecules which are generally required in DNA synthesis and repair. Antimetabolites bind to enzymes in place of the normal molecules and disrupt the metabolic pathways for DNA synthesis and repair. Methotrexate is an antimetabolite and a folic acid analog. It binds to the enzyme dihydrofolate reductase which is required for the production of the reduced form of folic acid and so it inhibits the synthesis of several bases of DNA. Alkylating agents are highly reactive organic molecules that bind directly to DNA and cause single strand or double strand breaks in DNA, or they crosslink DNA molecules. As a result, DNA replication cannot occur. Platinum drugs also inhibit DNA synthesis by DNA crosslinking. Topoisomerases control the coiling and uncoiling of DNA during DNA replication. Topoisomerase inhibitors interfere with the topoisomerase-DNA bond and cause a double strand break in DNA. Consequently, apoptosis occurs. Mitotic inhibitors like Taxol disrupt the mitotic spindle during mitosis so cells cannot divide. Hormone therapy is generally used for patients who have cancer originating from hormone-dependent tissues. Tamoxifen molecule has some similarities with estrogen molecule, therefore, for estrogen receptor positive breast cancer patients, if tamoxifen is given, it binds to estrogen receptor and blocks the receptor activation. Streptomyces species produce

anthracyclines (doxorubicin, daunorubicin, epirubicin, and idarubicin) and non-anthracycline antibiotics (bleomycin and actinomycin D) which are very cytotoxic to cells. They act as alkylating agents but also intercalate DNA and inhibit topoisomerase function. In addition, they can generate free radicals, which cause oxidative damage to cellular proteins, thus inhibiting their action. But anthracycline antibiotics cause cardiotoxicity. Doxorubicin (DOX) is an anthracycline antibiotic. It can act as an alkylating agent and bind directly to DNA and cause single strand or double strand breaks in DNA or it crosslinks DNA. As a result, DNA replication cannot occur. Cardiotoxicity is a major problem after treatment with DOX (Pelengaris & Khan, 2013).

Mutations in the cancer cells cause molecular differences in their structures. Monoclonal antibodies against these molecules are being used for the treatment of cancer. Trastuzumab is a monoclonal antibody which targets the HER2 receptor (epidermal growth factor receptor) on the cancer cell surface and inhibits the activation of the receptor. Cancer cells overexpress HER2 receptor to stimulate cell proliferation by binding high amounts of growth factor. Trastuzumab binds to HER2 receptor and blocks the signaling pathway of the receptor by inhibiting the activation of the receptor. As a result, tumor growth is inhibited. Small molecule inhibitors are also being used to target specific proteins in the cells. Unlike monoclonal antibodies, small molecule inhibitors can enter the cell. Imatinib is a Bcr-Abl tyrosine-kinase receptor inhibitor. Bcr-Abl is an abnormal protein which is only produced in cancer cells from the oncogene BCR-ABL. Therefore, imatinib is an ideal targeted drug for cancers overexpressing BCR-ABL oncogene (Pelengaris & Khan, 2013).

1.2.1 Research on New Drug Candidates

Cancer cells can escape from drug therapy in various ways called as multidrug resistance. Multidrug resistance occurs due to the presence of cells like cancer associated fibroblasts and cancer stem cells, and survival factors like fibroblast growth factor, epidermal growth factor, insulin-like growth factor, platelet derived

growth factor, and vascular endothelial growth factor (VEGF) in tumor microenvironment (Haider et al., 2020). The overexpression of some genes like P-gp, MDR1 (multidrug resistance gene) also causes multidrug resistance.(Haider et al., 2020). Drugs are taken by the cells can throw away from the cell by drug efflux transporter proteins in cancer cell membrane. The alteration of apoptotic pathways and changes in cell membrane also decreases the activity of the drugs. Inactivation of drugs due to changes in the tumor environment can occur. For example, DOX can be protonated and become inactive due to acidity of the tumor microenvironment (Haider et al., 2020). Epithelial to mesenchymal transition of cells also causes multidrug resistance which causes metastasis, cell shape changes (Haider et al., 2020). Therefore, new drug candidates are being investigated to overcome the multidrug resistance mechanism of cancer cells. For example, Özenver et al. (2018) extracted aloe-emodin from R. acetosella and studied the anticancer effect of aloe-emodin on CCRF-CEM (acute lymphoblastic leukemia cells). They showed that aloe-emodin causes apoptosis, ROS generation and cell cycle arrest in S phase. The IC_{50} value of aloe-emodin was found as 9.872 μM on CCRF-CEM cells. They proposed that aloe-emodin can be considered as a possible anticancer drug (Özenver et al., 2018). Liao et al. (2019) used chaetocin as an anticancer agent for the treatment of gastric cancer. IC_{50} values of chaetocin on three different gastric cancer cell lines (AGS, HGC-27, and NCI-N87) were re as 120 nM, 400 nM, and 820 nM, respectively. They showed that chaetocin induced apoptosis on AGS, and HGC-27 cells. Mitochondrial transmembrane potentials of AGS, and HGC-27 cells were decreased without increasing ROS levels. Thus, they suggested that chaetocin causes apoptosis on gastric cancer cells independent from ROS levels (X. Liao et al., 2019).

Lithocholic acid (LCA) is a hydrophobic bile acid and has been reported to have anticancer effect on breast cancer cells (Luu et al., 2018; Mikó et al., 2018), prostate cancer cells (Gafar et al., 2016), and neuroblastomas (Goldberg et al., 2011), and it is not toxic to normal cells. It was also shown that LCA suppresses cell apoptosis on mouse cardiomyocytes by preventing EphA2 phosphorylation which regulates cell death and differentiation in development and cancer (Jehle et al., 2012). Luu et al.,

(2018) reported that increasing concentrations of LCA decreased cell viability and lipogenic activity and increased apoptosis of breast cancer cells in vitro (Luu et al., 2018). Gafar et al. reported that cell death mechanism of LCA on prostate cancer cells by apoptosis, necrosis and autophagy (Gafar et al., 2016). Singh et al. (2017) prepared LCA containing polymer-drug conjugate (lithocholic acid-poly(ethylene glycol)-lactobionic acid; LPL) and loaded with DOX. They observed that free LCA and free DOX exhibited similar cell viability, and apoptosis. On the other hand, DOX loaded LPL nanoparticles demonstrated lower cell viability and higher cell apoptosis on liver cancer cells (Singh et al., 2017).

1.3 Drug Delivery Systems

Drugs used in chemotherapy are usually hydrophobic and toxic chemicals. Therefore, when injected into the body or orally taken, they cause unwanted side effects such as hair loss, nausea, vomiting, diarrhea, anemia, defective blood clotting, and immune deficiency on normal tissues. These drugs are also rapidly removed from the body by the reticuloendothelial system before reaching the tumor, which leads to an ineffective drug consumption (Y. Zhang et al., 2014).

Due to genomic instability, cancer cells can become resistant to chemotherapeutic drugs after a series of treatment with drugs. Some resistant cancer cells may be present after chemotherapy, which could proliferate and form a new tumor that is completely resistant to chemotherapy, meaning to the drugs applied previously. This phenomenon is called as 'multidrug resistance'. Multidrug resistant transport proteins are involved in drug efflux mechanism. These transport proteins can traverse a broad spectrum of drugs resulting in drug resistance in cancer cells by exporting most of the chemically dissimilar molecules (Pezzella et al., 2019). To minimize the side effects of drugs, drug carriers as controlled drug release systems and targeted drug delivery systems are being developed. Drug delivery systems protect the drug from rapid degradation or renal clearance and enhances drug concentration in the

target tissues, therefore, lower doses of drugs can be applied without causing side effects (Upponi & Torchilin, 2014).

1.3.1 Targeted Drug Delivery

Drug delivery systems should provide minimum side effects and maximum therapeutic effect. Therefore, especially for the cancer therapy, targeted drug delivery systems are being developed. Targeted drug delivery is a method of treatment that involves the increase in medicament in one or few body parts in comparison to others. Therefore, it delivers the medication only to areas of interest within the body. In these systems, drugs are either covalently or ionically conjugated to polymers or nano carriers or bound with hydrophobic interactions. These systems deliver the cargo to the cancer cells via two strategies: passive targeting and active targeting (Figure 1.1).

Passive Targeting: Cancer cells have self-sufficiency in growth factors so they can overproduce VEGF. Overproduction of VEGF causes disorganized vascular tissue around the tumor tissue. This vascular tissue is called as 'leaky vasculatures' since they leak more fluid than normal tissue due to larger pore sizes in capillaries around cancer tissue. Small molecules, and nanoparticles can accumulate in the targeted cancerous tissue because of leaky vasculatures in tumor and this phenomenon is called as 'enhanced permeability and retention (EPR) effect' in passive targeting.

Active Targeting: In this type of targeting, drug is conjugated with recognition ligands such as antibodies (Viravaidya-Pasuwat & Naruphontjirakul, 2019), low molecular ligands e.g., folic acids (Lale et al., 2015), proteins (Schieber et al., 2012), peptides (Nieberler et al., 2017), hyaluronic acid (K. Kim et al., 2019), carbohydrates (Venturelli et al., 2016), aptamers (Fu & Xiang, 2020) or recognition ligands (Peiris et al., 2018), which recognize the specific target molecules like receptors on the cancer cells, attach to these receptors and the bioactive agents are effective only in cancer area. Active targeting strategy can also be achieved through a manipulation

with physical or chemical stimuli (e.g., temperature, pH, magnetism, enzymes, etc.) (Upponi & Torchilin, 2014).

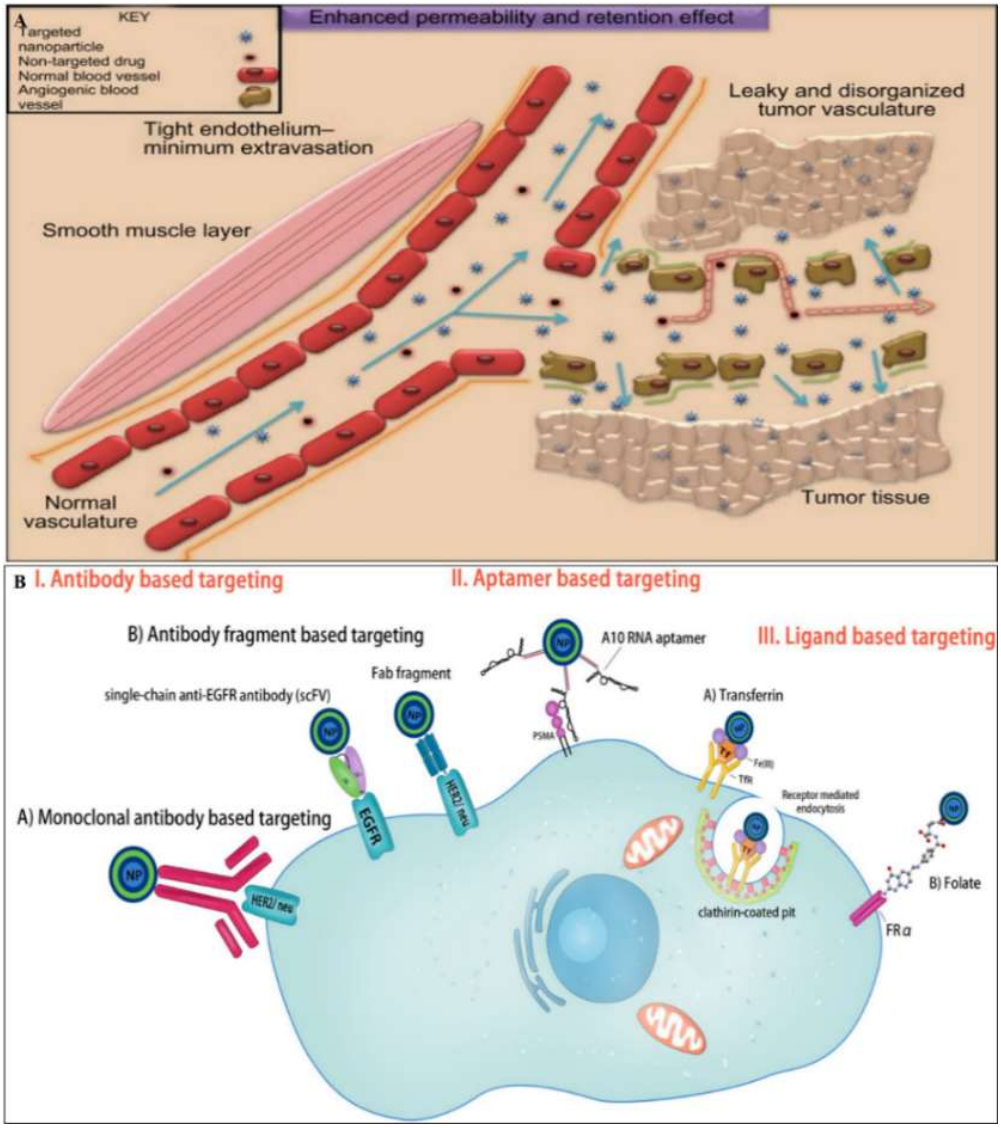

Figure 1.1. A) Passive targeting (Ranganathan et al., 2012). B) Active targeting (Bazak et al., 2015).

Besides the mentioned two strategies, there are also stimuli responsive delivery systems, which concentrate the bioactive agent in the tumor area since the properties and some biological molecules are different in their microenvironment than the healthy biological tissue.

1.3.1.1 Stimuli Responsive Drug Delivery

Cancer cells can induce angiogenesis by overexpression of angiogenic factors, some enzymes and cell surface receptors like epidermal growth factor, escape from apoptosis and immune cells, invade other tissues (metastasis), etc. These metabolic changes result in lower pH levels, higher intracellular levels of glutathione, higher reactive oxygen species and ATP levels, and hypoxia in the tumor microenvironment. Therefore, stimuli responsive (pH, enzyme, redox, temperature, or photosensitive) drug delivery systems are being developed to effectively release the anticancer drugs in tumor microenvironment (Faal Maleki et al., 2019).

1.3.1.1.1 Temperature Sensitive Delivery Systems

Temperature sensitive polymer-drug systems allow the release of entrapped/conjugated drug in response to heat shock stimuli. Nanoparticles may be developed as the temperature-sensitive carriers. Some polymers can show swelling and collapse transition according to its lower critical solution temperature (LCST) (Lee et al., 2015). Poly(N-isopropylacrylamide) (PNIPAAm) is a thermo-responsive polymer with a LCST at 32°C. It swells below LCST and collapse above LCST. Eskandari et al. (2020) prepared DOX loaded PNIPAAm nanoparticles and showed higher drug release at 40°C than 25°C. Higher DOX release was observed at 40°C due to squeezing of PNIPAAm nanoparticles above LCST (Eskandari et al., 2020). Kitano et al. (2021) synthesized a triblock copolymer made of poly(ethylene glycol) (PEG), poly(2-ureidoethyl methacrylate) (PUEM) and poly(2-(methacryloyl oxy)ethyl phosphorylcholine) (PMPC) (briefly PEUM), which has thermo-

responsive properties. Fullerene was added to the nanoparticle structure to add light-responsive behavior. Upon light irradiation, fullerene generates singlet oxygen and causes ROS-dependent apoptosis. DOX was added as an anticancer drug and release of DOX was higher at 50°C than 25°C due to swelling of the nanoparticle at 50°C (Kitano et al., 2022).

1.3.1.1.2 Magnetism Sensitive Delivery Systems

Magnetism is used as an external stimulus in drug delivery systems. Magnetic nanoparticles like ferric oxide particles can be added into the carriers or can be used as carriers after chemical modifications, so that they form particles sensitive to magnetism. Magnetic field is applied internally of externally to the area of tumor tissue and so magnetic nanoparticles accumulate in the tumor area. The release and the efficacy of the anti-cancer drug accumulate over there. Kheirkhah et al. (2018) prepared magnetic ferric oxide nanoparticles and covered them with gold layer. The particles were then coated with gellan gum and DOX was loaded to the particles with electrostatic interaction between DOX and the gellan gum. Then, they studied the anti-cancer effect of this system on intramedullary spinal cord tumors *in vivo* by implanting a neodymium magnet at the tumor site to create magnetic field around the tumor and to promote accumulation of DOX loaded magnetic nanoparticles at the desired area (Kheirkhah et al., 2018). García-Hevia et al. (2022) prepared DOX and Fe_3O_4 loaded magnetic nanoparticles from Carnauba wax and showed the more effective cytotoxic effect of these nanoparticles compared to free DOX on melanoma cells. They used magnetic nanoparticles (Fe_3O_4) to create hyperthermia around the tumor tissue to provide a synergistic treatment with DOX. They injected melanoma cells to C57BL/6 mice subcutaneously to form tumor. It was shown that DOX loaded magnetic particles more effectively accumulated in tumor tissue and decreased the volume of the tumor compared to DOX loaded nanoparticles, which did not contain Fe_3O_4 (García-Hevia et al., 2022).

1.3.1.1.3 Enzyme Sensitive Delivery Systems

Some enzymes are overexpressed by tumor cells. These enzymes can degrade the extracellular matrix and allow cancer cells to invade other tissues. Overexpression of these enzymes can be used to degrade some type of linkers like ester, peptide, glycoside, etc. This type of linkers can be used to conjugate anticancer drug to the nanoparticles and overexpressed enzymes around tumor microenvironment attack to and break these linkers releasing the anticancer drug in the tumor tissue (Chau et al., 2006). Matrix metalloproteinases (MMPs) are extracellular enzymes that degrade the extracellular matrix and are remodelling the tissue environment. MMPs are overexpressed by cancer cells and thus, they are responsible for cancer initiation, progression and metastasis. Therefore, MMP sensitive peptides can be conjugated to the anticancer drugs to deliver the drug in tumor tissue by using carrier nanoparticles with different hydrophobicity/hydrophilicity, structure, conformation, and/or charge (Yao et al., 2018). Chen et al. (2022) prepared enzymatic nanoreactors from sulfhydrylated polylysine (PL-SH) and 8arm-PEG-MAL with the usage of millifluidic technology. Glucose oxidase was loaded to nanoreactors as an enzymatic therapy for cancer. They induced tumor in BALB/c mice by injecting 4T1 cells subcutaneously. They showed that glucose oxidase loaded nanoreactors decreased the tumor volume without any change in body weight which indicates that glucose oxidase loaded nanoreactors are not cytotoxic to normal cells (N. Chen et al., 2022).

1.3.1.1.4 Hypoxia Sensitive Delivery Systems

In tumor microenvironment, oxygen levels are lower than normal tissue. These causes hypoxia around tumor and hypoxia influences tumors in many aspects including angiogenesis, epithelial to mesenchymal transition, invasiveness and metastasis. Hypoxia also increases drug resistance in cancer cells and activates some factors including hypoxia-inducible factors (HIFs), which could be targeted via their thiol groups. In tumor microenvironment, glutathione (GSH) levels are higher than

normal tissue due to hypoxic environment. Thus, GSH targeted drug delivery systems are gaining interest and being studied to deliver the anticancer drugs in tumor environment (Zeng et al., 2018). Gdowski et al. (2022) prepared a complex containing gemcitabine and sickle cell hemoglobin. Sickle cell hemoglobin can polymerize in hypoxic and acidic conditions and when it polymerizes, sickle cell hemoglobin can break tumor stroma and decrease the intratumoral pressure. They induced tumor in mice with the injection of BxPC3 pancreatic cancer cells subcutaneously and showed that gemcitabine containing sickle cell hemoglobin resulted in the lowest tumor volume among the free gemcitabine and sickle cell hemoglobin alone (Gdowski et al., 2022).

1.3.1.1.5 Light Sensitive Delivery Systems

Light is an external stimulus in drug delivery systems. It is also used for imaging reasons. In photochemical drug delivery, the applied light irradiation can dissociates chemical bonds and releases the drug in the tumor environment. In photoisomerization drug delivery, light can cause a reversible change on the bonds. This means that the release of the drug can be turned on and off. In photothermal drug delivery, light generates heat that allows the delivery of the drug. A chromophore or a thermo-responsive polymer can be used in photothermal drug delivery (Linsley & Wu, 2017). Wang et al. (2022) used flav7 (a fluorophore) and DOX loaded microneedles prepared from polycaprolactone. Flav7 was loaded to create a near-infrared light triggered drug delivery system. With the application of near-infrared light, temperature increases and so polycaprolactone melts. This provides the delivery of the drug from the microneedles. The researchers induced tumor in BALB/c mice by injecting 4T1 cells subcutaneously and showed that flav7 and DOX loaded microneedles accumulated in tumor tissue and decreased the tumor volume compared to free DOX and microneedles that do not contain DOX. They also showed that there were low signals of flav7 at normal tissues upon near-infrared imaging compared to tumor tissue (H. Wang et al., 2022).

1.3.1.1.6 pH Sensitive Delivery Systems

Cancer cells favor glycolysis than oxidative ATP production to supply the required ATP quickly. This results in hypoxia in the tumor area and pH values decrease to 6.5-7.2, 5.0-6.5, and 4.5-5.0, in the tumor microenvironment, endosomes, and lysosomes, respectively (Yi Li et al., 2019). In pH sensitive drug delivery, drugs are being conjugated to polymers with a pH sensitive linker like hydrazone, disulfide, azo, acetal, ortho ester, vinyl ether, amine, imine etc. (Chang et al., 2016). Amine derivatives are generally polycations that are positively charged in acidic environment. Polycation based nanoparticles are positively charged and they swell in tumor environment. Thus, an anticancer drug loaded in these nanoparticles is released (Ghaffar et al., 2020). Anticancer drugs can also be conjugated to the polymer with cis-aconityl linker and the release of the drug can be observed in lysosomal pH (4.5-5.0) while the polymer-drug conjugate is stable in normal physiological conditions (pH 7.4) (X. Huang et al., 2018). Thioether derivatives are protonated in acidic conditions and result in increase in the particle size. Thus, this phenomenon allows the higher drug release in acidic conditions than normal physiological conditions (M. Su et al., 2020). Acetal linkers are highly stable in normal physiological conditions while dissociate in mild acidic conditions. Therefore, acetal linkers are being used for drug delivery in cancer (Yamin Li et al., 2020).

Hydrazone derivatives (Figure 1.2) can respond to high levels of hydrogen ions and low pH levels and hydrazone groups are stable under normal physiological conditions (pH 7.4) (Faal Maleki et al., 2019). Etrych et al. (2014) conjugated DOX to N-(2-hydroxypropyl)methacrylamide (HPMA) copolymers via hydrazone bond and reported that drug release was faster at pH 5.0 than at pH 7.4 (Etrych et al., 2014). Lale et al. (2015) conjugated DOX to a pentablock copolymer via hydrazone bond and drug release studies showed that 89% of DOX was released at pH 5.0 and 29% of DOX was released at pH 7.4 (Lale et al., 2015). Zhang et al. (2022) conjugated DOX to supramolecular organic framework via hydrazone bond and they

showed that decrease in pH increased DOX release. Drug release studies showed that 80% of DOX was released at pH 4.5, 45% of DOX was released at pH 5.6 and 15% of DOX was released at pH 7.4 after 72 hours (Y.-C. Zhang et al., 2022).

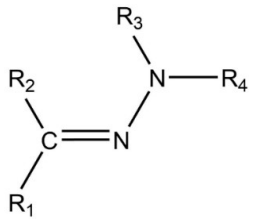

Figure 1.2. Hydrazone bond structure.

These results showed that hydrazone linkage causes drug release in acidic conditions while a slower drug release rate can be obtained under normal physiological conditions.

1.3.1.1.6.1 Conjugation of Drugs to Polymers or Nanocarriers

Drugs or antibodies can be bound to the polymers or nanoparticles via covalent bonds or via electrostatic interactions either by forming ionic or hydrophobic interactions. Ionic interactions are constructed between a positively charged group and a negatively charged group, and hydrophobic interactions form between molecules having no charged groups. In many cases, antibodies are conjugated to gold nanoparticles via electrostatic interaction or hydrophobic interaction (Jazayeri et al., 2016). In the literature, there are some studies that show the effect of electrostatic interaction in drug delivery and antibody conjugation. Murakami et al. (2021) used NanoAct® nanobeads (cellulose nanoparticles) to conjugate the antibody of influenza protein NP and showed that antibody was adsorbed onto NanoAct® nanobeads with a pH dependent manner. Decreasing pH increased adsorbed antibody amount (Murakami et al., 2021). Gandhi et al. (2019) studied the adsorption of trastuzumab antibody compared with the adsorption of emtansine conjugated trastuzumab. Emtansine conjugated trastuzumab is an antibody-drug conjugate commercially available as Kadcyla. Conjugation of hydrophobic drug emtansine to

the antibody was governed by increasing electrostatic interaction between the drug and the lysine residue of the antibody and also increasing hydrophobic protein-protein interactions. Results showed that drug conjugation increased the hydrophobicity and lowered colloidal stability of the antibody. As a result, more adsorption was observed in drug conjugated antibody compared to free antibody (Gandhi et al., 2019). Zhao et al. (2017) conjugated bovine serum albumin (BSA) to graphene oxide via electrostatic interaction and then, BSA conjugated graphene oxide was loaded into chitosan hydrogels. Results showed that increasing pH decreased BSA release from the hydrogels which had higher graphene oxide concentration, and explained as; electrostatic interaction between BSA and the graphene oxide protected the drug at pH 7.4 whereas at pH 6.8 higher BSA release was observed (Zhao et al., 2017). Nanogels were prepared from poly(ethylene glycol)-polyethylenimine (PEG-PEI) with different protonation degrees by Mauri et al. (2017) to investigate the effectiveness of electrostatic interaction in drug delivery systems. Therefore, they used an ionic (sodium fluorescein) and a nonionic (rhodamine B) dye to imitate drug loading. First, protonated and uncharged nanogels were prepared and then, dyes were loaded to nanogels. Results showed the same release profile for rhodamine B at pH 7.4 and pH 4.5 whether protonated nanogel or uncharged nanogel was used. On the contrary, protonated nanogel decreased the release rate of sodium fluorescein due to electrostatic interaction between negatively charged dye and protonated nanogel at pH 7.4 and pH 4.5 and uncharged nanogel increased the release rate and initial burst release of sodium fluorescein at pH 7.4 and pH 4.5 compared to protonated nanogel. Sodium fluorescein is weakly negative and protonated nanogel was highly positive so this may decrease the release rate by holding the dye with the nanogel due to electrostatic interaction (Mauri et al., 2017). These findings from the literature indicate that electrostatic interactions can be used in antibody conjugation and preparation of pH sensitive drug delivery system without changing the conformational structure of the drug and the antibody since electrostatic interaction is not a covalent bond.

1.4 Nanoparticles in Drug Delivery Systems

In drug delivery systems, drugs used in chemotherapy are given to the body with biocompatible nanoparticles to minimize the side effects of drugs. Nanoparticles are drug carriers, which have a size smaller than 100 nm in at least one dimension. Nanoparticles have a high surface area and an ability to cross cells and tissue barriers because of their small sizes. Liposomes, solid lipids nanoparticles, dendrimers, polymeric micelles, silicon or carbon materials, and magnetic nanoparticles are being tested as drug delivery systems (Wilczewska et al., 2012). There are studies showing that liposome-encapsulated DOX decreases cardiac toxicity of the drug, and albumin-stabilized paclitaxel allows higher tolerated doses in patients (Bertrand et al., 2014). Nanoparticles present in the market are shown in Figure 1.3.

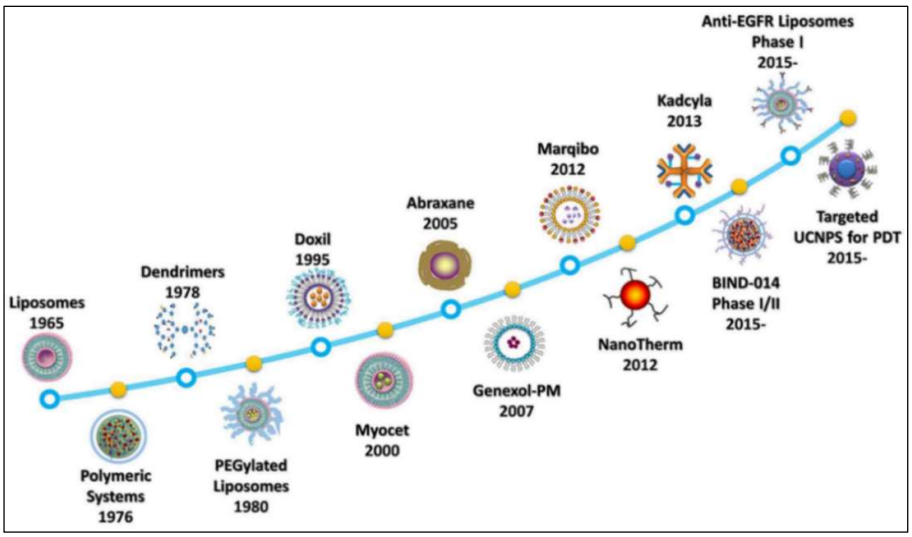

Figure 1.3. Nanoparticles in the market (Z. Li et al., 2017).

1.4.1 Polymeric Micelles

Polymeric micelles are nano-sized particles with a hydrophilic shell and a hydrophobic core. Due to the hydrophobic core, hydrophobic anticancer drugs can be loaded into these structures (Wilczewska et al., 2012). These systems are easy to prepare, can be synthesized in small and uniform particle size, can encapsulate large

amounts of drugs and provide controlled drug release. Therefore, it is common to use these nanoparticles in *in vitro* and *in vivo* studies (Y. Wang et al., 2017). In particular, encapsulating hydrophobic drugs into micelles increases bioavailability of the drug and decreases the side effects, so they are becoming advantageous in many applications (Torchilin, 2007). The characteristic size of polymeric micelles ranges from 5 to 50–100 nm, which makes them ideal candidates for the delivery of therapeutic and contrast agents to the tumor tissue. Amphiphilic copolymers can self-assemble to form micelles with hydrophobic core and hydrophilic corona. Therefore, drugs that are poorly soluble in water can be loaded into micelles (Owen et al., 2012). Micelles used as drug delivery vesicles should have some properties; they should;

- be small enough (~10 – 100 nm) for intravenous injection and penetration into tumor tissue
- be unrecognizable by the immune system to circulate into the body for a sufficient time
- accumulate in the target tissue and interact with the target cells
- have adjustable stability
- maintain high loading
- be eliminated from the body after degradation or dissolution
- improve the pharmacokinetic profile of loaded drug
- be produced reproducibly and be inexpensive (Hussein & Youssry, 2018; Owen et al., 2012).

Methoxy poly(ethylene glycol)-block-polycaprolactone (mPEG-b-PCL) (Figure 1.4) is a synthetic, amphiphilic, biocompatible and biodegradable polymer that is approved by FDA (Senevirathne et al., 2016). Poly(ethylene glycol) (PEG) and polycaprolactone (PCL) are biocompatible polymers and widely used in the production of drug delivery systems and tissue engineering scaffolds (Xiong et al., 2015). However, PCL is highly hydrophobic, its degradation is too slow for drug delivery applications, and it can be recognized by immune system rapidly (Mariani et al., 2019). On the other hand, PEG is hydrophilic and can escape from the immune

system. Scientists prepared or used copolymers or tri-block-polymers of PEG and PCL and produced nanoparticles or micelles as drug delivery vehicles, and evaluated in vitro and in vivo effects of these systems.

Theerasilp et al. (2017) prepared COOH-PEG-b-PCL micelles by solvent evaporation method that contain superparamagnetic iron oxide for imaging purposes and glucose was conjugated to micelle surface by EDC-NHS chemistry to target to prostate cancer cells. The superparamagnetic iron oxide encapsulation efficiency of micelles was found as 12%. The size of targeted and non-targeted micelles was found as 35.5 nm by dynamic light scattering. The non-targeted micelles had a zeta potential of -24.3 mV whereas targeted micelles' zeta potential was -17.2 mV, which confirms the conjugation of glucose on micelle surface. *In vitro* cell viability of prostate cancer cell line (PC-3) cells did not change with the addition of targeted or non-targeted micelles to the medium but the cellular uptake of targeted micelles increased compared to non-targeted micelles (Theerasilp et al., 2017).

Ribeiro et al. (2016) synthesized mPEG-b-PCL and NH_2-PEG-PCL to prepare docetaxel loaded polymeric micelles by thin film hydration method. Pyrazolyl-diamine units were added on amine group of the copolymers to stabilize the micelle structure. Then prazolyl-diamine units were radio-labeled with fac-[99mTc$(CO)_3(H_2O)_3$] for imaging. Hydrodynamic diameter of the prepared micelles (blank non-labeled micelles, docetaxel loaded non-labeled micelles, labeled blank micelles, docetaxel loaded labeled micelles) varied from 35.5 nm to 66.5 nm. Zeta potential of the prepared micelles varied from -1.4 mV to -8.4 mV. Drug loading and encapsulation efficiency of micelles were found as 3.2% and 63%, respectively. *In vitro* release of the drug was studied in media at different pH and higher release was observed at pH 5.0 than that of pH 7.4. The anti-proliferative activity of blank and docetaxel loaded micelles was assessed by the Alamar Blue assay on different human cancer cell lines (breast cancer (MDA-MB-231), prostate cancer (PC-3) and osteosarcoma (MNNG HOS) cell lines), and compared with that of free docetaxel. The viability of MDA-MB-231 and MNNG HOS cells decreased when docetaxel loaded micelles were used. On the contrary, the viability of PC-3 cells did not change

when compared to free drug. It may be due to the drug resistance of PC-3 cells. In comparison to the free drug, the drug loaded-micelles require lower docetaxel concentration to induce a similar therapeutic effect with reduced side effects. In vivo biodistribution studies were carried out with healthy BALB/c mice and researchers reported that radiolabeled micelles showed prolonged blood circulation time (Ribeiro et al., 2016).

Sengel-Turk et al. (2016) used PEG-b-PCL copolymers to prepare nimesulide loaded micelles. The group used nanoprecipitation method (N-method) and solvent evaporation method using either a homogenizer (H-method), or ultrasonication device (U-method) to prepare micelles. The mean particle size of the nanoparticles was 233.3 nm for U-method and 148.5 nm for N-method whereas 307.2 nm particle size was determined by the H-method. Zeta potential of micelles were found -20.5 mV for H-method, -25.6 mV for U-method and -17.7 mV for N-method. The encapsulation efficiencies of micelles were found as 97.42% for H-method, 96.19% for U-method and 73.05% for N-method. The amount of nimesulide released from micelles was approximately 63% for H-method, 54% for U-method, and 68% for N-method during the first 24 h. After a period of 7 days, nimesulide release was obtained nearly 64% for H-method, 57% for U-method, and 72% for N-method. The cytotoxic effect of the prepared micelles was tested on MCF-7 breast cancer cells. Nimesulide loaded PEG-b-PCL micelles that were produced by all of the techniques had a significant toxicity on the viability of MCF-7 cells compared to untreated and treated with free nimesulide groups (Sengel-Turk et al., 2017).

Hascicek et al. (2017) prepared fulvestrant loaded PEG-b-PCL micelles and PEG-b-PLGA (poly(ethylene glycol)-block-poly(lactide-co-glycolide)) micelles using different lengths of PEG, PCL and PLGA polymers, by a combined method of salting-out and solvent evaporation (Figure 1.4). The particle size of the nanoparticles ranged between 84.56 and 220.20 nm. Among the micelles, the higher hydrophilic form of the PEG-b-PCL had the smallest particle dimension. The dimension of the particles significantly increased when molecular weight of hydrophobic part (PLGA and PCL polymers) of the micelles was increased. The

encapsulation efficiencies of fulvestrant loaded PEG-b-PCL and PEG-b-PLGA micelles were found as 73.56% and 82.06%, respectively. PEG-b-PCL micelles showed much faster drug release than PEG-b-PLGA micelles, which may be caused by higher hydrophilic character and the faster degradation rate of PEG-b-PCL copolymer than those of PLGA. Cytotoxic effect of the free fulvestrant and fulvestrant loaded micelles were determined by in-vitro MTT assay using MCF-7 breast cancer cells, and the effects on the proliferation of MCF-7 cells was studied after 24 and 48 h. The highest cytotoxic effect was observed with fulvestrant loaded PEG-b-PCL micelles. Cellular uptake studies were also achieved with coumarin 6 loaded micelles, and PEG-b-PCL micelles had the higher cellular uptake than PEG-b-PLGA micelles (Hascicek et al., 2017).

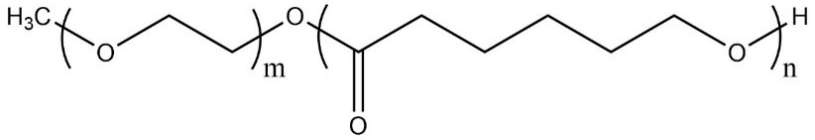

Figure 1.4. mPEG-b-PCL structure.

Polymeric micelles are being developed to provide a suitable drug delivery formulation for the treatment of diseases like cancer, and for imaging purposes. Drugs or imaging agents are either loaded to the micelles or conjugated to the polymers that form micelles. Targeting agents like antibodies are conjugated to the micelles to provide higher accumulation in the disease site. Table 1 summarize some of the studies related to the use of polymeric micelles for cancer treatment.

1.4.1.1 Polymeric Micelles under Clinical Trials

Polymeric micelles are being investigated with several clinical studies. They are used to treat several diseases like cancer, sickle cell disease, cystic fibrosis, etc. There are also some products of polymeric micelles that are in market and being used in the cancer treatment like Genexol-PM. Table 2 shows the polymeric micelles used in clinical trials.

Table 1.1. Studies about polymeric micelles for cancer treatment.

Drug Carrying System	Drug or Agent	Aim	Findings	Ref.
COOH-PDLLA-PEG-PDLLA-COOH and NH2-PDLLA-PEG-PDLLA-NH_2 hydrogel and 5,6-dimethylxanthenone-4-acetic acid (DMXAA) conjugated or Doxorubicin (DOX) loaded mPEG-b-PLGA micelles	DOX and DMXAA	- To obtain temperature sensitive hydrogel containing drug loaded and/or conjugated micelles for local delivery in tumor tissue - To increase DOX loading due to electrostatic interaction and hydrogen bonding with DMXAA - To provide DMXAA (vascular disrupting agent and anti-tumor immune response inducer) release - To provide synergistic effect on the cancer treatment with DOX and DMXAA	- Sustained release of drugs at pH 7.4 and pH 5.5 - After induction of tumor with injection of HeLa cells subcutaneously to BALB/c mice, mice were treated with DOX and DMXAA containing hydrogels. Dual drug containing hydrogels inhibited tumor growth for five weeks compared to free drugs and hydrogels that do not contain drugs. - Inhibition of vascular formation was also observed after treatment with DMXAA conjugated hydrogels	(Darge et al., 2021)
Micelles formed from PEG–b-poly(glutamic acid) (PEG–b-P(Glu)) copolymer and the poly(glutamic acid) (P(Glu)) homopolymer	1,2-diaminocyclohexane-platinum(II) (DACHPt)	-To evaluate the effect of size of micelles on tumor tissue	- Increasing ratio of P(Glu) in copolymer and homopolymer increased size of the micelles from 30 nm to 100 nm. - Penetration to tumor tissue was affected by size of the micelles (Only sub-50 nm (30 nm) micelles penetrated poorly permeable pancreatic tumors while sub-100 nm (30 nm, 50 nm, and 70 nm) micelles could penetrate hyperpermeable colon tumors)	(Cabral et al., 2011)

Table 1.1 (cont'd). Studies about polymeric micelles for cancer treatment.

Drug Carrying System	Drug or Agent	Aim	Findings	Ref.
poly 10-hydroxycamptothecin (pHCPT)-PEG micelles	10-hydroxycamptothecin (HCPT) and dexamethasone (DEX)	- To obtain a reactive oxygen species (ROS) responsive dual drug delivery system - To increase ROS level in tumor tissue with DEX - To obtain higher HCPT release due to reduction of keto groups in micelles with increased ROS	- Increased hydrogen peroxide levels increased HCPT release. - Tumor induced BALB/c mice showed higher accumulation of keto group containing micelles in tumor site compared to aliphatic micelles - DEX loaded keto micelles inhibited tumor growth more than keto micelles without DEX.	(Meng et al., 2021)
ROS-sensitive thioketal (TK) linkage-bridged diblock copolymer of PEG with polylactic acid-glycolic acid (PLGA) (PEG-TK-PLGA) micelles	Aggregation induced emission (AIE) photosensitizer TPA-BDTO (TB) and paclitaxel (PTX)	- To obtain a ROS sensitive micelles - To obtain a targeted drug delivery with the conjugation of cRGD peptide to the micelles	- AIE photosensitizer TB increased ROS generation after light irradiation so increased PTX release. - Inhibited tumor growth - Induced anti-tumor immune response - Upregulated PD-L1 expression to increase the effectiveness of anti-PD-L1 antibody for abscopal effect	(Xu et al., 2021)
pH sensitive, antibody conjugated DSPE-PEG immunomicelles by incorporation of pH-sensitive polyhistidine-polyethylene glycol (PHIS-PEG)	Paclitaxel (PTX)	- To obtain a pH sensitive drug delivery system - To obtain a micelle system that is stable at pH 7.4 and pH 6.8 but disintegrates at pH 5.0 (endosomal pH)	- Destabilization of micelles when pH drops to around 5.5 - Increased cytotoxicity due to pH sensitiveness - Increased tumor cell killing effect due to antibody conjugation	(Wu et al., 2013)

Table 1.1 (cont'd). Studies about polymeric micelles for cancer treatment.

Drug Carrying System	Drug or Agent	Aim	Findings	Ref.
Nanoparticles from mal-PAH-PEG-DMMA / poly (ethylene imine) – poly(ε-caprolactone) block polymers containing DTX and IR825 loaded MPPD/PEI-PCL micelles	IR825 and docetaxel (DTX)	- To obtain both pH sensitive and photoresponsive dual drug delivery system	- Charge reversal at pH 6.8 and so occurrence of micelle disintegration - Increased drug release at lower pH values - Increased temperature due to IR825 release compared to free IR825 - Increased cell toxicity and apoptosis on cancer cells and *in vivo* anti-tumor efficiency	(X. Wang et al., 2022)
H_2N-PEEP-b-PBYP-hyd-DOX micelles	Doxorubicin (DOX)	- To obtain targeted with a CD147 monoclonal antibody by EDC/NHS chemistry and pH sensitive drug delivery	- Increased release of DOX at pH 5.0 compared to pH 7.4 - Antibody conjugation increased cellular uptake of micelles	(Y.-K. Huang et al., 2021)
Folic acid conjugated poly(2-hydroxyethyl acrylate)-b-poly(N-vinylcaprolactam) micelles	5-fluorouracil	- To obtain a targeted drug delivery system against colon cancer	- Viability of mouse cardiomyocytes and colon fibroblasts did not change upon treatment. - Viabilities of colon cancer cell lines (DLD-1, CaCo-2, and HT-29) decreased *in vitro*	(Siemiaszko et al., 2021)
D-α-tocopherol polyethylene glycol 1000 succinate (TPGS) and pluronic F127 (F127) combined micelles	Baicalein	- To obtain baicalein loaded mixed micelles to enhance aqueous solubility of baicalein	- Mixed micelles showed high entrapment efficiency. - Increased cellular uptake - Increased anticancer efficiency on MDA-MB-231 cells - Enhanced apoptosis on MDA-MB-231 cells -Increased ROS generation	(Srivastava et al., 2021)

Table 1.1 (cont'd). Studies about polymeric micelles for cancer treatment.

Drug Carrying System	Drug or Agent	Aim	Findings	Ref.
Micelles from methoxy-poly(ethylene glycol)-b-poly(glutamic acid) (mPEG-b-P(Glu))	Active complex of oxaliplatin, (1,2-diaminocyclohexane) platinum(II) (DACHPt) (DACHPt/m)	- To obtain antibody fragment (Fab') conjugated drug loaded immunomicelles for pancreatic cancer treatment	- Enhanced antitumor efficiency - Rapid binding and internalization of Fab' conjugated micelles - Tumor was induced in BALB/c mice with injecting BxPC3 subcutaneously. Fab' conjugated micelles enhanced targeting ability of micelles *in vivo* compared to untargeted ones while both micelles showed similar accumulation in tumor tissue.	(Ahn et al., 2015)
Core-crosslinkable (photocrosslinking) micelles of genetically encoded resilin-/elastin-like diblock polypeptides	None	- To obtain targeted core-crosslinkable micelles under critical micelle concentration (CMC) to enhance micelle stability and to target αvβ3 integrin and DR5 receptors that are commonly upregulated in many solid tumors)	- Core-crosslinking increased the stability of micelles that were incubated with guanidinium hydrochloride (GuHCl), a potent chemical denaturant. - Decreased viability of Colo 205 cells and increased cellular uptake by K562 cells at lower concentrations compared to uncrosslinked micelles	(Weber et al., 2021)

Table 1.2. Clinical trials on polymeric micelles (*Clinical Trials*, 2022).

Clinical Trial Status	Clinical Study Title	Condition or Disease	Polymer or Formulation Name	Drugs or Agents
Phase 1	Study of NC-6004 in Combination With 5-FU and Cetuximab in Patients with Head and Neck Cancer	Head and Neck Neoplasms	NC-6004 (PEG-b-poly(glutamic acid) micelles)	Cisplatin 5-Fluorouracil Cetuximab
Phase 1	A Study to Evaluate the Safety and Pharmacokinetics of RadProtect® in Healthy Volunteers	Acute Radiation Syndrome	RadProtect® (ferrous iron containing PEG-b-poly(glutamic acid) micelles)	Amifostine
Phase 1 and Phase 2	Safety and Efficacy of an Antioxidant-rich Multivitamin Supplement in Cystic Fibrosis	Cystic Fibrosis	AquADEK (micelle formulation for oral administration)	Vitamin supplement
Phase 2	A Trial of Paclitaxel (Genexol®) and Cisplatin Versus Paclitaxel Loaded Polymeric Micelle (Genexol-PM®) and Cisplatin in Advanced Non-Small Cell Lung Cancer	Advanced Non-Small Cell Lung Cancer	Genexol-PM (Cremophor EL (polyoxyethylenated castor oil))	Paclitaxel Cisplatin

Table 1.2 (cont'd). Clinical trials on polymeric micelles (Clinical Trials, 2022).

Clinical Trial Status	Clinical Study Title	Condition or Disease	Polymer or Formulation Name	Drugs or Agents
Phase 2	A Study to Evaluate ONM-100, an Intraoperative Fluorescence Imaging Agent for the Detection of Cancer	- Breast Cancer - Head and Neck Squamous Cell Carcinoma - Colorectal Cancer - Prostate Cancer - Ovarian Cancer - Urothelial Carcinoma - Non-small Cell Lung Cancer	ONM-100 (a polymer micelle covalently conjugated to indocyanine green)	Indocyanine green
Phase 2	Dose-Finding Study of SC411 in Children with Sickle Cell Disease	Sickle Cell Disease	SC411 (DHA ethyl ester formulation)	Docosahexaenoic Acid
Phase 3	Paclitaxel Micelles for Injection / Paclitaxel Injection in Combination with Cisplatin for First-line Therapy of Advanced NSCLC	Advanced Non-Small-Cell Lung Cancer	Cremophor EL	Paclitaxel Cisplatin

Table 1.2 (cont'd). Clinical trials on polymeric micelles (Clinical Trials, 2022).

Clinical Trial Status	Clinical Study Title	Condition or Disease	Polymer or Formulation Name	Drugs or Agents
Phase 3	A Phase III Study of NK105 in Patients With Breast Cancer	Breast Cancer Nos Metastatic Recurrent	NK105 (PEG-polyaspartate micelles)	Paclitaxel
Phase 4	A Clinical Trial of Paclitaxel Loaded Polymeric Micelle in Patients with Taxane-Pretreated Recurrent Breast Cancer	Recurrent Breast Cancer	Genexol-PM	Paclitaxel

1.4.1.2 Polymeric Micelle Stability

Polymeric micelles used in cancer treatment applications should be biocompatible and stable. Stability of polymeric micelles is an important issue since they will expose to some force, like blood circulation shear forces, after injection to body. The micelles should protect their shape, size as well as the drug that they carry. During blood circulation, they should withstand dissociation and premature drug release until they reach to the tumor tissue. The stability of micelles can be determine via size distribution measurements, zeta potential measurements, morphology examination with either TEM or SEM, drug release studies under physiological and acidic (tumor tissue) conditions, etc.

Some factors affect the stability of micelles like hydrophobicity and hydrophilicity of polymers, hydrophobic chain length, crystallinity of hydrophobic chain, micelle preparation method, etc. Hydrophobic chain should be long enough to have a stable micelle formation. Studies showed that increasing hydrophobic chain length results in larger core size, which means higher drug loading capacity and lower polydispersity index (PDI). However, there must be a balance between hydrophilic chain length and hydrophobic chain length. The molecular weight of copolymers should not exceed 42-50 kDa to escape from renal clearance. Increase in molecular weight also results in higher micelle size and lower micelle stability. When polymers form micelles, some hydrophobic and hydrophilic interactions occur between polymer chains. If polymer chain is too long, these interactions weaken. Thus, micelle stability decreases. (Hussein & Youssry, 2018).

Hydrophobicity of hydrophobic block of the copolymer affects the stability of micelles. Increasing hydrophobicity results in increased stability. Studies showed that when PCL and poly(L-lactic acid) (PLLA) had the same molecular weight, PCL enhanced thermodynamic stability and decreased drug release rate compared to PLLA due to more hydrophobic nature of PCL (Hussein & Youssry, 2018).

Crystallinity of the hydrophobic chain affects the stability of micelles. Core fluidity increases above glass transition temperature (Tg) of hydrophobic chain and increasing core fluidity results in lower stability. Semi-crystalline nature of PCL may result in enhanced kinetic stability (Hussein & Youssry, 2018).

Drug-core interactions also affect the stability of micelles. Mikhail and Allen (2010) showed that conjugation and loading cause different effects. Docetaxel conjugated PEG-b-PCL micelles had higher stability, more uniform and spheroid shape than that of docetaxel loaded PEG-b-PCL micelles (Mikhail & Allen, 2010). The interaction of polymer and drug can be interpreted with a dimensionless energy parameter called Flory-Huggins interaction parameter (χ). Lower χ results in higher compatibility between the drug and hydrophobic core, thus leading to enhanced solubilization, as well as slower drug release (Hussein & Youssry, 2018).

Micelle preparation method also influences the polymeric micelle stability. There are different micelle preparation methods such as dialysis, emulsion-diffusion, solvent evaporation, co-solvent evaporation, etc. Studies showed that dialysis method results in larger and disperse particles while co-solvent evaporation method produces smaller and more uniform particles (Owen et al., 2012).

Miscibility of aqueous phase and organic phase also changes the polymeric micelle stability. Aliabadi et al. (2007) prepared mPEG-b-PCL micelles with tetrahydrofuran (THF), acetone and acetonitrile. They reported that THF caused larger particles (109 nm) while acetone and acetonitrile produced smaller particles (88 nm and 83 nm, respectively) with a lower PDI (0.504 for THF, 0.111 for acetone, and 0.104 for acetonitrile). Micelles prepared with THF also showed a second peak around 440 nm which results in higher PDI. Aliabadi et al. (2007) also studied the effect of organic: aqueous phase ratio on micelle size. Acetone was used as organic phase and organic: aqueous phase ratios were 1:2 and 1:6. Results showed that lower acetone:water ratios produced smaller particles (88 nm for 1:2 ratio and 63 nm for 1:6 ratio) (Aliabadi et al., 2007).

1.5 Immunomicelles

There are some active targeting strategies in drug delivery systems. In active targeting, antibodies, small molecules like folic acid, peptides like RGD peptide, some fragments of antibodies especially Fab' fragment can be used. Polymeric micelles, which carry an antibody or antibody fragment can easily recognize the receptors of the targeted cancer cells and specifically bound them. This type of micelles are called as immunomicelles.

Trastuzumab is an antibody against HER2 receptor on HER2 positive breast cancer cells and there are many drug delivery systems that are being studied which carry trastuzumab as a targeting agent. Bolu et al. (2020) prepared docetaxel loaded trastuzumab conjugated PEG-4 bis-MPA polyester dendron micelles. Trastuzumab was conjugated to PEG part of the micelles by EDC/NHS chemistry. They showed the higher cellular uptake of targeted micelles compared to untargeted micelles on MCF7 and SK-OV-3 cell lines, which are both HER2 positive cell lines. They also showed that micelles were located in cell periphery by using fluorophore conjugated antibody conjugated micelles (Bolu et al., 2020). Leach et al. (2020) prepared nanoparticles from maleimide functionalized PEG-PLGA and conjugated anti-delta-like ligand 4 (anti-DLL4) variable new antigen receptor (VNAR) with maleimide-cysteine chemistry. VNARs were discovered in sharks. They are immunoglobulin-based proteins and smaller than antibodies in size and show better thermostability than antibodies. Therefore, they are investigated for diagnostic and therapeutic applications. Anti-DLL4 VNAR conjugated nanoparticles showed higher cell internalization in pancreatic cancer cell lines and human umbilical vein endothelial cells (HUVECs) compared to untargeted nanoparticles. Anti-DLL4 VNAR conjugated nanoparticles also inhibited angiogenesis *in vitro* (Leach et al., 2020).

Click chemistry is a very simple and effective way for the conjugation of two molecules to each other. It is being widely used to modify organic molecules due to high yield and high selectivity in bioconjugation, drug discovery, materials science, and radiochemistry. Click reactions are bio-orthogonal, functional groups of

reactants and products do not interact with functionalized biomolecules. Click reactions are chosen due to mild conditions that reaction take place (such as room temperature, in water, etc.). They are also insensitive towards oxygen, and forms stereospecific products. In general, the conjugate can easily be purified, it is highly pure with high yield, and has almost no side products (Nwe & Brechbiel, 2009).

Click chemistry can be applied to cycloaddition reactions (such as the 1,3-dipolar family, and hetero Diels-Alder reactions), nucleophilic ring-opening reactions (e.g., epoxides, aziridines, cyclic sulfates, and so forth), carbonyl chemistry reactions (such as the formation of oxime ethers, hydrazones, and aromatic heterocycles), and addition reactions of carbon-carbon multiple bonds (such as epoxidation and dihydroxylation and azide-phosphine coupling; and Staudinger ligation) (Nwe & Brechbiel, 2009).

In our study, click chemistry was used to conjugate antibody (anti-CD73) by maleimide-cysteine reaction to the synthesized maleimide functionalized PEG-b-PCL polymer. Maleimide-cysteine click chemistry have been used by many scientists to create antibody-drug conjugates (Ravasco et al., 2019; van Leeuwen et al., 2017). In our case, maleimide functionalized PEG-b-PCL was synthesized to conjugate the antibody (anti-CD73) to PEG-b-PCL micelles through cysteine residue of the antibody to target the cancer drugs to the cancer cells.

1.6 Aim of the Study

The aim of the thesis was to develop PEG-b-PCL (poly(ethylene glycol)-block-polycaprolactone) micelles to carry bioactive agents to the cancer cells. In this study; controlled delivery of DOX and LCA from the prepared passively targeted micelles which will provide pH responsive release was aimed. It was aimed to have of DOX and LCA at the tumor area, so less side effects would occur in the body.

PEG-b-PCL was chosen as the copolymer due to its biocompatibility. DOX was one of the anticancer agents used due to its highly effective anticancer activity.

Additionally, LCA was the second anticancer agent used which is a possible effective anticancer agent.

In accordance with this purpose, mPEG-b-PCL copolymer was synthesized and characterized. DOX was added into the micelles either by covalent conjugation via pH sensitive hydrazone bond (DOX_{conj}-M) or by loading into PEG-b-PCL micelles (DOX_{ld}-M). Meantime, LCA was conjugated to the copolymer via ionic bonds with electrostatic interactions at two different temperatures as 60°C and 25°C and micelles were prepared (LCA_{60}**M and LCA_{25}**M, respectively; stars (**) define the ionic conjugation of the drugs). DOX_{conj}-M and DOX_{ld}-M as well as LCA_{60}**M and LCA_{25}**M were prepared to examine the effects of preparation parameters on the cytotoxicity of the micelles. The combinational effect of DOX_{conj}-M and LCA_{60}**M on the breast cancer cells was investigated using different amounts of micelles loaded with DOX and LCA. Also, micelles having both, DOX and LCA (loaded at 25°C) micelles were prepared (DL-M) to examine the cytotoxic effect of both drugs together. Apoptotic effects of the micelles on MDA-MB-231 cancer cells were determined and compared.

CHAPTER 2

MATERIALS AND METHODS

2.1 Materials

Adriamycin (trade name of DOX) was purchased from Deva Holding (Turkey) as lyophilized powder of 10 mg of Doxorubicin hydrochloride in injection vials. ε-caprolactone (ε-CL) was purchased from Acros Organics, USA. Lithocholic acid (LCA), methoxy poly(ethylene glycol) (mPEG) (Mn=5000 Da), tin(II) 2-ethylhexanoate, succinic anhydride, dimethylaminopyridine, dicyclohexylcarbodiimide, N-hydroxysuccinimide, hydrazine hydrate, glycine, sodium bicarbonate, trinitrobenzene sulfonic acid (TNBSA), polyvinyl alcohol, 3-(4,5-dimethylthiazol-2-yl)-2,5-diphenyltetrazolium bromide (MTT), coumarin 6, dimethylsulfoxide (DMSO), paraformaldehyde, crystal violet, and oil red O were the products of Sigma-Aldrich, Germany. Tetrahydrofuran, diethyl ether, methanol, trifluoroacetic acid, concentrated sulfuric acid, acetone, and ethanol were purchased from Merck, Germany. Leibovitz's L-15 medium, RPMI-1640, DMEM, fetal bovine serum (FBS), gentamicin, penicillin-streptomycin were the products of Biological Industries, Israel. MDA-MB-231 cells and A549 cells were taken from Ege University Bioengineering Department.

2.2 Methods

In the study, the first step was the synthesis and characterization of the polymers used for the production of micelles. Then DOX and LCA were conjugated to the polymers and micelles were prepared. The properties of the micelles and their efficacies on cancer cells were determined. Micelles without any drug addition,

formed from copolymer mPEG-b-PCL-CO-NH-NH_2 (M); micelles having DOX either covalently conjugated or loaded (DOX_{conj}-M and DOX_{ld}-M, respectively), micelles having ionically conjugated LCA at 60ºC (LCA_{60}**M) and at 25ºC (LCA_{25}**M), as well as micelles having both DOX and LCA (DL-M) were prepared. LCA and/or DOX release under normal (pH 7.4) and acidic (pH 6.8 and pH 5.5) conditions from LCA_{60}**M, LCA_{25}**M, DOX_{conj}-M, DOX_{ld}-M, and DL-M were studied.

In order to show the anticancer effect of LCA and DOX, the half-maximal inhibitory concentration (IC_{50}) of free drugs was investigated on triple negative breast cancer cells (MDA-MB-231), non-small cell lung cancer cells (A549) and melanoma cells (SK-MEL-30).

In vitro cytotoxic effect of micelles was investigated on MDA-MB-231 cells with MTT assay. Cell internalization of LCA_{60}**M and LCA_{25}**M were studied with coumarin 6 loaded samples. For cell internalization experiments of DOX containing micelles, coumarin 6 could not be used since DOX has fluorescence properties.

Cell migration assay and colony formation assay of MDA-MB-231 cells were conducted with LCA_{60}**M, LCA_{25}**M, DOX_{conj}-M, DOX_{ld}-M, and DL-M micelles. For all these micelles, lipid droplet formation, qRT-PCR analysis for apoptotic and anti-apoptotic genes, cell apoptosis in MDA-MB-231 cells were also determined.

For LCA_{60}**M, LCA_{25}**M, DOX_{conj}-M, DOX_{ld}-M, and DL-M micelles, the loss of mitochondrial transmembrane potential in MDA-MB-231 cells after the treatment of cells with micelles was analyzed with a fluorescent probe (DiOC6). For these micelles, also ROS generation in MDA-MB-231 cells after treatment was investigated. The effects of the same micelles on endothelial cell tube formation of HUVECs was also studied. Co-cultures of HUVECs and MDA-MB-231 cells were used to investigate the effect of cancer cells on endothelial cell tube formation with or without LCA_{60}**M, LCA_{25}**M, DOX_{conj}-M, DOX_{ld}-M, and DL-M. The studies, carried out during this theses content, are schematically shown in Figure 2.1. The details of the applied methodologies are given in the following sections.

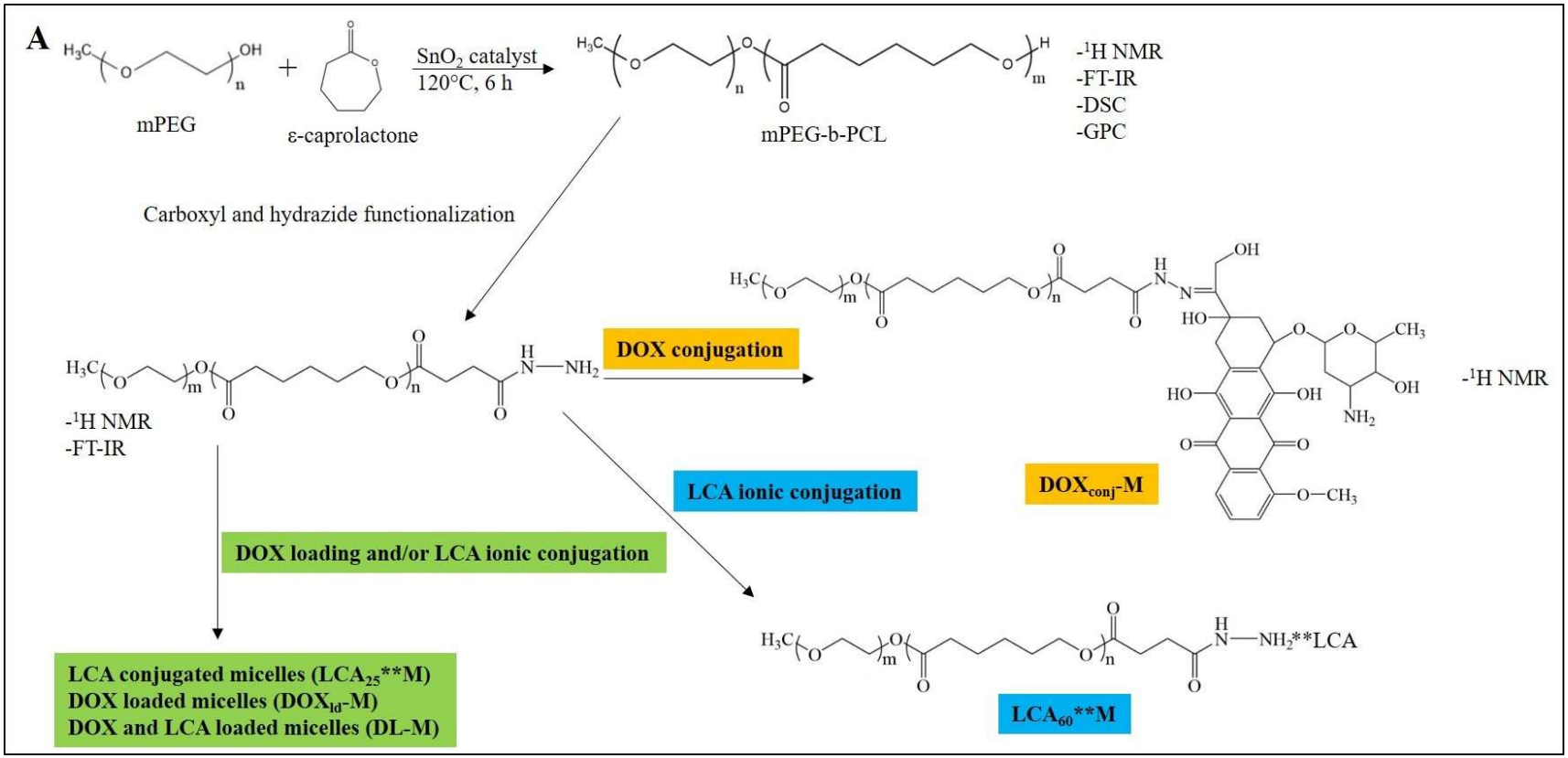

Figure 2.1. Schematic representation of studies carried out. A) Polymer synthesis.

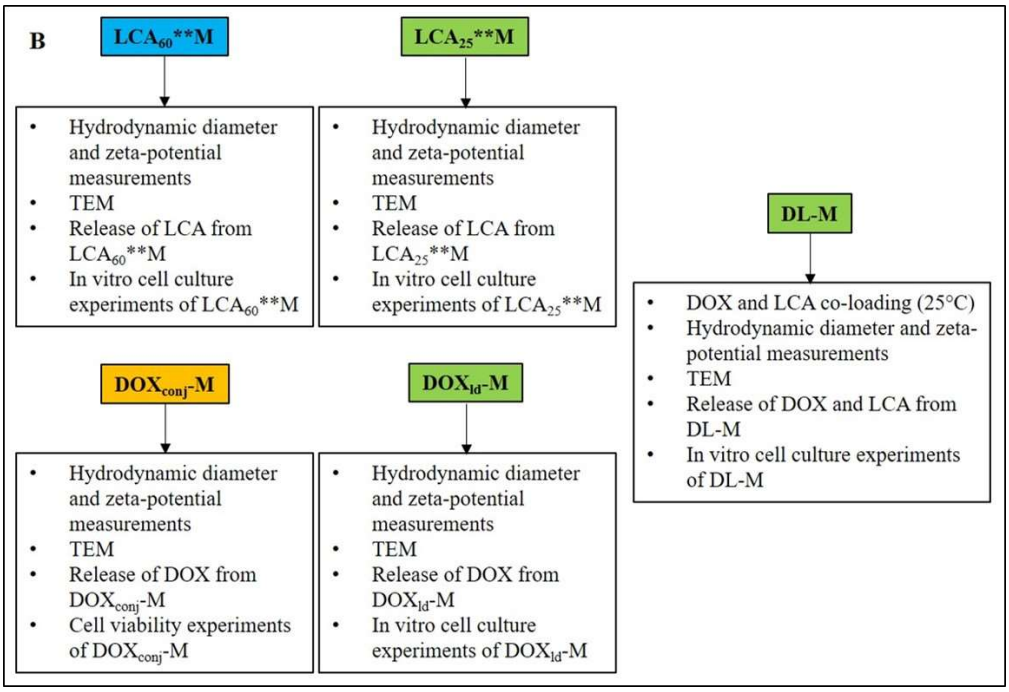

Figure 2.1 (cont'd). B) Micelles prepared.

2.2.1 Synthesis and Characterization of mPEG-b-PCL Copolymer

mPEG-b-PCL copolymer was synthesized by ring opening polymerization (Isik et al., 2020; Shuai et al., 2003). Firstly, ε-caprolactone was purified by vacuum distillation over CaH_2. mPEG (Mn = 5000 Da) was dried under vacuum at 105°C for 90 minutes. Predetermined amounts of ε-caprolactone were added into a 3-necked flask containing mPEG and tin(II)-2-ethylhexanoate (0.1% of ε-caprolactone in molar amount). The flask was then filled with argon gas, sealed, and stored in an oil bath at 120°C for 6 hours. After 6 hours, the product was dissolved in dichloromethane, precipitated in cold ethanol, and then dried under vacuum at 40°C. ^{1}H-NMR spectra of the copolymer were recorded on a Bruker Avance 400 DPX (USA) instrument at 400 MHz using deuterated chloroform. FT-IR spectra of the copolymer were recorded on a Perkin Elmer Spectrum 65 (Perkin Elmer Inc., USA) instrument. Diblock copolymer was thermally characterized at a heating rate of

10°C/min by using DSC (Scinco DSC N-650, Seoul, Korea). The number average molecular weight (Mn) of diblock copolymer was calculated by comparing integrals of characteristic peaks of the PCL block at 3.99 ppm (triplet) and mPEG block at 3.58 ppm (triplet) in the ^{1}H NMR spectra, by using the formulas given below (M. H. Huang et al., 2003, 2004). 44 is the molecular weight of the repeating unit of mPEG.

$$Degree\ of\ polymerization\ (DP)\ of\ mPEG = \frac{Mn\ of\ mPEG}{44}$$

$$DP\ of\ PCL = (DP\ of\ mPEG) \times \frac{Integral\ of\ peak\ at\ 3.99\ ppm\ (PCL\ block)}{Integral\ of\ peak\ at\ 3.58\ ppm\ (mPEG\ block)}$$

$$Mn\ of\ copolymer\ (Mn) = (Mn\ of\ mPEG)\ + 114\ \times (DP\ of\ PCL)$$

The weight average molecular weight (Mw) and the number average molecular weight (Mn) of diblock copolymer were also determined by GPC measurements. The polydispersity index of the copolymer was calculated according to the following formula (Bansal et al., 2015).

$$Polydispersity\ index\ (PI) = \frac{Weight\ average\ molecular\ weight\ (Mw)}{Number\ average\ molecular\ weight\ (Mn)}$$

2.2.2 Preparation of Micelles

Micelles were prepared either by emulsion-diffusion method or by solvent evaporation method using either distilled water or polyvinyl alcohol.

2.2.2.1 Emulsion-Diffusion Method

In the preparation of micelles, 50 mg of mPEG-b-PCL copolymer was dissolved in 5 mL of acetone and added dropwise into 50 mL of distilled water (Jette et al., 2004). The suspension was stirred for 6 hours at 200 rpm to form micelles, and then, water and acetone were evaporated under vacuum with a rotary evaporator. 25 mL of distilled water was added to the concentrated micelle suspension and passed through a 0.22 µm syringe filter. The hydrodynamic diameter and zeta potential of these

micelles (having no drugs) were determined using a Malvern Zetasizer Nano ZS (Malvern Instruments Ltd., MA). Transmission electron microscopy (TEM) was used to examine morphology of the micelles.

2.2.2.2 Solvent Evaporation Method

In the preparation of micelles, solvent evaporation method was used either with distilled water or using polyvinyl alcohol. These are described in the following sections.

2.2.2.2.1 Solvent Evaporation Method with Distilled Water

In the preparation of micelles, 10 mg of mPEG-b-PCL copolymer was dissolved in 2 mL of dichloromethane and added into 20 mL of distilled water under vigorous ultrasonication for 5 min (Han et al., 2011). Then, micelle suspension was mixed at 1000 rpm for 1 hour and at 200 rpm overnight to allow slow evaporation of dichloromethane and formation of the micelles. Micelles were collected by centrifugation at 14,000 rpm for 20 min at 4°C. Then, micelles were suspended with 5 mL of distilled water and passed through a 0.22 µm syringe filter. The hydrodynamic diameter and zeta potential of empty micelles were determined using a Malvern Zetasizer Nano ZS (Malvern Instruments Ltd., MA). Transmission electron microscopy (TEM) was used to examine morphology of the micelles.

2.2.2.2.2 Solvent Evaporation Method with Polyvinyl Alcohol

In the preparation of micelles, 10 mg of mPEG-b-PCL copolymer was dissolved in 2 mL of dichloromethane and added into 20 mL of 1% polyvinyl alcohol solution under vigorous ultrasonication for 5 min (Şengel Türk et al., 2009). Then, micelle suspension was mixed at 1000 rpm for 1 hour and at 200 rpm overnight to allow slow evaporation of dichloromethane and formation of the micelles. Micelles were

collected by centrifugation at 14,000 rpm for 20 min at 4°C. Then, micelles were suspended with 5 mL of distilled water and passed through a 0.22 µm syringe filter. The hydrodynamic diameter and zeta potential of these micelles (M) (having no drugs) were determined using a Malvern Zetasizer Nano ZS (Malvern Instruments Ltd., MA). Transmission electron microscopy (TEM) was used to examine morphology of the micelles.

2.2.3 Activation of mPEG-b-PCL Copolymer to Conjugate DOX

In order to conjugate DOX to the polymer via hydrazone bond, the synthesized polymer was activated chemically in two steps as described below. In the first step carboxyl group and then hydrazide group were added and the obtained polymer was characterized as described below.

In order to add carboxyl groups to polymer and produce mPEG-b-PCL-COOH polymer, mPEG-b-PCL, succinic anhydride and dimethylaminopyridine were dissolved (1:2:0.5 molar ratio) in tetrahydrofuran (50 mL) in a three-neck flask and reacted under N_2 atmosphere for 24 hours at 30°C (Isik et al., 2021; Lale et al., 2015). The carboxylated product (mPEG-b-PCL-COOH) was precipitated in cold diethyl ether, dried under vacuum. The obtained polymer was examined by ^{1}H-NMR (by Bruker Avance 400 DPX (USA) working at 400 MHz and using deuterated chloroform), and by Fourier Transform Infrared (FT-IR) (Perkin Elmer Spectrum 65, Perkin Elmer Inc., USA) analyses.

In order to add hydrazide groups to carboxylated polymer and produce of mPEG-b-PCL-CO-NH-NH_2, mPEG-b-PCL-COOH, dicyclohexylcarbodiimide and NHS were dissolved (1:1:1 molar ratio) in tetrahydrofuran (50 mL) and reacted under N_2 atmosphere for 24 hours at 30°C (Isik et al., 2021; Lale et al., 2015). Hydrazine hydrate was then added to this mixture and the reaction was continued for 12 hours. The product (mPEG-b-PCL-CO-NH-NH_2) was filtered, precipitated in cold diethyl

ether, and the precipitate was dried under vacuum. FT-IR spectrum was recorded (by Perkin Elmer Spectrum 65, Perkin Elmer Inc., USA).

For colorimetric detection of primary amine groups attached to the copolymer, TNBSA method was used (Isik et al., 2021). 5% TNBSA was diluted 500-fold with 0.1 M sodium bicarbonate buffer. 1 mg/mL mPEG-b-PCL-CO-NH-NH_2 was suspended in 0.1 M sodium bicarbonate buffer and 1 part of TNBSA was mixed with 2 parts of mPEG-b-PCL-CO-NH-NH_2 suspension. The solutions were incubated at 37°C for 2 hours and absorbances were measured at 335 nm using a plate reader (SpectraMax iD3, Molecular Devices, USA). The amount of primary amine was determined using the calibration curve constructed with different concentrations of glycine solutions (4 – 20 µg/mL which is equal to 0.53×10^{-7} – 27×10^{-7} mol amine/mL) prepared in sodium bicarbonate buffer (0.1 M, pH 8.5; Appendix A1 Figure 1).

2.2.3.1 Conjugation of DOX to Activated mPEG-b-PCL Copolymer

For conjugation of DOX to hydrazone group, two different methods were used as given below:

DMSO method: mPEG-b-PCL-CO-NH-NH_2 copolymer and DOX were dissolved (1:1 molar ratio) in DMSO (50 mL) and kept in dark, for 72 hours, under N_2 gas, at 30°C for reaction (Isik et al., 2021; Lale et al., 2015). The product was purified by dialysis (MWCO 3500, Spectrum Laboratories, USA) against deionized water at room temperature for 3 days by changing the water in every 6 hours. DOX conjugated mPEG-b-PLC-CO-NH-NH_2 was obtained after lyophilization. The yield of the synthesis was determined with the equation below;

$$The\ yield\ (\%) = \frac{Total\ amount\ of\ DOX\ conjugated\ polymer}{The\ sum\ of\ DOX\ and\ the\ polymer\ used\ for\ the\ synthesis} \times 100$$

MeOH-TFA method: mPEG-b-PCL-CO-NH-NH_2 copolymer and DOX were dissolved (1:1 molar ratio) in methanol (15 mL), a drop of TFA was added, left

overnight at 60°C (Isik et al., 2021; F. Wang et al., 2011). After the removal of methanol under vacuum, the residue was suspended in water and dialyzed (MWCO 3500, Spectrum Laboratories, USA) against deionized water at room temperature for 3 days by changing the water in every 6 hours. DOX conjugated mPEG-b-PLC-CO-NH-NH_2 was obtained after lyophilization. The yield of the synthesis was determined using the equation given above.

2.2.3.1.1 Determination of Conjugated DOX Content of the Copolymer

Conjugation of DOX to the copolymer was characterized by ^{1}H-NMR (by Bruker Avance 400 DPX (USA) analyses working at 400 MHz and using deuterated DMSO). Meanwhile, DOX conjugation efficiency was determined by using the following two methods:

Dissolution of the drug-polymer conjugate (Ch:MeOH (1:1) Method): DOX (10 mg) was dissolved in chloroform:methanol (Ch:MeOH; 1:1, v/v) and a calibration curve was constructed (1 - 70 µg DOX / mL; Appendix B1 Figure 1) by measuring absorbances at 440 nm with UV-visible spectrophotometer (Isik et al., 2021). 10 mg of pristine mPEG-b-PCL-CO-NH-NH_2 copolymer (as blank solution) and/or 10 mg of DOX conjugated copolymer were dissolved in 1 mL of Ch:MeOH (1:1, v/v). DOX content of the DOX-copolymer conjugate was calculated by using the following equation;

$$Conjugated\ drug\ content\ (\mu g\ /\ mg\ polymer) = \frac{(Abs\ of\ DOX\ conj\ poly - Abs\ poly)\ /\ X}{10}$$

where; *Abs of DOX conj poly* = Absorbance of DOX conjugated copolymer,

Abs poly = Absorbance of pristine copolymer.

X = The slope of the calibration curve, which is 0.014 for Ch:MeOH

10 = Dilution factor (the samples were diluted 10 times before the measurements).

Drug conjugation efficiencies of the copolymer was calculated with the equation given below;

$$Conjugation\ efficiency = \frac{Total\ conjugated\ DOX\ to\ the\ polymer}{DOX\ content\ used\ for\ the\ synthesis} \times 100$$

Breaking the pH sensitive bond in acidic media: For this method, three different media (HCl (0.1 M), concentrated HCl (12 M) and concentrated H_2SO_4 (18.3 M)) were used to determine the conjugated DOX content (Isik et al., 2021). HCl (0.1 M) was used to compare the results with literature (Lale et al., 2015). For each media, the wavelength having maximum absorbance values was determined, and the calibration curves were prepared accordingly (Appendix C1 Figure 1, Appendix D1 Figure 1, and Appendix E1 Figure 1). Pristine copolymer (10 mg) having no drug was also dissolved in the mentioned media and used as blank solution (in order to eliminate any effect caused by the polymer). DOX-polymer conjugates (10 mg) were dissolved in the solutions, and the amount of the conjugated drug content on the copolymer was determined spectroscopically by using the following equation;

$$Conjugated\ drug\ content\ (\mu g\ /\ mg\ polymer) = \frac{(Abs\ of\ DOX\ conj\ poly - Abs\ poly)\ /\ X}{10}$$

where; *Abs of DOX conj poly* = Absorbance of DOX conjugated copolymer,

Abs poly = Absorbance of pristine copolymer.

X = The slope of the calibration curves, which are 0.0211, 0.02 and 0.0415 for HCl (0.1 M), HCl (12 M) and H_2SO_4, respectively.

10 = Dilution factor (the samples were diluted 10 times before the measurements).

Conjugation efficiencies of the copolymer was calculated with using the equation given below;

$$Conjugation\ efficiency = \frac{Total\ conjugated\ DOX\ to\ the\ polymer}{Total\ DOX\ content\ used\ for\ the\ synthesis} \times 100$$

The procedures are given below;

HCl (0.1 M and 12 M) method: DOX (10 mg) was dissolved in 0.1 M HCl or 12 M HCl, separately (Isik et al., 2021). Wavelengths where the maximum absorption was observed (λ-max) were determined as 480 nm for 0.1 M HCl and at 504 nm for 12 M HCl media. Calibration curves were constructed (using concentrations as 1 - 50 µg DOX/mL for 0.1 M HCl, and 1 - 55 µg DOX/mL for 12 M HCl) by measuring absorbances with UV-visible spectrophotometer at determined λ-max wavelength (Appendix C1 Figure 1 and Appendix D1 Figure 1, respectively) (Lale et al., 2015). Similarly, 10 mg DOX conjugated copolymer was suspended in 5 mL of 0.1 M HCl or in 12 M HCl, separately, and probe sonication was applied with 10% amplitude for 5 min. Solutions were kept at 37°C for 48 hours to break the hydrazone bonds of DOX conjugation. Then, copolymers were separated by centrifugation (14000 rpm for 10 min), and the absorbances of the supernatant at 480 nm for 0.1 M HCl and at 504 nm for 12 M HCl were measured by UV-visible spectrophotometer. As blank solution, 10 mg pristine copolymer prepared in the same way in 0.1 M HCl or 12 M HCl was used. The amount of the DOX in the supernatant was calculated from the formula given above.

H_2SO_4 (18.3 M) method: DOX was dissolved in concentrated (18.3 M) sulfuric acid (Isik et al., 2021). A calibration curve was constructed with different concentrations of the DOX (1 - 40 µg/mL) by measuring absorbances at 543 nm with a UV-visible spectrophotometer (Appendix E1 Figure 1). 1 mg of DOX conjugated mPEG-b-PCL-CO-NH-NH_2 was dissolved in 1 mL of concentrated sulfuric acid. The same amount of pristine copolymer dissolved in 1 mL of concentrated sulfuric acid was used as blank solution and the conjugated DOX content was calculated from the formula given above.

2.2.3.2 Addition of LCA to Activated mPEG-b-PCL Copolymers and Characterization Studies

Addition of LCA to mPEG-b-PCL-CO-NH-NH_2 polymer was carried out in two methods: In the first method, exactly similar conditions used for DOX conjugation

were applied. The copolymer mPEG-b-PCL-CO-NH-NH_2 (2.2 g), LCA (50 mg) and a drop of trifluoroacetic acid were added into methanol (75 mL) and mixed overnight at 60°C. NH_2 groups of the copolymer and the acid groups of LCA form salt and stay together by electrostatic interactions. After the removal of methanol under vacuum, the salt residue was suspended in water and dialyzed against water for 3 days at room temperature within a dialysis tubing (MWCO 3500 Da, Spectrum Laboratories, USA). The remaining solution was lyophilized, and the product (mPEG-b-PCL-CO-NH-NH_2**LCA mixture) was obtained. In the second method, the similar steps were carried out except the reaction was carried out at room temperature. LCA existence was confirmed by ^{1}H-NMR (by Bruker Avance 400 DPX (USA) working at 400 MHz, using deuterated DMSO). Amount of LCA was determined by using a calibration curve constructed by dissolving different concentrations of free LCA in concentrated sulfuric acid (1 – 100 µg/mL which is equal to 2.65 µM – 265 µM; Appendix F1 Figure 1) and measuring absorbances at 311 nm with a UV-visible spectrophotometer (Hitachi U-2800A, Hitachi Ltd., Japan). Concentrated sulfuric acid was chosen since it can dissolve both mPEG-b-PCL-CO-NH-NH_2 and LCA. As reference group, mPEG-b-PCL-CO-NH-NH_2 copolymer (which does not have LCA) was dissolved in concentrated sulfuric acid and used as reference.

2.2.4 Critical Micelle Concentration of mPEG-b-PCL Copolymers, mPEG-b-PCL-CO-NH-NH_2 Copolymers and DOX Conjugated Copolymers

Critical Micelle Concentrations (CMC) of mPEG-b-PCL copolymers, mPEG-b-PCL-CO-NH-NH_2 copolymers, and DOX conjugated copolymers were determined using a pyrene fluorescent probe. For this purpose, 20 mg of each polymer was dissolved in 5 mL of tetrahydrofuran, then 40 mL of deionized water was added, and the solution was left in fume hood for evaporation of tetrahydrofuran. Dilutions were made to prepare different concentrations of pyrene solution in 0.6 mM acetone ($0.5x10^{-3}$ – 0.5 g/L). Then, 10 µL of pyrene solution prepared was added to 1 mL of

polymer solutions and the solutions were kept in an incubator overnight. The excitation spectra were scanned from 250 to 360 nm at a fixed emission wavelength of 390 nm with bandwidth 1 nm using a microplate reader. Intensity ratio at 338 and 333 nm (I_{338}/I_{333}) were measured and plotted against the logarithm of polymer concentrations. CMC was calculated from the intersection of the two tangent plots (Mohanty et al., 2015).

2.2.5 Optimization of LCA Ionically Conjugated (LCA_{60}**M) and DOX Conjugated (DOX_{conj}-M) Micelle Preparation

In micelle preparation, co-solvent evaporation method was applied. To optimize the parameters, the method was achieved either with application of sonication or without sonication, as described in the following sections.

2.2.5.1 Co-Solvent Evaporation Method with Sonication

DOX covalent conjugated and LCA ionic conjugated micelles were prepared as follows: mPEG-b-PCL-CO-NH-NH_2**LCA or mPEG-b-PCL-CO-NH-NH_2-DOX polymers (10 mg) were dissolved in 2 mL of THF or acetone, and added into 20 mL of 0.5% (w/v), 0.75% (w/v), 1% (w/v), 1.5% (w/v), or 2% (w/v) polyvinyl alcohol solutions under vigorous ultrasonication for 5 min at room temperature. Then, micelle suspension was mixed at 1000 rpm overnight to allow evaporation of organic solvent and formation of the micelles. Micelles were collected by centrifugation at 14,000 rpm for 20 min at 4°C. For washing, micelles were dispersed in distilled water and centrifuged again. Washing step was repeated twice. Then, micelles were suspended with 5 mL of distilled water and passed through a 0.22 µm syringe filter. The hydrodynamic diameter and zeta potential of LCA loaded micelles or DOX conjugated micelles were determined using a Malvern Zetasizer Nano ZS (Malvern Instruments Ltd., MA).

2.2.5.2 Co-Solvent Evaporation Method without Sonication

Micelles were prepared co-solvent evaporation method (Aliabadi et al., 2007). Briefly, 30 mg of mPEG-b-PCL-CO-NH-NH_2**LCA or mPEG-b-PCL-CO-NH-NH_2-DOX copolymers were dissolved in 0.5 mL of acetone. Then, 3 mL of water, 1% PVA, 1.5% PVA, or 2% PVA was added dropwise to the organic phase under vigorous agitation. Then, micelle suspension was mixed at 1100 rpm for 5 hours to allow evaporation of organic solvent and formation of the micelles. Micelles were collected by centrifugation at 14,000 rpm for 20 min at 4°C. For washing, micelles were dispersed in distilled water and centrifuged again. Washing step was repeated twice. Then, micelles were suspended with 5 mL of distilled water and passed through a 0.22 µm syringe filter.

During the reaction of the mPEG-b-PCL-CO-NH-NH_2 polymer with LCA, LCA did not covalently conjugate to the polymer via hydrazone bond. In the purification step, dialysis was used. Since LCA did not dissolve in water, a salt of the polymer and LCA was obtained due to the electrostatic interaction between –NH_2 group of the polymer and the –COOH group of LCA (mPEG-b-PCL-CO-NH-NH_2**LCA salt) instead of covalent hydrazone bond formation between two chemicals. After freeze-drying of this salt, LCA amount was calculated and then micelles were prepared. The electrostatic interaction can be reconstructed between LCA and the polymer during micelle preparation step.

Since, LCA does not form hydrazone bond, LCA ionically conjugated micelles were also prepared at room temperature to examine whether they show the similar behavior. LCA loaded micelles (LCA_{25}**M) were prepared using mPEG-b-PCL-CO-NH-NH_2 as the polymer to create an electrostatic interaction between –NH_2 of the polymer and –COOH of LCA. Briefly, 3 mg of LCA and 30 mg of mPEG-b-PCL-CO-NH-NH_2 were dissolved in 0.5 mL of acetone. Then, 3 mL of 1% PVA was added dropwise to the organic phase under vigorous agitation. Then, micelle suspension was mixed at 1100 rpm for 5 hours to allow evaporation of organic solvent and formation of the micelles. Micelles were collected by centrifugation at

14,000 rpm for 20 min at 4°C. For washing, micelles were dispersed in distilled water and centrifuged again. Washing step was repeated twice. Then, micelles were suspended with 5 mL of distilled water and passed through a 0.22 µm syringe filter.

Transmission electron microscopy (TEM) was used to examine the physical forms of the prepared micelles. The hydrodynamic diameter and zeta potential of these micelles were measured using a Malvern Zetasizer Nano ZS (Malvern Instruments Ltd., MA). The micelles were freeze-dried (FreeZone 6 Plus, Labconco Corp., USA) for 1 day and stored in dried form for further experiments.

Encapsulation efficiency of LCA containing micelles was calculated using equation below. Amount of LCA was determined by using a calibration curve constructed by dissolving free LCA in concentrated sulfuric acid (1 – 100 µg/mL which is equal to 2.65 µM – 265 µM; Appendix F1 Figure 1) and by measuring absorbances at 311 nm with a UV-visible spectrophotometer (Hitachi U-2800A, Hitachi Ltd., Japan).

$$Encapsulation\ efficiency\ of\ LCA\ (\%) = \frac{(The\ amount\ of\ LCA\ inside\ the\ micelles)}{(The\ initial\ amount\ of\ LCA)} \times 100$$

Drug loading capacities of LCA or DOX containing micelles were calculated using equation below, after dissolving weighted amount of freeze-dried micelles in concentrated sulfuric acid, and by measuring the absorbances at 311 nm for LCA and at 543 nm for DOX with UV-visible spectrophotometer (Hitachi U-2800A, Hitachi Ltd., Japan). LCA and DOX contents were detected using the calibration curves. Micelles of copolymers prepared without any drug (having no LCA nor DOX) were also dissolved in concentrated sulfuric acid and used as background.

$$Drug\ loading\ capacity\ (\%) = \frac{(The\ amount\ of\ drug\ inside\ the\ micelles)}{(The\ amount\ of\ micelles)} \times 100$$

2.2.6 Preparation of DOX and/or LCA Loaded Micelles

After the optimization studies, DOX and/or LCA loaded micelles were prepared using the selected parameters in the section above. For this purpose, 30 mg of mPEG-

b-PCL-CO-NH-NH_2 polymer and 3 mg of DOX and/or 3 mg of LCA were dissolved in 0.5 mL of acetone containing 5 µL of triethylamine. Then, 3 mL of 1% PVA was added dropwise to the organic phase under vigorous agitation. Then, micelle suspension was mixed at 1100 rpm for 5 hours to allow evaporation of organic solvent and formation of the micelles. Micelles were collected by centrifugation at 14,000 rpm for 20 min at 4°C. For washing, micelles were dispersed in distilled water and centrifuged again. Washing step was repeated twice. Then, micelles were suspended with 5 mL of distilled water and passed through a 0.22 µm syringe filter. The micelles were freeze-dried (FreeZone 6 Plus, Labconco Corp., USA) for 1 day and stored in dried form for further experiments.

Encapsulation efficiencies and drug loading capacities of DOX_{ld}-M or DL-M were calculated using equation below, after dissolving weighted amounts of freeze-dried micelles in concentrated sulfuric acid, and by measuring the absorbances at 311 nm for LCA and at 543 nm for DOX with UV-visible spectrophotometer (Hitachi U-2800A, Hitachi Ltd., Japan). LCA contents and DOX contents were detected using the calibration curves. Micelles of copolymers having no LCA or no DOX were also dissolved in concentrated sulfuric acid and used as background.

$$Encapsulation\ efficiency\ (\%) = \frac{(The\ amount\ of\ drug\ inside\ the\ micelles)}{(The\ initial\ amount\ of\ drug\ added)} \times 100$$

$$Drug\ loading\ capacity\ (\%) = \frac{(The\ amount\ of\ drug\ inside\ the\ micelles)}{(The\ amount\ of\ micelles)} \times 100$$

2.2.7 Release Studies

2.2.7.1 Release of LCA from LCA_{60}**M or LCA_{25}**M

Release of LCA from the micelles was studied in three different media having pH values of 7.4, 6.8 and 5.0. For this study, LCA_{60}**M or LCA_{25}**M (10 mg) were suspended in 1 mL of phosphate buffered saline (PBS, 0.1 M and pH 7.4) or 1 mL of citrate-phosphate buffer (CPB, 0.15 M; pH 5.0 or pH 6.8) (n = 6). Free LCA were

dispersed in PBS-7.4, or CPB-5 or CPB-6.8 (1 mg LCA/ mL) was used as the control group. Micelle solutions and free LCA solutions were transferred to a dialysis bag (MWCO is 3500 Da; Spectrum Laboratories, USA), placed in 4 mL of PBS-7.4 or CPB-5 or CPB-6.8 and incubated in a beaker thermostatic shaker (37°C, 80 rpm) (Nüve ST-30, Turkey). At predetermined time intervals 2 mL of the release media was removed and replaced with fresh PBS-7.4 or CPB-5 or CPB-6.8. Drawn samples were freeze-dried, dissolved in ethanol. The absorbance of the samples was measured at 238 nm with a UV-Vis spectrophotometer (Hitachi U-2800A, Hitachi Ltd., Japan). The amount of LCA in the release media was determined using the calibration curve of LCA prepared in ethanol (Appendix G1 Figure 1). To evaluate the release mechanism of LCA from micelles, the data obtained were fitted to zero order (cumulative percent release of LCA versus time plot), first order (log cumulative percent of LCA remaining versus time plot), Higuchi model (cumulative percent of LCA release versus square root of time plot), and Korsmeyer-Peppas (log cumulative percent release of LCA versus log time plot) models.

In zero order release kinetics, the release rate of the drug is constant over a period of time (Costa & Sousa Lobo, 2001).

$Q_t = Q_0 + K_0 t$

where Q_t is the cumulative drug amount released at time t, Q_0 is the initial amount of drug present in the micelles, K_0 is the zero order rate constant and t is the time (Costa & Sousa Lobo, 2001).

In first order release kinetics, the release rate is dependent on the concentration of drug (Costa & Sousa Lobo, 2001).

$Q_t = Q_0 \exp(-K_1 t)$ or $\ln Q_t = \ln Q_0 - K_1 t$

where Q_t is the cumulative drug amount released at time t, Q_0 is the initial amount of drug present in the micelles, K_1 is the first order rate constant and t is the time (Costa & Sousa Lobo, 2001).

In Higuchi model, there are some assumptions;

- Initial drug concentration in the drug delivery system is much higher than the drug solubility.
- Diffusion of drug occurs only in one dimension.
- Drug particles much smaller than system thickness.
- Swelling of matrix and dissolution is negligible.
- In the release environment perfect sink conditions are maintained (Shaikh et al., 2015).

$Q_t = Q_\infty + K_H \sqrt{t}$

where Q_t is the cumulative drug amount released at time t, Q_∞ is the total drug amount that released, K_H is the Higuchi model rate constant and t is the time (Costa & Sousa Lobo, 2001).

In Korsmeyer-Peppas model;

$M_t / M_\infty = K_p t^n$

where M_t / M_∞ is the fraction of drug release at time t, K_p is the Korsmeyer-Peppas model rate constant, t is the time and n is the exponent of release (Costa & Sousa Lobo, 2001).

There are two models that the release profile of an active agent in a system can be fitted depending on the value of n (exponent of release): Fickian (n=0.43) and non-Fickian models (n=0.85). Drug release is governed by diffusion in the Fickian model. In the non-Fickian model, drug release is governed by swelling and relaxation of polymer chains. When $0.43<n<0.85$, release kinetic is through anomalous transport and the drug release mechanism is governed by both diffusion and swelling (Bruschi, 2015).

2.2.7.2 Release of DOX from DOX_{conj}-M or DOX_{ld}-M

Release of DOX from DOX_{conj}-M or DOX_{ld}-M micelles was studied exactly in the same way as applied to LCA micelles. Except, the fluorescence of the samples was

measured using an excitation wavelength of 480 nm and an emission wavelength of 590 nm for DOX release with a microplate reader (SpectraMax iD3, Molecular Devices, USA). The amount of DOX in the release media was determined using the calibration curve of DOX prepared in ethanol (Appendix H1 Figure 1). To evaluate the release mechanism of DOX from micelles, release data were fitted to zero order (cumulative percent release of DOX versus time plot), first order (log cumulative percent of DOX remaining versus time plot), Higuchi model (cumulative percent of DOX release versus square root of time plot), and Korsmeyer-Peppas (log cumulative percent release of DOX versus log time plot) models.

2.2.7.3 Release of LCA and DOX from DL-M

Release of LCA and DOX from micelles were carried out by following the processes explained above. Similarly, release data were fitted to zero order (cumulative percent release of LCA versus time plot), first order (log cumulative percent of LCA or DOX remaining versus time plot), Higuchi model (cumulative percent of LCA or DOX release versus square root of time plot), and Korsmeyer-Peppas (log cumulative percent release of LCA or DOX versus log time plot) models.

2.2.8 *In Vitro* Cell Culture Experiments

In *in vitro* cell culture experiments, three types of cells were used. Namely, MDA-MB-231 Cells, A549 Cells and SK-MEL-30 Cells. MDA-MB-231 cells and A549 cells were kindly supplied by Ege University, Bioengineering Department.

2.2.8.1 Determination of IC_{50} of LCA on MDA-MB-231 Cells, A549 Cells and SK-MEL-30 Cells

Cytotoxic effects of different concentrations of LCA on MDA-MB-231 triple negative breast cancer cells, A549 non-small cell lung cancer cells, and SK-MEL-30

melanoma cells were studied. For this purpose, first MDA-MB-231 cells were cultured in Leibovitz's L-15 medium supplemented with 15% FBS, 0.1% gentamicin and 0.1% penicillin-streptomycin at 37°C in 5% CO_2 atmosphere in CO_2 incubator. A549 cells were cultured in Dulbecco's modified Eagle medium (DMEM) supplemented with 10% fetal bovine serum, 0.1% gentamicin and 0.1% penicillin-streptomycin at 37°C in 5% CO_2 atmosphere in CO_2 incubator. SK-MEL-30 cells were cultured in RPMI-1640 medium supplemented with 10% fetal bovine serum, and 1% penicillin-streptomycin at 37°C in 5% CO_2 atmosphere in CO_2 incubator. Then, cells were seeded in a 96-well plate at a density of 2500 cells/well in 100 µL medium and allowed to adhere overnight. The following day, the media were changed with media that contained different concentrations of LCA (from 0 µM to 210 µM; prepared from 75 mM stock solution of LCA) in 0.4% ethanol and cells were incubated for 48 hours. Thereafter, media were discarded and wells were washed with sterile PBS (0.1 M, pH 7.4). To assess the cell viability MTT solution (100 µL of 0.5 mg/mL) was added to each well. After 4 hours of incubation, solutions in the wells were discarded and the formazan crystals formed inside the cells were solubilized in 100 µL of 10% SDS in 0.01 M HCl overnight. Then, solutions in the wells were transferred to a new 96-well plate and the absorbance was measured at 550 nm using SpectraMax iD3 (Molecular Devices, USA). Cell viability was calculated as percentage of the untreated control containing 0.4% ethanol and the IC_{50} value of LCA was determined by GraphPad Prism 8 (GraphPad Software, USA). The absorbance values obtained by MTT were entered into the program and the program calculated the normalized absorbance values by converting the absorbance values to percentages. The program gave the IC_{50} value from the graph.

Modifications were needed in the MTT method, for the cancer cell lines with low adhesion properties in cell culture studies. After the cells were incubated for 48 hours with different concentrations of LCA, the media were not discarded and 10 µL of 5 mg/mL MTT solution was added to each well. As negative control, cells treated with 0.4% ethanol containing medium were used. After 4 hours of incubation, solutions in the wells were discarded and the formazan crystals were solubilized in 50 µL of

DMSO for 20 min on an orbital shaker. Then, the solutions in the wells were transferred to a new 96-well plate and the absorbance was measured at 570 nm (SpectraMax iD3, Molecular Devices, USA). Cell viability was calculated as the percentage of the negative control, and IC_{50} value was determined with GraphPad Prism 8 (GraphPad Software, USA). Morphology of cells was examined with inverted phase contrast microscope (Nikon Eclipse TS100, Nikon Corp, USA) and photographed.

2.2.8.2 Determination of IC_{50} of DOX on MDA-MB-231 Cells, A549 Cells and SK-MEL-30 Cells

Cytotoxic effects of different concentrations of DOX on MDA-MB-231 triple negative breast cancer cells, A549 non-small cell lung cancer cells, and SK-MEL-30 melanoma cells were studied. For this purpose, first MDA-MB-231 cells were cultured in Leibovitz's L-15 medium supplemented with 15% FBS, 0.1% gentamicin and 0.1% penicillin-streptomycin at 37°C in 5% CO_2 atmosphere in CO_2 incubator. A549 cells were cultured in Dulbecco's modified Eagle medium supplemented with 10% fetal bovine serum, 0.1% gentamicin and 0.1% penicillin-streptomycin at 37°C in 5% CO_2 atmosphere in CO_2 incubator. SK-MEL-30 cells were cultured in RPMI-1640 medium supplemented with 10% fetal bovine serum, and 1% penicillin-streptomycin at 37°C in 5% CO_2 atmosphere in CO_2 incubator. Then, cells were seeded in a 96-well plate at a density of 2500 cells/well in 100 µL medium and allowed to adhere overnight. The following day, the media were changed with media that contained different concentrations of DOX (from 0 µM to 90 µM; prepared from 400 µM stock solution of DOX) in 0.4% water and cells were incubated for 48 hours. Thereafter, 10 µL of 5 mg/mL MTT solution was added to each well. As negative control, cells treated with 0.4% water containing medium were used. After 4 hours of incubation, solutions in the wells were discarded and the formazan crystals formed inside the cells were solubilized in 50 µL of DMSO for 20 min on an orbital shaker. Then, the solutions in the wells were transferred to a new 96-well plate and the

absorbance was measured at 570 nm (SpectraMax iD3, Molecular Devices, USA). Cell viability was calculated as the percentage of the negative control, and IC_{50} value was determined with GraphPad Prism 8 (GraphPad Software, USA).

2.2.8.3 Cytotoxicity Studies of Micelles

Cytotoxic effects of DOX and LCA carrying micelles as well as empty micelles were evaluated using cancer cells, as explained in the following sections.

2.2.8.3.1 Cytotoxicity of Empty Micelles (M), LCA_{60}**M, and LCA_{25}**M

The cytotoxic effect of different concentrations of LCA_{60}**M and empty micelles (M) on the MDA-MB-231 triple negative breast cancer cell line, A549 non-small cell lung cancer cell line and SK-MEL-30 melanoma cell line was investigated in Leibovitz's L-15 medium supplemented with 15% fetal bovine serum, 0.1% gentamicin and 0.1% penicillin-streptomycin for MDA-MB-231, Dulbecco's modified Eagle medium supplemented with 10% fetal bovine serum, 0.1% gentamicin and 0.1% penicillin-streptomycin for A549, and RPMI-1640 medium supplemented with 10% fetal bovine serum, and 1% penicillin-streptomycin for SK-MEL-30 at 37°C in 5% CO_2 atmosphere in carbon dioxide incubator. MDA-MB-231, A549, and SK-MEL-30 cells were seeded in a 96-well plate at a density of 2500 cells/well in 100 µl medium and allowed to adhere overnight. The next day, the media were replaced with the media containing different concentrations of LCA_{60}**M (0.125 mg/mL to 5 mg/mL) and M (0.125 mg/mL to 5 mg/mL), and the cells were incubated with the micelles for 48 hours. Cells not incubated with LCA_{60}**M or M were used as the control and the control was considered as 100% viable when calculating the cell viability. After 48 hours, the media were discarded and 100 µL of MTT solution (0.5 mg/mL) was added to each well to evaluate the cell viability. After 4 hours of incubation, the solutions in the wells were discarded. Formazan crystals inside the cells were dissolved in 50 µL DMSO for 20 min on an

orbital shaker. The solutions in the wells were then transferred to a new 96-well plate and the absorbance was measured at 570 nm using SpectraMax iD3 (Molecular Devices, USA).

As mentioned above, modifications were made to the MTT method for healthier viability measurements. After the cells were incubated for 48 hours with different concentrations of M (0.0125 mg/mL to 3 mg/mL), the media were not discarded and 10 µL of 5 mg/mL MTT solution was added to each well. After 4 hours of incubation, the solutions in the wells were discarded and formazan crystals were dissolved in 50 µL of DMSO for 20 min on an orbital shaker. The solutions in the wells were then transferred to a new 96-well plate and the absorbance was measured at 570 nm using SpectraMax iD3 (Molecular Devices, USA). Cells not incubated with blank micelles were used as the positive control and assumed as 100% viable. Then, cell viability was calculated.

With the MTT method, studies on dose-dependent cytotoxicity of LCA_{60}**M were repeated. After the cells were incubated for 48 hours with different concentrations of LCA_{60}**M (25-550 µg/mL for MDA-MB-231 and 0.125 mg/mL to 2.75 mg/mL for A549 and SK-MEL-30), the media were not discarded and 10 µL of 5 mg/mL MTT solution was added to each well. After 4 hours of incubation, the solutions in the wells were discarded and the formazan crystals were dissolved in 50 µL of DMSO for 20 min on an orbital shaker. The solutions in the wells were then transferred to a new 96-well plate and the absorbance was measured at 570 nm using SpectraMax iD3 (Molecular Devices, USA). Cells not incubated with LCA_{60}**M were used as the positive control and assumed as 100% viable. Then, cell viability was calculated.

In order to compare the cytotoxic effect of LCA_{25}**M with LCA_{60}**M, cell viability studies were carried out. Cytotoxic effect of LCA_{25}**M and LCA_{60}**M on MDA-MB-231 triple negative breast cancer cells were studied at 37°C in 5% CO_2 incubator. MDA-MB-231 cells were seeded in a 96-well plate at a density of 2500 cells/well in 100 µL medium and allowed to adhere overnight. The next day, the media were changed and replaced with media containing 1.5 mg/mL micelles

dispersed in complete medium. Free LCA containing complete medium was used to check the effectiveness of micelles compared to free drug. MTT assay was carried out according to the procedure to evaluate cytotoxicity of LCA_{25}**M and LCA_{60}**M. As the positive control, cells incubated only in media were used and their viability was considered as 100% viability.

2.2.8.3.2 Cytotoxicity of DOX_{conj}-M and DOX_{ld}-M on MDA-MB-231 Cells

DOX_{conj}-M, and DOX_{ld}-M were treated with MDA-MB-231 triple negative breast cancer cells at 37°C in 5% CO_2 incubator to compare the cytotoxic effect of conjugated drug and loaded drug on triple negative breast cancer cells. MDA-MB-231 cells were seeded in a 96-well plate at a density of 2500 cells/well in 100 µL medium land allowed to adhere overnight. The next day, the media were changed and replaced with media containing 1.5 mg/mL micelles dispersed in complete medium. Free DOX containing complete medium was used to check the effectiveness of micelles compared to free drug. MTT assay was carried out according to the procedure given in the previous section to evaluate cytotoxicity of micelles. As the positive control, cells incubated only in media were used and their viability was considered as 100% viability.

2.2.8.3.3 Cytotoxicity of Mixed Micelles (DOX_{conj}-M and LCA_{60}**M) on MDA-MB-231 Cells

In order to determine whether there is a synergistic effect of DOX and LCA, the micelles having each drug (LCA_{60}**M and DOX_{conj}-M prepared under the same conditions) were mixed in certain proportions and cell viability studies were performed. Cytotoxic effect of mixed micelles on MDA-MB-231 triple negative breast cancer cells were studied at 37°C in 5% CO_2 incubator. MDA-MB-231 cells were seeded in a 96-well plate at a density of 2500 cells/well in 100 µL medium and allowed to adhere overnight. The next day, the media were replaced with media

containing 1.5 mg/mL micelles dispersed in complete medium. Micelles were mixed in 1:1, 1:2, and 2:1 (LCA_{60}**M:DOX_{conj}-M) ratios. Free LCA and/or free DOX containing complete medium was used to check the effectiveness of micelles compared to free drugs. MTT assay was carried out according to the procedure given in the previous section to evaluate cytotoxicity of micelles. As the positive control, cells incubated only in media were used and their viability was considered as 100% viability.

2.2.8.3.4 Cytotoxicity of DL-M on MDA-MB-231 Cells

Cytotoxic effect of DL-M on MDA-MB-231 triple negative breast cancer cells were studied at 37°C in 5% CO_2 incubator. MDA-MB-231 cells were seeded in a 96-well plate at a density of 2500 cells/well in 100 µL medium and allowed to adhere overnight. The next day, the media were changed and replaced with media containing 1.5 mg/mL micelles dispersed in complete medium. Free LCA and/or free DOX containing complete medium was used to check the effectiveness of micelles compared to free drugs. MTT assay was carried out according to the procedure given in the previous section to evaluate cytotoxicity of micelles. As the positive control, cells incubated only in media were used and their viability was considered as 100% viability.

2.2.8.4 Determination of Cell Internalization of Micelles Using Coumarin 6

Cell internalization was studied using coumarin 6 dye as the fluorescent probe to determine if the micelles were taken into the cells by endosomal route. Due to the hydrophobic structure, coumarin 6 was trapped in the core of the micelles. During the preparation process of the LCA_{60}**M, and LCA_{25}**M, 1% (w/v) coumarin 6 was added to the organic solvent. Then, coumarin 6 loaded micelles (C6-LCA_{60}**M and C6-LCA_{25}**M) were freeze-dried. Coumarin 6 was not used for the cell internalization of DOX containing micelles since DOX has fluorescence properties.

Cell internalization of free coumarin 6, free DOX, C6-LCA_{60}**M, C6-LCA_{25}**M, DOX_{conj}-M, DOX_{ld}-M and DL-M were studied using MDA-MB-231 cells at 37°C. The cells were seeded on coverslips at a density of 10^5 cells/well in 1 mL medium and allowed to adhere overnight. The next day, the media were changed with media containing free coumarin 6 (50 ng/mL), or free DOX (80 nM), or C6-LCA_{60}**M (1.5 mg/mL), or C6-LCA_{25}**M (1.5 mg/mL), or DOX_{conj}-M (1.5 mg/mL), or DOX_{ld}-M (1.5 mg/mL), or DL-M (1.5 mg/mL) in complete medium. All samples were incubated for 1, 2, 4 and 6 hours. At the given time intervals, cells were washed with cold PBS and fixed with 4% paraformaldehyde at room temperature. Cell nuclei were stained with DAPI and cell internalization of free coumarin 6, free DOX, C6-LCA_{60}**M, C6-LCA_{25}**M, DOX_{conj}-M, DOX_{ld}-M, and DL-M were examined by confocal microscopy (Zeiss Cell Observer SD, Germany) and images were taken.

2.2.8.5 Cell Migration Assay

Cell migration was studied using MDA-MB-231 at 37°C in 5% CO_2 atmosphere in carbon dioxide incubator by incubating the cells either with M, LCA_{60}**M, LCA_{25}**M, DOX_{conj}-M, DOX_{ld}-M or DL-M. The cell migration assay was carried out with transwell chambers for 24-well plates that have 8.0 µm porosity (Greiner) (He et al., 2017). Cells were seeded on cell inserts at a density of 60.000 cells/transwell in 200 µL of serum-free medium containing free LCA (108 µM for MDA-MB-231), or free DOX (80 nM for MDA-MB-231), or M (1.5 mg/mL), or LCA_{60}**M (1.5 mg/mL), or LCA_{25}**M (1.5 mg/mL), or DOX_{conj}-M (1.5 mg/mL), or DOX_{ld}-M (1.5 mg/mL), or DL-M (1.5 mg/mL). 500 µL of serum containing medium was added in the bottom chambers. After 48 hours, non-migrated cells were removed with a cotton swab. 4% paraformaldehyde was used to fix the migrated cells and cells were stained with 0.2% crystal violet. Afterwards, chambers were washed with water and left to dry. Images were taken with an inverted phase contrast microscope (Nikon Eclipse TS100, Nikon Corp, USA) and cells were counted from

three random fields with ImageJ software. The percentage of migrated cells was normalized with respect to control (cells only).

2.2.8.6 Colony Formation Assay

Colony formation of MDA-MB-231 cells after incubation with M, LCA_{60}**M, LCA_{25}**M, DOX_{conj}-M, DOX_{ld}-M or DL-M was studied at 37°C in 5% CO_2 atmosphere in CO_2 incubator. MDA-MB-231 cells were seeded at a density of 2.000 cells/well in 6-well plate and allowed to grow for 24 h. Then, cells were treated with free LCA (108 µM for MDA-MB-231) or free DOX (80 nM for MDA-MB-231) or M (1.5 mg/mL) or LCA_{60}**M (1.5 mg/mL) or LCA_{25}**M (1.5 mg/mL) or DOX_{conj}-M (1.5 mg/mL) or DOX_{ld}-M (1.5 mg/mL) or DL-M (1.5 mg/mL) for one week. Thereafter, colonies were fixed with 4% paraformaldehyde for 20 min and 0.2% crystal violet was used to stain the colonies. Colonies were counted manually. The experiment was performed for three times (He et al., 2017). Untreated cells were used as control.

2.2.8.7 Determination of Lipid Droplets in MDA-MB-231 Cells

In order to determine apoptosis in cancer cells, the number of lipid droplets was determined for groups having free LCA, free DOX, M, LCA_{60}**M, LCA_{25}**M, DOX_{conj}-M, DOX_{ld}-M and DL-M. For this purpose, MDA-MB-231 cells were seeded on 24-well plate at a density of 100.000 cells/well in 1 mL medium and allowed to adhere overnight. The next day, the media were replaced with media that contained free LCA (108 µM for MDA-MB-231) or free DOX (80 nM for MDA-MB-231) or M (1.5 mg/mL) or LCA_{60}**M (1.5 mg/mL) or LCA_{25}**M (1.5 mg/mL) or DOX_{conj}-M (1.5 mg/mL) or DOX_{ld}-M (1.5 mg/mL) or DL-M (1.5 mg/mL) dispersed in complete medium. The cells were incubated for 48 hours, then, washed with PBS and fixed with 4% paraformaldehyde for 20 min. After removing the paraformaldehyde, 60% isopropanol was added to each well and kept for 5 min.

Later on, the cells were incubated in oil red O staining solution for 30 min, followed by incubation with Weigert's hematoxylin for 10 min. Finally, the cells were washed with water 3 times. Then, cell morphology and lipid droplets inside cells were examined using inverted phase contrast microscope (Nikon Eclipse TS100, Nikon Corp, USA) and photographed (Luu et al., 2018).

2.2.8.8 Detection of Apoptosis in Cancer Cells with qRT-PCR

Apoptotic gene expression of MDA-MB-231 triple negative breast cancer cell line was studied by incubating in media containing M or LCA_{60}**M or LCA_{25}**M or DOX_{conj}-M or DOX_{ld}-M or DL-M at 37°C in carbon dioxide (5% CO_2) incubator for 24 h. For this purpose, first MDA-MB-231 cells were seeded in a 6-well plate at a density of 10^6 cells/well in 3 mL medium and allowed to adhere overnight. The next day, the media were changed with media containing free LCA (108 µM for MDA-MB-231) or free DOX (80 nM for MDA-MB-231) or M (1.5 mg/mL) or LCA_{60}**M (1.5 mg/mL) or LCA_{25}**M (1.5 mg/mL) or DOX_{conj}-M (1.5 mg/mL) or DOX_{ld}-M (1.5 mg/mL) or DL-M (1.5 mg/mL) dispersed in complete medium and incubated for 24 hours. Untreated cells were used as the control. Next day, total RNA was isolated with Roche High Pure RNA Isolation Kit (Switzerland) and cDNA was synthesized using Roche Transcriptor High Fidelity cDNA Synthesis Kit (Switzerland), both according to the manufacturer's instructions. For PCR analysis, LightCycler® FastStart DNA Master SYBR Green I (Switzerland) was used. Gene expression levels of pro-apoptotic (Bax, p53) and anti-apoptotic (Bcl-2 and Bcl-xL) genes were calculated relative to the reference β-actin gene using ΔΔCT method. The sequences of the primers are given in Table 2.1.

Table 2.1. Primers used in qRT-PCR studies.

Primer	**Sequence**
Bax forward	CCCGAGAGGTCTTTTTCCGAG
Bax reverse	CCAGCCCATGATGGTTCTGAT
p53 forward	CCTCAGCATCTTATCCGAGTGG
p53 reverse	TGGATGGTGGTACAGTCAGAGC
Bcl-2 forward	GGTGGGGTCATGTGTGTGG
Bcl-2 reverse	CGGTTCAGGTACTCAGTCATCC
Bcl-xL forward	GAGCTGGTGGTTGACTTTCTC
Bcl-xL reverse	TCCATCTCCGATTCAGTCCCT
β-actin forward	ATGTGGCCGGAGGACTTGATT
β-actin reverse	AGTGGGGTGGCTTTTAGGATG

2.2.8.9 Determination of Cell Apoptosis with Annexin V-FITC Assay

Apoptotic effect of M or LCA_{60}**M or LCA_{25}**M or DOX_{conj}-M or DOX_{ld}-M and DL-M on MDA-MB-231 cells was studied using FITC Annexin V-PI kit. For this purpose, the cells were seeded in a 6-well plate at a density of 10^6 cells/well in 3 mL medium and allowed to adhere overnight. The next day, the media were changed with media that contained free LCA (108 μM for MDA-MB-231), or free DOX (80 nM for MDA-MB-231), or M (1.5 mg/mL), or LCA_{60}**M (1.5 mg/mL), or LCA_{25}**M (1.5 mg/mL), or DOX_{conj}-M (1.5 mg/mL), or DOX_{ld}-M (1.5 mg/mL), or DL-M (1.5 mg/mL) dispersed in complete medium and incubated for 24 hours. Cells treated with IC_{50} value of LCA (108 μM) or DOX (80 nM) containing medium was used as the negative control. Then, media were discarded, and wells were washed with sterile PBS (0.1 M, pH 7.4). Cells were detached with cell scraper and collected by centrifugation at 2000 rpm for 5 min, and then incubated with FITC Annexin V and propidium iodide according to FITC Annexin V-PI kit protocol (BioLegend, USA). Apoptosis analysis was carried out with a flow cytometry (BD Accuri C6,

USA). First, cells from each group were counted and dilutions were made to obtain 10^6 cells/ml for each group. The data were gated to exclude debris using unstained cell suspension. Then cells stained with Annexin V-FITC and propidium iodide were analyzed with flow cytometry and live and apoptotic cells were determined according to the gate. The percentages of apoptotic and live cells were determined according to the untreated control group.

2.2.8.10 Mitochondrial Transmembrane Potential Detection

Change in mitochondrial transmembrane potential is an early indicator in apoptosis. 3,3'-Dihexyloxacarbocyanine iodide (DiOC6) is a membrane permeable fluorescent probe that dyes mitochondria. But, DiOC6 cannot dye mitochondria if the cell is in apoptotic stage since the mitochondrial transmembrane integrity is lost. For this purpose, MDA-MB-231 cells were seeded in a 6-well plate at a density of 10^6 cells/well in 3 mL medium and allowed to adhere overnight. The next day, the media were changed with the media that contained free LCA (108 µM for MDA-MB-231) or free DOX (80 nM for MDA-MB-231) or M (1.5 mg/mL) or LCA_{60}**M (1.5 mg/mL) or LCA_{25}**M (1.5 mg/mL) or DOX_{conj}-M (1.5 mg/mL) or DOX_{ld}-M (1.5 mg/mL) or DL-M (1.5 mg/mL) dispersed in complete medium and incubated for 24 hours. Cells treated with IC_{50} value of LCA (108 µM) or DOX (80 nM) containing medium was used as the negative control. Then, media was discarded, and wells were washed with sterile PBS (0.1 M, pH 7.4). Cells were detached with a cell scraper and collected by centrifugation, and then incubated with 40 nM of DiOC6 for 30 minutes. Mitochondrial transmembrane potential analysis were carried out with a flow cytometry (BD Accuri C6, USA). First, cells from each group were counted and dilutions were made to obtain 10^6 cells/ml for each group. Then the data were gated to exclude debris using unstained cell suspension. Cells stained with DiOC6 was analyzed with flow cytometry. Loss of mitochondrial transmembrane potential was observed with the decrease of the percentages in V1-R section compared to control group (Yadav et al., 2015).

2.2.8.11 Reactive Oxygen Species (ROS) Determination

In the cases where the cells are in the apoptotic stage, ROS concentration increases. Therefore, ROS determination was carried out to check the status of the cells after the treatment of micelles, according to Cellular ROS Assay Kit (Abcam) protocol. The fluorescent probe of 2',7'-Dichlorofluorescin diacetate (DCFDA) binds to ROS in the cell. MDA-MB-231 cells were either seeded on coverslips placed in 24-well plates at a density of 10^5 cells/well in 1 mL medium for confocal microscopy imaging, or on 96-well plates at a density of 2500 cells/well in 100 µL medium to determine the ROS concentration of cells. In each case, cells were incubated overnight to adhere. The next day, the media were changed with media containing IC_{50} concentration of free LCA (108 µM for MDA-MB-231) or free DOX (80 nM for MDA-MB-231) or M (1.5 mg/mL) or LCA_{60}**M (1.5 mg/mL) or LCA_{25}**M (1.5 mg/mL) or DOX_{conj}-M (1.5 mg/mL) or DOX_{ld}-M (1.5 mg/mL) or DL-M (1.5 mg/mL) which were dispersed in complete medium and incubated for 24 hours. After that, media from the wells were discarded, the cells were stained with 20 µM DCFDA solution for 30 minutes and washed with PBS. The cells on coverslips were examined with confocal microscopy (Zeiss), and fluorescence intensity of the cells in 96-well plates was measured using SpectraMax iD3 (Molecular Devices, USA) to determine the ROS concentration of cells. Medium in 0.4% ethanol was used as the negative control. Tert-butyl hydroperoxide (TBHP) control group was incubated only with 50 µM TBHP for 4 hours prior to staining with DCFDA.

2.2.8.12 Endothelial Cell Tube Formation Assay

Angiogenesis is important for the cell growth. Therefore, tube formation assay was performed to determine the effects of micelles on reducing angiogenesis of endothelial cells and thus preventing metastasis (Bielenberg & Zetter, 2015). For this purpose, human umbilical vein endothelial cells were cultured in endothelial cell (EC) medium containing 10% FBS. First, 50 µL of Matrigel solution (Corning) was

put in 96-well plates and incubated for 30-60 min at 37°C in an incubator. Then, $40x10^3$ HUVEC/well and/or $40x10^3$ MDA-MB-231 cells/well were seeded on Matrigel. Later on, 150 µL of medium was placed and cells were incubated for 2, 4, 8, and 24 hours. After each time point, images were taken with an inverted microscope and tube formation was examined using ImageJ software (National Institutes of Health, Bethesda, MD). The total endothelial tube lengths and number of nodes were measured using ImageJ Software Angiogenesis Analyzer Tool from three independent experiments and the values were averaged. Groups examined and the media composition used for the groups are given in Table 2.2.

Table 2.2. Groups for endothelial cell tube formation assay.

Group name	Cells	Medium and treatment
Control-1	HUVEC	EC medium
Control-2	HUVEC	EC:L15 medium (1:1)
Free LCA-1	HUVEC	EC medium, free LCA
Free LCA-2	HUVEC	EC:L15 medium (1:1), free LCA
Free DOX-1	HUVEC	EC medium, free DOX
Free DOX-2	HUVEC	EC:L15 medium (1:1), free DOX
Co-culture control	HUVEC:MDA-MB-231	EC:L15 medium (1:1)
Co-culture free LCA	HUVEC:MDA-MB-231	EC:L15 medium (1:1), free LCA
Co-culture free DOX	HUVEC:MDA-MB-231	EC:L15 medium (1:1), free DOX
HUVEC1-L60	HUVEC	EC medium, LCA_{60}**M
HUVEC1-L25	HUVEC	EC medium, LCA_{25}**M
HUVEC2-L60	HUVEC	EC:L15 medium (1:1), LCA_{60}**M
HUVEC2-L25	HUVEC	EC:L15 medium (1:1), LCA_{25}**M
HUVEC1-DM1	HUVEC	EC medium, DOX_{conj}-M
HUVEC1-DM2	HUVEC	EC medium, DOX_{ld}-M
HUVEC1-DLM	HUVEC	EC medium, DL-M
HUVEC2-DM1	HUVEC	EC:L15 medium (1:1), DOX_{conj}-M
HUVEC2-DM2	HUVEC	EC:L15 medium (1:1), DOX_{ld}-M
HUVEC2-DLM	HUVEC	EC:L15 medium (1:1), DL-M
HUVEC1-EM	HUVEC	EC medium, M
HUVEC2-EM	HUVEC	EC:L15 medium (1:1), M
Co-culture L60	HUVEC:MDA-MB-231	EC:L15 medium (1:1), LCA_{60}**M
Co-culture L25	HUVEC:MDA-MB-231	EC:L15 medium (1:1), LCA_{25}**M
Co-culture DM1	HUVEC:MDA-MB-231	EC:L15 medium (1:1), DOX_{conj}-M
Co-culture DM2	HUVEC:MDA-MB-231	EC:L15 medium (1:1), DOX_{ld}-M
Co-culture DLM	HUVEC:MDA-MB-231	EC:L15 medium (1:1), DL-M
Co-culture EM	HUVEC:MDA-MB-231	EC:L15 medium (1:1), M

2.2.9 Statistical Analysis

All data are presented as mean ± standard deviation. Results were analyzed using one-way analysis of variance (ANOVA) and Tukey's multiple comparison test.

CHAPTER 3

RESULTS AND DISCUSSIONS

3.1 Synthesis and Characterization of mPEG-b-PCL Copolymer

The synthesized mPEG-b-PCL copolymer was examined by ^{1}H NMR and FT-IR. The chemical structure of the mPEG-b-PCL copolymer is shown in Figure 3.1 (Protons in the chemical structure of the polymer are numbered in order to indicate peaks in NMR spectra.).

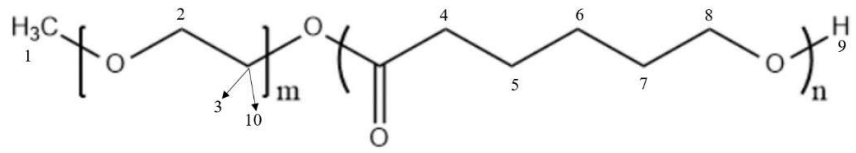

Figure 3.1. Chemical structure of mPEG-b-PCL polymer (For protons numbered 3 and 10: the number of –CH_2– protons in polyethylene glycol is 3. The number of –CH_2– protons where the polyethylene glycol is linked to the polycaprolactone by ester bond is 10. –CH_2– protons numbered as 3 linked to oxygen by ether bond. –CH_2– protons numbered as 10 linked to polycaprolactone by ester bond.).

^{1}H NMR spectra of the copolymer synthesized and the mPEG polymer used in the synthesis are shown in Figure 3.2-A and Figure 3.2-B, respectively. The protons belonging to the observed peaks in the ^{1}H NMR spectra and the literature values are given in Table 3.1.

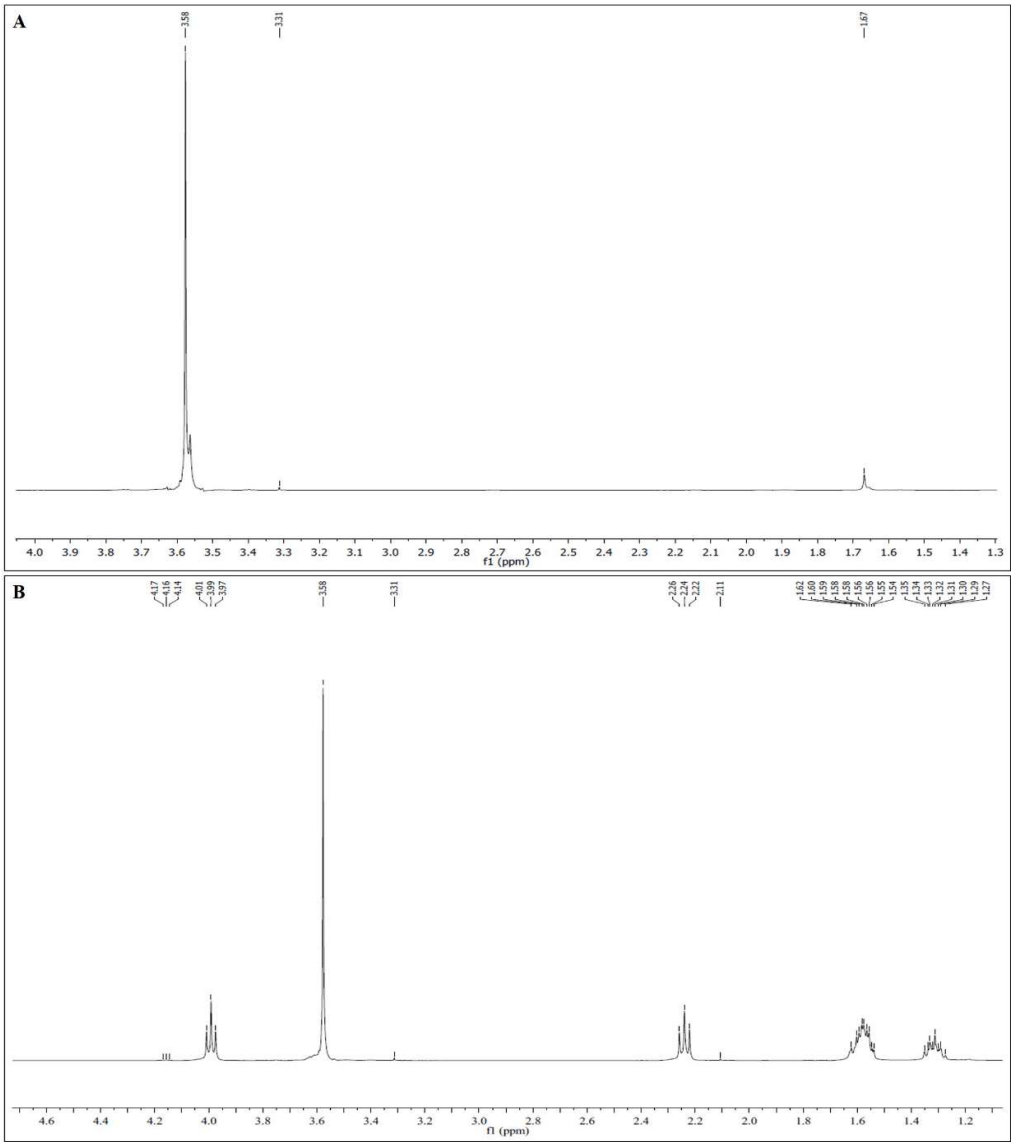

Figure 3.2. A) ^{1}H NMR spectra of mPEG, B) ^{1}H NMR spectra of mPEG-b-PCL.

Table 3.1. Comparison of ^{1}H NMR values of synthesized mPEG-b-PCL copolymer with those reported in literature.

Proton	Synthesized copolymer	(Gao et al., 2015)	(Shuai et al., 2003, 2004)
H_1	3.31 ppm, singlet (3H)	3.35 ppm, singlet (3H)	3.38 ppm, singlet (3H)
H_2 ve H_3	3.58 ppm, singlet (4H)	3.65 ppm, singlet (4H)	3.65 ppm, singlet (4H)
H_4	2.24 ppm, triplet (2H)	2.30 ppm, triplet (2H)	2.30 ppm, triplet (2H)
H_5 ve H_7	1,54-1,62 ppm, multiplet (4H)	1.60-1.70 ppm, multiplet (4H)	1.60-1.70 ppm, multiplet (4H)
H_6	1.27-1.35 ppm, multiplet (2H)	1.30-1.50 ppm, multiplet (2H)	1.35-1.45 ppm, multiplet (2H)
H_8	3.99 ppm, triplet (2H)	4.10 ppm, triplet (2H)	4.06 ppm, triplet (2H)
H_9	2.11 ppm, singlet (1H)	2.05 ppm, singlet (1H)	-
H_{10}	4.16 ppm, triplet (2H)	4.25 ppm, triplet (2H)	4.25 ppm, triplet (2H)

Figure 3.2-A shows the singlet peak of $–CH_2–$ protons in the mPEG polymer at 3.58 ppm, and the singlet peak of $CH_3–$ protons in the mPEG polymer at 3.31 ppm. Since there is only one methyl group in the polymer, the intensity of singlet peak at 3.31 ppm is very low. The small and wide singlet peak seen at 1.67 ppm belongs to the –OH group at the end of the polymer. When these data are compared with the ^{1}H NMR spectra of synthesized copolymers, the intensity of triplet peak seen at 4.16 ppm was less than the other peaks because there was only one $–CH_2–$ group that is bonded to polycaprolactone with ester bond. The singlet peak seen in the synthesized copolymers at 3.58 ppm is the peak of $–CH_2–$ protons of the mPEG polymer (except for the $–CH_2–$ group, which binds the polycaprolactone). The reason for this peak to have more intensity than other peaks is that all $–CH_2–$ protons of mPEG polymer resonate at the same location. Because all $–CH_2–$ protons in mPEG are equivalent protons.

The ^{1}H NMR spectra of the synthesized copolymer were slightly different in their peak values compared to the literature (Table 3.1). The reason for this difference could be due to the different types of mPEG and ε-caprolactone used in the synthesis. Different chemical shift values are reported in the literature for the same copolymer used in this study (Gao et al., 2015; Shuai et al., 2003, 2004; Tanaka et al., 2010).

FT-IR spectroscopy (PerkinElmer Spectrum 65) was also used to confirm the chemical structure of the synthesized copolymers. Figure 3.3 shows the FT-IR spectra of mPEG polymer, ε-caprolactone monomer and synthesized copolymer. The peaks specific to the chemical bonds observed in the FT-IR spectra of the synthesized copolymer are given in Table 3.2. The reason of the wave number differences in four characteristic peaks present in the copolymer between the copolymer, the mPEG polymer, and the ε-caprolactone monomer are due to the alteration of the bond strengths. In addition, the two characteristic peaks observed in the mPEG polymer and the two characteristic peaks in the ε-caprolactone monomer are also present in the FT-IR spectra of the copolymer, which shows that the synthesis is successful. According to Tanaka et al. (2010), the absorbance peak at 2875 cm^{-1} was ascribed to C-H stretching vibrations of the mPEG polymer. The absorbance peak at 2937 cm^{-1} was ascribed to C-H stretching vibrations of the ε-caprolactone monomer. The absorbance peak at 1725 cm^{-1} was ascribed to C=O stretching vibrations of the ε-caprolactone monomer (Tanaka et al., 2010). Shuai et al. (2003) showed that the mPEG-b-PCL copolymer had a peak showing stretching vibration of C-H bonds between 2800 cm^{-1} and 2900 cm^{-1}. The absorbance peak observed at 1726 cm^{-1} was ascribed the stretching vibration of C=O bonds in the polycaprolactone part of the copolymer. The absorbance peak observed at 1105 cm^{-1} was ascribed the stretching vibration of C-O bonds in the mPEG part of the copolymer (Shuai et al., 2003). In the mPEG-b-PCL copolymer, these three peaks are observed.

Table 3.2. Chemical bonds assigned to the peaks in the FT-IR spectra of synthesized copolymers

Bond	Wave number of peaks observed in the FT-IR spectra (cm^{-1})		
	mPEG	**ε -caprolactone**	**Synthesized Copolymer**
C-H	2889	2936	2894 ve 2946
C-O	1104	-	1106
C=O	-	1732	1725

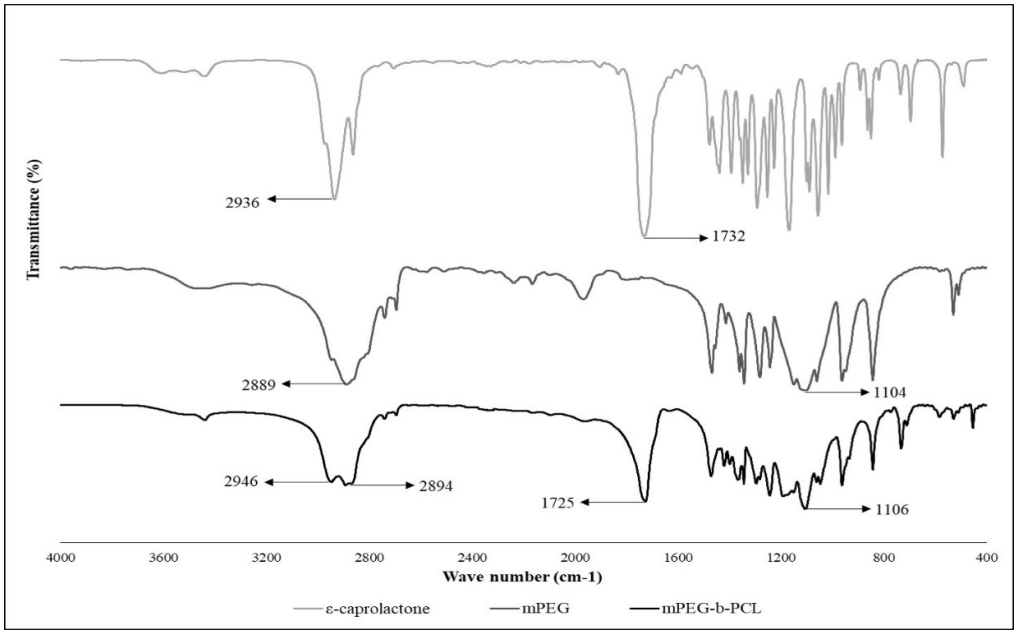

Figure 3.3. FT-IR spectra of mPEG-b-PCL polymer synthesized, mPEG polymer and the ε-caprolactone monomer.

The number average molecular weight (Mn) of the copolymer synthesized was determined by integration of the peaks present in the ^{1}H NMR spectra (Table 3.3). The value found is quite close to the estimated value (15,700 Da) before starting the synthesis (15,000 Da). The number average (Mn) and weight average (Mw) molecular weights of the synthesized copolymer were determined by GPC. The values detected were a bit higher than ^{1}H NMR results, but it is accepted that the differences were not significant.

The polydispersity index (PDI) is the ratio of the Mw of a polymer to the Mn and is always greater than 1, and generally about 1.5 for most of the polymers synthesized in the lab. When the PDI value is equal to 1 that means all polymer chains in a polymer sample have the same length and the same weight. This is a hypothetically ideal case for polymers.

Table 3.3. Molecular weights and polydispersity index of the synthesized mPEG-b-PCL copolymer.

Mn (kDa) (with NMR)	Mn (kDa) (with GPC)	Mw (kDa) (with GPC)	Polydispersity index (PDI)
15.7	16.7	24.7	1.49

The differential scanning calorimeter (DSC) was used to determine the thermal properties of the synthesized copolymers. Figure 3.4-A shows the DSC curve of the mPEG polymer having a number average molecular weight of 5,000 Da used in the synthesis. A sharp peak in phase transitions seen in the DSC curve indicates that the substance is pure. A sharp peak is also observed in the DSC curve of the mPEG polymer. This curve is the melting curve and the melting temperature of the mPEG polymer is 67°C. The DSC curve in Figure 3.4-B shows two adjacent melting peaks. Since the copolymers are composed of two different polymers (PEG and PCL), there must be a separate melting peak for both. Peng et al. (2015) showed that the melting temperature of mPEG-b-PCL copolymers with the average molecular weight of 16 kDa was found to be 61°C as a result of DSC measurement (Peng et al., 2015). Baimark (2009) showed that the melting temperature of the mPEG polymer, with the average molecular weight of 5000 Da was found to be 61°C. The mPEG-b-PCL copolymer with an average molecular weight of 40 kDa was found to be 58°C as a result of DSC measurement (Baimark, 2009). Danafar et al. (2014) showed that the melting temperature of mPEG-b-PCL copolymer with the average molecular weight of 22.7 kDa was found to be 58.68°C as a result of DSC measurements (Danafar et al., 2014). There is few degrees difference with the melting temperatures of the synthesized copolymers and the data given in the literature, which is not a significant difference. As a result, the synthesized copolymer is similar to the literature.

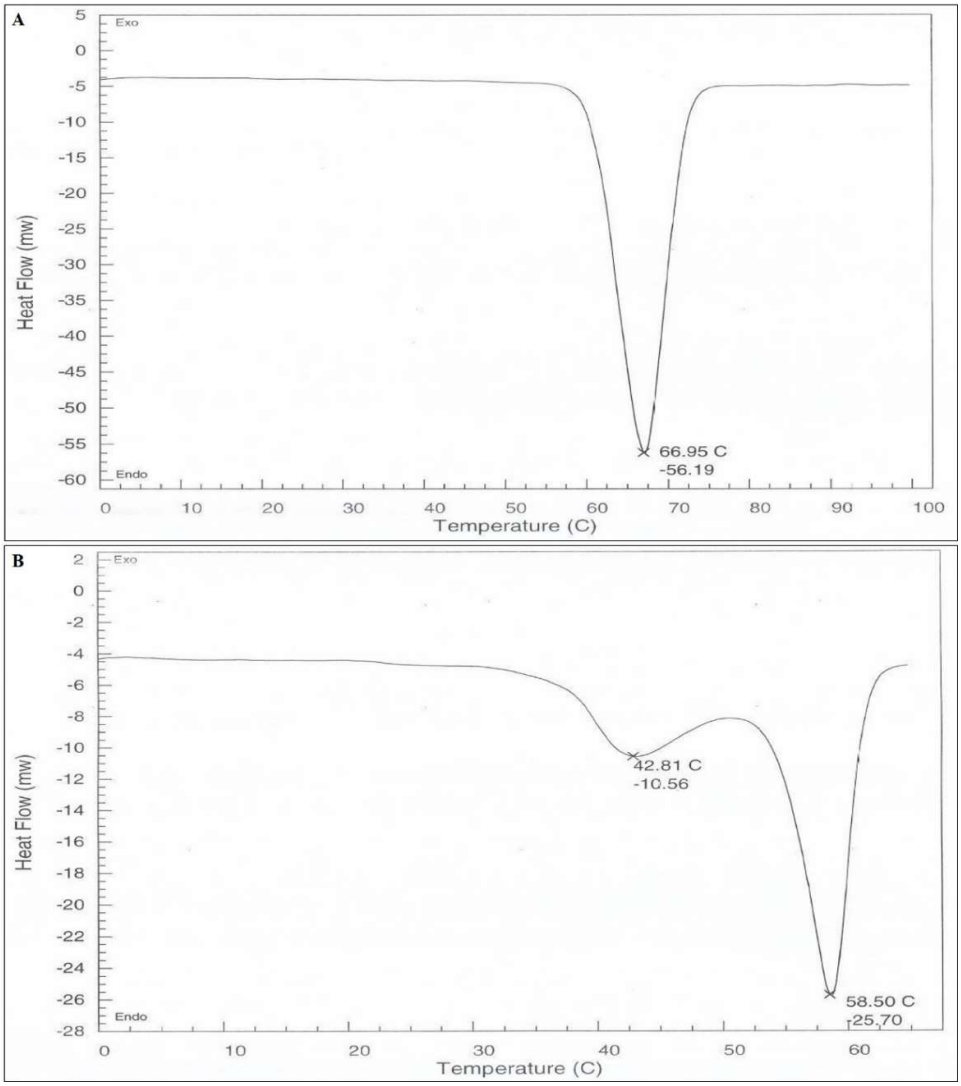

Figure 3.4. DSC curves of A) mPEG polymer and B) mPEG-b-PCL copolymer.

3.2 Characterization of Micelles

Hydrodynamic diameter and zeta potential values of the micelles obtained by emulsion-diffusion method were found as 85.4±28.3 nm and -2.66±0.27 mV, respectively. Figure 3.5-A shows the size distribution chart of micelles. It is the zeta

potential value that determines the stability of micelles in the solution. The micelles are stable if the zeta potential is far from zero in plus or minus directions. The zeta potential of the prepared micelles was -2.66 mV. Meanwhile, there are more negative values reported in literature. For example; Bernabeu et al. (2016) as -31.7 mV (Bernabeu et al., 2016), and Xiong et al. (2015) as -21.4 mV (Xiong et al., 2015). This shows that the prepared micelles are not stable. Micelle morphologies can be seen in Figure 3.6-A and Figure 3.6-B. As seen from TEM images, these micelles do not have a uniform shape and size. Therefore, we changed the micelle preparation method.

Solvent evaporation method was applied for micelle preparation. This time, hydrodynamic diameter and zeta potential values were found as 175.2±2.4 nm and -4.76±0.5 mV, respectively. Figure 3.5-B shows the size distribution of micelles. The size distribution is very wide which shows that there are very small and very large particles in the suspension. Also, zeta potential was much lower than the values reported in literature. Micelle morphologies can be seen in Figure 3.6-C and Figure 3.6-D. As seen from TEM images, these micelles have uniform shape but there are also polymer aggregates. Therefore, solvent evaporation method was slightly changed and 1% polyvinyl alcohol solution was used as water phase to increase the stability of micelles. Since PVA is a surfactant, it is used as a stabilizing agent in the preparation of polymeric micelles (Şengel Türk et al., 2009; Xiao et al., 2013). Hydrodynamic diameter and zeta potential values of micelles were found as 150±24.1 nm and -11.07±0.8 mV, respectively. Figure 3.5-C shows the size distribution chart of micelles. These micelles were stable, and as seen from TEM images, they had a uniform shape and size (Figure 3.6-E and Figure 3.6-F). Therefore, solvent evaporation method with PVA was chosen as the best method for micelle preparation.

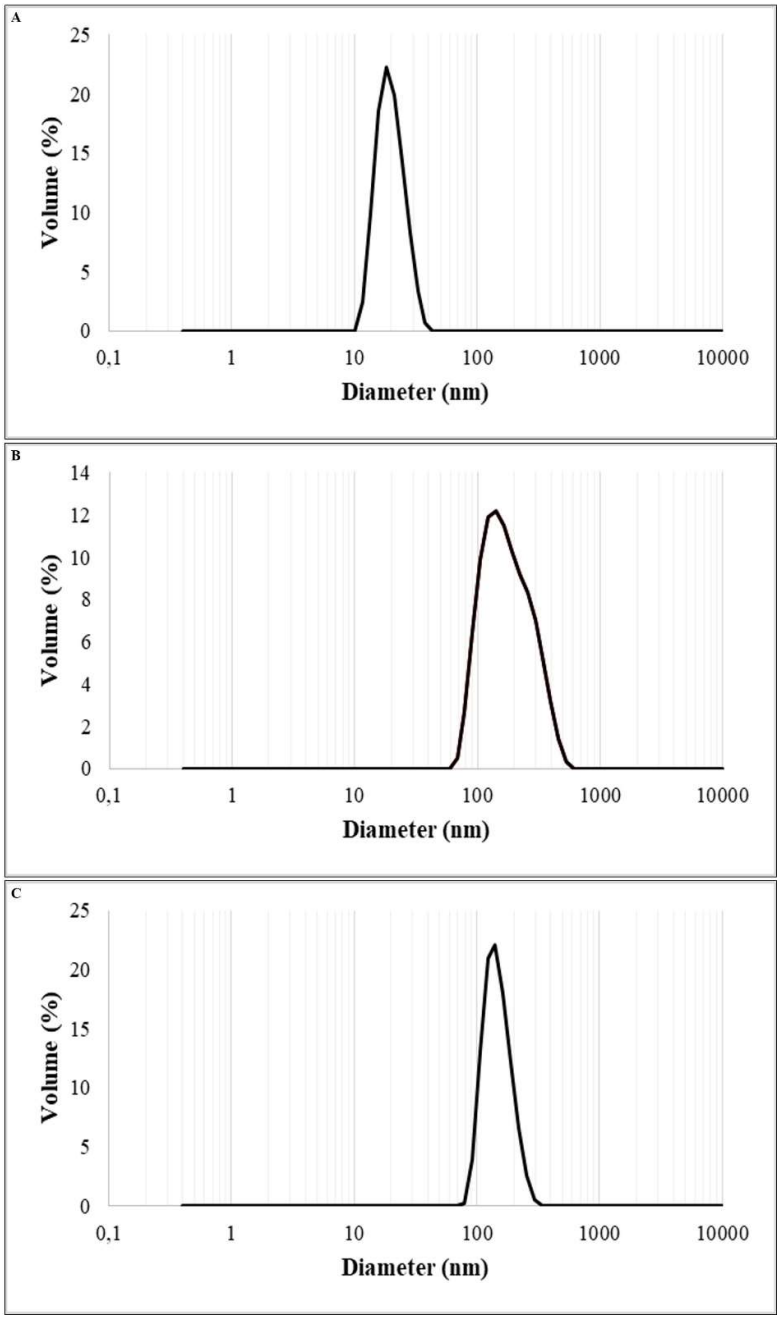

Figure 3.5. Size distribution of mPEG-b-PCL empty micelles prepared by A) Emulsion-diffusion method, B) Solvent evaporation method (Water phase is distilled water.). C) Solvent evaporation method (Water phase is 1% polyvinyl alcohol.).

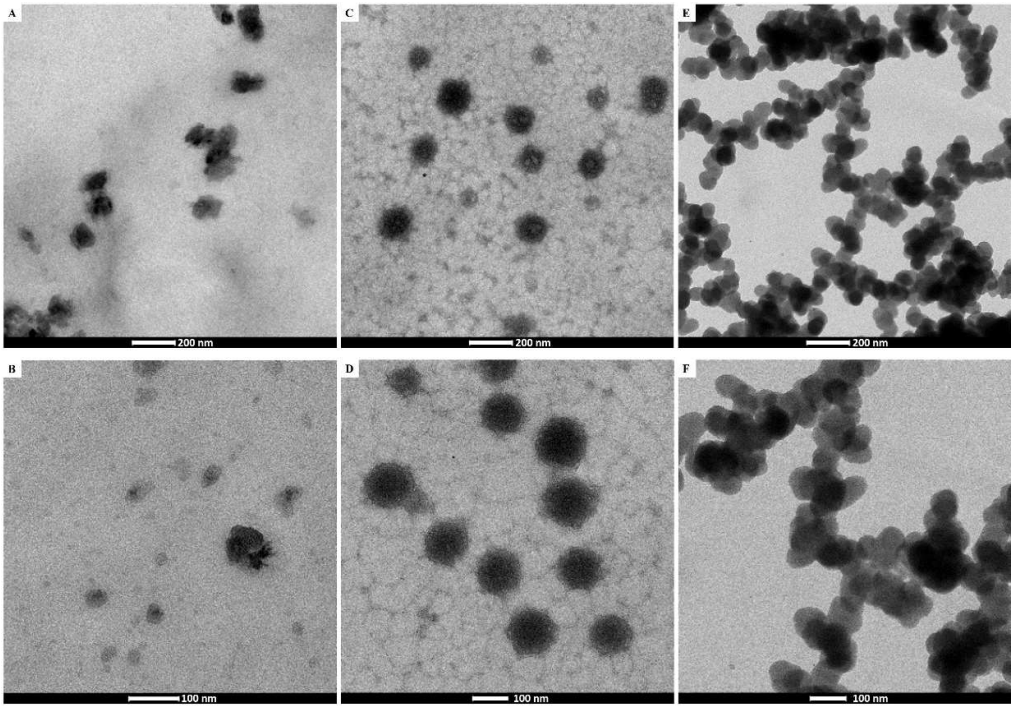

Figure 3.6. TEM images of micelles prepared by A) Emulsion-diffusion method, B) Emulsion-diffusion method, C) Solvent evaporation method (Water phase is distilled water.), D) Solvent evaporation method (Water phase is distilled water.), E) Solvent evaporation method (Water phase is 1% polyvinyl alcohol.). Scale bar is 200 nm in parts A, C and E. Scale bar is 100 nm in parts B, D and F.

3.3 Characterization of DOX and LCA Conjugated mPEG-b-PCL Copolymer

The mPEG-b-PCL copolymer and its carboxylated and aminated forms, mPEG-b-PCL-COOH and mPEG-b-PCL-CO-NH-NH_2, were synthesized following a consecutive process to obtain amphiphilic block copolymer ending with hydrazide groups (Figure 3.7). FT-IR spectra of mPEG-b-PCL, mPEG-b-PCL-COOH and mPEG-b-PCL-CO-NH-NH_2 polymers are given in Figure 3.8. The absorbance peaks observed at 3443 cm^{-1} belong to the stretching vibrations of –NH_2 bonds (Isik et al., 2021; Lale et al., 2015); peaks at 2866 cm^{-1} and 2945 cm^{-1} are belong to C-H

stretching vibrations. The absorbance peaks at 1722 cm^{-1} were evaluated as C=O stretching vibrations of PCL unit, and the peak at 1103 cm^{-1} was ascribed to C-O stretching vibrations of mPEG unit in the copolymer (Y. Chen et al., 2016; Isik et al., 2021). ^{1}H NMR results of the products obtained in every step showed that hydrazide functionalization of mPEG-b-PCL copolymer was achieved successfully (Figure 3.9-A, B, and C). For ^{1}H NMR spectrum of mPEG-b-PCL-COOH copolymer the peak at 2.64 shows the $–CH_2–CH_2–$ group from succinic anhydride (Isik et al., 2021; Lale et al., 2015). The peaks at 1.36-1.43 ppm (multiplet), 1.56-1.70 ppm (multiplet), 2.31 ppm (triplet), 4.06 ppm (triplet) and 4.23 ppm (triplet) belong to the methylene protons of PCL block in the copolymer. The peak at 3.65 ppm (triplet) was assigned to the methylene protons of mPEG block in the copolymer (Y. Chen et al., 2016; Isik et al., 2021).

DOX conjugation was verified using ^{1}H NMR spectroscopy (Figure 3.10) (Gatti et al., 2018; Isik et al., 2021; Ye et al., 2015). ^{1}H NMR results also showed that MeOH-TFA method was more efficient than DMSO method since some impurities were observed in ^{1}H NMR spectrum of DOX conjugated copolymer prepared with DMSO method The yield for DOX conjugated polymer synthesis was higher in MeOH-TFA method (92.1%) than DMSO method (78.9%).

LCA conjugation was also verified using ^{1}H NMR spectroscopy (Figure 3.11). Hydrazone bond can be formed between an aldehyde or ketone group and a hydrazide. LCA did not have an aldehyde or ketone group on it. But it has a carboxylic acid group on it and so an electrostatic interaction forming ionic conjugation can occur between amine group of the polymer and carboxylic acid group of LCA regardless of the reaction (R. Su et al., 2021).

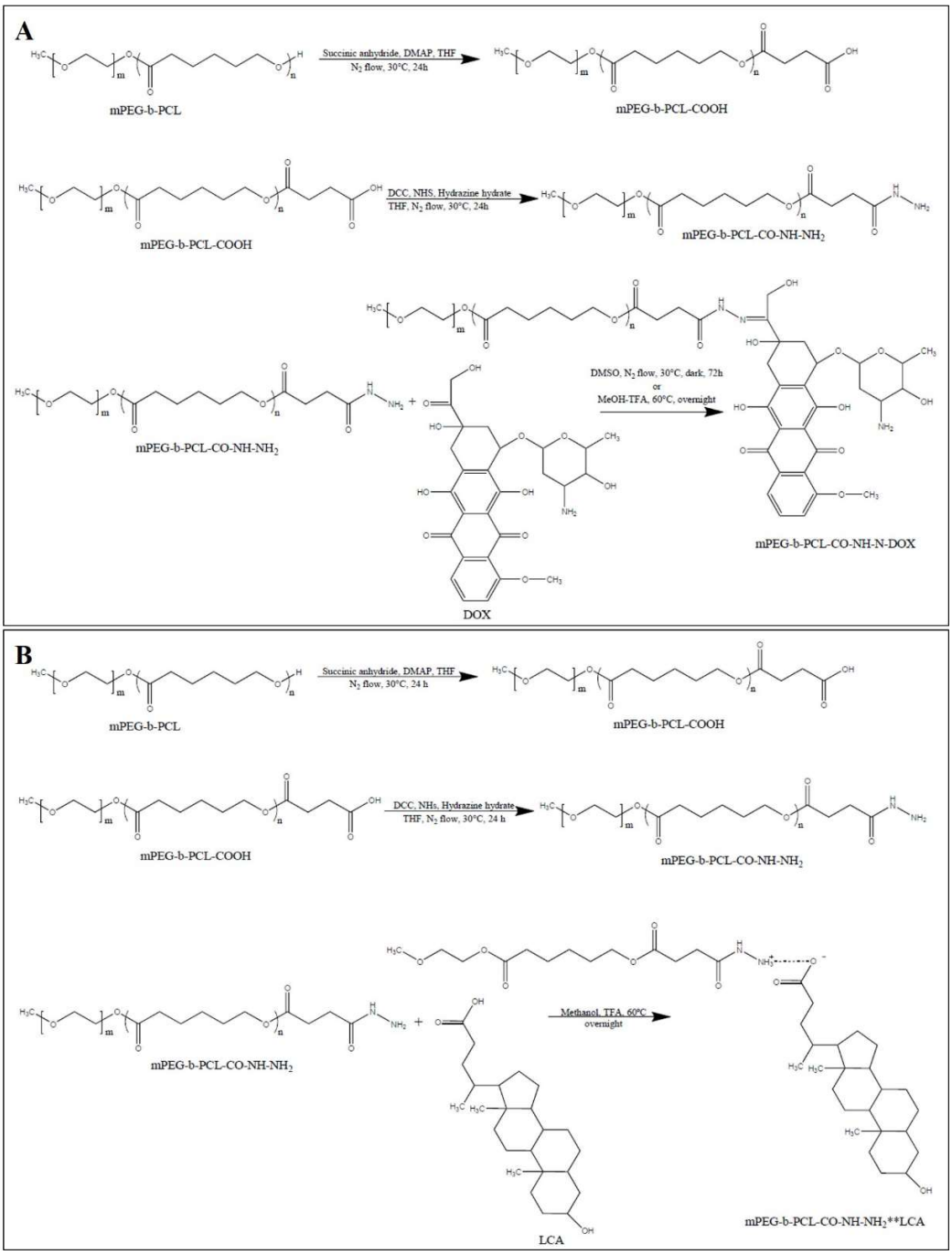

Figure 3.7. A) Reaction scheme for hydrazide functionalization of mPEG-b-PCL copolymer and conjugation of DOX. B) Reaction scheme for hydrazide functionalization of mPEG-b-PCL copolymer and ionic conjugation of LCA at 60ºC.

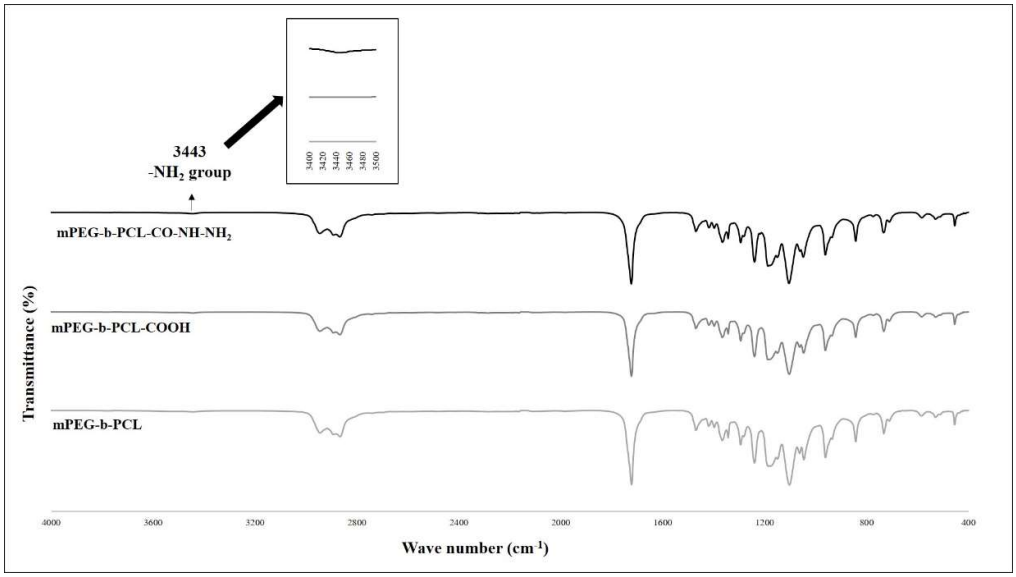

Figure 3.8. FT-IR spectra of mPEG-b-PCL, mPEG-b-PCL-COOH, and mPEG-b-PCL-CO-NH-NH_2.

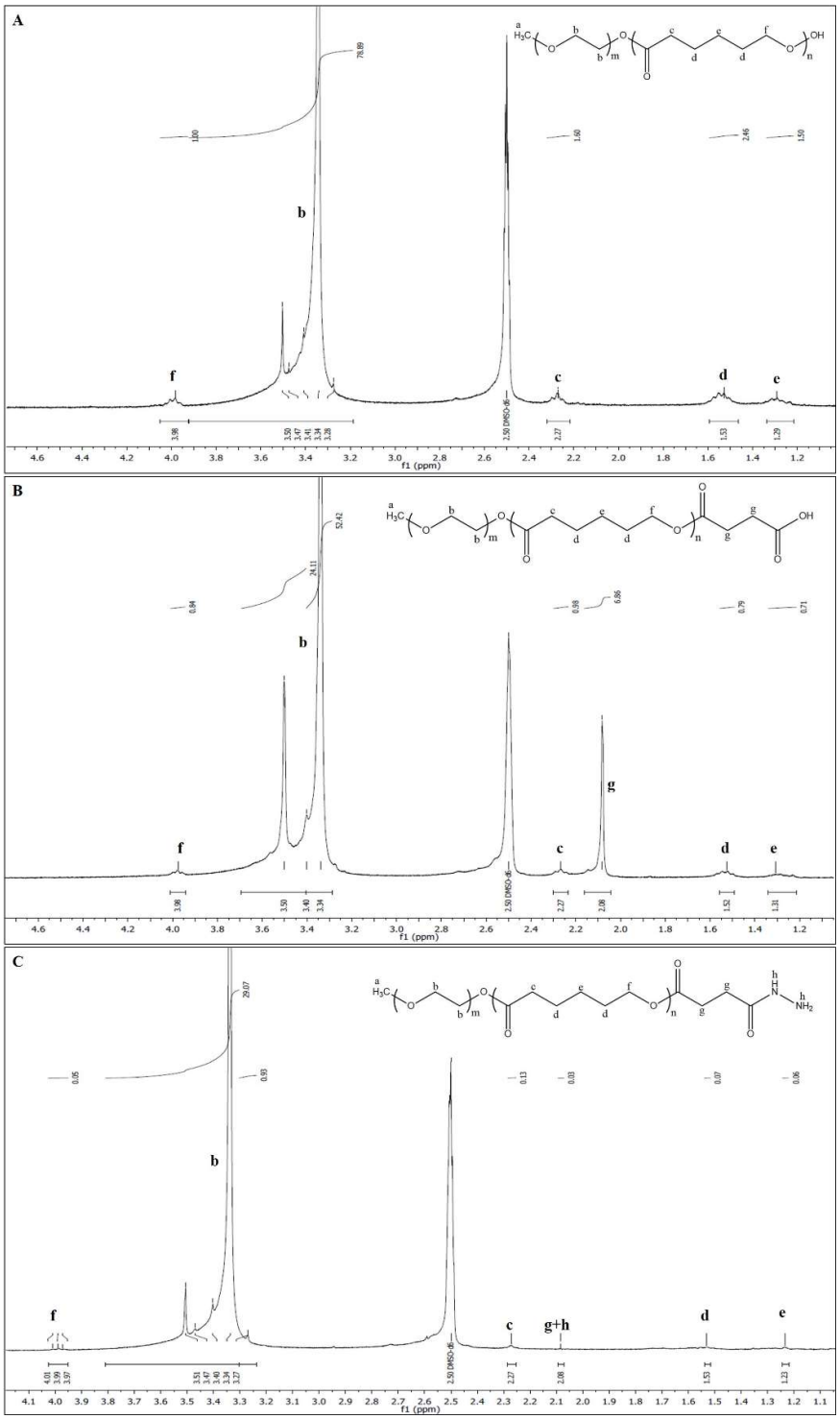

Figure 3.9. ^{1}H NMR spectra of A) mPEG-b-PCL in $CDCl_3$, B) mPEG-b-PCL-COOH in $CDCl_3$, C) mPEG-b-PCL-CO-NH-NH_2 in $CDCl_3$.

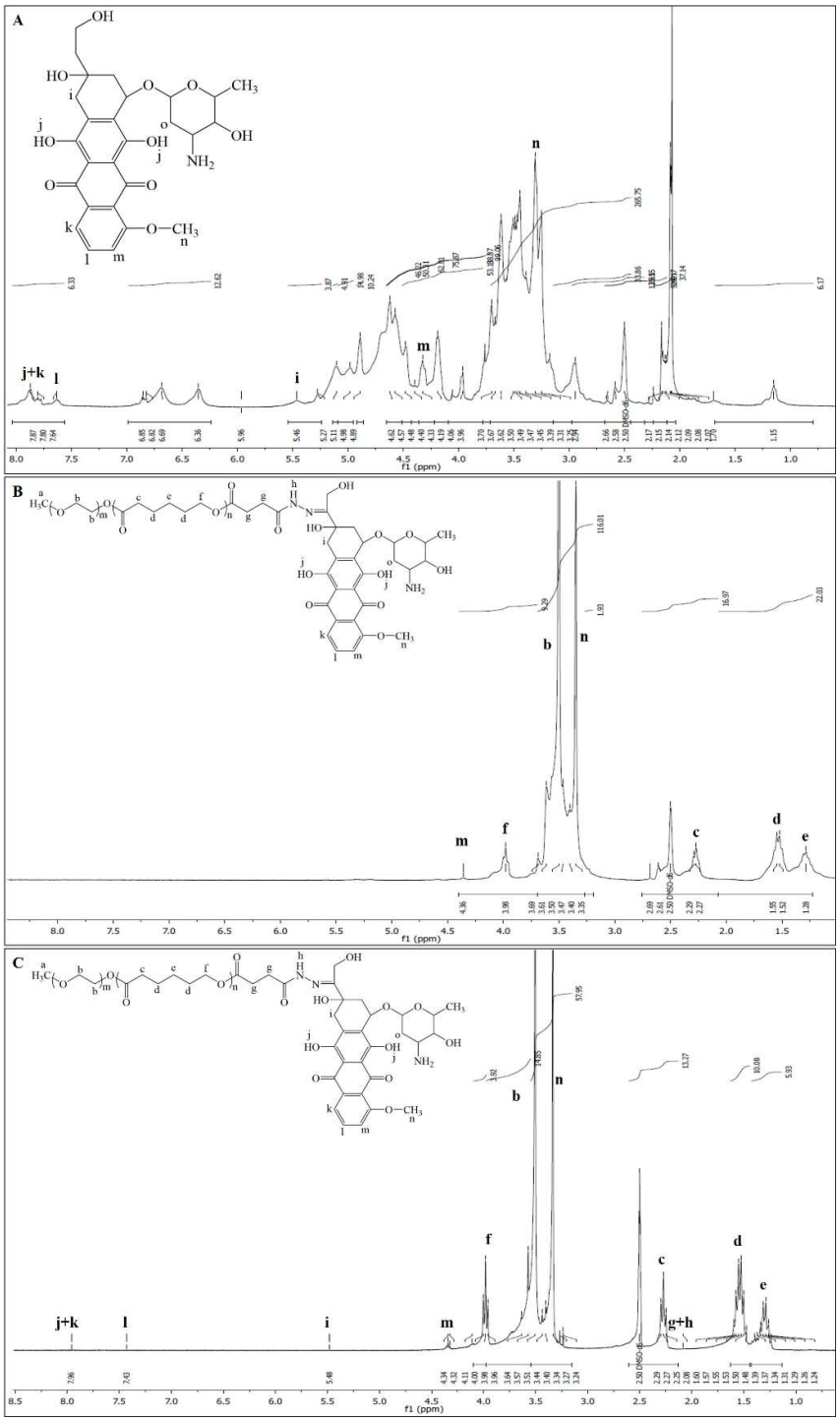

Figure 3.10. ^{1}H NMR spectra of A) DOX in $CDCl_3$, B) mPEG-b-PCL-CO-NH-N-DOX with DMSO method in DMSO-d6, and C) mPEG-b-PCL-CO-NH-N-DOX with MeOH-TFA method in DMSO-d6.

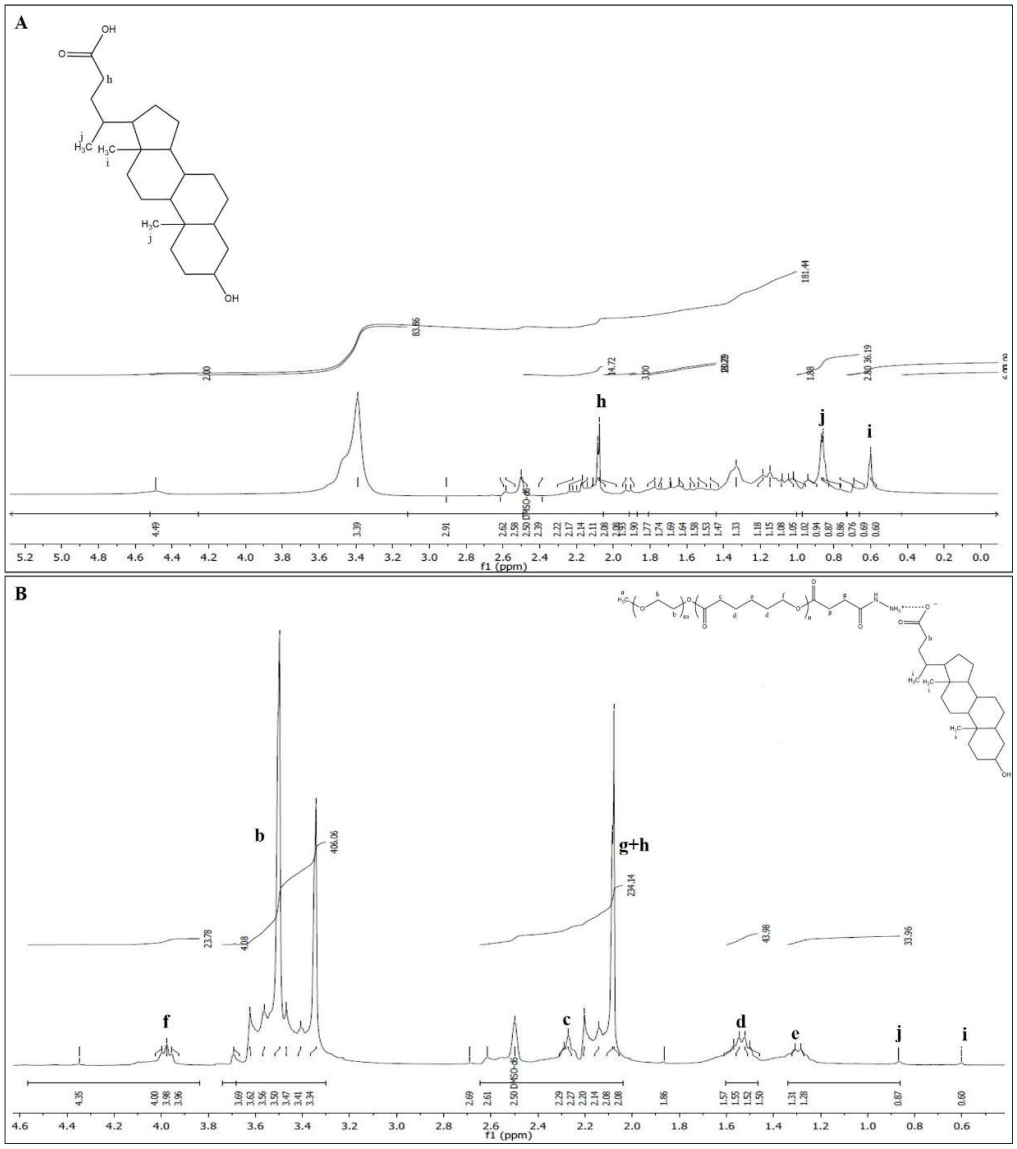

Figure 3.11. ^{1}H NMR spectra of A) LCA in $CDCl_3$, and B) mPEG-b-PCL-CO-NH-N_2**LCA salt in DMSO-d6.

To determine hydrazide functionalization in the mPEG-b-PCL-CO-NH-NH_2 polymer, colorimetric primary amine detection assay was conducted. The hydrazide amount in mPEG-b-PCL-CO-NH-NH_2 polymer was calculated and found as 45.6 mol% (100 mol polymer contains 45.6 mol -NH_2 group (hydrazide group)). Similary, other studies used the same TNBSA assay to determine hydrazide groups in the polymer and found as 8.2 mol%, 5.6 mol%, and 63 mol%, respectively (del Rosario

et al., 2010; Etrych et al., 2001, 2014). This means that the obtained hydrazide functionalization was within the acceptable limits. It is even better than the studies of Etrych et al. (Etrych et al., 2001, 2014).

DOX was conjugated to mPEG-b-PCL-CO-NH-NH_2 copolymer either in DMSO or in MeOH-TFA solutions. The DOX contents of the DOX-copolymer conjugates were determined spectroscopically with two different methods: 1. dissolution of the polymer-drug conjugates in Ch:MeOH (1:1); 2. breaking the pH sensitive bonds between the polymer and the drug using three different acidic media (HCl (0.1 M), HCl (12 M) and H_2SO_4 (18.3 M)). The results demonstrated that, MeOH-TFA was better than the DMSO for the conjugation of DOX, since the amount of DOX conjugation was found to be higher. Meanwhile, when two methods were compared, the results obtained for Ch:MeOH (1:1) and HCl (0.1 M) in DMSO media did not show any significant difference (Table 3.4 and Table 3.5). On the other hand, when the medium was changed to MeOH:TFA, a significant difference between Ch:MeOH (1:1) and HCl (0.1 M) was observed. This shows that, using acidic media to determine the conjugation content and conjugation efficiency resulted in higher amount of conjugation. In the second method, acidity of the media was changed to compare the conjugation efficiencies, and stronger acids were used. H_2SO_4 (18.3 M) method resulted in higher DOX amount than the ones obtained for HCl (0.1 M) and HCl (12 M) methods (Table 3.4 and Table 3.5) (Isik et al., 2021). In the literature, there are also DOX conjugations via hydrazone bond. del Rosario et al. (2010) found DOX conjugation efficiency to hydrazide group in amphiphilic copolymers as 6.5% (del Rosario et al., 2010). Etrych et al. (2001, 2014) used N-(2-hydroxypropyl) methacrylamide polymer to conjugate DOX via hydrazone bond, and reported 12 wt%, and 9 wt% conjugation in two different studies (Etrych et al., 2001, 2014). The reported values were lower than the ones we found in our study. That might be because of the differences of the polymers used.

It is highly possible that DOX can degrade in H_2SO_4 but calibration curve of free DOX in H_2SO_4 shows that R^2 is 0.9936 which means that even if the DOX is degraded in H_2SO_4 we can still measure it. Thus, we assumed that degradation

products of DOX gave max absorption at 543 nm (Isik et al., 2021). It is known that DOX is not stable in solutions with a pH less than 3; DOX breaks up into a red-colored, water insoluble aglycone (adriamycinone) and a water soluble, reducing amino sugar (daunosamine) (National Center for Biotechnology Information, 2022). For example, treatment of DOX with mild acids (e.g. 1 N HCl) selectively cleaves the glycosidic bond between the aglycone and the sugar group components. Thus, quantification of conjugated DOX after mild acid hydrolysis is based on released adriamycinone component (Configliacchi et al., 1996).

Table 3.4. DOX conjugation content on copolymer synthesized.

Conjugation Media*	**Conjugation contents (µg DOX/mg polymer)***			
	Ch:MeOH (1:1) Method	HCl (0.1 M) Method	HCl (12 M) Method	H_2SO_4 (18.3 M) Method
DMSO, at 30°C	1.91 ± 0.01	2.08 ± 0.05	3.24 ± 0.14[a]	3.93 ± 0.12[a]
MeOH-TFA, at 60°C	4.15 ± 0.03[b]	6.45 ± 0.10[b]	7.99 ± 0.05[b]	12.87 ± 0.07[b]

* n=3, [a] shows the significant differences between conjugation content of DMSO media, [b] shows the significant differences between conjugation content methods of MeOH-TFA media.

Table 3.5. DOX conjugation efficiencies.

Conjugation Media*	**Conjugation efficiencies found with different methods (%)***			
	Ch:MeOH (1:1) Method	HCl (0.1 M) Method	HCl (12 M) Method	H_2SO_4 (18.3 M) Method
DMSO, at 30°C	4.59 ± 0.03	5.00 ± 0.13	7.77 ± 0.33[a]	9.44 ± 0.29[a]
MeOH-TFA, at 60°C	11.61 ± 0.09[b]	18.05 ± 0.27[b]	22.36 ± 0.14[b]	36.04 ± 0.20[b]

* n=3, [a] shows the significant differences between conjugation content of DMSO media, [b] shows the significant differences between conjugation content methods of MeOH-TFA media.

In order to determine the LCA content in the mPEG-b-PCL-CO-NH-NH_2**LCA, the salt was dissolved in concentrated sulfuric acid since it is a good solvent for both, mPEG-b-PCL-CO-NH-NH_2 and LCA (Appendix F1 Figure 1). The amount of LCA was found as 26.63 ± 0.20 µg LCA/mg mPEG-b-PCL-CO-NH-NH_2**LCA.

3.4 Critical Micelle Concentration of mPEG-b-PCL Copolymers, mPEG-b-PCL-CO-NH–NH_2 Copolymers, and DOX Conjugated Copolymers

After administration of micelles into the body, they should remain their form until reaching the target site and if the micellar formulation is above its CMC, it means that micellar formulation will protect its form in the body. Therefore, stability of micelles is verified by measuring their critical micelle concentration (CMC). Pyrene is a fluorescent probe and used to determine CMC of micellar formulations. Pyrene is hydrophobic and due to its hydrophobicity pyrene locates in the hydrophobic domain of the micelles. Upon the formation of micelles, excitation wavelength of pyrene changes from 333 nm to 338 nm and the fluorescence intensity ratio at 338 nm and 333 nm (I_{338}/I_{333}) was plotted against the logarithm of polymer concentration (Mohanty et al., 2015). Our polymer had a 33:67 ratio of hydrophilic to hydrophobic block length and CMC values of mPEG-b-PCL polymers, mPEG-b-PCL-CO-NH-NH_2 copolymers, and DOX conjugated mPEG-b-PCL-CO-NH-NH_2 copolymers were found as 14.1×10^{-3} mg/mL, 9.8×10^{-3} mg/mL, and $7.1\times10_{-3}$ mg/mL, respectively (Figure 3.12). At low concentrations, the intensity ratio did not change and when the polymer concentration reached to CMC value, which shows the formation of micelles, the intensity ratio increases. The CMC value is affected by the hydrophilic-hydrophobic proportion of the polymer and increases with increasing hydrophilic block length. Increase in CMC value decreases the stability of micellar formulations. Similar results were reported in the literature. Mohanty et al. (2015) synthesized mPEG-b-PCL copolymers with different ratios of hydrophilic to hydrophobic block lengths (80:20, 60:40, 40:60, and 20:80). The CMC values were found as 8.2×10^{-3} mg/mL, 5.9×10^{-3} mg/mL, 4.8×10^{-3} mg/mL, and 3.9×10^{-3} mg/mL, respectively

(Mohanty et al., 2015). Shuai et al. (2004) also synthesized mPEG-b-PCL copolymers with different ratios of hydrophilic to hydrophobic block lengths (50:50, and 17:83). The CMC values were found as 20×10^{-3} mg/mL, and 12×10^{-3} mg/mL, respectively (Shuai et al., 2004). In our copolymers, hydrophilic to hydrophobic block length ratio was 33:67, and the detected CMC is acceptable.

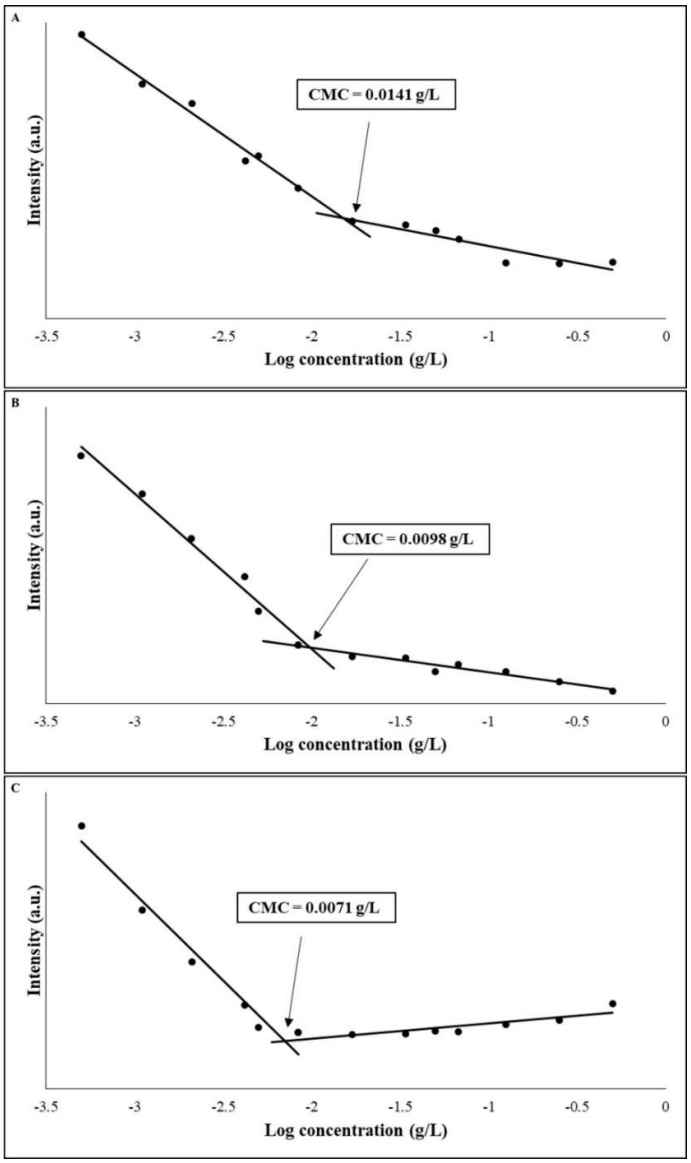

Figure 3.12. Plot of intensity ratio (I_{338}/I_{333}) of the excitation spectra of pyrene against log concentration of A) mPEG-b-PCL copolymers, B) mPEG-b-PCL-CO-NH-NH_2 copolymers, and C) DOX conjugated copolymers.

3.5 Optimization of Preparation Parameters for Micelles

Micelles were prepared by applying co-solvent evaporation method either with sonication or without sonication in order to optimize the preparation parameters, which are described in the following sections.

3.5.1 Co-Solvent Evaporation Method with Sonication

LCA loaded micelles obtained by co-solvent evaporation method with sonication of mPEG-b-PCL-CO-NH-NH_2**LCA mixture (at 60°C) prepared in a solution either with THF or acetone and different amounts of PVA. The micelles obtained were characterized by measuring their hydrodynamic diameter and zeta potential. Table 3.6 shows hydrodynamic diameters, zeta potentials and polydispersity index of the micelles. Figure 3.13 shows the size distribution of micelles.

Table 3.6. Hydrodynamic diameters, zeta potentials and polydispersity index of LCA loaded micelles (at 60°C) prepared by co-solvent evaporation method with sonication.

Experiments	Size (Z-average, nm)	Zeta potential (mV)	Polydispersity index (PDI)
0.5% PVA – THF	527.4	-3.56	0.457
0.75% PVA – THF	181.6	-22.8	0.301
1% PVA – THF	2210	-21.2	1.000
1.5% PVA – THF	4523	-6.81	1.000
2% PVA – THF	5037	-6.08	1.000
0.5% PVA – acetone	5589	0.594	1.000
0.75% PVA – acetone	255.4	-16.9	0.374
1% PVA – acetone	625.3	-18	0.633
1.5% PVA – acetone	2335	-5.37	1.000
2% PVA – acetone	1123	-4.21	0.807

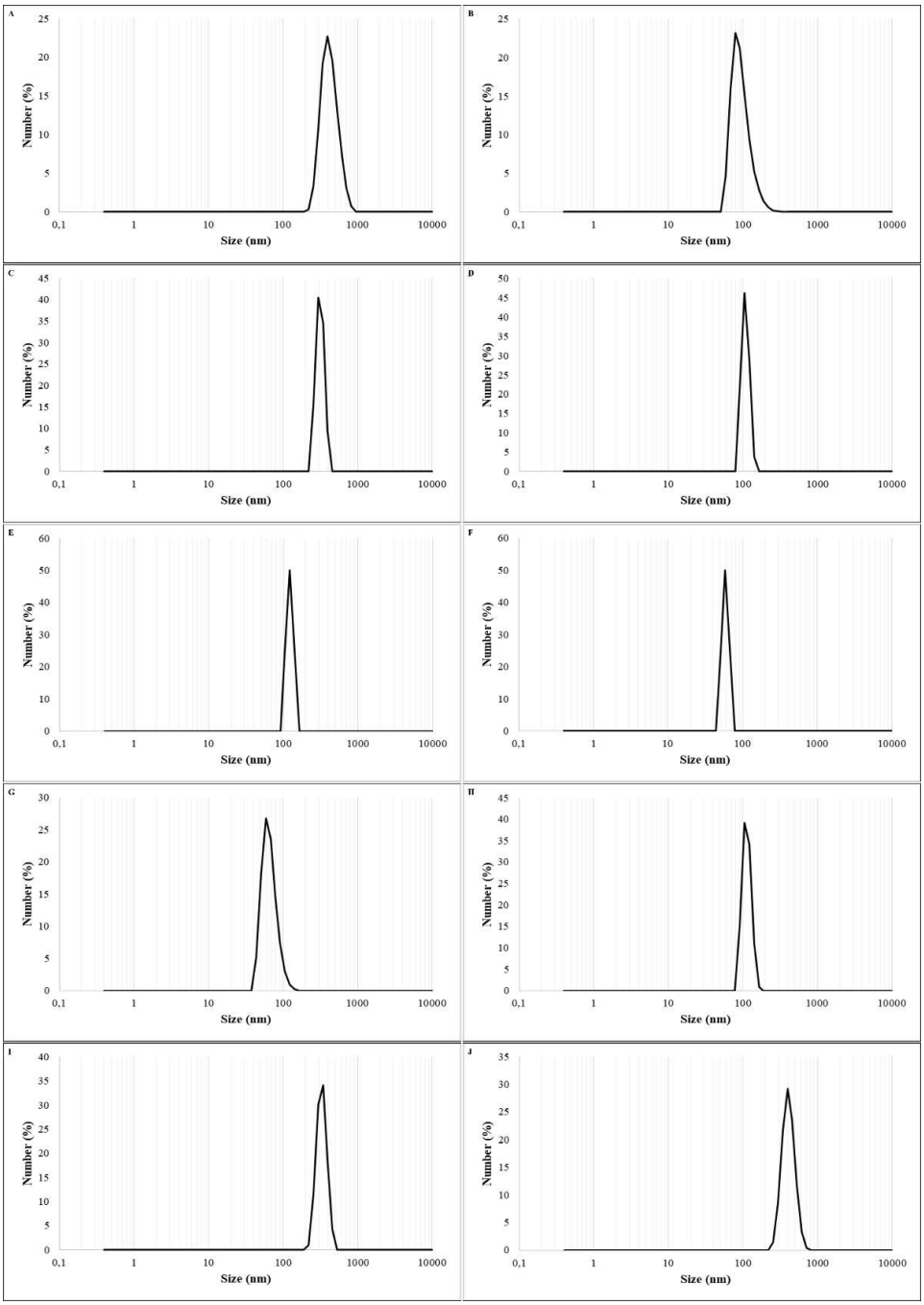

Figure 3.13. Size distribution of LCA loaded micelles (at 60°C) prepared with A) 0.5% PVA – THF, B) 0.75% PVA – THF, C) 1% PVA – THF, D) 1.5% PVA – THF, E) 2% PVA – THF, F) 0.5% PVA – acetone, G) 0.75% PVA – acetone, H) 1% PVA – acetone, I) 1.5% PVA – acetone, and J) 2% PVA – acetone.

It is the zeta potential value and polydispersity index, which determine the stability of micelle solutions (Owen et al., 2012). Most of the micelle suspensions had high zeta potential values (between -16.9 mV and -22.8 mV for 0.75% PVA and 1% PVA groups, see Table 3.6). However, polydispersity index of all suspensions were quite high. Although their size distributions were narrow, their average hydrodynamic diameters were large and this resulted in high PDI. Therefore, micelle preparation method was changed to obtain better polydispersity index, zeta potential and hydrodynamic diameter values.

3.5.2 Co-Solvent Evaporation Method without Sonication

Co-solvent evaporation method without sonication was applied to both, LCA conjugated and DOX conjugated micelles.

3.5.2.1 Co-Solvent Evaporation Method without Sonication for the Preparation of LCA Conjugated Micelles

In this method, micelles were prepared using mPEG-b-PCL-CO-NH-NH_2**LCA copolymer (at 60°C), by co-solvent evaporation method, but no sonication was applied. Table 3.7 shows hydrodynamic diameters, zeta potentials and polydispersity index values and Figure 3.14 shows the size distribution chart of the micelles obtained.

Table 3.7. Hydrodynamic diameters, zeta potentials and polydispersity index of LCA_{60}**M prepared by co-solvent evaporation method without sonication (n=3).

Experiments	Size (Z-average, nm)	Zeta potential (mV)	Polydispersity index (PDI)
Water – acetone	101.7 ± 4.3	-5.42 ± 1.74	0.159
1% PVA – acetone	86.9 ± 0.3	-7.54 ± 2.16	0.085
1.5% PVA – acetone	89.9 ± 6.8	-9.02 ± 1.98	0.332
2% PVA – acetone	102.9 ± 13.1	-9.12 ± 3.72	0.355

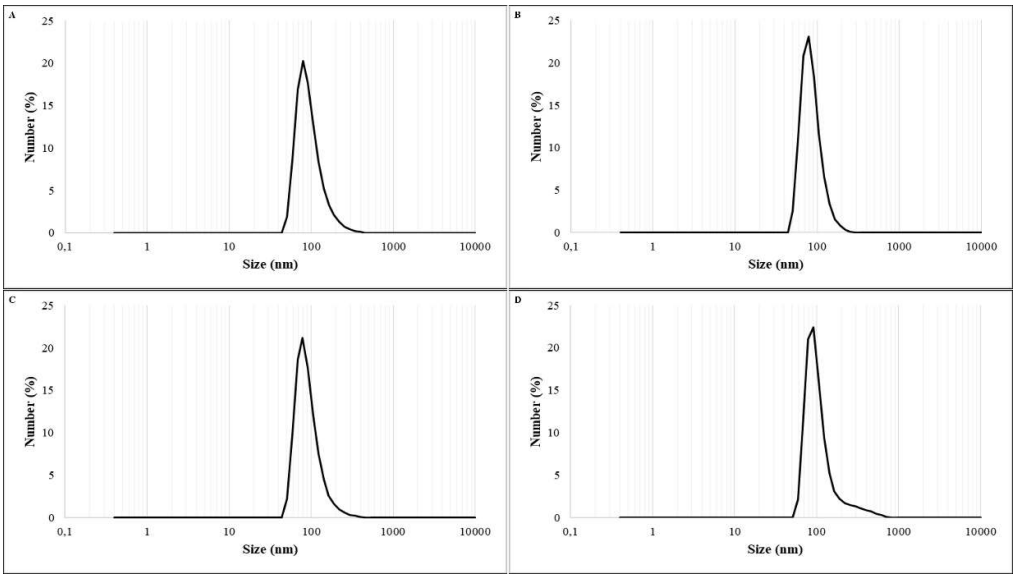

Figure 3.14. Size distribution charts of LCA_{60}**M prepared with A) water – acetone, B) 1% PVA – acetone, C) 1.5% PVA – acetone, and D) 2% PVA – acetone.

Polydispersity index of the micelles prepared without sonication was lower than the micelles prepared with sonication method. Hydrodynamic diameters were also smaller than those prepared with the previous method. Therefore, this method was chosen to prepare micelles having LCA and DOX conjugations.

PVA is a surfactant and used to increase micelle stability. PDI value increased up to 0.355 when PVA concentration was increased to 2%. When water was used instead of 1% PVA, the size, zeta potential and PDI values of LCA_{60}**M increased. When 1% PVA was used to prepare micelles, PDI was very low (0.085), a uniform size distribution chart could be obtained with an average hydrodynamic diameter of 86.9 ± 0.3 nm. Its zeta potential was also higher than micelles prepared with water. 1% PVA gives better results compared to water since PVA is a surfactant and provides micelle stability during preparation (Şengel Türk et al., 2009; Xiao et al., 2013). Therefore, these conditions were chosen for micelle preparation.

LCA_{25}**M was also prepared with the same method using 1% PVA. Table 3.8 shows hydrodynamic diameter, zeta potential and polydispersity index value and Figure 3.15 shows the size distribution chart of the micelles obtained.

Table 3.8. Hydrodynamic diameters, zeta potentials and polydispersity index of LCA_{25}**M prepared by co-solvent evaporation method without sonication (n=3).

Experiments	Size (Z-average, nm)	Zeta potential (mV)	Polydispersity index (PDI)
1% PVA – acetone	228.2 ± 10.8	-18.83 ± 0.49	0.036

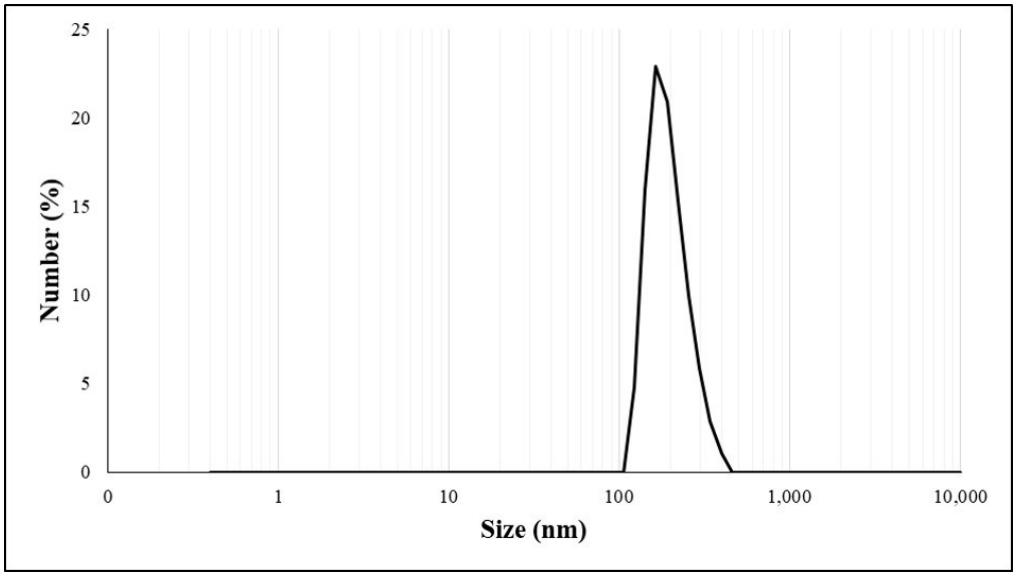

Figure 3.15. Size distribution chart of LCA_{25}**M prepared with 1% PVA – acetone.

LCA_{25}**M showed higher hydrodynamic diameter than LCA_{60}**M. On the other hand, zeta potential of LCA_{60}**M was lower than LCA_{25}**M and PDI of LCA_{25}**M was lower than LCA_{60}**M. Zeta potential results suggested that micelles prepared at 25°C was more stable than at 60°C but micelle preparation at 25°C results in bigger micelles than at 60°C.

The encapsulation efficiencies and drug loading capacities of micelles were calculated (Table 3.9). LCA_{60}**M prepared with water-acetone showed significantly higher encapsulation efficiency and drug loading capacity than LCA_{60}**M prepared with 1% PVA-acetone. LCA_{60}**M prepared with 2% PVA-acetone showed significantly higher encapsulation efficiency and drug loading capacity than LCA_{60}**M prepared with 1% PVA-acetone. LCA_{25}**M prepared with 1% PVA-acetone showed higher encapsulation efficiency than LCA_{60}**M but their drug loading capacities were similar.

Table 3.9. Encapsulation efficiencies (EE) and drug loading capacities (DLC) of LCA_{60}**M and LCA_{25}**M (n=3).

Experiments	**LCA_{60}**M**		**LCA_{25}**M**	
	EE (%)	**DLC (%)**	**EE (%)**	**DLC (%)**
Water – acetone	63.58 ± 2.49^{a}	6.54 ± 0.52	-	-
1% PVA – acetone	$52.90 \pm 1.13^{a,b}$	7.18 ± 1.25	95.19 ± 4.66	6.21 ± 0.30
1.5% PVA – acetone	58.44 ± 4.44	6.41 ± 0.85	-	-
2% PVA – acetone	65.34 ± 5.95^{b}	6.80 ± 0.12	-	-

a, and b indicate statistically significant groups ($p<0.05$).

3.5.2.2 Co-Solvent Evaporation Method without Sonication for the Preparation of DOX Conjugated Micelles (DOX_{conj}-M) and DOX Loaded Micelles (DOX_{ld}-M)

DOX_{conj}-M obtained by co-solvent evaporation method without sonication from DOX conjugated copolymers were also characterized with hydrodynamic diameters and zeta potentials. Table 3.10 shows hydrodynamic diameters, zeta potentials and polydispersity index. Figure 3.16 shows the size distribution chart of micelles.

Table 3.10. Hydrodynamic diameters, zeta potentials and polydispersity index of DOX_{conj}-M prepared by co-solvent evaporation method without sonication (n=3).

Experiments	Size (Z-average, nm)	Zeta potential (mV)	Polydispersity index (PDI)
Water – acetone	165.3 ± 34.9	-1.04 ± 0.49	0.204
1% PVA – acetone	121.6 ± 16.3	-6.61 ± 1.49	0.206
1.5% PVA – acetone	120.2 ± 21.1	-2.61 ± 0.01	0.548
2% PVA – acetone	123.5 ± 23.9	-1.47 ± 0.55	0.741

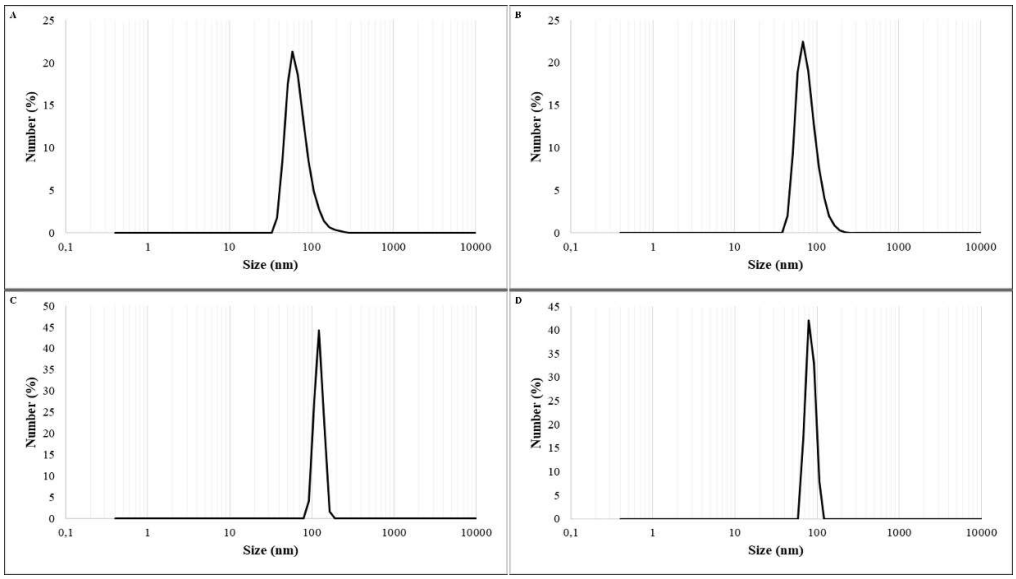

Figure 3.16. Size distribution charts of DOX_{conj}-M prepared with A) water – acetone, B) 1% PVA – acetone, C) 1.5% PVA – acetone, and D) 2% PVA – acetone.

When PVA concentration was higher than 1%, PDI of DOX_{conj}-M increased and zeta potential decreased. When water was used instead of 1% PVA, zeta potential of DOX_{conj}-M decreased because PVA is a surfactant and it is used to form more stable nanoparticles while preparation and higher zeta potential means more stable micelles (Şengel Türk et al., 2009; Xiao et al., 2013). When 1% PVA was used to prepare micelles, PDI was low (0.206) and a uniform size distribution chart was obtained

with an average hydrodynamic diameter of 86.9 ± 0.3 nm. Its zeta potential was also higher than micelles prepared with water, 1.5% PVA, and 2% PVA.

DOX_{ld}-M obtained by co-solvent evaporation method without sonication using 1% PVA were also characterized with hydrodynamic diameters and zeta potentials. Table 3.11 shows hydrodynamic diameter, zeta potential and polydispersity index. Figure 3.17 shows the size distribution chart of micelles.

Table 3.11. Hydrodynamic diameters, zeta potentials and polydispersity index of DOX_{ld}-M prepared by co-solvent evaporation method without sonication (n=3).

Experiments	Size (Z-average, nm)	Zeta potential (mV)	Polydispersity index (PDI)
1% PVA – acetone	265.3 ± 25.60	-10.75 ± 0.78	0.353

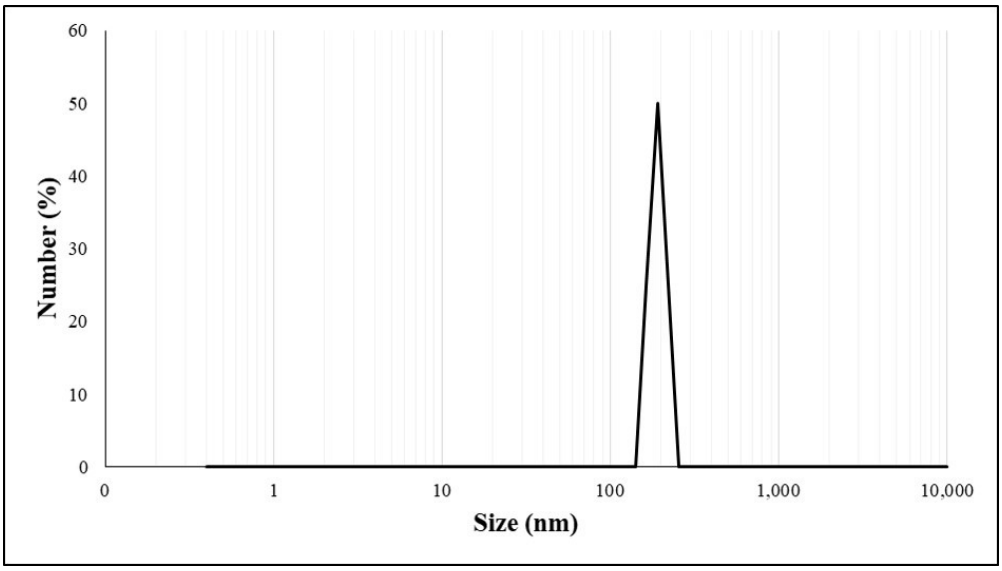

Figure 3.17. Size distribution chart of DOX_{ld}-M prepared with 1% PVA – acetone.

DOX_{ld}-M showed higher hydrodynamic diameter than DOX_{conj}-M. On the other hand, zeta potential of DOX_{conj}-M was lower than DOX_{ld}-M. These results suggested that drug loading forms more stable micelles than conjugated ones.

The encapsulation efficiencies and drug loading capacities of micelles were calculated (Table 3.12). DOX_{conj}-M prepared with water-acetone showed significantly lower drug loading capacity than DOX_{conj}-M prepared with 1%, 1.5%, and 2% PVA-acetone. Although some values were higher than the ones prepared by co-solvent evaporation method without sonication method using 1% PVA, due to low PDI and high zeta potential of the latter one, that method was chosen for further studies. Micelle stability is affected by micelle preparation method (Hussein & Youssry, 2018) and so this affects the drug loading capacities of micelles. This may cause the lower drug loading capacity when water is used. Loading of DOX also decreased the drug loading capacity compared to DOX_{conj}-M. This also shows that micelle characteristics is affected by the micelle preparation technique. Moulahoum et al. (2022) synthesized carboxylic acid terminated mPEG-b-PCL copolymers and DOX loading was done. They achieved 38% EE for DOX with a hydrodynamic diameter of 145.6 nm (PDI = 0.386) and zeta potential of -37.2 mV (Moulahoum et al., 2022). DOX_{conj}-M is smaller and DOX_{ld}-M is bigger in size compared to those reported in the literature. Zeta potential of DOX_{conj}-M and DOX_{ld}-M was lower than the literature. This may be due to the differences in the copolymer. For example, the copolymer synthesized by Moulahoum et al. (2022) was 2510 Da (Moulahoum et al., 2022) while the copolymer in this study was 16 kDa. But encapsulation efficiency of DOX_{ld}-M was found higher than those reported in the literature.

Table 3.12. DLC of DOX_{conj}-M and DOX_{ld}-M an EE of DOX_{ld}-M (n=3).

Experiments	**DOX_{conj}-M**	**DOX_{ld}-M**	
	DLC (%)	**EE (%)**	**DLC (%)**
Water – acetone	8.24 ± 2.60^{x}	-	-
1% PVA – acetone	13.54 ± 1.13	83.32 ± 4.54	8.62 ± 0.47
1.5% PVA – acetone	13.71 ± 1.94	-	-
2% PVA – acetone	13.82 ± 1.79	-	-

^{x} indicate statistically significant sand lowest group ($p<0.05$).

Both LCA_{60}**M and DOX_{conj}-M showed good results in hydrodynamic diameter, zeta potential, and PDI when they were prepared with 1% PVA compared to water, 1.5% PVA, and 2% PVA.

3.5.2.3 Co-Solvent Evaporation Method without Sonication for the Preparation of DOX and LCA Loaded Micelles (DL-M)

DL-M obtained by co-solvent evaporation method without sonication were also characterized with hydrodynamic diameters and zeta potentials. Table 3.13 shows hydrodynamic diameter, zeta potential and polydispersity index. Figure 3.18 shows the size distribution chart of micelles. The encapsulation efficiencies and drug loading capacities of micelles were also calculated (Table 3.14).

Table 3.13. Hydrodynamic diameters, zeta potentials and polydispersity index of DL-M prepared by co-solvent evaporation method without sonication (n=3).

Experiments	Size (Z-average, nm)	Zeta potential (mV)	Polydispersity index (PDI)
1% PVA – acetone	162.5 ± 15.9	-6.34 ± 0.89	0.502

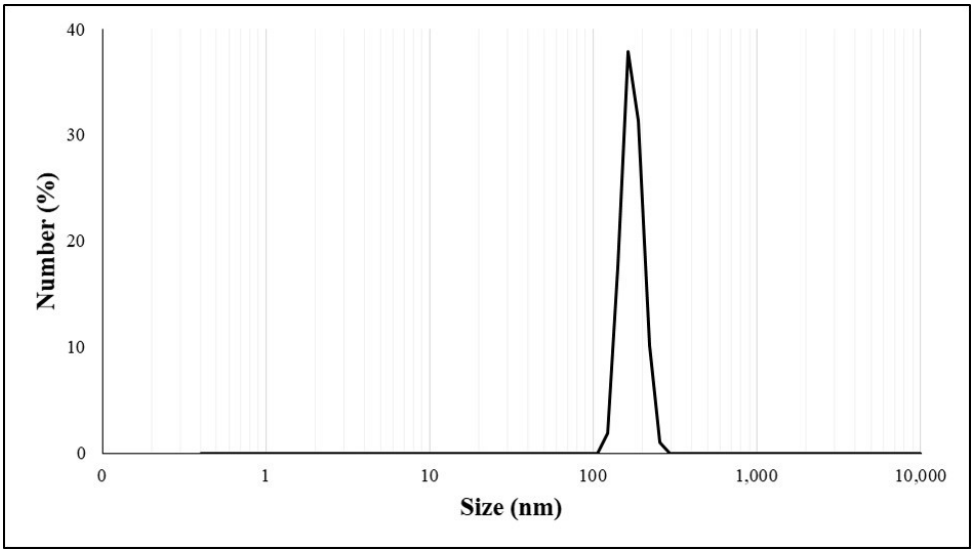

Figure 3.18. Size distribution chart of DL-M prepared with 1% PVA – acetone.

Table 3.14. DLC and EE of DL-M (n=3).

Experiments	DOX		LCA	
	EE (%)	DLC (%)	EE (%)	DLC (%)
1% PVA – acetone	78.82 ± 4.52	8.76 ± 0.50	90.18 ± 9.63	10.02 ± 1.07

DL-M showed smaller hydrodynamic diameter than LCA_{25}**M and DOX_{ld}-M while lower zeta potential was observed in DL-M than LCA_{25}**M and DOX_{ld}-M which suggested that DL-M is less stable than LCA_{25}**M and DOX_{ld}-M. DOX and LCA encapsulation efficiencies of DL-M were lower than LCA_{25}**M and DOX_{ld}-M on the other hand drug loading capacities did not change.

Therefore, for further studies (as drug release and in vitro cell culture experiments) the micelles were prepared by co-solvent evaporation method without sonication method using 1% PVA. Figure 3.19 shows TEM images of micelles obtained by co-solvent evaporation method without sonication. Results showed that LCA_{60}**M and LCA_{25}**M forms uniform, round micelles. LCA_{60}**M forms more uniform micelles compared to DOX_{conj}-M because there are some small and big micelles in DOX_{conj}-M group. DOX_{ld}-M seems more uniform than DOX_{conj}-M and there was no difference in the shape of LCA_{25}**M and DOX_{ld}-M but DOX_{ld}-M was smaller than LCA_{25}**M. On the other hand, DL-M formed uniform and smallest micelles among the groups.

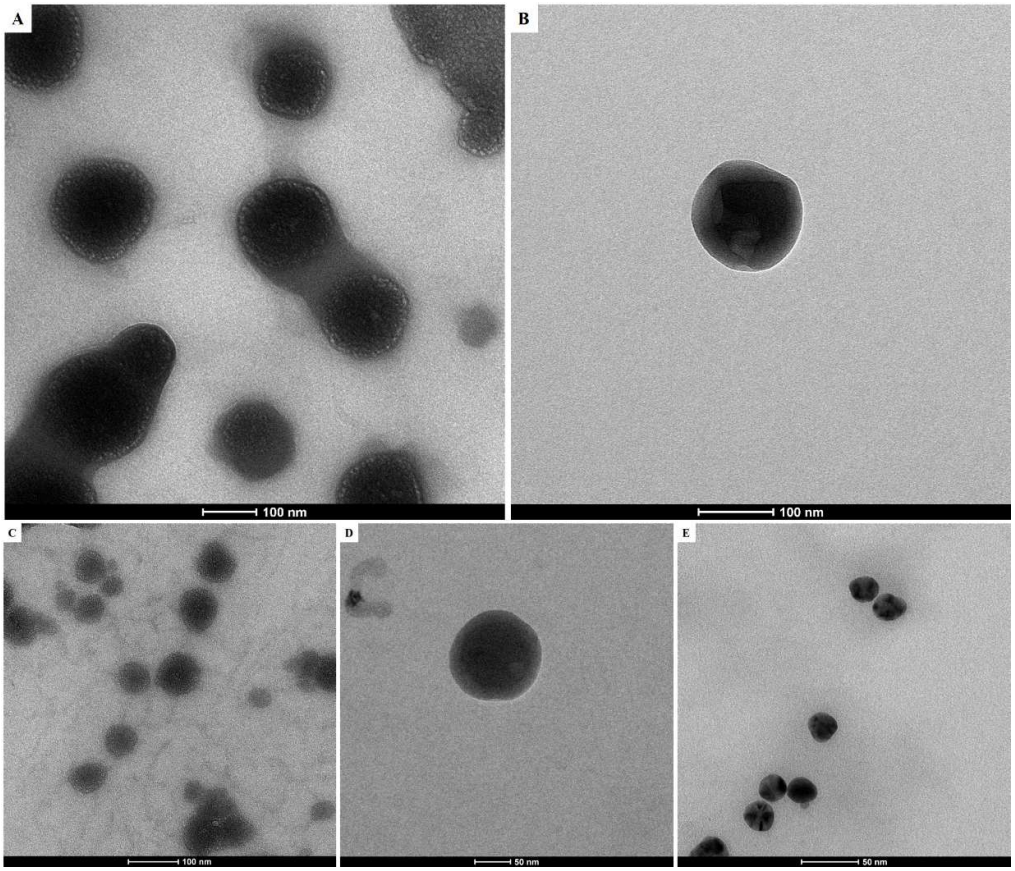

Figure 3.19. TEM images of A) LCA_{60}**M, B) LCA_{25}**M, C) DOX_{conj}-M, D) DOX_{ld}-M, and E) DL-M prepared by co-solvent evaporation method without sonication using 1% PVA as water phase.

3.6 Release Studies

Cancer cells prefer glycolysis rather than oxidative ATP production in order to provide the required ATP quickly. This results in hypoxia in the tumor microenvironment. The pH of the tumor microenvironment, endosomes and lysosomes are 6.5-7.2, 5.0-6.5 and 4.5-5.0, respectively. Therefore, release studies are carried out in different media having different pH to simulate the tumor microenvironment, endosomes and lysosomes, respectively (Yi Li et al., 2019).

3.6.1 Release of LCA from LCA_{60}**M and LCA_{25}**M

Release studies showed that under acidic conditions LCA release rate was higher from both micelles, LCA_{60}**M and LCA_{25}**M, due to the breaking of electrostatic interactions between LCA and the copolymer (Figure 3.20). There was no significant difference between the drug release profiles of physiological and acidic release conditions till 5 hours for LCA_{60}**M, but after 5 hours, the LCA release rate significantly increased in medium at pH 5 compared to other release media ($p<0.05$). The release rate was significantly faster at pH 6.8 and pH 5 than that of at pH 7.4 ($p<0.05$). On the other hand, there was no significant difference between the drug release profiles of physiological and acidic release conditions till 4 hours for LCA_{25}**M, but after 4 hours, the LCA release rate significantly increased in medium at pH 5 and pH 6.8 compared to physiological conditions ($p<0.05$). The release rate was significantly faster at pH 6.8 and pH 5 than that of at pH 7.4 ($p<0.05$). There was no significant difference between the drug release profiles at pH 5.0 and pH 6.8 till 8 hours for LCA_{25}**M, but after 8 hours, the LCA release rate significantly increased in medium pH 5.0 compared to pH 6.8 ($p<0.05$).

Meanwhile, LCA release rate was lower compared to the free drug for both micelles, indicating an electrostatic interaction between LCA and the copolymers. Similar results showing fast release at low pH from the nanoparticles with electrostatic interaction between the drug and the polymer in acidic media were reported in literature. For example, Su et al. (2021) conjugated DOX to carbon dots via electrostatic interaction and then extracellular vesicles were loaded with DOX conjugated carbon dots. Electrostatic interaction was used to avoid early burst drug release. They reported that at pH 7.4, DOX stayed in the inner core of the extracellular vesicles due to electrostatic interaction between DOX and carbon dots. On the other hand, at pH 5.0, DOX was released from the vesicles due to electrorepulsion between DOX and carbon dots (R. Su et al., 2021). Similarly, Cha et al. (2009) prepared paclitaxel loaded mPEG-b-oligo(l-aspartic acid)-b-PCL micelles. Aspartic acid was used to form ionically stable micelles. Ionically stable

micelles showed slower drug release compared to unstable micelles at pH 7.4. They observed 45% of paclitaxel was released from ionically stable micelles after 24 h (Cha et al., 2009).

In our study, after 24 hours, 46% of LCA was released from the LCA_{60}**M and 52% of LCA was released from the LCA_{25}**M under physiological conditions while 78% of LCA was released from the LCA_{60}**M and 77% of LCA was released from the LCA_{25}**M under acidic conditions (pH 5.0). Similar release behavior was observed under similar conditions with the literature. Meanwhile, after 48 hours, 48% and 87% of LCA were released from LCA_{60}**M and 54% and 84% of LCA were released from LCA_{25}**M in media at physiological pH and acidic pH (5.0), respectively. After 4 days, the amount of LCA released was 100% at pH 5.0 for both micelles, while it was 83% from LCA_{60}**M and 85% from LCA_{25}**M at pH 6.8 and only 52% from LCA_{60}**M and 60% from LCA_{25}**M at pH 7.4. These results showed that LCA release was faster in acidic media and the data found is similar to the findings reported in the literature. Results showed that micelle preparation did not affect the release profile of LCA under physiological and acidic conditions. It was expected that release should be faster in acidic conditions due to breakage of electrostatic interactions between the polymer and LCA in acidic media and results from both micelles showed that behavior so results suggested that pH responsive drug delivery was achieved with ionic conjugation.

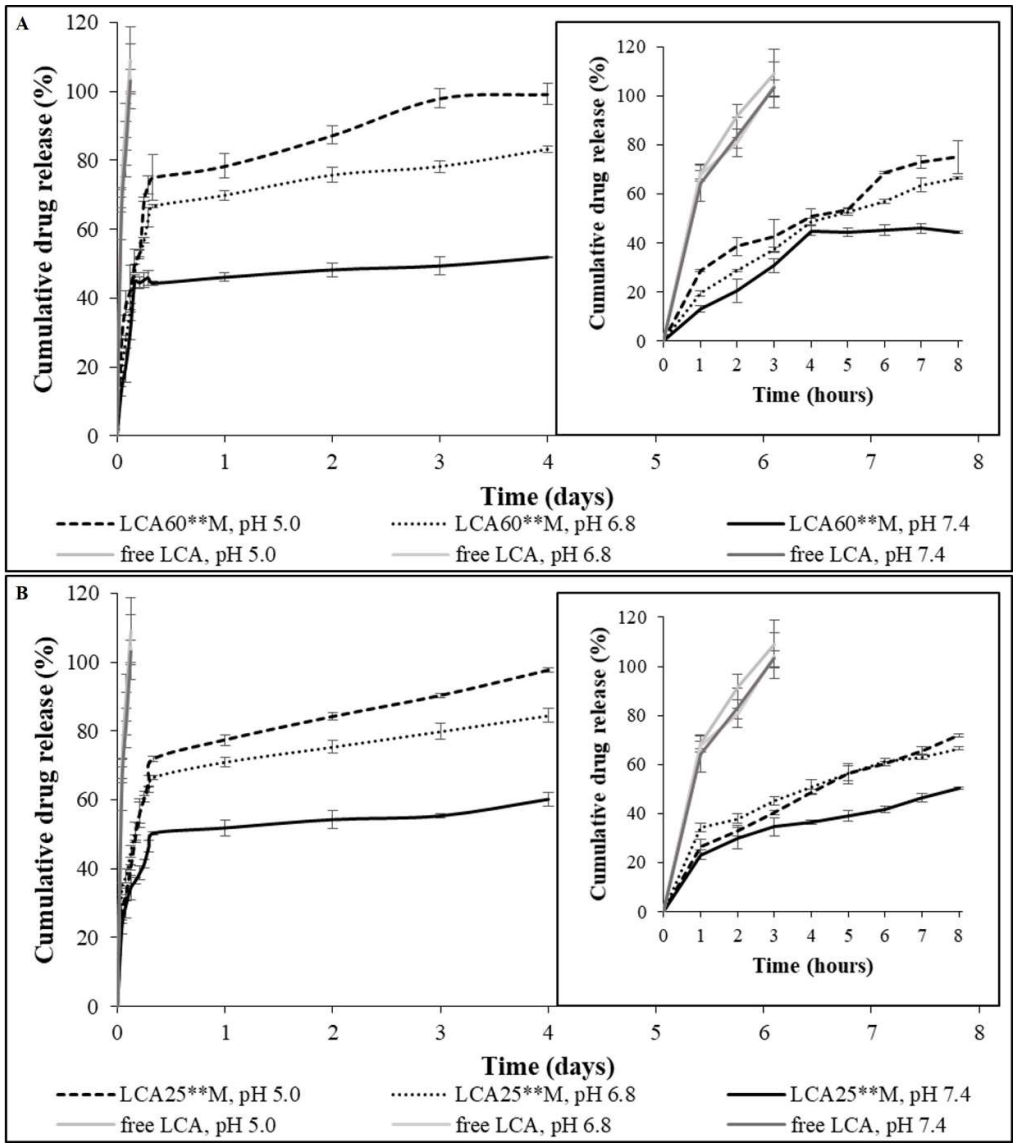

Figure 3.20. Cumulative drug release profiles from dialysis membrane of A) free LCA and LCA_{60}**M and B) free LCA and LCA_{25}**M under physiological conditions (PBS, 0.1 M and pH 7.4) and acidic conditions (CPB-pH 5.0 and CPB-pH 6.8; 0.15 M) at 37°C (n=6).

Release data were used to investigate the kinetic model that fitted best for the release profile of LCA from the micelles (zero order, first order, Higuchi model, and Korsmeyer-Peppas model). Rate constants (K_0, K_1, K_H, and K_P), n value and

coefficients of determination (R^2) are given in Table 3.15. Korsmeyer-Peppas model was found as the best fit model for drug release from both micelles at pH 7.4 (PBS, 0.1 M and pH 7.4) and at pH 6.8 (CPB, 0.15 M and pH 6.8). Meanwhile, first order model was found as the best fit model for the drug release from both micelles in acidic conditions (CPB, 0.15 M and pH 5.0).

Table 3.15. *In vitro* release kinetic parameters of LCA_{60}**M and LCA_{25}**M.

Micelles	Release Kinetic Models		pH 7.4	pH 6.8	pH 5.0
LCA_{60}M**	**Zero order**	K_0	0.430	0.611	0.674
		R^2	-1.883	-1.754	-2.944
	First order	K_1	-0.008	-0.008	-0.006
		R^2	0.793	0.811	0.958
	Higuchi model	K_H	7.713	0.074	13.567
		R^2	-0.516	0.627	0.239
	Korsmeyer-Peppas model	K_P	0.132	0.186	0.255
		n (exponent of release)	0.185	0.188	0.121
		R^2	0.979	0.980	0.865
LCA_{25}M**	**Zero order**	K_0	0.836	1.133	0.193
		R^2	-1.473	-2.166	-3.052
	First order	K_1	-0.008	-0.007	0.018
		R^2	0.682	0.740	0.921
	Higuchi model	K_H	8.730	0.067	13.444
		R^2	0.119	0.588	0.083
	Korsmeyer-Peppas model	K_P	0.231	0.362	0.477
		n (exponent of release)	0.215	0.176	-0.382
		R^2	0.932	0.9629	0.831

3.6.2 Release of DOX from DOX_{conj}-M or DOX_{ld}- M

Release studies showed that under acidic conditions DOX release rate was higher from both, DOX_{conj}-M and DOX_{ld}-M micelles (Figure 3.21). There was no significant difference between the drug release profiles of physiological and acidic release condition (pH 6.8) till 2 days for DOX_{conj}-M, but after 2 days, the DOX release rate significantly increased in medium at pH 6.8 compared to pH 7.4 resembling physiological media ($p<0.05$). The release rate was significantly faster at pH 5 than other release media after 2 hours ($p<0.05$) which showed that pH sensitive hydrazone bond breaks in acidic media and increases the drug release rate. On the other hand, there was no significant difference between the drug release profiles of physiological and acidic release conditions till 2 hours for DOX_{ld}-M, but after 2 hours, the DOX release rate significantly increased in medium at pH 5 and pH 6.8 compared to physiological conditions ($p<0.05$). There was no significant difference between the drug release profiles at pH 5.0 and pH 6.8 till 5 hours for DOX_{ld}-M, but after 5 hours, the DOX release rate significantly increased in medium pH 5.0 compared to pH 6.8 ($p<0.05$). This may be due to increasing solubility of DOX in acidic media.

Meanwhile, DOX release rate was lower compared to the free drug release from dialysis membrane for both micelles. Similar results showing fast release at low pH from the nanoparticles in acidic media were reported in literature. For example, Liao et al. (2021) conjugated DOX to poly(2-(diethylamino) ethyl methacrylate)-polypropargyl methacrylate via hydrazone bond and prepared micelles from DOX conjugated polymer. Diethylamino groups in poly(2-(diethylamino) ethyl methacrylate) become protonated in acidic environment which fastens the release of the drug. Hydrazone bond between polymer and DOX breaks in acidic environment. Therefore, they achieved a dual pH responsive with hydrazone bonded DOX and charge reversible poly(2-(diethylamino) ethyl methacrylate). Results showed that DOX release was higher at pH 5 than pH 6.8 and 7.4. After 48 h, they observed that

63.43% of DOX was released at pH 5.0, 28.48% of DOX was released at pH 6.8, and 13.18% of DOX was released at pH 7.4 (J. Liao et al., 2021).

In our study, higher burst release of DOX occurred in DOX_{ld}-M after 8 hours compared to DOX_{conj}-M. After 8 hours, the amounts of DOX released were 60% for the DOX_{conj}-M and 79% for the DOX_{ld}-M at pH 5.0 while it was 40% from the DOX_{conj}-M and 61% from the DOX_{ld}-M at pH 6.8 and only 41% from the DOX_{conj}-M and 51% from the DOX_{ld}-M at pH 7.4. Higher burst release occurred in DOX_{ld}-M compared to DOX_{conj}-M because DOX was conjugated to the polymer via hydrazone bond covalently so this decreased the release rate in DOX_{conj}-M group. On the other hand, DOX was loaded into the micelles in DOX_{ld}-M which resulted in higher burst release after 8 h. After 24 hours, 47% of DOX was released from the DOX_{conj}-M and 54% of DOX was released from the DOX_{ld}-M under physiological conditions while 62% of DOX was released from the DOX_{conj}-M and 86% of DOX was released from the DOX_{ld}-M under acidic conditions (pH 5.0). Meanwhile, after 48 hours, 52% and 64% of DOX were released from the DOX_{conj}-M and 57% and 92% of DOX were released from the DOX_{ld}-M in media at physiological pH and acidic pH (5.0), respectively. After 4 days, the amounts of DOX released were 71% for the DOX_{conj}-M and 100% for the DOX_{ld}-M at pH 5.0 while it was 64% from the DOX_{conj}-M and 91% from the DOX_{ld}-M at pH 6.8 and only 58% from the DOX_{conj}-M and 64% from the DOX_{ld}-M at pH 7.4. Qi et al. (2018) prepared DOX loaded pH sensitive micelle system with PEG-dihydrazone-PLA. Dihydrazone bond breaks in acidic environment and fastens the release of the drug. They also prepared DOX loaded PLA-PEG-PLA micelles to compare the effectiveness of dihydrazone bond in acidic conditions. Release results showed that at pH 7.4, 40% of DOX was released from PLA-PEG-PLA micelles while 38% of DOX released from PEG-Dihydrazone-PLA micelles. At pH 5, 40% of DOX released from PLA-PEG-PLA micelles while 75% of DOX released from PEG-Dihydrazone-PLA micelles. These results showed that they achieved a pH sensitive drug delivery system with dihydrazone bond (Qi et al., 2018). Similar release behavior was observed under similar conditions with the literature. Our results showed that DOX release was faster

in acidic media and DOX conjugation resulted in slower drug release compared to DOX loading. This shows that we achieved a pH sensitive drug delivery system with hydrazone bond in DOX_{conj}-M. Results showed that conjugation and loading of the drug affected the release profile of DOX under physiological and acidic conditions. It was expected that release should be faster in acidic conditions due to breakage of hydrazone bond between the polymer and DOX in acidic media and results from DOX_{conj}-M showed that behavior so results suggested that pH responsive drug delivery was achieved with hydrazone bond conjugation. DOX_{ld}-M also showed a pH sensitive behavior due to higher solubility of DOX in acidic media than physiological media.

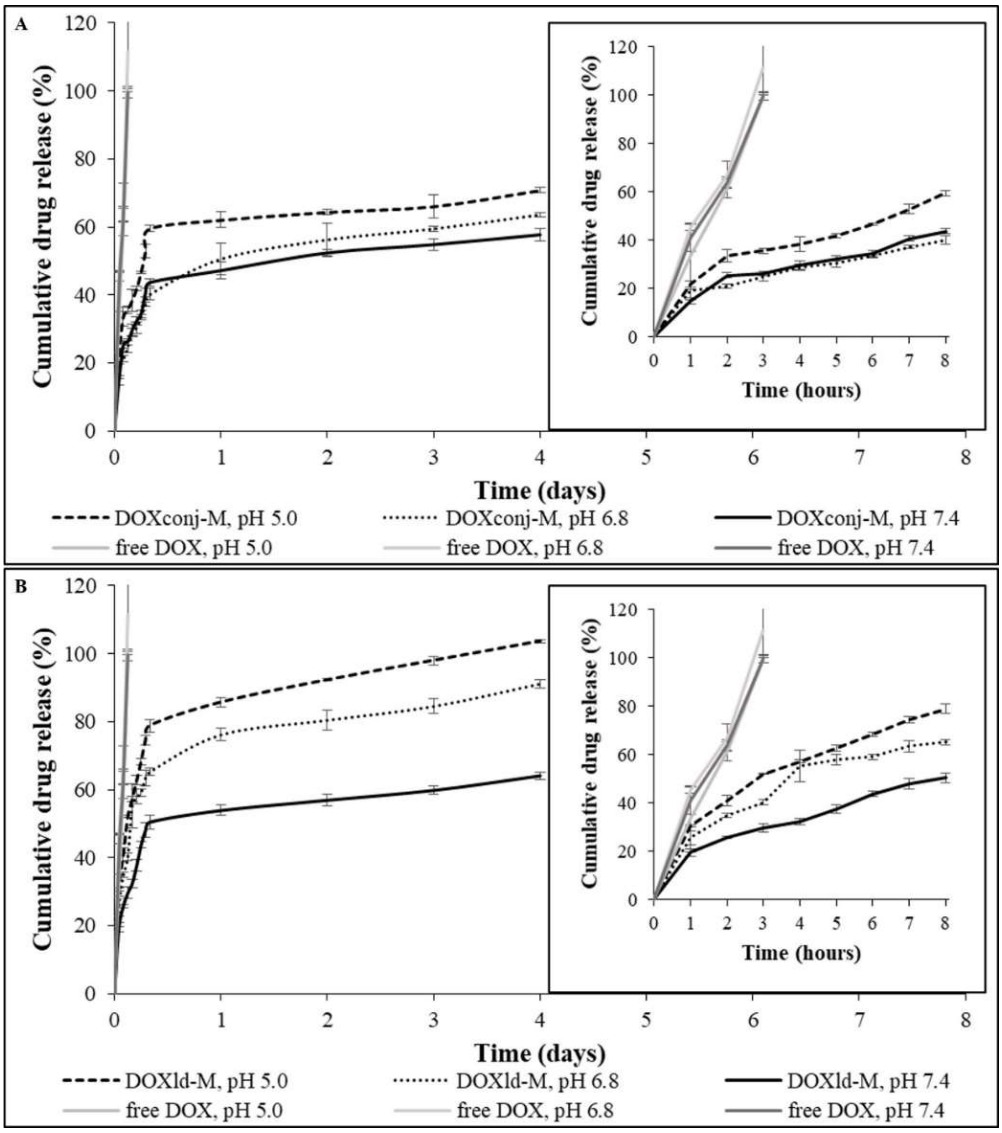

Figure 3.21. Cumulative drug release profiles from dialysis membrane of A) free DOX and DOX_{conj}-M; B) free DOX and DOX_{ld}**M under physiological conditions (PBS, 0.1 M and pH 7.4) and acidic conditions (CPB-pH 5.0 and CPB-pH 6.8; 0.15 M) at 37°C (n=6).

Release data were fitted to the different the kinetic models (zero order, first order, Higuchi model, and Korsmeyer-Peppas model) to determine the best fitted model for the release profile of DOX from the micelles. Rate constants (K_0, K_1, K_H, and K_P), n value and coefficients of determination (R^2) are given in Table 3.16. Korsmeyer-

Peppas model which shows that drug release occurs from a polymeric system was found as the best fit model for drug release from both micelles at pH 7.4 (PBS, 0.1 M and pH 7.4) and at pH 6.8 (CPB, 0.15 M and pH 6.8). Meanwhile, first order model which shows the faster drug release was found as the best fit model for the drug release from both micelles in acidic conditions (CPB, 0.15 M and pH 5.0).

Table 3.16. *In vitro* release kinetic parameters of DOX_{conj}-M and DOX_{ld}-M.

Micelles	Release Kinetic Models		pH 7.4	pH 6.8	pH 5.0
DOX_{conj}-M	**Zero order**	K_0	0.617	0.683	0.557
		R^2	-1.387	-1.741	-3.210
	First order	K_1	-0.009	-0.008	-0.006
		R^2	0.616	0.679	0.933
	Higuchi model	K_H	7.8552	0.111	9.885
		R^2	0.240	0.778	-0.028
	Korsmeyer-Peppas model	K_P	0.163	0.198	0.199
		n (exponent of release)	0.232	0.203	0.130
		R^2	0.926	0.951	0.478
DOX_{ld}-M	**Zero order**	K_0	0.739	1.012	1.140
		R^2	-1.669	-1.577	-0.794
	First order	K_1	-0.008	-0.008	-0.10
		R^2	0.612	0.598	0.919
	Higuchi model	K_H	8.791	0.069	14.225
		R^2	0.097	0.647	0.095
	Korsmeyer-Peppas model	K_P	0.208	0.278	0.254
		n (exponent of release)	0.215	0.222	0.238
		R^2	0.920	0.913	0.518

3.6.3 Release of LCA and DOX from DL-M

LCA release studies showed that under acidic conditions (pH 5 and 6.8) LCA release rate was higher from the DL-M due to breaking of electrostatic interaction between LCA and the polymer (Figure 3.22-A). There was significant difference between the drug release profiles of physiological and acidic release conditions (pH 5 and 6.8) till 1h for LCA release, but after 1 h, the LCA release rate significantly increased in medium at pH 6.8 and pH 5 compared to physiological media ($p<0.05$). The release rate was significantly faster at pH 5 than other release media after 7 h ($p<0.05$) which showed that electrostatic conjugation between LCA and the copolymer. Meanwhile, LCA release rate was lower compared to the free LCA release from dialysis membrane. After 24 hours, 57% of LCA was released from DL-M and 52% of LCA was released from the LCA_{25}**M under physiological conditions while 93% and 77% of LCA were released from DL-M LCA_{25}**M under acidic conditions (pH 5.0), respectively. Meanwhile, after 48 hours, 56% and 54% of LCA were released from DL-M and LCA_{25}**M at physiological pH, respectively. 95% and 84% of LCA were released from DL-M and LCA_{25}**M at acidic pH (5.0), respectively. After 4 days, 100% release occurred at pH 5.0 for both micelles, while it was 92% from DL-M and 85% from LCA_{25}**M at pH 6.8 and only 63% was released from both types of micelles at pH 7.4. Release behavior of the micelles at pH 7.4 was not different between DL-M and LCA_{25}**M. At pH 5, release rate was faster in DL-M than LCA_{25}**M after 24 h and 48 h. But after 4 days, 100% of LCA was released from both types of micelles under acidic conditions (pH 5). These results showed that DL-M fastens the LCA release from micelles compared to LCA_{25}**M. This behavior may be a result of co-loading of DOX with LCA. Since there is another drug in the micelle, LCA may not conjugate the polymer via electrostatic interaction to the polymer due to hindrance of amino groups in the copolymer by DOX. DOX may take place in front of the amino groups of the copolymer so LCA might not have conjugated efficiently with the copolymer.

DOX release studies showed that under acidic conditions DOX release rate was higher from DL-M compared to the physiological condition (Figure 3.22-B). There was no significant difference between the drug release profiles of physiological and acidic release condition (pH 6.8) till 8 h, but after 8 h, the DOX release rate significantly increased in medium at pH 6.8 compared to physiological media ($p<0.05$). The release rate was significantly faster at pH 5 than other release media after 6 hours ($p<0.05$). Meanwhile, DOX release rate was lower compared to the free drug. After 24 hours, 52% and 54% of DOX was released from DL-M and from DOX_{ld}-M under physiological conditions, respectively while 79% and 86% of DOX were released from DL-M and DOX_{ld}-M under acidic conditions (pH 5.0), respectively. Meanwhile, after 48 hours, 57% of DOX was released at physiological pH from both types of micelles whereas 88% and 92% release of DOX were observed from DL-M and DOX_{ld}-M at acidic pH (5.0). After 4 days, DOX release reached 100% for both micelles at pH 5.0 while it was 81% from DL-M and 91% from DOX_{ld}-M at pH 6.8 and only 61% from DL-M and 64% from DOX_{ld}-M at pH 7.4. Release behaviors at pH 7.4 were similar for DL-M and DOX_{ld}-M. At pH 5, DOX release rate was faster in DOX_{ld}-M than DL-M after 24 h and 48 h. But after 4 days, they both reached 100% release of DOX at pH 5. These results suggest that DOX release was slowed down after co-loading with LCA. LCA may compete with the DOX when release occurs. These results are in line with the LCA release behavior of DL-M since LCA release rate was faster after 24 h and 48 h compared to LCA_{25}**M and DOX release rate was slower after 24 h and 48 h compared to DOX_{ld}-M.

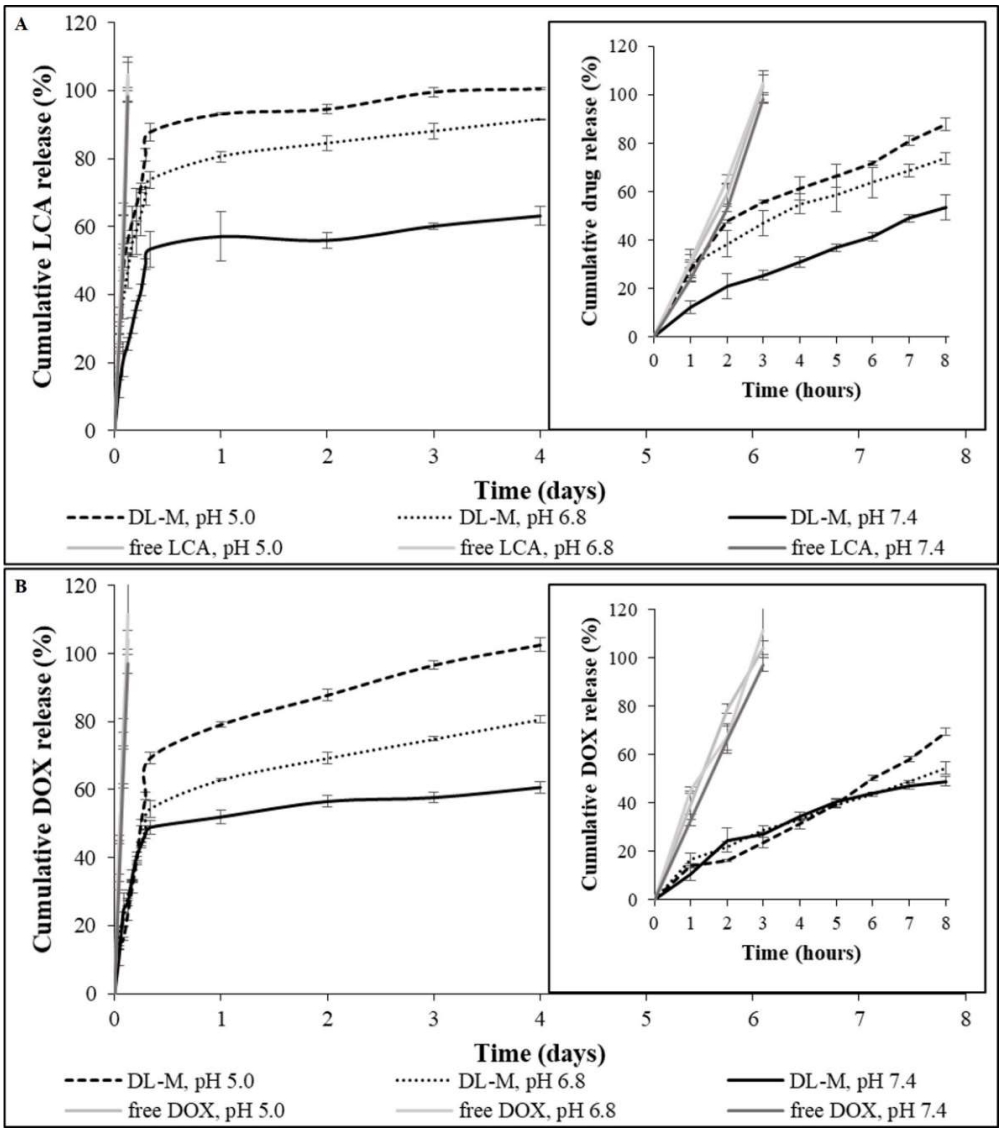

Figure 3.22. Cumulative drug release profiles from dialysis membrane of A) free LCA and DL-M B) free DOX and DL-M under physiological conditions (PBS, 0.1 M and pH 7.4) and acidic conditions (CPB-pH 5.0 and CPB-pH 6.8; 0.15 M) at 37°C (n=6).

Release data were fitted to the different the kinetic models (zero order, first order, Higuchi model, and Korsmeyer-Peppas model) to determine the best fitted model for the release profiles of LCA and DOX from the DL-M. Rate constants (K_0, K_1, K_H, and K_P), n value and coefficients of determination (R^2) are given in Table 3.17. Korsmeyer-Peppas model was found as the best fitted model for both LCA and DOX

release from DL-M at pH 7.4 (PBS, 0.1 M and pH 7.4) and at pH 6.8 (CPB, 0.15 M and pH 6.8). Meanwhile, first order model was found as the best fit model for both LCA and DOX release from the DL-M in acidic conditions (CPB, 0.15 M and pH 5.0).

Table 3.17. *In vitro* release kinetic parameters of DL-M for LCA and DOX.

Drugs	Release Kinetic Models		pH 7.4	pH 6.8	pH 5.0
LCA	Zero order	K_0	0.627	0.982	0.766
		R^2	-0.743	-1.670	-0.716
	First order	K_1	-0.011	-0.008	-0.010
		R^2	0.591	0.684	0.931
	Higuchi model	K_H	8.727	0.065	14.648
		R^2	0.270	0.606	-0.125
	Korsmeyer-Peppas model	K_P	0.135	0.284	0.186
		n (exponent of release)	0.287	0.203	0.215
		R^2	0.910	0.924	0.607
DOX	Zero order	K_0	0.597	0.747	0.791
		R^2	-0.632	-0.911	0.447
	First order	K_1	-0.011	-0.10	-0.015
		R^2	0.589	0.648	0.932
	Higuchi model	K_H	8.518	0.088	12.772
		R^2	0.124	0.782	0.771
	Korsmeyer-Peppas model	K_P	0.128	0.175	0.115
		n (exponent of release)	0.301	0.261	0.344
		R^2	0.919	0.936	0.897

3.7 *In vitro* Cell Culture Experiments

Cancer cell lines were used to study the anticancer effect of micelles in *in vitro* conditions. For this purpose, the first step was to determine IC_{50} values of the drugs on cells.

3.7.1 Determination of IC_{50} of LCA on MDA-MB-231 Cells, A549 Cells and SK-MEL-30 Cells

Different concentrations of LCA in 0.4% ethanol was added to medium and MDA-MB-231, A549, and SK-MEL-30 cells were incubated at 37°C for 48 hours and MTT assay was carried out to determine cell viability. Appendix I1 Figure 1 shows cell viability results. IC_{50} values of LCA on MDA-MB-231, A549, and SK-MEL-30 cells were calculated with GraphPad Prism 8 software and found as 139.30±9.8 µM, 23.44±4.91 µM, and 85.00±6.32 µM, respectively. Appendix J1 Figure 1 shows normalized absorbance versus LCA concentration graphs that were obtained from software and R^2 values were found as 0.919, 0.9491, and 0.9696, respectively. If R^2 values are above 0.9, it means that the results are very close to the regression line, which shows the best fit with the model for calculating IC_{50} values.

After the MTT method was changed, the same method was repeated for the cytotoxicity studies of free LCA (for MDA-MB-231 Figure 3.23; for A549 and SK-MEL-30 Appendix K1 Figure 1). With these results, IC_{50} values were calculated in GraphPad program (for MDA-MB-231 Figure 3.24; for A549 and SK-MEL-30 Appendix L1 Figure 1). The IC_{50} value of free LCA on MDA-MB-231 cells was found to be 107.5 ± 4.6 µM. The R^2 value of the graph is also 0.9856. The IC_{50} value was found on A549 cells at a concentration of 79.0 ± 20.3 µM. However, the R^2 value of the graph is 0.6217. In other words, LCA does not show cytotoxic effects on A549 cells. Looking at the graph (Appendix L1 Figure 1-A), the normalized absorbance value increased with the increasing concentrations. This proves that LCA does not show cytotoxic effects on A549 cells. IC_{50} value on SK-MEL-30 cells was

found as 132.7 ± 9.0 µM. Luu et al. (2018) found that LCA reduces cell proliferation and causes cell apoptosis on MDA-MB-231 and MCF7 cells. In addition, they found the IC_{50} values of LCA on MDA-MB-231 and MCF7 cells as 144.8 µM and 104.9 µM, respectively (Luu et al., 2018). He et al. (2017) found the IC_{50} value of LCA on MCF7 cells as 150.3 µM (He et al., 2017). Gafar et al. (2016) found the IC_{50} values of LCA on prostate cancer cell lines (PC-3 and DU-145) as 32.0 µM and 30.4 µM, respectively (Gafar et al., 2016). When IC_{50} values we found in our study are compared with the values reported in the literature, similar results were obtained with MDA-MB-231 and SK-MEL-30 cells. SK-MEL-30 cells showed higher IC_{50} value than MDA-MB-231 cells. This can be due to SK-MEL-30 cells' aggressiveness. Cell morphologies of MDA-MB-231, A549, and SK-MEL-30 cells are shown in Figure 3.25, Appendix M1 Figure 1, and Appendix N1 Figure 1, respectively. Normal cell morphology can be seen in the control groups of cells. It can be seen from images that cell number decreases and cell morphology changes at IC_{50} value.

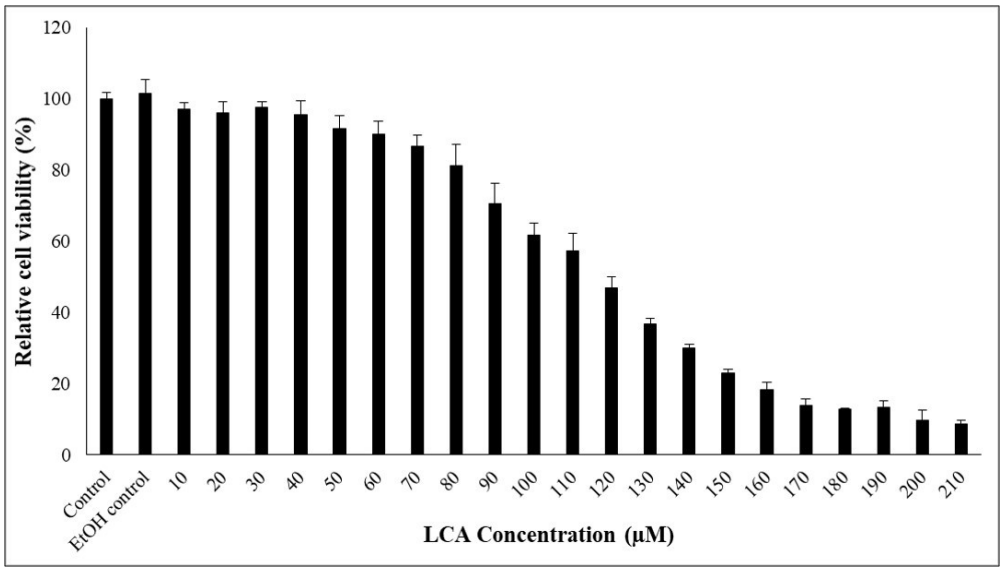

Figure 3.23. Cell viability results of MDA-MB-231 cells after 48 hours incubation with different LCA concentrations (n=4). Positive control is the cells not incubated with LCA or ethanol.

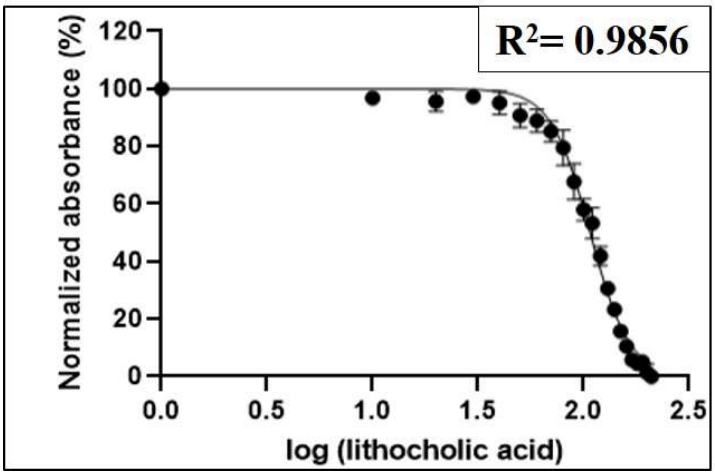

Figure 3.24. Normalized absorbance against the LCA concentration plots of MDA-MB-231 cells obtained using GraphPad Prism 8 software after modifying the MTT method (n=4).

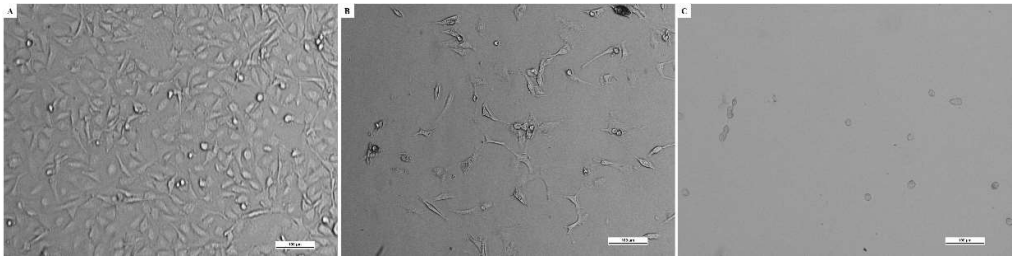

Figure 3.25. Morphology of MDA-MB-231 cells after 48 hours incubation with A) 0 µM (control), B) 108 µM and C) 200 µM LCA. Scale bars are 100 µm.

3.7.2 Determination of IC_{50} of DOX on MDA-MB-231 Cells, A549 Cells and SK-MEL-30 Cells

Different concentrations of DOX was added to cell medium and MDA-MB-231, A549, and SK-MEL-30 cells were incubated at 37°C for 48 hours and MTT assay was done to determine cell viability. Figure 3.26 shows cell viability results of MDA-MB-231 and Appendix O1 Figure 1 shows cell viability results of A549 and SK-MEL-30. IC_{50} values of DOX on MDA-MB-231, A549, and SK-MEL-30 cells was calculated with GraphPad Prism 8 software and found as 79.98 ± 4.37 nM, 1191.24

± 10.49 nM, and 384.59 ± 4.00 nM, respectively. In the literature, IC_{50} values of DOX on MDA-MD-231 cells, A549 cells, and SK-MEL-30 cells are 1262 nM, 1146 nM, and 46.96 nM, respectively (Yang et al., 2013). When IC_{50} values are compared with literature values, IC_{50} values of DOX on MDA-MB-231 cells were found lower than literature value and IC_{50} value of DOX on SK-MEL-30 cells was found higher than the value reported in literature. These can be due to the difference in passage numbers or mutagenicity of cell lines in cell cultures. Figure 3.27 shows normalized absorbance vs DOX concentration graphs of MDA-MB-231 cells, and Appendix P1 Figure 1 shows normalized absorbance vs DOX concentration graphs of A549 and SK-MEL-30 cells that were obtained from software and R^2 values were found as 0.9575, 0.9074, and 0.9705, respectively. This means that data were very close to the fitted regression line.

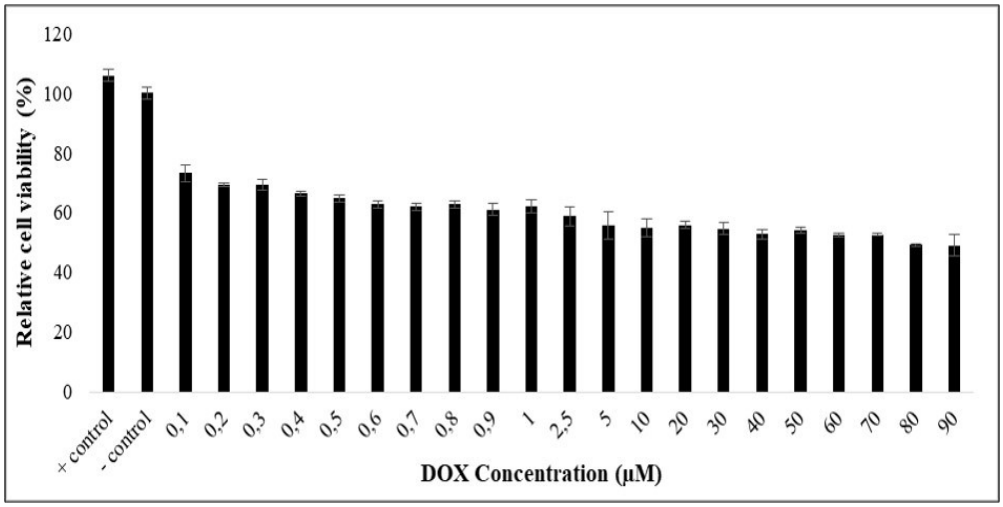

Figure 3.26. Cell viability results of MDA-MB-231 cells after treatment with different concentrations of DOX (n=4).

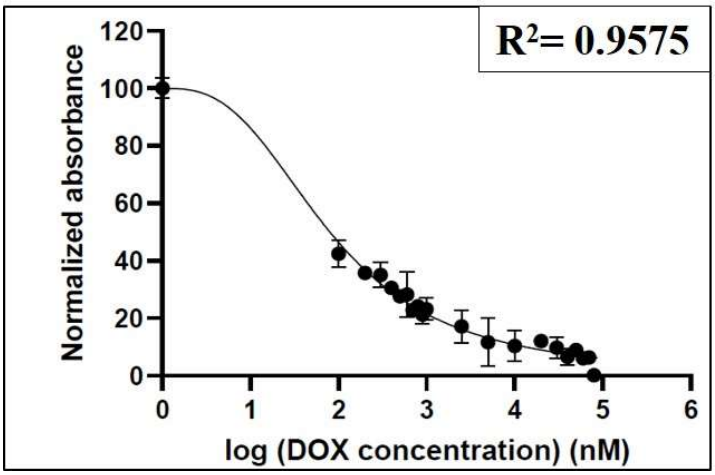

Figure 3.27. Normalized absorbance vs. DOX concentration charts of MDA-MB-231 cells after data fitting using GraphPad Prism 8 software.

3.7.3 Cytotoxicity Studies of Micelles

3.7.3.1 Cytotoxicity of LCA_{60}**M and LCA_{25}**M on MDA-MB-231 Cells

Cytotoxic effect of LCA_{60}**M on MDA-MB-231, A549, and SK-MEL-30 cells was studied with old MTT method and results are presented in Appendix Q1 Figure 1. Micelles having no drug (M) were also used as the control group. The mPEG-b-PCL copolymer used in micellar preparation is a polymer known to be biocompatible. However, as can be seen from the Appendix Q1 Figure 1, it was observed that these micelles (M) had a cytotoxic effect and these findings were thought to be experimental errors. While performing MTT, the medium, in which the cells were incubated, was withdrawn and fresh MTT solution was added into wells. However, it was realized that the cells adhering to the polymer were also pulled out while the media were taken out, so the viability was found to be lower than the expected real values. Therefore, the test was modified and fresh MTT solution was added without withdrawing the cell media, and cytotoxicity studies of micelles were repeated (Figure 3.28 for MDA-MB-231; Appendix R1 Figure 1 for A549 and SK-MEL-30).

As a result, it was found that blank micelles (M) were not cytotoxic on all three cell types examined in this study.

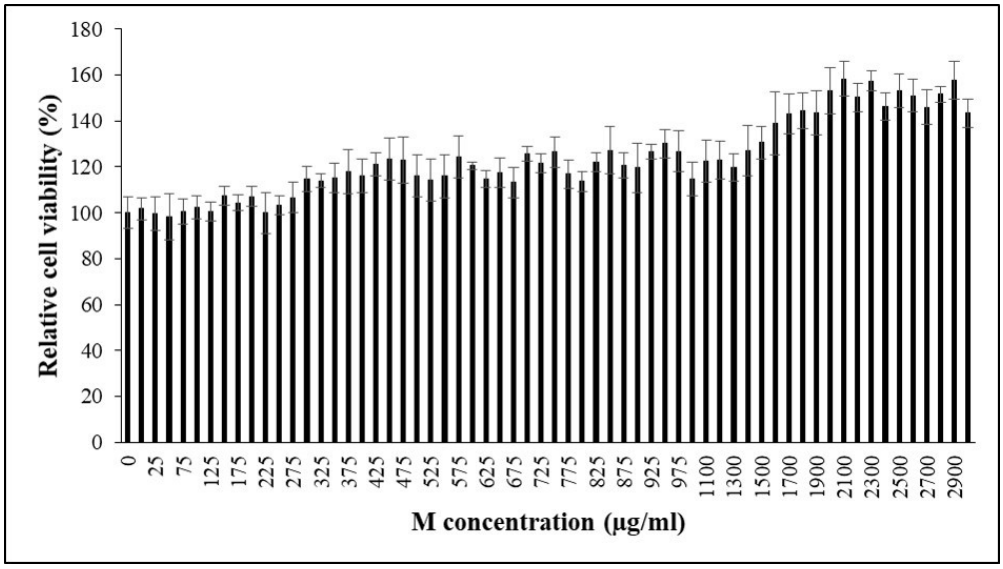

Figure 3.28. The cytotoxic effect of different concentrations of M on MDA-MB-231 cells (n=4).

Later, cytotoxicity studies of LCA_{60}**M were performed (Figure 3.29 for MDA-MB-231; and Appendix S1 Figure 1 for A549 and SK-MEL-30) by applying the same technique. It was determined that LCA_{60}**M did not show any cytotoxic effect on A549 and SK-MEL-30 cells. LCA_{60}**M reduced cell viability by 50% at a concentration of 225 µg/mL on MDA-MB-231 cells. 225 µg/mL LCA_{60}**M contain 16 µM LCA. This was lower than the IC_{50} value of free LCA (108 µM) on MDA-MB-231 cells. In other words, LCA_{60}**M were more effective than free LCA on MDA-MB-231 cells. Cancer cells have some drug resistance mechanisms and drug efflux mechanism is one of them. Free drug enters the cell via diffusion and when the cancer cell recognizes the free drug in its structure, transports it out from the cell via drug efflux pumps, which are overexpressed in cancer cells. Therefore, the drug concentration in the cell cannot reach the cytotoxic levels. On the other hand, nanoparticles can enter the cell via endocytosis, so the cell cannot recognize the drug

inside the particle and controlled release of the drug occurs. This increases the drug concentration in the cell. Thus, lower drug concentration in the nanoparticle can show cytotoxic effect on cancer cells while higher free drug concentration is needed to show cytotoxic effect on cancer cells (Zhou et al., 2019). Similar to our results, Feng et al. (2018) prepared DOX loaded micelles and showed their cytotoxic effect on MCF-7 and SMMC-7721 cells. They found that DOX loaded micelles were more cytotoxic than free DOX (Feng et al., 2018). Zhang et al. (2016) prepared DOX conjugated and arsenite loaded vesicles and showed their cytotoxic effect on MCF-7 and MCF-7/ADR (DOX resistant) cells. They found that DOX conjugated vesicles were more effective than free DOX (L. Zhang et al., 2016).

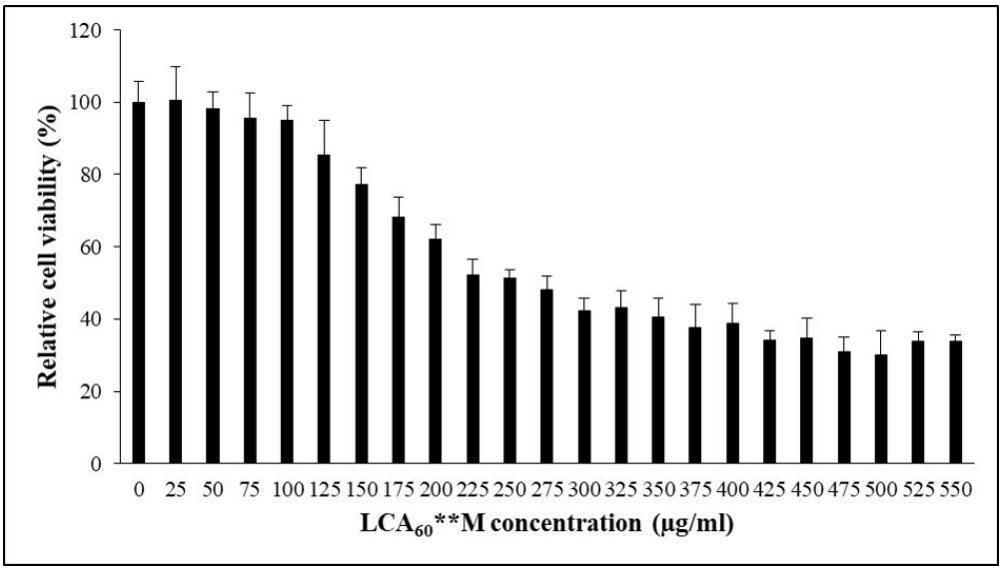

Figure 3.29. Cytotoxic effect of different concentrations of LCA_{60}**M on MDA-MB-231 cells (n=4).

Different micelle preparation methods can result in differences in cell viability. To evaluate the differences in cell viability of LCA_{60}**M and LCA_{25}**M, MTT assay was carried out (Figure 3.30). Results showed that there was no significant difference between LCA_{60}**M and LCA_{25}**M in cell viability since 1.5 mg/mL LCA_{60}**M and 1.5 mg/mL LCA_{25}**M contains 108 µM LCA and 93 µM LCA, respectively. Both micelles caused significant decrease in cell viability compared to free LCA,

which was an expected result due to higher cell internalization of LCA loaded micelles than free LCA. Free LCA is highly hydrophobic and therefore to carry them in micelles increase their solubility in and internalization by the cells. This showed that micelle preparation method did not affect the cell viabilities of MDA-MB-231 cells since drug loading capacity is one of the important parameters which affect the cell viability.

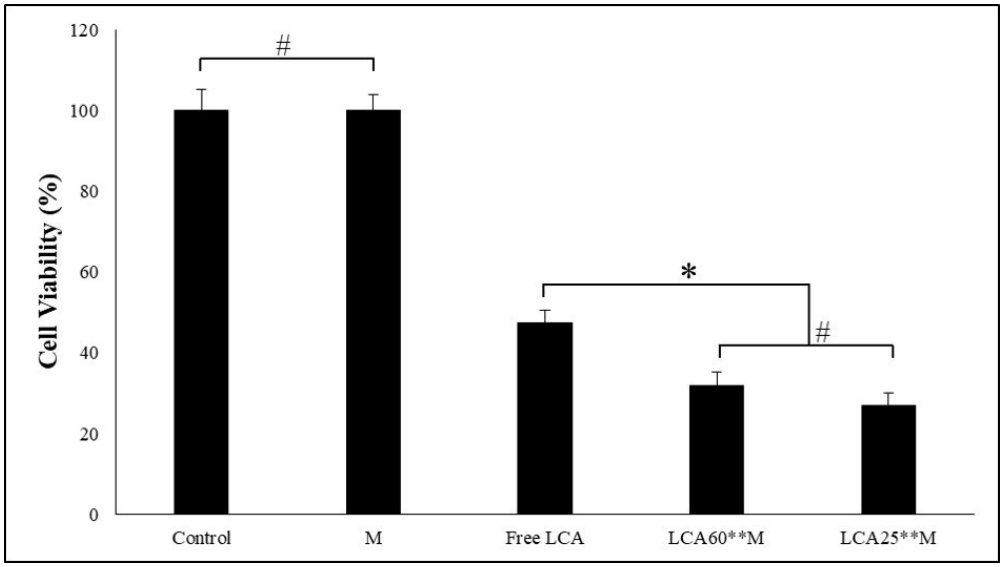

Figure 3.30. Cytotoxic effect of LCA_{60}**M and LCA_{25}**M compared to free LCA on MDA-MB-231 cells (n=4). * shows the significant difference between the groups and # shows the non-significant difference between the groups ($p<0.05$; n=4).

3.7.3.2 Cytotoxicity of DOX_{conj}-M and DOX_{ld}-M on MDA-MB-231 Cells

Viability of MDA-MB-231 cells was assessed after treatment with DOX_{conj}-M and DOX_{ld}-M to see the differences caused by different drug loading mechanisms into the micelle (Figure 3.31). Results showed that DOX loading or DOX conjugation to micelles did not cause any difference in cell viabilities. Both DOX_{conj}-M and DOX_{ld}-M decreased the cell viability. 1.5 mg/mL DOX_{conj}-M and 1.5 mg/mL DOX_{ld}-M contained 374 µM and 238 µM, respectively. But this difference did not result a difference in cell viability between these two groups. This result is similar to IC_{50}

study of free DOX. Increasing free DOX concentration did not cause a further decrease in cell viability after IC_{50} concentration of DOX (80 nM). Cancer cells have different mechanisms like drug efflux mechanism due to high mutation rate of cancer cells which multidrug resistance transporter proteins are involved in drug efflux mechanism during which drugs are sent outside the cell to escape from cell death (Yakun Chen et al., 2009; Ferreira et al., 2005). DOX enters cell via endocytosis but can be recognized by the cell and cell can send it to outside by drug efflux mechanism. Although our MDA-MB-231 cells used in this study are not DOX resistant cell line, but they were at high passage numbers which were between 25 and 30 and some cells might have become resistant due to mutations. Ciocan-Cartita et al. (2020) studied the effect of passage number on mutagenicity of MDA-MB-231 cells. They showed that mutations were increased in passage 12 and 24 compared to passage 0. They also showed that increasing number of passages increases expression of drug resistance genes (Ciocan-Cartita et al., 2020). On the other hand, DOX_{ld}-M caused a significant decrease in cell viability compared to free DOX. But DOX conjugation and DOX loading had similar effect on MDA-MB-231 cells in terms of cell viability while DOX_{conj}-M had higher drug loading capacity than DOX_{ld}-M. On the other hand, cell internalization studies showed that DOX_{ld}-M directly localized in the cell nuclei so DOX_{ld}-M may be a better treatment for breast cancer treatment.

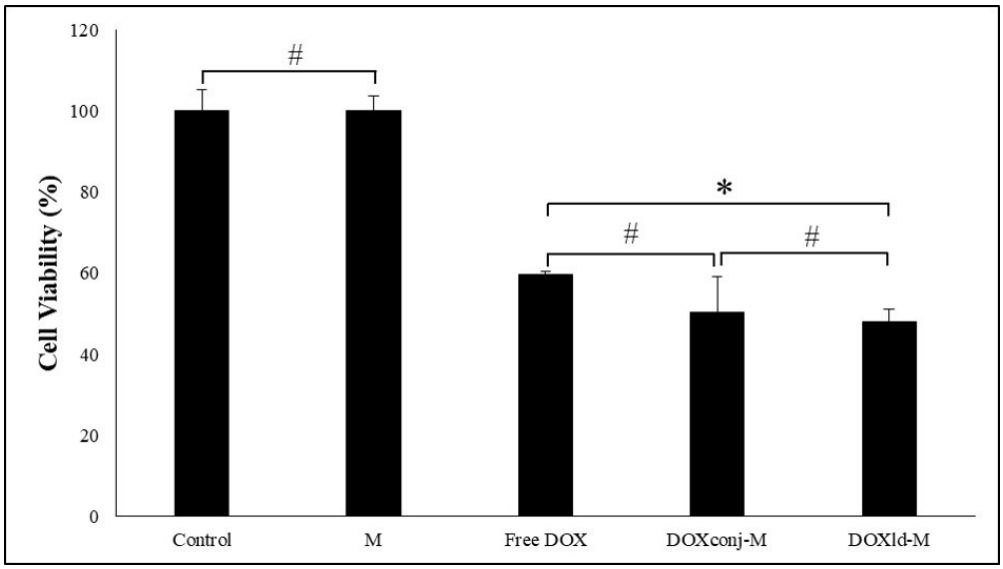

Figure 3.31. Cytotoxic effect of DOX_{conj}-M and DOX_{ld}-M compared to free DOX (80 nM) on MDA-MB-231 cells (n=4). * shows the significant difference between the groups and # shows the non-significant difference between the groups ($p<0.05$; n=4).

3.7.3.3 Cytotoxicity of Mixed Micelles (DOX_{conj}-M and LCA_{60}**M) on MDA-MB-231 Cells

In order to examine synergistic effect of LCA and DOX together on MDA-MB-231 cells, LCA_{60}**M and DOX_{conj}-M were mixed in certain proportions (1:1 (w/w), which is 0.75 mg/mL LCA_{60}**M and 0.75 mg/mL DOX_{conj}-M), 1:2 (w/w), which is 0.5 mg/mL LCA_{60}**M and 1 mg/mL DOX_{conj}-M), and 2:1 (w/w), which is 1 mg/mL LCA_{60}**M and 0.5 mg/mL DOX_{conj}-M), respectively) (Figure 3.32). Free drug formulations of these mixtures were also used as control such as: free LCA:free DOX 1:1 (w/w) (which is 54 µM LCA and 107.25 nM DOX), 1:2 (w/w) (which is 36 µM LCA and 143 nM DOX), and 2:1 (w/w) (which is 72 µM LCA and 71.5 nM DOX). Results showed that there was no synergistic effect of mixed micelles on cell viabilities of MDA-MB-231 cells. In fact, LCA_{60}**M mixing did not affect the cell viability in 1:1 (w/w) and 1:2 (w/w) ratios. Cell viabilities after treatment with mixed micelles in 1:1 (w/w) and 1:2 (w/w) ratios were found similar with cell viabilities

after treatment with same amounts of DOX_{conj}-M ($p>0.05$). When micelles were mixed in 2:1 (w/w) ratio, cell viabilities were found similar with cell viabilities observed after treatment with same amount of LCA_{60}**M. These results showed that there was no synergistic effect of LCA and DOX in cell viability. Therefore, mixture of micelles were not used for further experiments. Instead of mixing micelles, DOX and LCA were loaded in the micelles when micelles were prepared and DL-M was obtained.

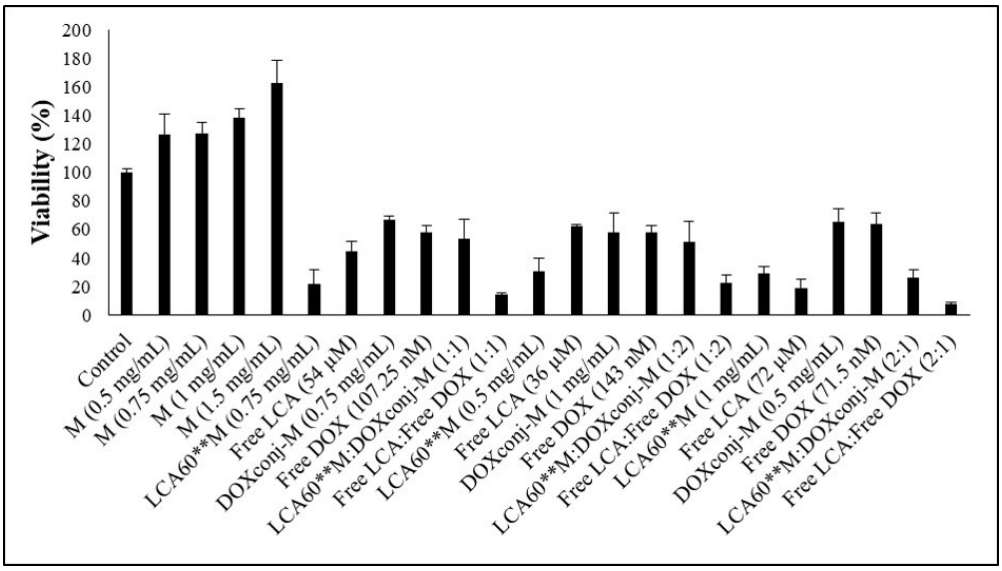

Figure 3.32. Cell viabilities of MDA-MB-231 cells after treatment with mixed micelles compared to LCA_{60}**M and DOX_{conj}-M (n=4).

3.7.3.4 Cytotoxicity of DL-M on MDA-MB-231 Cells

DOX and LCA were loaded together into micelles and cell viability studies were carried out to see the effectiveness of both DOX and LCA on MDA-MB-231 cells (Figure 3.33). LCA_{25}**M contains 93 µM LCA. DOX_{ld}-M contains 238 µM DOX. DL-M contains 242 µM DOX and 400 µM LCA in it.

Results showed that there was no significant difference between DOX_{ld}-M and DL-M ($p>0.05$). On the other hand LCA_{25}**M decreased cell viability significantly compared to DL-M ($p<0.05$). DL-M had higher LCA concentration than LCA_{25}**M,

but this did not decrease the cell viability after treatment with DL-M. This may be due to the multidrug mechanism in MDA-MB-231 cells. Cells may recognize DOX and since DOX and LCA enter the cells together via endocytosis of micelles, LCA may exposed to same drug efflux mechanism with DOX. In order to make this part clear, DL-M was further investigated in terms of cell migration, colony formation, lipid droplet formation, apoptosis, ROS generation, etc.

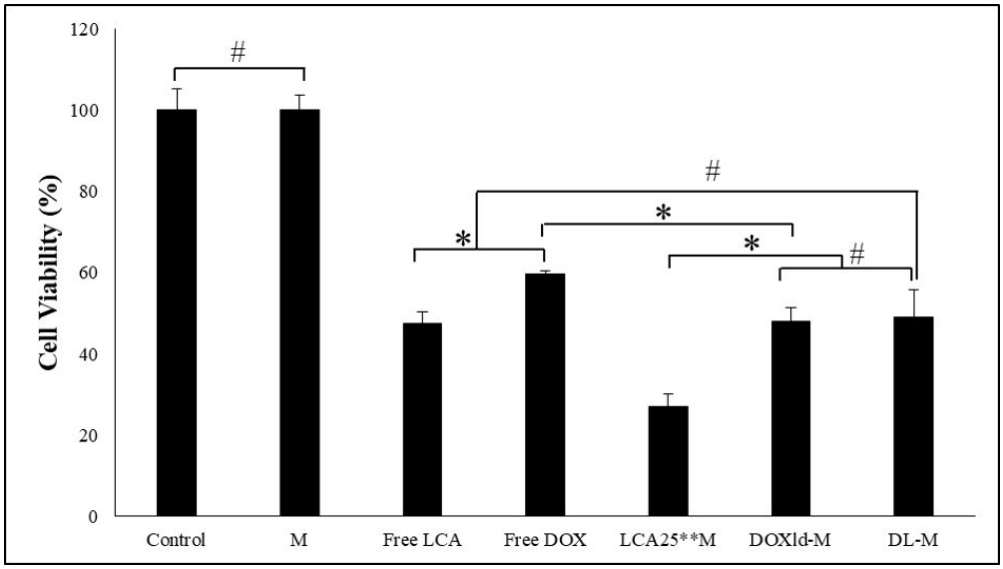

Figure 3.33. Cytotoxic effect of DL-M compared to LCA_{25}**M and DOX_{ld}-M on MDA-MB-231 cells (n=4). * shows the significant difference between the groups and # shows the non-significant difference between the groups ($p<0.05$; n=4).

3.7.4 Determination of Cell Internalization of Micelles

Cell internalization of micelles loaded with coumarin 6 was examined with confocal microscopy. Effect of free coumarin 6 on cells was also examined as the control group. Results showed that, cell internalization of free coumarin 6 reached highest in 1 hour, but then decreased after 2 h (Figure 3.34-A). On the other hand, cell internalization of C6-LCA_{60}**M and C6-LCA_{25}**M occurred after 1 h and reached to the highest concentration after 4 hours (Figure 34-B and C). After 6 h, it started to decrease. Similar to our study, Gu et al. (2020) prepared coumarin 6 loaded polymer-

lipid hybrid nanoparticles to study their cellular uptake and found that cellular uptake of nanoparticles reached a peak after 3 hours and then decreased (Gu et al., 2020). Jannu et al. (2021) prepared LCA conjugated tryptophan based micelles to deliver niclosamide for the treatment of prostate cancer and they conjugated a ligand that targets EphA2 receptor on cells to micelles to target prostate cancer cells. They used two cell lines: PC-3 cells (high expression of EphA2 receptor) and H4 cells (low expression of EphA2 receptor). They observed that fluorescence intensity of coumarin 6 loaded, targeted micelles increased with time up to 24 h in PC3 cells while H4 cells showed lower fluorescence intensity of coumarin 6 than PC3 cells and cellular uptake of micelles reached a peak after 3 hours for H4 cells (Jannu et al., 2021). In our case, LCA_{60}**M and LCA_{25}**M demonstrated similar behavior as the ones reported in literature.

Figure 3.34-D shows the cell internalization of free DOX. Cell internalization of free DOX occurred after 1 h and reached the highest concentration at 4 h. Similar to free DOX, DOX_{conj}-M was also internalized after 1 h by the cells and reached the highest at 4 h (Figure 3.34-E). Figure 3.34-F shows the cell internalization of DOX_{ld}-M and Figure 3.34-G shows the cell internalization of DL-M. Both DOX_{ld}-M and DL-M showed that micelles are localized in cell nuclei after 1 h because DOX fluorescence and DAPI (dye for cell nuclei) were overlapped in the images and cell nuclei was observed as purple. Cai et al. (2014) prepared DOX conjugated hyaluronan nanoparticles and they also observed the localization of DOX conjugated nanoparticles in cell nuclei (Cai et al., 2014). Okur et al. (2016) prepared DOX loaded PEG-dextran nanoparticles and they also observed that DOX loaded nanoparticles were localized in cell nuclei (Okur et al., 2016). It is also known that DOX cause DNA damage in cells (Shin et al., 2015) so cell nuclei internalization of DOX_{ld}-M and DL-M shows that these micelles may possess much better efficiency in the treatment of breast cancer.

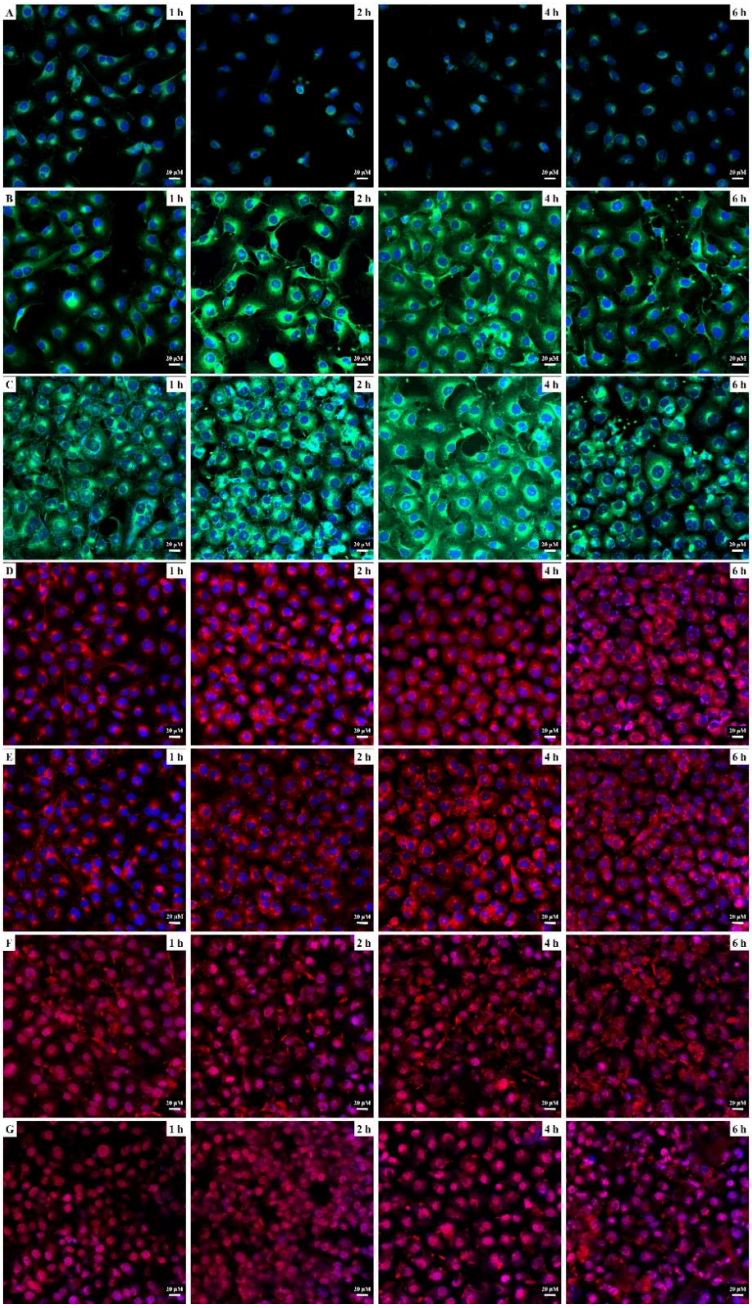

Figure 3.34. Cell internalization after 1h, 2h, 4h and 6h of A) free coumarin 6 and B) C6-LCA$_{60}$**M, C) C6-LCA25**M, D) free DOX, E) DOXconj-M, F) DOXld-M, and G) DL-M. Cell nuclei was stained with DAPI. Blue is DAPI, green is coumarin 6, and red is DOX in images. In the B and C sections green color in the cells designate cell internalized coumarin 6 loaded micelles. In the E, F, and G sections red color in the cells designate DOX conjugated or loaded micelles inside the cells.

3.7.5 Cell Migration Assay

Metastasis occurs in the late stages of cancer. Cancer cells separate from the primary cancer site, enter the lymph or blood system, locates a new place in the body and forms new tumor there. To simulate the migration of cancer cells *in vitro*, transwell migration assay was carried out (Figure 3.35). MDA-MB-231 cells are metastatic breast cancer cells. The effect of free LCA, free DOX, LCA_{60}**M, LCA_{25}**M, DOX_{conj}-M, DOX_{ld}-M, and DL-M treatment on the migration behavior of MDA-MB-231 cells was investigated. M and untreated cells were used as control.

Results showed that LCA_{60}**M and LCA_{25}**M were more effective than free LCA. DOX_{conj}-M, DOX_{ld}-M, and DL-M inhibited cell migration compared to free DOX significantly. Inhibition of cell migration of DL-M did change compared to LCA_{25}**M. on the other hand, there was a significant decrease in cell migration after treatment with DL-M compared to treatment with DOX_{conj}-M, and DOX_{ld}-M.

He et al. (2017) synthesized amide derivatives of LCA to find the most potent LCA derivative on cancer cells. They used the most potent derivative in cell migration assay. 10 µM of LCA derivative inhibited the MDA-MB-231 cell migration by 50% compared to control group (untreated group) (He et al., 2017). Their LCA derivative concentration was lower than the LCA concentration used in this study because they synthesized a derivative which was more cytotoxic than LCA. In our studies, results also showed a 60% decrease in cell migration for free LCA, LCA_{60}**M, and LCA_{25}**M.

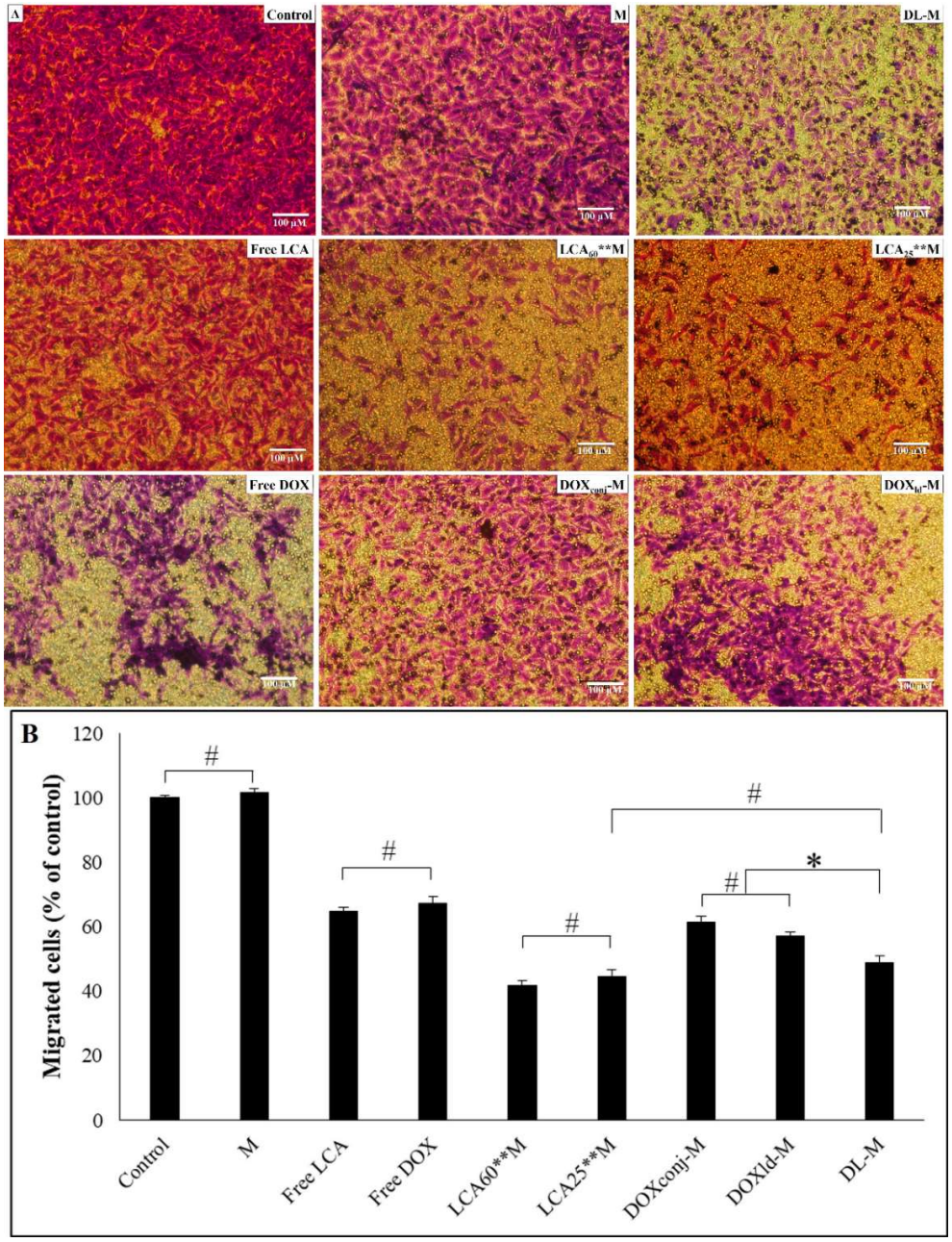

Figure 3.35. A) Images of MDA-MB-231 cells migrated from the top of the transwell to the bottom of the transwell after treatment. B) Normalized plot of migrated cells after transwell migration assay. IC_{50} concentration of LCA (108 µM) and DOX (80 nM) was used in free LCA and free DOX groups. Transwell migration assay was carried out for 48 hours and then, cells were fixed with 4% paraformaldehyde and stained with 0.2% crystal violet. After that, cells were counted from three independent experiments. * shows the significant difference between the groups and # shows the non-significant difference between the groups ($p<0.05$; n=3).

3.7.6 Colony Formation Assay

Cancer cells have the ability to form a tumor from single cell. To simulate this behavior *in vitro*, colony formation assay was carried out. After treatment, it was expected that cell proliferation ability of cancer cells would decrease. To determine anti-proliferative effects of micelles prepared (LCA_{60}**M, LCA_{25}**M, DOX_{conj}-M, DOX_{ld}-M, and DL-M), colony formation assay was carried out (Figure 3.36). The results showed that all drug containing micelles showed the similar anti-proliferative effect with the free LCA and free DOX while the control (nothing applied) and M (empty micelles) groups showed the highest proliferation. He et al. (2017) synthesized amide derivatives of LCA to find the most potent LCA derivative on cancer cells. They used the most potent derivative in colony formation assay at 2.5 µM and 5 µM concentrations on MCF-7 and MCF-7/ADR cells. Similarly, they showed that increasing concentrations of LCA derivative decreased colony number and colony size of MCF-7 and MCF-7/ADR cells. At 5 µM concentration of LCA derivative they found that colony formation decreased to 20% compared to control (100%) (He et al., 2017). Their LCA derivative concentration was lower than the LCA concentration used in this study because they synthesized a derivative which is more cytotoxic than LCA. Our results also showed a 50% decrease in colony formation for free LCA, free DOX, LCA_{60}**M, and LCA_{25}**M, DOX_{conj}-M, DOX_{ld}-M, and DL-M.

Xie et al. (2019) prepared hybrid micelles from polyethylenimine-polycaprolactone and gadolinium(III)-conjugated polyethyleneglycol-polycaprolactone and DOX and miR-34a were co-loaded into micelles. Colony formation assay was carried out on MDA-MB-231 cells and results showed that 15 µM DOX containing micelles decreased colony number by approximately 30% while 15 µM DOX and miR-34a containing micelles decreased colony number by approximately 55% (Xie et al., 2019). DOX_{conj}-M, DOX_{ld}-M, and DL-M contained 374 µM, 238 µM, and 242 µM DOX, respectively, which contains much higher DOX than the micelles prepared by Xie et al. (2019). DOX_{conj}-M, DOX_{ld}-M, and DL-M also decreased the colony

formation ability of MDA-MB-231 cells by 50%. This might be resulted by the higher inhibition of colony formation with DOX_{conj}-M, DOX_{ld}-M, and DL-M, compared to the literature values because they reached 55% inhibition with the usage of miR-34a together with DOX.

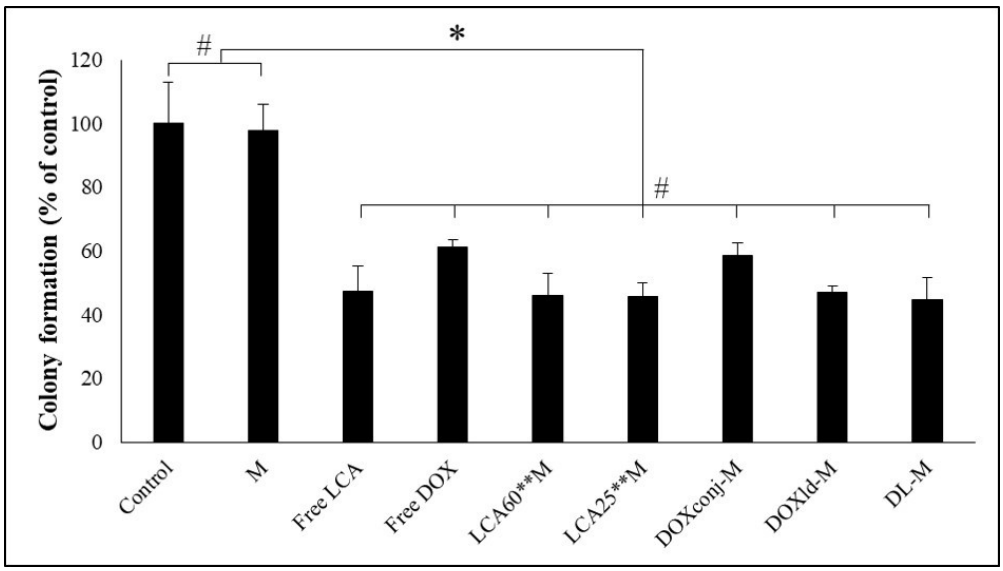

Figure 3.36. Normalized plot of colonies after colony formation assay. IC_{50} concentration of LCA (108 µM) and DOX (80 nM) was used in free LCA and free DOX groups. Colony formation assay was carried out for a week and then, colonies were counted manually from three independent experiments. * shows the significant difference between the groups and # shows the non-significant difference between the groups ($p<0.05$; n=3).

3.7.7 Determination of Lipid Droplets in MDA-MB-231 Cells

In breast cancer cells, lipogenic activity is prominent for cell survival and proliferation (Luu et al., 2018). High number of lipid droplets in control and M groups was observed (Figure 3.37). Lipid droplets were lower in free LCA, LCA_{60}**M, and LCA_{25}**M groups compared to control and M groups and morphology of cells also changed after the treatment. It seems like cells lost their cytoplasm and shrinked after treatment with free LCA, LCA_{60}**M, and LCA_{25}**M. It was observed that LCA_{60}**M and LCA_{25}**M inhibited lipid droplet formation

more than free LCA group and cell morphology changed more compared to free LCA group. These results showed that treatment with LCA_{60}**M and LCA_{25}**M decreased lipogenic activity of MDA-MB-231 cells. Similarly, Luu et al. (2018) showed that treatment with increasing concentrations of free LCA from 0 to 200 µM decreased number of lipid droplets of MDA-MB-231 cells (Luu et al., 2018). On the other hand, free DOX, DOX_{conj}-M, and DOX_{ld}-M did not change lipid droplet formation but changed the cell morphology. Cells appeared to be enlarged in DOX containing groups. Lower number of lipid droplets was observed after treatment with DL-M. Anti-lipogenic activity of LCA was studied and it was shown that LCA reduces SREBP-1c expression of breast cancer cells. Some lipogenic enzymes like FASN also were shown to be downregulated after treatment with LCA (Luu et al., 2018). Therefore, it was thought that LCA containing micelles inhibit lipogenesis while DOX containing micelles had no effect on lipogenesis *in vitro*.

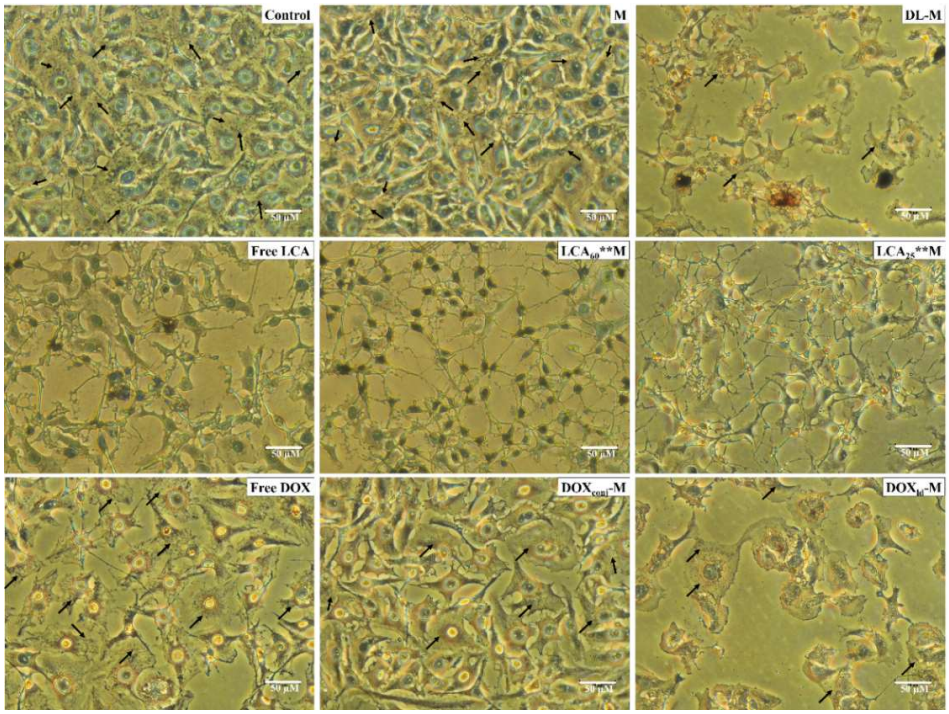

Figure 3.37. Images of MDA-MB-231 cells stained for lipid droplets with oil red after treatment. Hematoxylin was used to counterstain the cells. IC_{50} concentration of LCA (108 µM) and DOX (80 nM) was used in free LCA group and free DOX group. Black arrows show the lipid droplets. They are seen as small gray dots inside the cells (in the cytoplasm).

3.7.8 Detection of Apoptosis in Cancer Cells with qRT-PCR

Expression of pro-apoptotic genes as Bax and p53 increases if cells are in apoptotic stage, meanwhile expression of anti-apoptotic genes Bcl-2 and Bcl-xL decreases if cells are in apoptotic stage. LCA causes cell death by apoptosis, necrosis and autophagy in prostate cancer cells (Gafar et al., 2016). Therefore, we investigated the apoptotic effect of free LCA, LCA_{60}**M, LCA_{25}**M, free DOX, DOX_{conj}-M, DOX_{ld}-M and DL-M on MDA-MB-231 cells.

In our study, after the treatment with free LCA, LCA_{60}**M, and LCA_{25}**M, expression of Bax gene significantly increased in LCA_{60}**M, and LCA_{25}**M groups compared to free LCA group, which shows that LCA_{60}**M and LCA_{25}**M had better anticancer efficacy than that of free LCA.

Free DOX demonstrated higher Bax gene expression than all groups. On the other hand, there was no significant difference in Bax gene expressions of DOX_{conj}-M, DOX_{ld}-M and DL-M groups. In all these groups Bax gene expression was higher compared to the control (untreated cells) and M groups (Figure 3.38-A). There was no significant difference in the expression of p53 gene between free LCA, LCA_{60}**M, and LCA_{25}**M groups but the expression of p53 gene in free LCA, LCA_{60}**M, and LCA_{25}**M groups was significantly higher than control (untreated cells) and M group. Free DOX provided more p53 gene expression than all groups. The p53 gene expression of DOX_{conj}-M, DOX_{ld}-M and DL-M increased compared to the control and M groups.

For the micelles containing DOX, the order for p53 gene expressions was as follows: DOX_{conj}-M, the highest, followed by DL-M and DOX_{ld}-M, the lowest (Figure 3.38-B). The expression of Bcl-2 gene was significantly higher in free LCA, LCA_{60}**M, and LCA_{25}**M groups compared to control (untreated cells) and M group. Free DOX and DOX_{conj}-M likewise increased Bcl-2 gene expression. On the other hand, DOX_{ld}-M and DL-M significantly reduced Bcl-2 gene expression (Figure 3.38-C). There was no change in the gene expressions of Bcl-xL of free LCA, LCA_{60}**M,

and LCA_{25}**M groups compared to control group (untreated cells), but was higher compared to M group. Free DOX and DOX_{conj}-M likewise increased Bcl-xL gene expression. On the other hand, DOX_{ld}-M and DL-M significantly reduced Bcl-xL gene expression (Figure 3.38-D). These results were in line with the literature. For example, Luu et al. (2018) reported no change in Bcl-2 gene expressions in MDA-MB-231 cells when used free LCA in concentrations between 0-200 µM (Luu et al., 2018). But our results of p53 and Bax gene expressions were higher than reported in literature (Luu et al., 2018). Our results showed that LCA_{60}**M and LCA_{25}**M were highly effective and induced apoptosis in MDA-MB-231 cells. On the other hand, DOX_{ld}-M and DL-M were more effective than other groups.

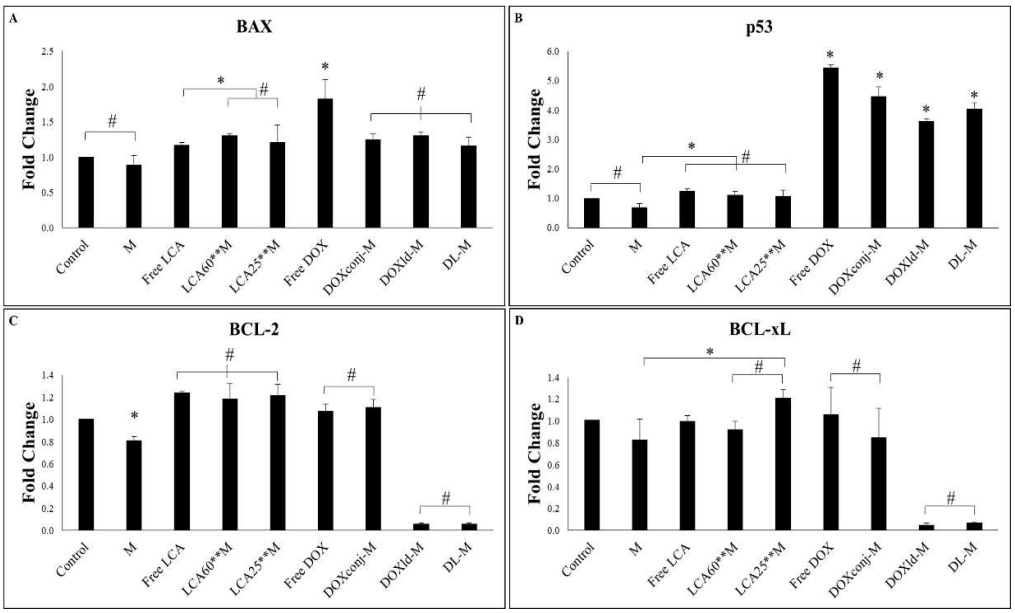

Figure 3.38. qRT-PCR results of A) Bax, B) p53, C) Bcl-2, and D) Bcl-xL genes of MDA-MB-231 cells after free LCA, LCA_{60}**M, LCA_{25}**M, free DOX, DOX_{conj}-M, DOX_{ld}-M, DL-M, and M treatment for 24 hours (n=3). IC_{50} concentration of LCA (108 µM) and DOX (80 nM) was used in free LCA group and free DOX group. * shows the significant differences between the groups ($p<0.05$) and # shows non-significant differences ($p>0.05$).

3.7.9 Determination of Cell Apoptosis with Annexin V-FITC Assay

Apoptosis of MDA-MB-231 cells after treatment with free LCA, LCA_{60}**M, LCA_{25}**M, free DOX, DOX_{conj}-M, DOX_{ld}-M and DL-M was determined by Annexin V-FITC assay (Figure 3.39-A, B, C, D, E, F, G, H, and I). Results showed that free LCA, LCA_{60}**M, LCA_{25}**M, and DL-M induced higher apoptosis in MDA-MB-231 cells compared to the control (untreated cells) and M groups. Free DOX, DOX_{conj}-M and DOX_{ld}-M increased the apoptosis compared to control, M, free LCA, LCA_{60}**M, LCA_{25}**M, and DL-M groups. Results indicated that LCA_{60}**M, LCA_{25}**M, and DL-M caused about 10-fold increase in the number of total apoptotic (early and late) cells (Figure 3.39-J). Total number of apoptotic cells in LCA_{60}**M, LCA_{25}**M, and DL-M was significantly higher than free LCA group. These results indicated that LCA_{60}**M, LCA_{25}**M, and DL-M formulations are more effective on MDA-MB-231 cells than free LCA. Similarly, Luu et al. (2018) reported that 150 and 200 µM free LCA caused apoptosis in MDA-MB-231 cells due to inhibition of lipogenesis after treatment with LCA. Lipogenesis inhibition decreases cell proliferation so cell death occurs but this pathway has not proven for MDA-MB-231 cells yet (Luu et al., 2018). According to our results, 108 µM free LCA, or LCA_{60}**M, LCA_{25}**M and DL-M containing 108 µM LCA also caused apoptosis of MDA-MB-231 cells. The highest apoptotic cell number was observed in DOX_{ld}-M group. There was no significant difference between free DOX and DOX_{conj}-M but they caused the second highest apoptotic cell number.

Gao et al. (2017) prepared honokiol and DOX loaded mPEG-b-PCL micelles. Honokiol was used due to its anti-oxidative, anti-inflammatory, and anti-depressant effects as well as possible anticancer activity. Annexin V-FITC analysis results showed that honokiol loaded micelles did not cause apoptosis on C6 glioma cells. On the other hand, DOX loaded micelles and DOX and honokiol co-loaded micelles increased apoptosis (Gao et al., 2017). In our study, DOX containing groups also caused more apoptosis than LCA containing micelles. These results are in line with our qRT-PCR, and ROS generation results.

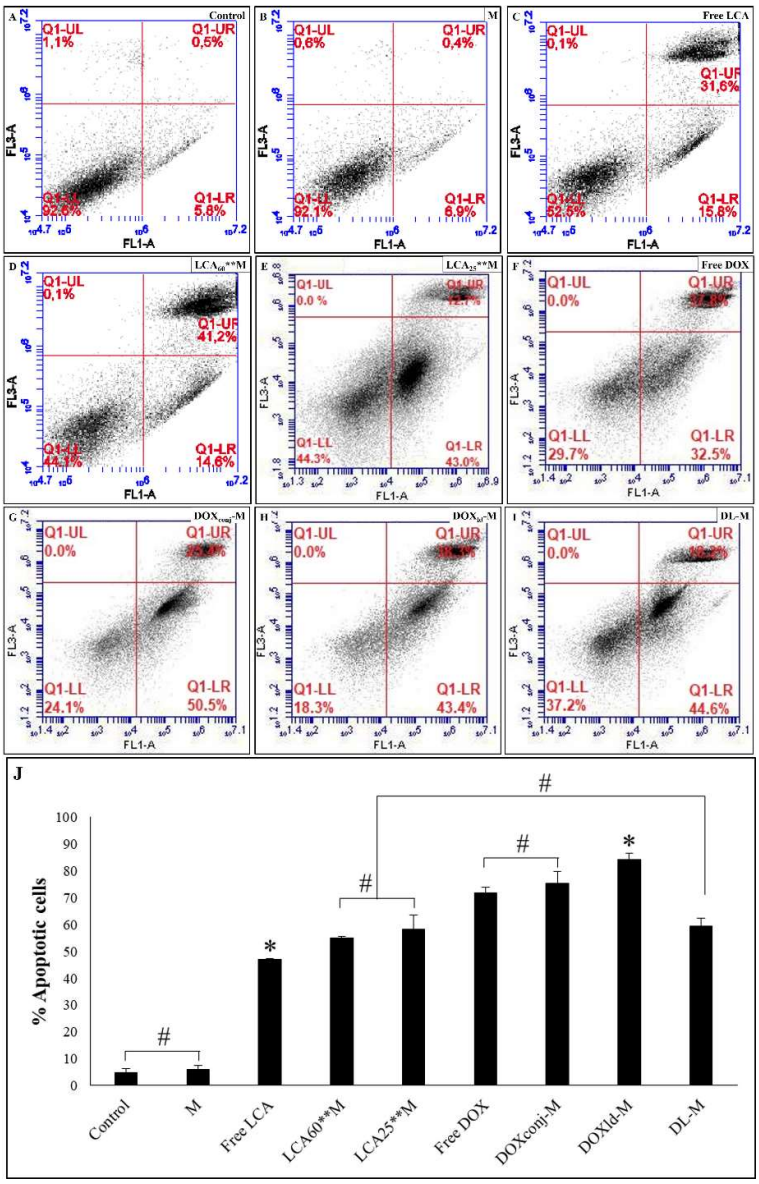

Figure 3.39. Annexin-V/FITC apoptosis assay results of MDA-MB 231 cells A) without treatment (control group: untreated cells). Annexin-V/FITC apoptosis assay results of MDA-MB 231 cells after treatment with B) M, C) free LCA, D) LCA_{60}**M, E) LCA_{25}**M, F) free DOX, G) DOX_{conj}-M, H) DOX_{ld}-M, and I) DL-M for 24 h. Q1-LL: viable cells. Q1-UL: dead cells. Q1-UR: late apoptotic cells. Q1-LR: early apoptotic cells. J) Percentage of apoptotic cells after 24 h incubation (n=3). IC_{50} concentration of LCA (108 µM) and DOX (80 nM) was used in free LCA group and free DOX group and LCA_{60}**M containing the same amount as the IC_{50} concentration. All micelles were added in the same amount with LCA_{60}**M. * shows the significant differences ($p<0.05$) between the groups and # shows the nonsignificant differences ($p>0.05$).

3.7.10 Mitochondrial Transmembrane Potential Detection

DiOC6 is a cell membrane permeable dye which can stain intact mitochondria. In apoptosis, loss of mitochondrial transmembrane potential occurs and therefore DiOC6 cannot stain the mitochondria. In Figure 3.40, mitochondrial transmembrane potential analysis results are given. M did not change the mitochondrial transmembrane potential, while treatment with free LCA, LCA_{60}**M and LCA_{25}**M caused a loss of mitochondrial transmembrane potential as a result of cell apoptosis. Free LCA, LCA_{60}**M and LCA_{25}**M decreased mitochondrial transmembrane potential by 41.8 ± 3.0%, 30.4 ± 0.9%, and 57.1 ± 0.5, respectively. LCA_{25}**M decreased mitochondrial transmembrane potential more than the LCA_{60}**M. On the other hand, there was no significant difference between LCA_{60}**M and LCA_{25}**M in other apoptosis determination assays like qRT-PCR, annexin-V analysis and ROS determination.

Yadav et al. (2015) showed that a LCA derivative induced loss of mitochondrial transmembrane potential in MDA-MB-231 cells, whereas it did not change mitochondrial transmembrane potential in MCF-7 cells, suggesting that LCA derivative can has selective activity against MDA-MB-231 cells (Yadav et al., 2015). Our results showed that LCA_{60}**M and LCA_{25}**M caused decrease in mitochondrial transmembrane potential related to apoptosis. Treatment with free DOX, DOX_{conj}-M, DOX_{ld}-M, and DL-M also decreased mitochondrial transmembrane potential by 44.4 ± 0.7%, 41.8 ± 2.8%, 43.0 ± 1.7%, and 38.8 ± 1.3%, respectively. All micelles containing DOX and/or LCA decreased mitochondrial transmembrane potential, which lead to apoptosis of the cells.

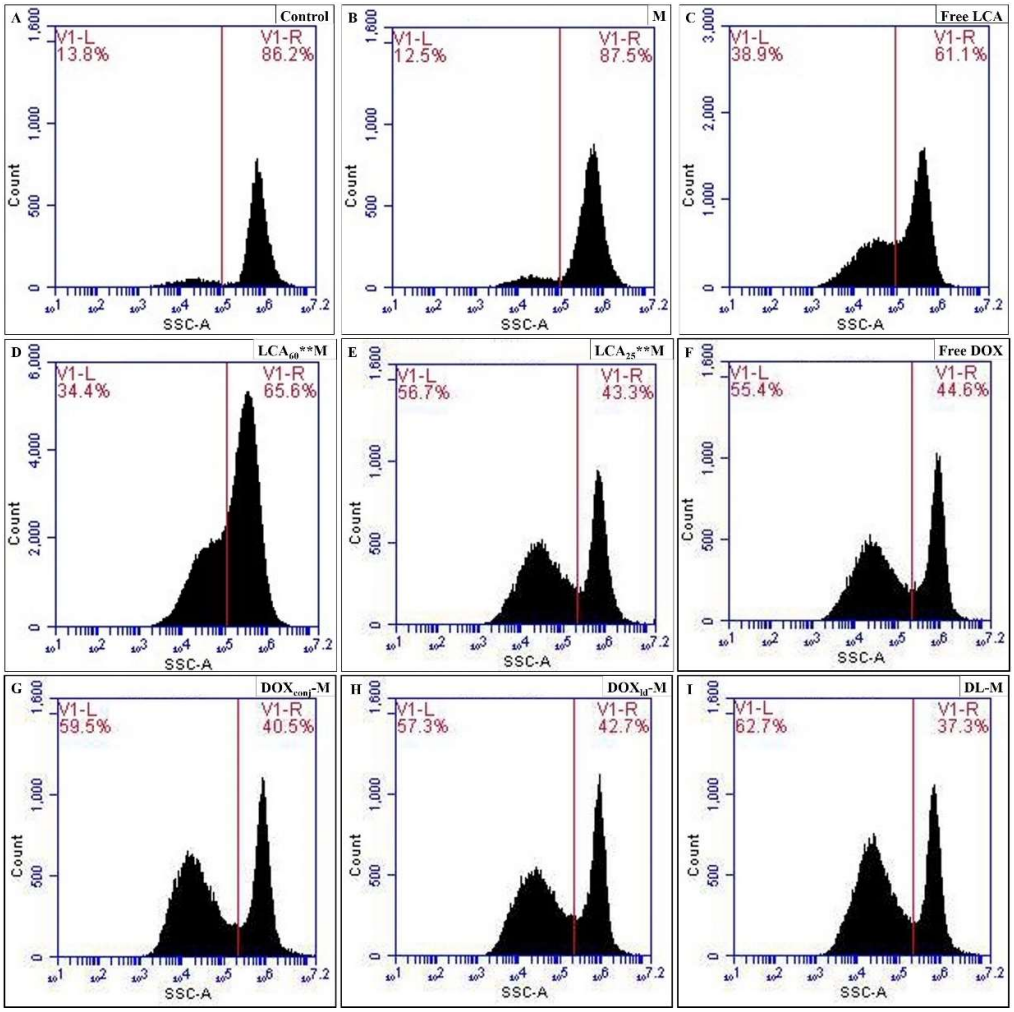

Figure 3.40. Mitochondrial transmembrane potential measurements of MDA-MB-231 cells A) without treatment (control group: untreated cells) using DiOC6. Mitochondrial transmembrane potential measurements of MDA-MB-231 cells after treatment with B) M, C) free LCA, D) LCA_{60}**M, E) LCA_{25}**M, F) free DOX, G) DOX_{conj}-M, H) DOX_{ld}-M, and I) DL-M for 24 h using DiOC6. V1-L: viable cells. V1-R: dead cells.

3.7.11 Reactive Oxygen Species (ROS) Determination

DCFDA is a fluorescent probe and used to detect ROS in the cell. In this study, ROS was determined with confocal microscopy and results showed that free LCA, LCA_{60}**M, LCA_{25}**M, free DOX, DOX_{conj}-M, DOX_{ld}-M, DL-M, and TBHP increased ROS levels in cells compared to control and M groups (Figure 3.41-A).

TBHP was used as the control group since it increases ROS levels of cells because TBHP forms radical species which increase ROS in the cell. ROS also determined with measuring fluorescence intensity (Figure 3.41-B). Results showed that free LCA, LCA_{60}**M, and LCA_{25}**M significantly increased ROS generation compared to control and M. Effect of LCA on ROS was also reported by Sreekanth et al. (2013), where they synthesized tamoxifen conjugated LCA and showed that tamoxifen conjugated LCA caused an increase in ROS level when treated with MDA-MB-231 cells (Sreekanth et al., 2013).

In our study, the highest ROS generation was observed in DOX_{conj}-M group. There was no significant difference between DOX_{ld}-M, and DL-M in ROS generation but both DOX_{ld}-M, and DL-M significantly increased ROS generation compared to free DOX group. These results showed that DOX conjugated or DOX loaded micelles had higher effect on ROS generation than free DOX, which may result in higher apoptotic activity since ROS generation is an early indicator of apoptosis. Cheng et al. (2020) prepared DOX loaded mixed micelles from Pluronic F127 and phenylboronic ester grafted Pluronic P123. Phenylboronic ester was used to give ROS sensitivity to micelles. They observed that ROS unsensitive and ROS sensitive DOX loaded mixed micelles increased ROS generation in DOX resistant MCF7 cells compared to free DOX by 5.49 fold and 8.96 fold, respectively (Cheng et al., 2020). In our study, DOX_{conj}-M, DOX_{ld}-M, and DL-M increased ROS generation compared to free DOX by 3.37 fold, 2.47 fold, and 2.30 fold, respectively. These results showed that treatment with DOX_{conj}-M, DOX_{ld}-M, and DL-M can increase the effectiveness of DOX on DOX resistant cells.

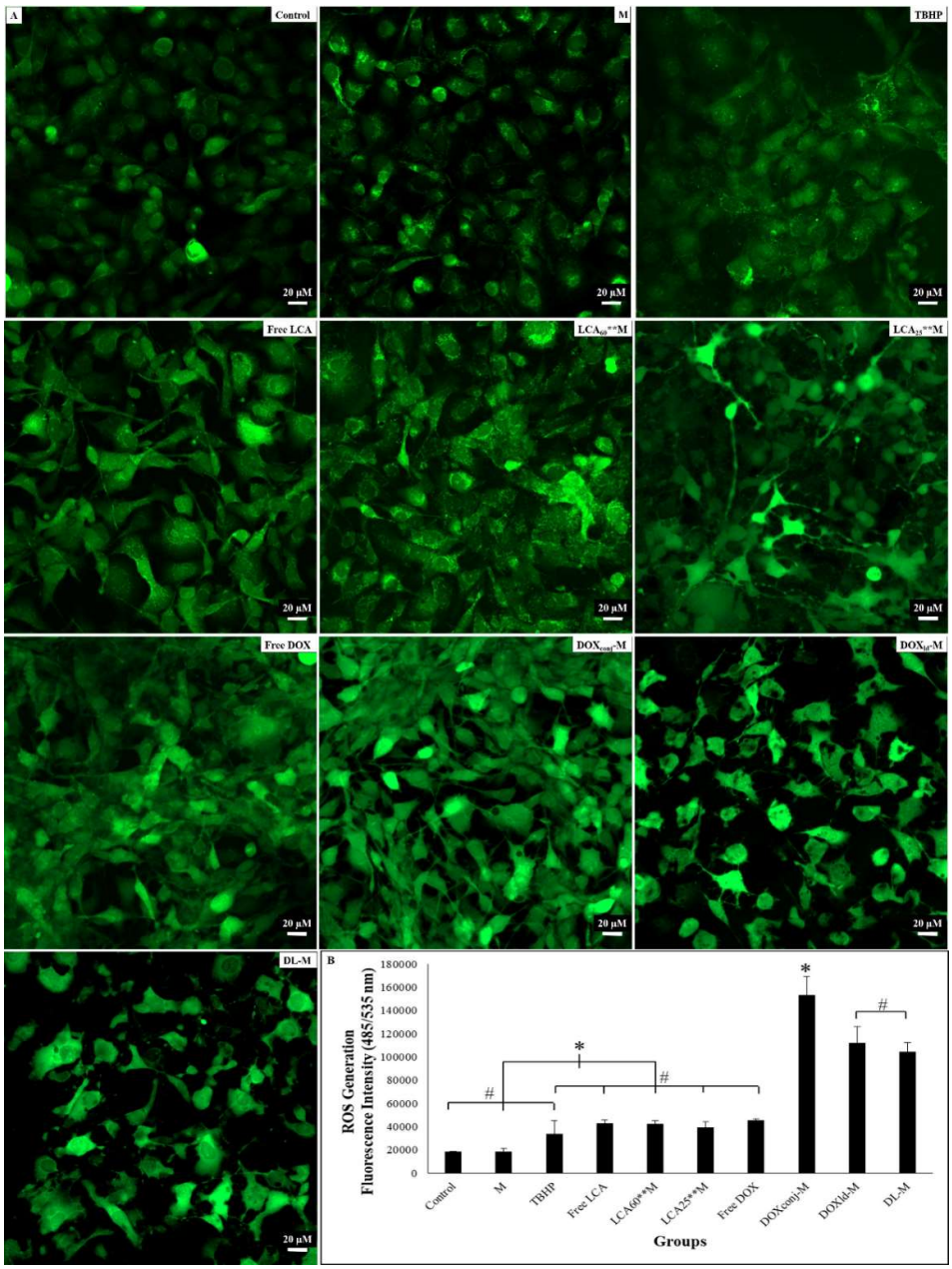

Figure 3.41. A) ROS determination with confocal microscopy after treatment with TBHP, M, free LCA, LCA_{60}**M, LCA_{25}**M, free DOX, DOX_{conj}-M, DOX_{ld}-M, and DL-M for 24 h (TBHP: Tert-butyl hydroperoxide). B) ROS determination by measuring fluorescence intensity using microplate reader after treatment with TBHP, M, free LCA, LCA_{60}**M, LCA_{25}**M, free DOX, DOX_{conj}-M, DOX_{ld}-M, and DL-M for 24 h (n=4). * shows the significant differences between the groups ($p<0.05$) and # shows non-significant differences ($p>0.05$). DCFDA is a green fluorescent dye that stains ROS in cells.

3.7.12 Endothelial Cell Tube Formation Assay

Cancer cells overexpress vascular endothelial growth factors to stimulate the formation of new blood vessel so the cancer cells can easily access to the nutrients. Tube formation assay was carried out to determine the effect of LCA and DOX carrying micelles on the new vessel formation ability of endothelial cells. Results showed that co-culture of MDA-MB-231 cells with HUVECs stimulated tube formation (Figure 3.42, Figure 3.43, Figure 3.44 and Figure 3.45). Tube formation was suppressed after treatment with free LCA at IC_{50} concentration (108 µM) and LCA_{60}**M and LCA_{25}**M that contained the same amount with the IC_{50} concentration of LCA. On the other hand, free DOX increased tube formation compared to control groups. DOX_{conj}-M, DOX_{ld}-M and DL-M reduced tube formation relative to free DOX. There were more meshes in co-cultures of MDA-MB-231 cells and HUVECs compared to the control groups (untreated cells) which means that cancer cells increased the vessel formation of endothelial cells. Co-culture of endothelial cells with cancer cells increases angiogenesis of endothelial cells, because cancer cells overexpress some growth factors like VEGF. Breast cancer cells also overexpress VEGF, which results in increased new blood vessel formation and increased permeability of vessels. This causes metastasis.

There is a system called 'blood-brain barrier' in brain and there are vessels in the blood-brain barrier, which decrease permeability. This prevents brain from components as well as bioactive agents and drugs in the circulating blood. Metastatic breast cancer cells increase the permeability of these vessels in the blood-brain barrier so this causes metastasis in the brain. Treatment with M resulted in similar mesh formation as the control groups (untreated cells). Free LCA in IC_{50} concentration (108 µM) treatment inhibited the tube formation of HUVECs (Figure 3.46-A and B). A significant decrease was observed in tube length and number of nodes after treatment with LCA. Free DOX significantly increased the number of nodes and total tube length compared to the control and co-culture control groups.

For the DOX containing micelles, DOX_{conj}-M caused the highest number of nodes and DOX_{ld}-M caused the lowest number of nodes. In fact, DOX_{ld}-M resulted in lower number of nodes than LCA_{60}**M and LCA_{25}**M. However, co-cultures treated with DOX_{ld}-M resulted in a higher number of nodes than LCA_{60}**M and LCA_{25}**M. Micelles containing DOX did not differ in total tube length compared to the control. Co-cultures after free LCA treatment showed tube formation but a significant decrease in tube length and number of nodes was observed compared to untreated co-culture control. Micelles containing DOX in the co-culture groups did not differ from the control in the number of nodes and total tube length. There was no significant difference in number of nodes between the co-culture control and co-cultures treated with empty micelles (M) after 2h and 8h incubations. Meantime, after 4h incubation, co-culture control group had significantly higher number of nodes than the co-culture treated with empty micelles (M). Total tube length of co-culture control group was significantly higher than the co-cultures treated with M after 2h, 4h, and 8 h. Tube formation significantly decreased after treatment with LCA_{60}**M and LCA_{25}**M that contained the same amount with the IC_{50} concentration of LCA.

Kundu et al. (2017) studied the effects of hydrophobic and hydrophilic bile acids on angiogenesis to investigate the liver repair after cholestatic liver disease. They examined the effect of LCA on angiogenesis. After overnight incubation, it was observed that LCA inhibited tube formation even at low concentrations (12.5 and 25 μM). Due to the hydrophobic and toxic nature of LCA they did not use concentrations higher than 25 μM and a significant decrease was observed in tube length and number of nodes after treatment with LCA. They observed approximately 2-fold decrease in number of nodes and total tube length compared to control (Kundu et al., 2017). Free LCA of IC_{50} concentration (108 μM) was used in this study and a significant decrease in tube length was also observed. On the other hand, LCA_{60}**M and LCA_{25}**M caused a 2-fold decrease in number of nodes and a 1.5-fold decrease in total tube length compared to M. These results showed that micelle formulation of LCA and free LCA were both effective in inhibition of angiogenesis. Zhu et al.

(2017) prepared curcumin loaded methoxy polyethylene glycol–polylactide micelles and showed their effect on angiogenesis using HUVECs. They observed that curcumin loaded micelles inhibited tube formation compared to free curcumin group (Zhu et al., 2017). Our results also showed that LCA_{60}**M and LCA_{25}**M significantly inhibited the tube formation compared the control group.

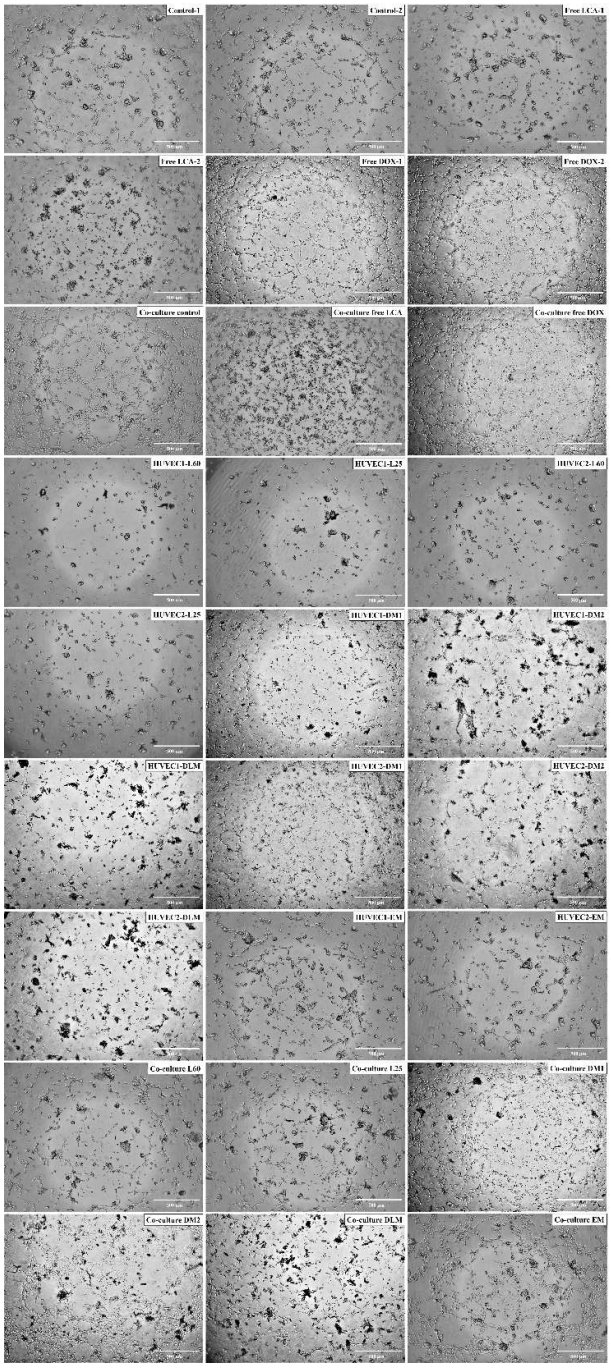

Figure 3.42. Images of tube formation assay after 2 hours of incubation. Scale bar is 500 µm. 40×10^3 HUVECs and 40×10^3 MDA-MB-231 cells were used in the experiments. 1: EC medium, 2: EC:L15 medium (1:1), EM: mPEG-b-PCL micelles (M), L60: LCA_{60}**M, L25: LCA_{25}**M, DM1: DOX_{conj}-M, DM2: DOX_{ld}-M, DLM: DL-M.

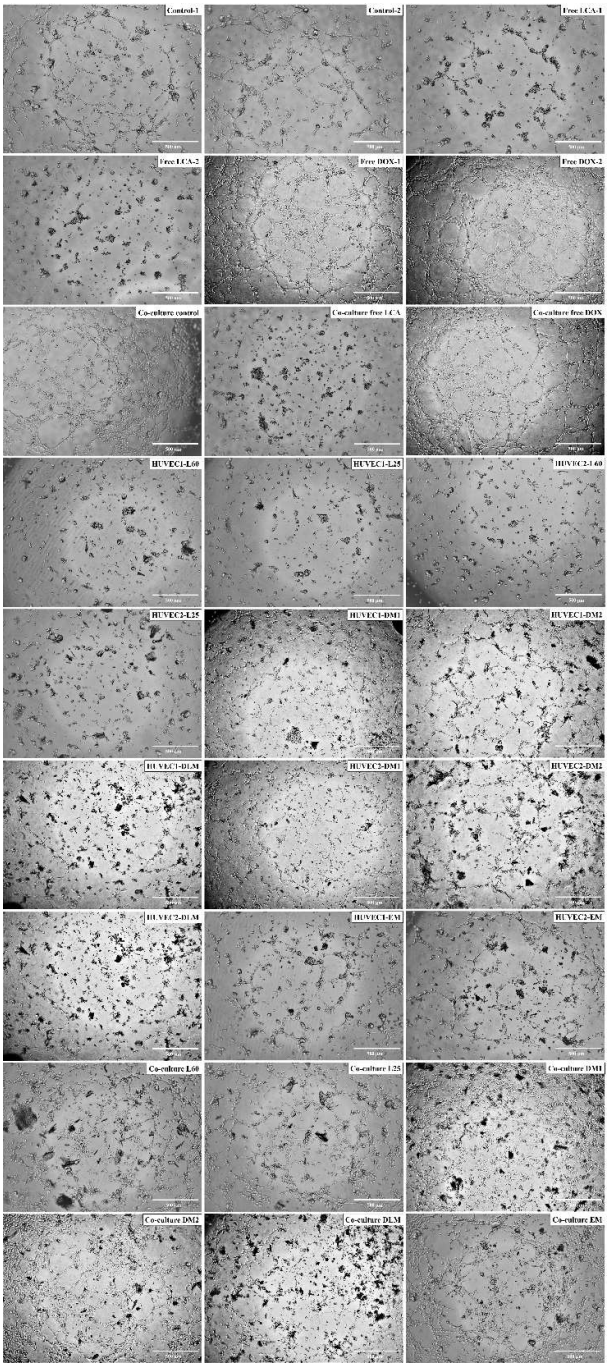

Figure 3.43. Images of tube formation assay after 4 hours of incubation. Scale bar is 500 µm. 40×10^3 HUVECs and 40×10^3 MDA-MB-231 cells were used in the experiments. 1: EC medium, 2: EC:L15 medium (1:1), EM: mPEG-b-PCL micelles (M), L60: LCA_{60}**M, L25: LCA_{25}**M, DM1: DOX_{conj}-M, DM2: DOX_{ld}-M, DLM: DL-M.

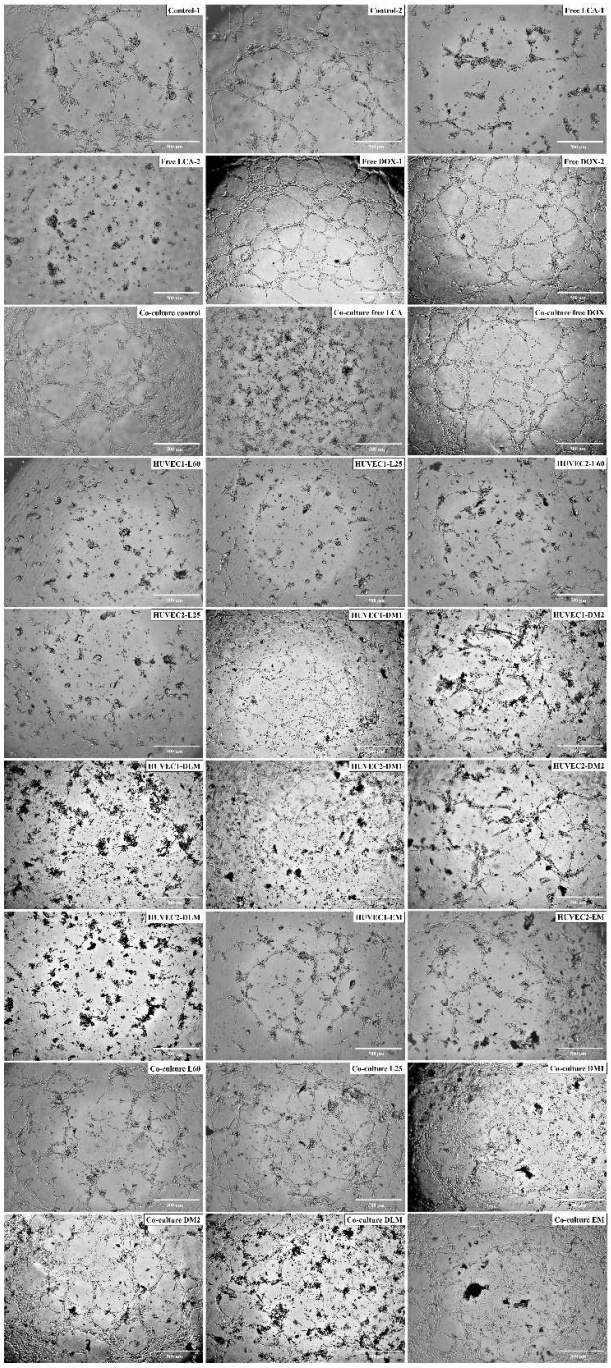

Figure 3.44. Images of tube formation assay after 8 hours of incubation. Scale bar is 500 µm. 40×10^3 HUVECs and 40×10^3 MDA-MB-231 cells were used in the experiments. 1: EC medium, 2: EC:L15 medium (1:1), EM: mPEG-b-PCL micelles (M), L60: LCA_{60}**M, L25: LCA_{25}**M, DM1: DOX_{conj}-M, DM2: DOX_{ld}-M, DLM: DL-M.

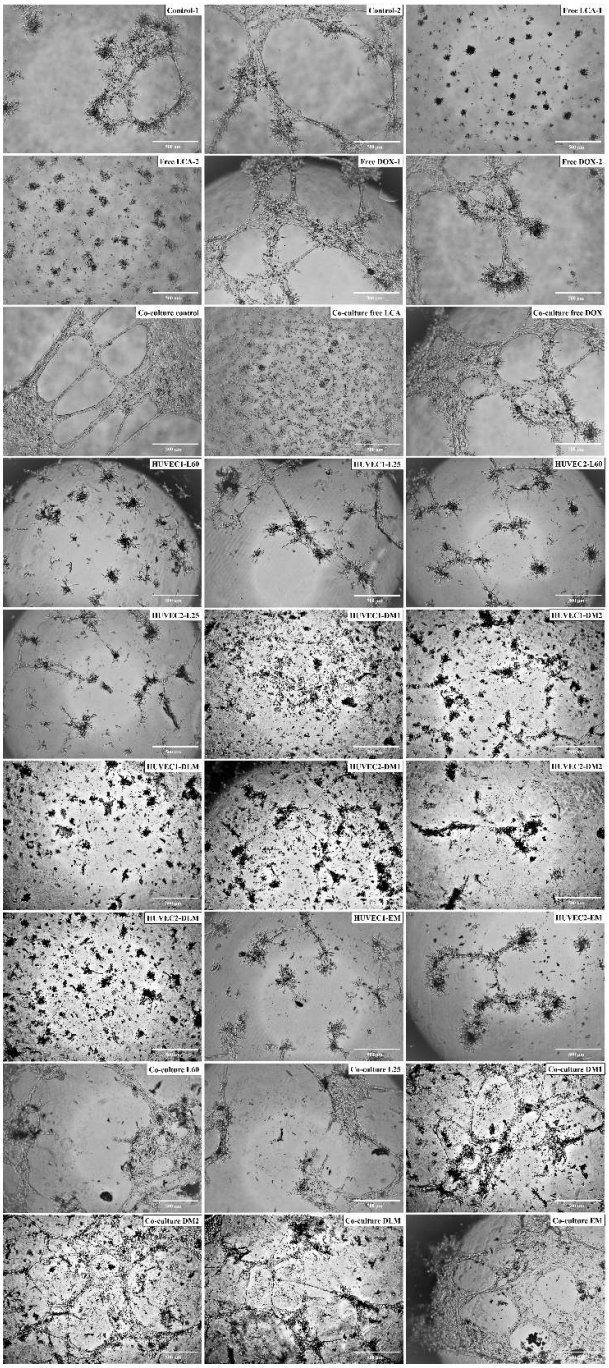

Figure 3.45. Images of tube formation assay after 24 hours of incubation. Scale bar is 500 µm. 40×10^3 HUVECs and 40×10^3 MDA-MB-231 cells were used in the experiments. 1: EC medium, 2: EC:L15 medium (1:1), EM: mPEG-b-PCL micelles (M), L60: LCA_{60}**M, L25: LCA_{25}**M, DM1: DOX_{conj}-M, DM2: DOX_{ld}-M, DLM: DL-M.

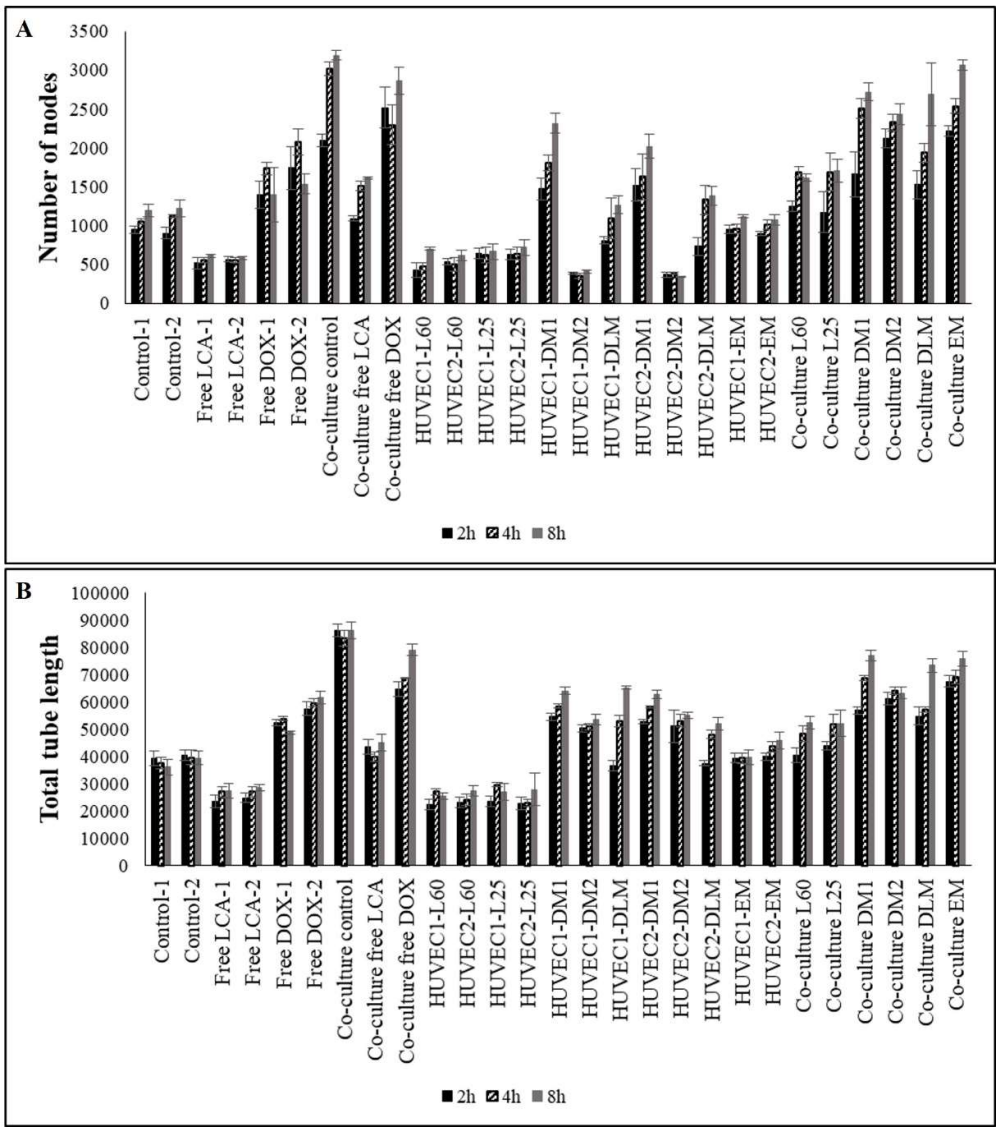

Figure 3.46. A) Quantification of tube formation in terms of number of nodes. B) Quantification of tube formation in terms of total tube lengths. IC50 concentrations (108 µM and 80 nM) were used in the free LCA and free DOX groups and LCA_{60}**M containing the same amount as the IC_{50} concentration of LCA was weighed. All micelles were added in the same amount with LCA_{60}**M. Images of HUVECs were taken after 2, 4, and 8 hours of incubation at 37°C from three independent experiments and number of nodes and total tube length were measured using ImageJ software (n=3). 1: EC medium, 2: EC:L15 medium (1:1), EM: empty micelles, L60: LCA_{60}**M, L25: LCA_{25}**M, DM1: DOX_{conj}-M, DM2: DOX_{ld}-M, DLM: DL-M.

CHAPTER 4

CONCLUSIONS

In this study, mPEG-b-PCL copolymer was synthesized and micelles (M) were prepared by solvent evaporation method without sonication. DOX was covalently conjugated via pH responsive hydrozone bonds to the copolymer, and the conjugation efficiency was 36.04%. LCA was ionically conjugated to the copolymer at two different temperatures as 60ºC and 25ºC, and the encapsulation efficiencies were 53% and 95%, respectively. The micelles prepared from these copolymers were coded as DOX_{conj}-M, DOX_{ld}-M, LCA_{60}**M, and LCA_{25}**M, respectively. Also, micelles loaded with DOX without conjugation (DOX_{ld}-M). and micelles having both drugs together (DL-M) were prepared

Characterization studies showed that all micelles had uniform shape with nano size structures about 80 – 200 nm, which is suitable for intravenous injection. Zeta potential and polydispersity index results showed that micelles were very stable. Drug release studies demonstrated faster LCA and DOX release under acidic conditions (pH 5.0) than under normal physiological conditions (pH 7.4). LCA release profile showed that LCA_{60}**M, LCA_{25}**M, and DL-M favors first order release under acidic conditions, while under normal conditions release follows Korsmeyer-Peppas kinetic model. DOX release profile also showed that DOX_{conj}-M, DOX_{ld}-M, and DL-M favors first order release under acidic conditions, while under normal conditions release follows Korsmeyer-Peppas kinetic model.

All micelles demonstrated higher cytotoxic effect on MDA-MB-231 cells compared to control group having only micelles without any drug. Migration of micelles was lower in all groups. Lipogenic activity was lower in LCA_{60}**M, and LCA_{25}**M than DOX containing ones as DOX_{conj}-M, DOX_{ld}-M, and DL-M groups. Apoptotic activity of micelles was evaluated with qRT-PCR and Annexin V-FITC analysis and results demonstrated that DOX_{ld}-M and DL-M was even more apoptotic than other

groups. Increased ROS generation in all micelles is an indicator of apoptosis. Loss of mitochondrial transmembrane potential of the cells tretaed with all types of micelles showed that cancer cells were in apoptotic stage. Endothelial cell tube formation was also inhibited after treating cells with LCA_{60}**M and LCA_{25}**M, showing the prevantion of the proliferation of the cancer cells.

Upto this point, all micelles prepared and loaded with anticancer drugs (DOX or LCA of both as DOX + LCA) demonstrated very high efficiency in preventing the growth and proliferation of cancer cells. These micelles demonstrating pH responsive delivery of the anticancer drugs can be good candidates as carriers for the therapy of cancer patients.

REFERENCES

Ahn, J., Miura, Y., Yamada, N., Chida, T., Liu, X., Kim, A., Sato, R., Tsumura, R., Koga, Y., Yasunaga, M., Nishiyama, N., Matsumura, Y., Cabral, H., & Kataoka, K. (2015). Antibody fragment-conjugated polymeric micelles incorporating platinum drugs for targeted therapy of pancreatic cancer. *Biomaterials*, *39*, 23–30. https://doi.org/10.1016/j.biomaterials.2014.10.069 0142-9612/©

Aliabadi, H. M., Elhasi, S., Mahmud, A., Gulamhusein, R., Mahdipoor, P., & Lavasanifar, A. (2007). Encapsulation of hydrophobic drugs in polymeric micelles through co-solvent evaporation: The effect of solvent composition on micellar properties and drug loading. *International Journal of Pharmaceutics*, *329*(1–2), 158–165. https://doi.org/10.1016/j.ijpharm.2006.08.018

Baimark, Y. (2009). Surfactant-free nanospheres of methoxy poly (ethylene glycol)-b-poly (ε-caprolactone) for controlled release of ibuprofen. *Journal of Applied Sciences*, *9*(12), 2287–2293. https://doi.org/10.3923/jas.2009.2287.2293

Bansal, K. K., Kakde, D., Purdie, L., Irvine, D. J., Howdle, S. M., Mantovani, G., & Alexander, C. (2015). New biomaterials from renewable resources-amphiphilic block copolymers from δ-decalactone. *Polymer Chemistry*, *6*(40), 7196–7210. https://doi.org/10.1039/c5py01203a

Bazak, R., Houri, M., El Achy, S., Kamel, S., & Refaat, T. (2015). Cancer active targeting by nanoparticles: a comprehensive review of literature. *Journal of Cancer Research and Clinical Oncology*, *141*(5), 769–784. https://doi.org/10.1007/s00432-014-1767-3

Bernabeu, E., Gonzalez, L., Legaspi, M. J., Moretton, M. A., & Chiappetta, D. A. (2016). Paclitaxel-loaded TPGS-b-PCL nanoparticles: in vitro cytotoxicity and cellular uptake in MCF-7 and MDA-MB-231 cells versus mPEG-b-PCL nanoparticles and Abraxane®. *Journal of Nanoscience and Nanotechnology*, *16*, 160–170. https://doi.org/10.1166/jnn.2016.10739

Bertrand, N., Wu, J., Xu, X., Kamaly, N., & Farokhzad, O. C. (2014). Cancer nanotechnology: The impact ofpassive and active targeting in the era of modern cancer biology. *Advanced Drug Delivery Reviews*, *66*, 2–25. https://doi.org/10.1016/j.addr.2013.11.009

Bielenberg, D. R., & Zetter, B. R. (2015). The contribution of angiogenesis to the process of metastasis. *The Cancer Journal*, *21*(4), 267–273. https://doi.org/10.1097/PPO.0000000000000138

Bolu, B. S., Golba, B., Sanyal, A., & Sanyal, R. (2020). Trastuzumab targeted micellar delivery of docetaxel using dendron–polymer conjugates. *Biomaterials Science*, *8*, 2600–2610. https://doi.org/10.1039/c9bm01764j

Bruschi, M. L. (2015). Mathematical models of drug release. In M. L. Bruschi (Ed.), *Strategies to Modify the Drug Release from Pharmaceutical Systems* (2nd ed., pp. 63–86). Elsevier/Woodhead publishing. https://doi.org/10.1016/B978-0-08-100092-2.00005-9

Cabral, H., Matsumoto, Y., Mizuno, K., Chen, Q., Murakami, M., Kimura, M., Terada, Y., Kano, M. R., Miyazono, K., Uesaka, M., Nishiyama, N., & Kataoka,

K. (2011). Accumulation of sub-100 nm polymeric micelles in poorly permeable tumours depends on size. *Nature Nanotechnology*, *6*, 815–823. https://doi.org/10.1038/NNANO.2011.166

Cai, S., Alhowyan, A. A. B., Yang, Q., Forrest, W. C. M., Shnayder, Y., & Forrest, M. L. (2014). Cellular uptake and internalization of hyaluronan based doxorubicin and cisplatin conjugates.pdf. *Journal of Drug Targeting*, *22*(7), 648–657. https://doi.org/10.3109/1061186X.2014.921924

Cha, E. J., Kim, J. E., & Ahn, C. H. (2009). Stabilized polymeric micelles by electrostatic interactions for drug delivery system. *European Journal of Pharmaceutical Sciences*, *38*(4), 341–346. https://doi.org/10.1016/j.ejps.2009.08.006

Chang, M., Zhang, F., Wei, T., Zuo, T., Guan, Y., Lin, G., & Shao, W. (2016). Smart linkers in polymer-drug conjugates for tumor-targeted delivery. *Journal of Drug Targeting*, *24*(6), 475–491. https://doi.org/10.3109/1061186X.2015.1108324

Chau, Yi., Dang, N. M., Tan, F. E., & Langer, R. (2006). Investigation of targeting mechanism of new dextran- peptide-methotrexate conjugates using biodistribution study in matrix-metalloproteinase-overexpressing tumor xenograft model. *Journal of Pharmaceutical Sciences*, *95*(3), 542–551. https://doi.org/10.1002/jps.20548

Chen, N., Li, S., Li, X., Zhan, Q., Li, L., Long, L., Zhao, J., Hou, X., & Yuan, X. (2022). Construction of enzymatic nanoreactors with high catalytic activity in millifluidic systems for cancer therapy. *Chemical Engineering Journal*, *429*, 132305. https://doi.org/10.1016/j.cej.2021.132305

Chen, W., Li, L., Zhang, X., Liang, Y., Pu, Z., Wang, L., & Mo, J. (2017). Curcumin: a calixarene derivative micelle potentiates anti-breast cancer stem cells effects in xenografted, triple-negative breast cancer mouse models. *Drug Delivery*, *24*(1), 1470–1481. https://doi.org/10.1080/10717544.2017.1381198

Chen, Y., Zhang, Y. X., Wu, Z. F., Peng, X. Y., Su, T., Cao, J., He, B., & Li, S. (2016). Biodegradable poly(ethylene glycol)-poly(ϵ-carprolactone) polymeric micelles with different tailored topological amphiphilies for doxorubicin (DOX) drug delivery. *RSC Advances*, *6*, 58160–58172. https://doi.org/10.1039/c6ra06040d

Chen, Yakun, Tang, Y., Chen, S., & Nie, D. (2009). Regulation of drug resistance by human pregnane X receptor in breast cancer. *Cancer Biology and Therapy*, *8*(13), 1265–1272. https://doi.org/10.4161/cbt.8.13.8696

Cheng, X., Lv, X., Xu, J., Zheng, Y., Wang, X., & Tang, R. (2020). Pluronic micelles with suppressing doxorubicin efflux and detoxification for efficiently reversing breast cancer resistance. *European Journal of Pharmaceutical Sciences*, *146*, 105275. https://doi.org/10.1016/j.ejps.2020.105275

Ciocan-Cartita, C. A., Jurj, A., Zanoaga, O., Cojocneanu, R., Pop, L. A., Moldovan, A., Moldovan, C., Zimta, A. A., Raduly, L., Pop-Bica, C., Buse, M., Budisan, L., Virag, P., Irimie, A., Gomes Dias, S. M., Berindan-Neagoe, I., & Braicu, C. (2020). New insights in gene expression alteration as effect of doxorubicin drug resistance in triple negative breast cancer cells. *Journal of Experimental and*

Clinical Cancer Research, *39*(1), 241. https://doi.org/10.1186/s13046-020-01736-2

Clinical Trials. (2022). https://clinicaltrials.gov/ct2/results?cond=&term=micelle&cntry=&state=&city=&dist=

Configliacchi, E., Razzano, G., Rizzo, V., & Vigevani, A. (1996). HPLC methods for the determination of bound and free doxorubicin, and of bound and free galactosamine, in methacrylamide polymer-drug conjugates. *Journal of Pharmaceutical and Biomedical Analysis*, *15*(1), 123–129. https://doi.org/10.1016/0731-7085(96)01825-0

Costa, P., & Sousa Lobo, J. M. (2001). Modeling and comparison of dissolution profiles. *European Journal of Pharmaceutical Sciences*, *13*(2), 123–133. https://doi.org/10.1016/S0928-0987(01)00095-1

Couraud, S., Zalcman, G., Milleron, B., Morin, F., & Souquet, P. J. (2012). Lung cancer in never smokers - A review. *European Journal of Cancer*, *48*(9), 1299–1311. https://doi.org/10.1016/j.ejca.2012.03.007

Danafar, H., Davaran, S., Rostamizadeh, K., Valizadeh, H., & Hamidi, M. (2014). Biodegradable m-PEG/PCL core-shell micelles: Preparation and characterization as a sustained release formulation for curcumin. *Advanced Pharmaceutical Bulletin*, *4*, 501–510. https://doi.org/10.5681/apb.2014.074

Darge, H. F., Hanurry, E. Y., Birhan, Y. S., Mekonnen, T. W., Andrgie, A. T., Chou, H.-Y., Lai, J.-Y., & Tsai, H.-C. (2021). Multifunctional drug-loaded micelles encapsulated in thermo-sensitive hydrogel for in vivo local cancer treatment: Synergistic effects of anti- vascular and immuno-chemotherapy. *Chemical Engineering Journal*, *406*, 126879. https://doi.org/10.1016/j.cej.2020.126879

del Rosario, L. S., Demirdirek, B., Harmon, A., Orban, D., & Uhrich, K. E. (2010). Micellar nanocarriers assembled from doxorubicin-conjugated amphiphilic macromolecules (DOX-AM). *Macromolecular Bioscience*, *10*(4), 415–423. https://doi.org/10.1002/mabi.200900335

Eskandari, P., Abousalman-Rezvani, Z., Hajebi, S., Roghani-Mamaqani, H., & Salami-Kalajahi, M. (2020). Controlled release of anti-cancer drug from the shell and hollow cavities of poly(N-isopropylacrylamide) hydrogel particles synthesized via reversible addition-fragmentation chain transfer polymerization. *European Polymer Journal*, *135*(July), 109877. https://doi.org/10.1016/j.eurpolymj.2020.109877

Etrych, T., Jel´ınkova, M., Rihova, B., & Ulbrich, K. (2001). New HPMA copolymers containing doxorubicin bound via pH-sensitive linkage: synthesis and preliminary in vitro and in vivo biological properties. *Journal of Controlled Release*, *73*, 89–102. https://doi.org/10.1016/S0168-3659(01)00281-4

Etrych, T., Šubr, V., Laga, R., Říhová, B., & Ulbrich, K. (2014). Polymer conjugates of doxorubicin bound through an amide and hydrazone bond: Impact of the carrier structure onto synergistic action in the treatment of solid tumours. *European Journal of Pharmaceutical Sciences*, *58*(1), 1–12. https://doi.org/10.1016/j.ejps.2014.02.016

Faal Maleki, M., Jafari, A., Mirhadi, E., Askarizadeh, A., Golichenari, B.,

Hadizadeh, F., Jalilzadeh Moghimi, S. M., Aryan, R., Mashreghi, M., & Jaafari, M. R. (2019). Endogenous stimuli-responsive linkers in nanoliposomal systems for cancer drug targeting. *International Journal of Pharmaceutics*, *572*, 118716. https://doi.org/10.1016/j.ijpharm.2019.118716

Feng, H., Chu, D., Li, Z., Guo, Z., Jin, L., Fan, B., Zhang, J., & Li, J. (2018). A DOX-loaded polymer micelle for effectively inhibiting cancer cells. *RSC Advances*, *8*(46), 25949–25954. https://doi.org/10.1039/c8ra04089c

Ferreira, M. J. U., Gyémánt, N., Madureira, A. M., Tanaka, M., Koós, K., Didziapetris, R., & Molnár, J. (2005). The effects of jatrophane derivatives on the reversion of MDR1- and MRP-mediated multidrug resistance in the MDA-MB-231 (HTB-26) cell line. *Anticancer Research*, *25*(6 B), 4173–4178.

Fouad, Y. A., & Aanei, C. (2017). Revisiting the hallmarks of cancer. *American Journal of Cancer Research*, *7*(5), 1016–1036. https://doi.org/10.1016/j.jmwh.2009.11.004

Fu, Z., & Xiang, J. (2020). Aptamer-functionalized nanoparticles in targeted delivery and cancer therapy. *International Journal of Molecular Sciences*, *21*(23), 1–39. https://doi.org/10.3390/ijms21239123

Gafar, A. A., Draz, H. M., Goldberg, A. A., Bashandy, M. A., Bakry, S., Khalifa, M. A., AbuShair, W., Titorenko, V. I., & Sanderson, J. T. (2016). Lithocholic acid induces endoplasmic reticulum stress, autophagy and mitochondrial dysfunction in human prostate cancer cells. *PeerJ*, *4*, e2445. https://doi.org/10.7717/peerj.2445

Gandhi, A. V., Randolph, T. W., & Carpenter, J. F. (2019). Conjugation of emtansine onto trastuzumab promotes aggregation of the antibody-drug conjugate by reducing repulsive electrostatic interactions and increasing hydrophobic interactions. *Journal of Pharmaceutical Sciences*, *108*, 1973–1983. https://doi.org/10.1016/j.xphs.2019.01.029

Gao, X., Wang, S., Wang, B., Deng, S., Liu, X., Zhang, X., Luo, L., Fan, R., Xiang, M., You, C., Wei, Y., Qian, Z., & Guo, G. (2015). Improving the anti-ovarian cancer activity of docetaxel with biodegradable self-assembly micelles through various evaluations. *Biomaterials*, *53*, 646–658. https://doi.org/10.1016/j.biomaterials.2015.02.108

Gao, X., Yu, T., Xu, G., Guo, G., Liu, X., Hu, X., Wang, X., Liu, Y., Mao, Q., You, C., & Zhou, L. (2017). Enhancing the anti-glioma therapy of doxorubicin by honokiol with biodegradable self-assembling micelles through multiple evaluations. *Scientific Reports*, *7*, 43501. https://doi.org/10.1038/srep43501

García-Hevia, L., Casafont, I., Oliveira, J., Teran, N., Fanarraga, M. L., Gallo, J., & Banobre-Lopez, M. (2022). Magnetic lipid nanovehicles synergize the controlled thermal release of chemotherapeutics with magnetic ablation while enabling non-invasive monitoring by MRI for melanoma theranostics. *Bioactive Materials*, *8*, 153–164. https://doi.org/10.1016/j.bioactmat.2021.06.009

Garmpis, N., Damaskos, C., Garmpi, A., Kalampokas, E., Kalampokas, T., Spartalis, E., Daskalopoulou, A., Valsami, S., Kontos, M., Nonni, A., Kontzoglou, K., Perrea, D., Nikiteas, N., & Dimitroulis, D. (2017). Histone deacetylases as new

therapeutic targets in triple-negative breast cancer: Progress and promises. *Cancer Genomics and Proteomics*, *14*, 299–313. https://doi.org/10.21873/cgp.20041

Gatti, S., Agostini, A., Palmiero, U. C., Colombo, C., Peviani, M., Biffi, A., & Moscatelli, D. (2018). Hydrazone linked doxorubicin-PLA prodrug nanoparticles with high drug loading. *Nanotechnology*, *29*, 305602. https://doi.org/10.1088/1361-6528/aac0d3

Gdowski, A., Hayatshahi, H., Fudala, R., Joshi, R., Liu, J., Vishwanatha, J. K., Jeyarajah, R., Guzik, P., & Ranjan, A. P. (2022). Novel use of hypoxia-inducible polymerizable protein to augment chemotherapy for pancreatic cancer. *Pharmaceutics*, *14*, 128. https://doi.org/10.3390/pharmaceutics14010128

Ghaffar, A., Yameen, B., Latif, M., & Malik, M. I. (2020). pH-sensitive drug delivery systems. In M. R. Shah, M. Imran, & S. Ullah (Eds.), *Metal Nanoparticles for Drug Delivery and Diagnostic Applications* (eBook, pp. 259–278). Elsevier. https://doi.org/10.1016/C2018-0-00172-3

Goldberg, A. A., Beach, A., Davies, G. F., Harkness, T. A. A., LeBlanc, A., & Titorenko, V. I. (2011). Lithocholic bile acid selectively kills neuroblastoma cells, while sparing normal neuronal cells. *Oncotarget*, *2*(10), 761–782. https://doi.org/10.18632/oncotarget.338

Gu, J., Chen, Y., Tong, L., Wang, X., Yu, D., & Wu, H. (2020). Astaxanthin-loaded polymer-lipid hybrid nanoparticles (ATX-LPN): Assessment of potential otoprotective effects. *Journal of Nanobiotechnology*, *18*(1), 1–17. https://doi.org/10.1186/s12951-020-00600-x

Haider, T., Pandey, V., Banjare, N., Gupta, P. N., & Soni, V. (2020). Drug resistance in cancer: mechanisms and tackling strategies. *Pharmacological Reports*, *72*, 1125–1151. https://doi.org/10.1007/s43440-020-00138-7

Han, M., Diao, Y. Y., Jiang, H. L., Ying, X. Y., Chen, D. W., Liang, W. Q., & Gao, J. Q. (2011). Molecular mechanism study of chemosensitization of doxorubicin-resistant human myelogenous leukemia cells induced by a composite polymer micelle. *International Journal of Pharmaceutics*, *420*(2), 404–411. https://doi.org/10.1016/j.ijpharm.2011.09.009

Hascicek, C., Sengel-Turk, C. T., Gumustas, M., Ozkan, A. S., Bakar, F., Das-Evcimen, N., Savaser, A., & Ozkan, Y. (2017). Fulvestrant-loaded polymer-based nanoparticles for local drug delivery: Preparation and in vitro characterization. *Journal of Drug Delivery Science and Technology*, *40*, 73–82. https://doi.org/10.1016/j.jddst.2017.06.001 1773-2247/©

He, X. L., Xing, Y., Gu, X. Z., Xiao, J. X., Wang, Y. Y., Yi, Z., & Qiu, W. W. (2017). The synthesis and antitumor activity of lithocholic acid and its derivatives. *Steroids*, *125*(June), 54–60. https://doi.org/10.1016/j.steroids.2017.06.009

Huang, M. H., Li, S., Coudane, J., & Vert, M. (2003). Synthesis and characterization of block copolymers of ε-caprolactone and DL-lactide initiated by ethylene glycol or poly(ethylene glycol). *Macromolecular Chemistry and Physics*, *204*(16), 1994–2001. https://doi.org/10.1002/macp.200350054

Huang, M. H., Li, S., Hutmacher, D. W., Schantz, J. T., Vacanti, C. A., Braud, C., &

Vert, M. (2004). Degradation and cell culture studies on block copolymers prepared by ring opening polymerization of ε-caprolactone in the presence of poly(ethylene glycol). *Journal of Biomedical Materials Research - Part A*, *69*(3), 417–427. https://doi.org/10.1002/jbm.a.30008

Huang, X., Liao, W., Xie, Z., Chen, D., & Zhang, C. Y. (2018). A pH-responsive prodrug delivery system self-assembled from acid-labile doxorubicin-conjugated amphiphilic pH-sensitive block copolymers. *Materials Science and Engineering C*, *90*, 27–37. https://doi.org/10.1016/j.msec.2018.04.036

Huang, Y.-K., Tian, H.-R., Zhang, M.-Z., He, J.-L., Liu, J., & Ni, P.-H. (2021). Monoclonal nntibody-conjugated polyphosphoester-hyd-DOX prodrug nanoparticles for targeted chemotherapy of liver cancer cells. *Chinese Journal of POLYMER SCIENCE*, *39*, 1392–1402. https://doi.org/10.1007/s10118-021-2582-3

Hussein, Y. H. A., & Youssry, M. (2018). Polymeric micelles of biodegradable diblock copolymers: Enhanced encapsulation of hydrophobic drugs. *Materials*, *11*(5), 688. https://doi.org/10.3390/ma11050688

Isik, G., Hasirci, N., Tezcaner, A., & Kiziltay, A. (2020). Multifunctional periodontal membrane for treatment and regeneration purposes. *Journal of Bioactive and Compatible Polymers*, *35*(2), 117–138. https://doi.org/10.1177/0883911520911659

Isik, G., Tezcaner, A., Hasirci, N., & Kiziltay, A. (2021). Determination of doxorubicin amount conjugated to mPEG-b-PCL copolymer via pH sensitive hydrazone bond. *Turkish Bulletin of Hygiene and Experimental Biology*. https://doi.org/10.5505/TurkHijyen.2022.04317

Jannu, A. K., Puppala, E. R., Gawali, B., Syamprasad, N. P., Alexander, A., Marepally, S., Chella, N., Gangasani, J. K., & Naidu, V. G. M. (2021). Lithocholic acid-tryptophan conjugate (UniPR126) based mixed micelle as a nano carrier for specific delivery of niclosamide to prostate cancer via EphA2 receptor. *International Journal of Pharmaceutics*, *605*(June), 120819. https://doi.org/10.1016/j.ijpharm.2021.120819

Jazayeri, M. H., Amani, H., Pourfatollah, A. A., Pazoki-Toroudi, H., & Sedighimoghaddam, B. (2016). Various methods of gold nanoparticles (GNPs) conjugation to antibodies. *Sensing and Bio-Sensing Research*, *9*, 17–22. https://doi.org/10.1016/j.sbsr.2016.04.002

Jehle, J., Staudacher, I., Wiedmann, F., Schweizer, P. A., Becker, R., Katus, H. A., & Thomas, D. (2012). Regulation of apoptosis in HL-1 cardiomyocytes by phosphorylation of the receptor tyrosine kinase EphA2 and protection by lithocholic acid. *British Journal of Pharmacology*, *167*(7), 1563–1572. https://doi.org/10.1111/j.1476-5381.2012.02117.x

Jette, K. K., Law, D., Schmitt, E. A., & Kwon, G. S. (2004). Preparation and drug loading of poly(ethylene glycol)-block-poly(ε- caprolactone) micelles through the evaporation of a cosolvent azeotrope. *Pharmaceutical Research*, *21*(7), 1184–1191. https://doi.org/10.1023/B:PHAM.0000033005.25698.9c

Kheirkhah, P., Denyer, S., Bhimani, A. D., Arnone, G. D., Esfahani, D. R., Aguilar, T., Zakrzewski, J., Venugopal, I., Habib, N., Gallia, G. L., Linninger, A.,

Charbel, F. T., & Mehta, A. I. (2018). Magnetic Drug Targeting: A Novel Treatment for Intramedullary Spinal Cord Tumors. *Scientific Reports*, *8*, 11417. https://doi.org/10.1038/s41598-018-29736-5

Kim, H. M., Lee, J., & Koo, J. S. (2017). Clinicopathological and prognostic significance of programmed death ligand-1 expression in breast cancer: A meta-analysis. *BMC Cancer*, *17*, 690. https://doi.org/10.1186/s12885-017-3670-1

Kim, K., Choi, H., Choi, E. S., Park, M. H., & Ryu, J. H. (2019). Hyaluronic acid-coated nanomedicine for targeted cancer therapy. *Pharmaceutics*, *11*(7), 1–22. https://doi.org/10.3390/pharmaceutics11070301

Kitano, K., Ishihara, K., & Yusa, S. (2022). Preparation of a thermo-responsive drug carrier consisting of a biocompatible triblock copolymer and fullerene. *Journal of Materials Chemistry B*, *Bioinspired Surfaces Engineering for Biomaterials*, Advance Article. https://doi.org/10.1039/d1tb02183d

Kundu, S., Bansal, S., Muthukumarasamy, K. M., Sachidanandan, C., Motiani, R. K., & Bajaj, A. (2017). Deciphering the role of hydrophobic and hydrophilic bile acids in angiogenesis using in vitro and in vivo model systems. *Med. Chem. Comm.*, *8*, 2248–2257. https://doi.org/10.1039/c7md00475c

Lale, S. V., Kumar, A., Naz, F., Bharti, A. C., & Koul, V. (2015). Multifunctional ATRP based pH responsive polymeric nanoparticles for improved doxorubicin chemotherapy in breast cancer by proton sponge effect/endo-lysosomal escape. *Polymer Chemistry*, *6*(11), 2115–2132. https://doi.org/10.1039/c4py01698j

Leach, A., Smyth, P., Ferguson, L., Steven, J., Greene, M. K., Branco, C. M., McCann, A. P., Porter, A., Barelle, C. J., & Scott, C. J. (2020). Anti-DLL4 VNAR targeted nanoparticles for targeting of both tumour and tumour associated vasculature. *Nanoscale*, *12*, 14751–14763. https://doi.org/10.1039/d0nr02962a

Lee, B. K., Yun, Y. H., & Park, K. (2015). Smart nanoparticles for drug delivery: Boundaries and opportunities. *Chemical Engineering Science*, *125*, 158–164. https://doi.org/10.1016/j.ces.2014.06.042

Li, Yamin, Li, R., Chakraborty, A., Ogurlu, R., Zhao, X., Chen, J., & Xu, Q. (2020). Combinatorial Library of Cyclic Benzylidene Acetal-Containing pH-Responsive Lipidoid Nanoparticles for Intracellular mRNA Delivery. *Bioconjugate Chemistry*, *31*, 1835–1843. https://doi.org/10.1021/acs.bioconjchem.0c00295

Li, Yi, Yang, H. Y., Thambi, T., Park, J. H., & Lee, D. S. (2019). Charge-convertible polymers for improved tumor targeting and enhanced therapy. *Biomaterials*, *217*, 119299. https://doi.org/10.1016/j.biomaterials.2019.119299

Li, Z., Tan, S., Li, S., Shen, Q., & Wang, K. (2017). Cancer drug delivery in the nano era: An overview and perspectives (Review). *Oncology Reports*, *38*(2), 611–624. https://doi.org/10.3892/or.2017.5718

Liao, J., Peng, H., Liu, C., Li, D., Yin, Y., Lu, B., Zhenga, H., & Wang, Q. (2021). Dual pH-responsive-charge-reversal micelle platform for enhanced anticancer therapy Jianhong. *Materials Science and Engineering C*, *118*, 111527. https://doi.org/10.1016/j.msec.2020.111527

Liao, X., Fan, Y., Hou, J., Chen, X., Xu, X., Yang, Y., Shen, J., Mi, P., Huang, X.,

Zhang, W., Cao, H., Hong, X., Hu, T., & Zhan, Y. (2019). Identification of chaetocin as a potent non-ROS- mediated anticancer drug candidate for gastric cancer. *Journal of Cancer*, *10*(16), 3678–3690. https://doi.org/10.7150/jca.32803

Linsley, C. S., & Wu, B. M. (2017). Recent advances in light-responsive on- demand drug-delivery systems. *Therapeutic Delivery*, *8*(2), 89–107. https://doi.org/10.4155/tde-2016-0060

Luu, T. H., Bard, J. M., Carbonnelle, D., Chaillou, C., Huvelin, J. M., Bobin-Dubigeon, C., & Nazih, H. (2018). Lithocholic bile acid inhibits lipogenesis and induces apoptosis in breast cancer cells. *Cellular Oncology*, *41*(1), 13–24. https://doi.org/10.1007/s13402-017-0353-5

Mariani, E., Lisignoli, G., Borzì, R. M., & Pulsatelli, L. (2019). Biomaterials: Foreign bodies or tuners for the immune response? *International Journal of Molecular Sciences*, *20*, 636. https://doi.org/10.3390/ijms20030636

Martinez, J. C., & Otley, C. C. (2001). The management of melanoma and nonmelanoma skin cancer: a review for the primary care physician. *Mayo Clinic Proceedings*, *76*(12), 1253–1265. https://doi.org/10.4065/76.12.1253

Mauri, E., Chincarini, G. M. F., Rigamonti, R., Magagnin, L., Sacchetti, A., & Rossi, F. (2017). Modulation of electrostatic interactions to improve controlled drug delivery from nanogels. *Materials Science and Engineering C*, *72*, 308–315. https://doi.org/10.1016/j.msec.2016.11.081

Meng, Q., Hu, H., Jing, X., Sun, Y., Zhou, L., Zhu, Y., Yu, B., Cong, H., & Shen, Y. (2021). A modular ROS-responsive platform co-delivered by 10-hydroxycampto- thecin and dexamethasone for cancer treatment. *Journal of Controlled Release*, *340*, 102–113. https://doi.org/10.1016/j.jconrel.2021.10.027

Mikhail, A. S., & Allen, C. (2010). Poly(ethylene glycol)- b -poly(ε-caprolactone) micelles containing chemically conjugated and physically entrapped docetaxel: Synthesis, characterization, and the influence of the drug on micelle morphology. *Biomacromolecules*, *11*(5), 1273–1280. https://doi.org/10.1021/bm100073s

Mikó, E., Vida, A., Kovács, T., Ujlaki, G., Trencsényi, G., Márton, J., Sári, Z., Kovács, P., Boratkó, A., Hujber, Z., Csonka, T., Antal-Szalmás, P., Watanabe, M., Gombos, I., Csoka, B., Kiss, B., Vígh, L., Szabó, J., Méhes, G., … Bai, P. (2018). Lithocholic acid, a bacterial metabolite reduces breast cancer cell proliferation and aggressiveness. *Biochimica et Biophysica Acta - Bioenergetics*, *1859*(9), 958–974. https://doi.org/10.1016/j.bbabio.2018.04.002

Mohanty, A. K., Jana, U., Manna, P. K., & Mohanta, G. P. (2015). Synthesis and evaluation of MePEG-PCL diblock copolymers: surface properties and controlled release behavior. *Progress in Biomaterials*, *4*(2–4), 89–100. https://doi.org/10.1007/s40204-015-0040-4

Moulahoum, H., Ghorbanizamani, F., Bayir, E., Timur, S., & Zihnioglu, F. (2022). A polyplex human saliva peptide histatin 5-grafted methoxy PEG-b-polycaprolactone polymersome for intelligent stimuli-oriented doxorubicin delivery. *Journal of Drug Delivery Science and Technology*, *67*, 102958.

https://doi.org/10.1016/j.jddst.2021.102958
Murakami, K., Nagatoishi, S., Kasahara, K., Nagai, H., Sasajima, Y., Sasaki, R., & Tsumoto, K. (2021). Electrostatic-triggered exothermic antibody adsorption to the cellulose nanoparticles. *Analytical Biochemistry*, *63*, 114337. https://doi.org/10.1016/j.ab.2021.114337
National Center for Biotechnology Information. (2022). *PubChem compound summary for CID 31703, doxorubicin*. Https://Pubchem.Ncbi.Nlm.Nih.Gov/Compound/Doxorubicin. https://pubchem.ncbi.nlm.nih.gov/compound/Doxorubicin
Nieberler, M., Reuning, U., Reichart, F., Notni, J., Wester, H. J., Schwaiger, M., Weinmüller, M., Räder, A., Steiger, K., & Kessler, H. (2017). Exploring the role of RGD-recognizing integrins in cancer. *Cancers*, *9*(9), 1–33. https://doi.org/10.3390/cancers9090116
Nwe, K., & Brechbiel, M. W. (2009). Growing applications of '"click chemistry"' for bioconjugation in contemporary biomedical research. *CANCER BIOTHERAPY AND RADIOPHARMACEUTICALS*, *24*(3), 289–302. https://doi.org/10.1089=cbr.2008.0626
Okur, A. C., Erkoc, P., & Kizilel, S. (2016). Targeting cancer cells via tumor-homing peptide CREKA functional PEG nanoparticles. *Colloids and Surfaces B: Biointerfaces*, *147*, 191–200. https://doi.org/10.1016/j.colsurfb.2016.08.005
Owen, S. C., Chan, D. P. Y., & Shoichet, M. S. (2012). Polymeric micelle stability. *Nano Today*, *7*(1), 53–65. https://doi.org/10.1016/j.nantod.2012.01.002
Özenver, N., Saeed, M., Demirezer, L. Ö., & Efferth, T. (2018). Aloe-emodin as drug candidate for cancer therapy. *Oncotarget*, *9*(25), 17770–17796. https://doi.org/10.18632/oncotarget.24880
Parvani, J. G., & Jackson, M. W. (2017). Silencing the roadblocks to effective triple negative breast cancer treatments by siRNA nanoparticles. *Endocrine-Related Cancer*, *24*(4), R81–R97. https://doi.org/10.1530/ERC-16-0482
Peiris, P. M., He, F., Covarrubias, G., Raghunathan, S., Turan, O., Lorkowski, M., Gnanasambandam, B., Wu, C., Schiemann, W. P., & Karathanasis, E. (2018). Precise targeting of cancer metastasis using multi-ligand nanoparticles incorporating four different ligands. *Nanoscale*, *10*(15), 6861–6871. https://doi.org/10.1039/c8nr02513d
Pelengaris, S., & Khan, M. (2013). *The Molecular Biology of Cancer: A Bridge From Bench to Bedside.* (S. Pelengaris & M. Khan (Eds.); 2nd ed.). UK: John Wiley & Sons, Inc.
Peng, W., Jiang, X., Zhu, Y., Omari-Siaw, E., Deng, W., Yu, J., Xu, X., & Zhang, W. (2015). Oral delivery of capsaicin using MPEG-PCL nanoparticles. *Acta Pharmacologica Sinica*, *36*, 139–148. https://doi.org/10.1038/aps.2014.113
Pezzella, F., Tavassoli, M., & Kerr, D. (Eds.). (2019). *Oxford Textbook of Cancer biology* (1st ed.). Oxford University Press. https://doi.org/10.1201/9781315373560
Qi, P., Wu, X., Liu, L., Yu, H., & Song, S. (2018). Hydrazone-containing triblock copolymeric micelles for pH-controlled drug delivery. *Frontiers in Pharmacology*, *9*, 1–11. https://doi.org/10.3389/fphar.2018.00012

Ranganathan, R., Madanmohan, S., Kesavan, A., Baskar, G., Krishnamoorthy, Y. R., Santosham, R., Ponraju, D., Rayala, S. K., & Venkatraman, G. (2012). Nanomedicine: Towards development of patient-friendly drug-delivery systems for oncological applications. *International Journal of Nanomedicine*, *7*, 1043–1060. https://doi.org/10.2147/IJN.S25182

Ravasco, J. M. J. M., Faustino, H., Trindade, A., & Gois, P. M. P. (2019). Bioconjugation with Maleimides: A Useful Tool for Chemical Biology. *Chemistry - A European Journal*, *25*(1), 43–59. https://doi.org/10.1002/chem.201803174

Ribeiro, E., Alho, I., Marques, F., Gano, L., Correia, I., Correia, J. D. G., Casimiro, S., Costa, L., Santos, I., & Fernandes, C. (2016). Radiolabeled block copolymer micelles for image-guided drug delivery. *International Journal of Pharmaceutics*, *515*, 692–701. https://doi.org/10.1016/j.ijpharm.2016.11.004

Schieber, C., Bestetti, A., Lim, J. P., Ryan, A. D., Nguyen, T. L., Eldridge, R., White, A. R., Gleeson, P. A., Donnelly, P. S., Williams, S. J., & Mulvaney, P. (2012). Conjugation of transferrin to azide-modified cdse/zns core-shell quantum dots using cyclooctyne click chemistry. *Angewandte Chemie - International Edition*, *51*(42), 10523–10527. https://doi.org/10.1002/anie.201202876

Senevirathne, S. A., Washington, K. E., Biewer, M. C., & Stefan, M. C. (2016). PEG based anti-cancer drug conjugated prodrug micelles for the delivery of anti-cancer agents. *Journal of Materials Chemistry B*, *4*(3), 360–370. https://doi.org/10.1039/c5tb02053k

Sengel-Turk, C. T., Hascicek, C., Bakar, F., & Simsek, E. (2017). Comparative Evaluation of Nimesulide-Loaded Nanoparticles for Anticancer Activity Against Breast Cancer Cells. *AAPS PharmSciTech*, *18*(2), 393–403. https://doi.org/10.1208/s12249-016-0514-2 Research

Şengel Türk, C. T., Sezgin Bayindir, Z., & Badilli, U. (2009). Preparation of polymeric nanoparticles using different stabilizing agents. *Journal of Faculty of Pharmacy of Ankara University*, *38*(4), 257–268. https://doi.org/10.1501/eczfak_0000000543

Shaikh, H. K., Kshirsagar, R. V., & Patil, S. G. (2015). Mathematical models for drug release characterization: A review. *World Journal of Pharmacy and Pharmaceutical Sciences*, *4*(04), 324–338.

Shin, H.-J., Kwon, H.-K., Lee, J.-H., Gui, X., Achek, A., Kim, J.-H., & Choi, S. (2015). Doxorubicin-induced necrosis is mediated by poly-(ADP-ribose) polymerase 1 (PARP1) but is independent of p53. *Scientific Reports*, *5*, 15798. https://doi.org/10.1038/srep15798

Shuai, X., Ai, H., Nasongkla, N., Kim, S., & Gao, J. (2004). Micellar carriers based on block copolymers of poly(ε-caprolactone) and poly(ethylene glycol) for doxorubicin delivery. *Journal of Controlled Release*, *98*(3), 415–426. https://doi.org/10.1016/j.jconrel.2004.06.003

Shuai, X., Merdan, T., Unger, F., Wittmar, M., & Kissel, T. (2003). Novel biodegradable ternary copolymers hy-PEI-g-PCL-b-PEG: Synthesis, characterization, and potential as efficient nonviral gene delivery vectors. *Macromolecules*, *36*(15), 5751–5759. https://doi.org/10.1021/ma034390w

Siemiaszko, G., Niemirowicz-Laskowska, K., Markiewicz, K. H., Misztalewska-Turkowicz, I., Dudź, E., Milewska, S., Misiak, P., Kurowska, I., Sadowska, A., Car, H., & Wilczewska, A. Z. (2021). Synergistic effect of folate-conjugated polymers and 5-fluorouracil in the treatment of colon cancer. *Cancer Nanotechnology*, *12*, 31. https://doi.org/10.1186/s12645-021-00104-9

Singh, B., Jang, Y., Maharjan, S., Kim, H. J., Lee, A. Y., Kim, S., Gankhuyag, N., Yang, M. S., Choi, Y. J., Cho, M. H., & Cho, C. S. (2017). Combination therapy with doxorubicin-loaded galactosylated poly(ethyleneglycol)-lithocholic acid to suppress the tumor growth in an orthotopic mouse model of liver cancer. *Biomaterials*, *116*, 130–144. https://doi.org/10.1016/j.biomaterials.2016.11.040

Sreekanth, V., Bansal, S., Motiani, R. K., Kundu, S., Muppu, S. K., Majumdar, T. D., Panjamurthy, K., Sengupta, S., & Bajaj, A. (2013). Design, synthesis, and mechanistic investigations of bile acid-tamoxifen conjugates for breast cancer therapy. *Bioconjugate Chemistry*, *24*(9), 1468–1484. https://doi.org/10.1021/bc300664k

Srivastava, S., Kumar, A., Yadav, P. K., Kumar, M., Mathew, J., Pandey, A. C., & Chourasia, M. K. (2021). Formulation and performance evaluation of polymeric mixed micelles encapsulated with baicalein for breast cancer treatment. *Drug Development and Industrial Pharmacy*. https://doi.org/10.1080/03639045.2021.2007394

Su, M., Xiao, S., Shu, M., Lu, Y., Zeng, Q., Xie, J., Jiang, Z., & Liu, J. (2020). Enzymatic multifunctional biodegradable polymers for pH- and ROS-responsive anticancer drug delivery. *Colloids and Surfaces B: Biointerfaces*, *193*, 111067. https://doi.org/10.1016/j.colsurfb.2020.111067

Su, R., Xiong, X., Li, Y., Wei, X., Zheng, S., Zhao, J., & Zhou, S. (2021). A pH-triggered fluorescence-switchable extracellular vesicle for tracing drug release and improving drug delivery. *Biomaterials Science*, *9*, 5812–5823. https://doi.org/10.1039/d1bm00862e

Subramanian, J., & Govindan, R. (2008). Molecular genetics of lung cancer in people who have never smoked. *The Lancet Oncology*, *9*(7), 676–682. https://doi.org/10.1016/S1470-2045(08)70174-8

Tanaka, K., Kanazawa, T., Shibata, Y., Suda, Y., Fukuda, T., Takashima, Y., & Okada, H. (2010). Development of cell-penetrating peptide-modified MPEG-PCL diblock copolymeric nanoparticles for systemic gene delivery. *International Journal of Pharmaceutics*, *396*(1–2), 229–238. https://doi.org/10.1016/j.ijpharm.2010.06.028

Theerasilp, M., Sunintaboon, P., Sungkarat, W., & Nasongkla, N. (2017). Glucose-installed, SPIO-loaded PEG-b-PCL micelles as MR contrast agents to target prostate cancer cells. *Applied Nanoscience*, *7*(8), 711–721. https://doi.org/10.1007/s13204-017-0610-y

Torchilin, V. P. (2007). Micellar nanocarriers: Pharmaceutical perspectives. *Pharmaceutical Research*, *24*(1), 1–16. https://doi.org/10.1007/s11095-006-9132-0

Upponi, J. R., & Torchilin, V. P. (2014). Passive vs. Active Targeting: An Update

of the EPR Role in Drug Delivery to Tumors. In M. J. Alonso & M. Garcia-Fuentes (Eds.), *Nano- Oncologicals: New Targeting and Delivery Approaches* (pp. 3–45). Cham: Springer International Publishing. https://doi.org/10.1007/978-3-319-08084-0_1

van Leeuwen, L. A. G., Hinchy, E. C., Murphy, M. P., Robb, E. L., & Cochemé, H. M. (2017). Click-PEGylation – A mobility shift approach to assess the redox state of cysteines in candidate proteins. *Free Radical Biology and Medicine*, *108*(January), 374–382. https://doi.org/10.1016/j.freeradbiomed.2017.03.037

Venturelli, L., Nappini, S., Bulfoni, M., Gianfranceschi, G., Dal Zilio, S., Coceano, G., Del Ben, F., Turetta, M., Scoles, G., Vaccari, L., Cesselli, D., & Cojoc, D. (2016). Glucose is a key driver for GLUT1-mediated nanoparticles internalization in breast cancer cells. *Scientific Reports*, *6*, 1–14. https://doi.org/10.1038/srep21629

Viravaidya-Pasuwat, K., & Naruphontjirakul, P. (2019). Development of anti-her2-targeted doxorubicin–core-shell chitosan nanoparticles for the treatment of human breast cancer. *International Journal of Nanomedicine*, *14*, 4105–4121. https://doi.org/10.2147/IJN.S198552

Wang, F., Wang, Y. C., Dou, S., Xiong, M. H., Sun, T. M., & Wang, J. (2011). Doxorubicin-tethered responsive gold nanoparticles facilitate intracellular drug delivery for overcoming multidrug resistance in cancer cells. *ACS Nano*, *5*(5), 3679–3692. https://doi.org/10.1021/nn200007z

Wang, H., Wang, W., Li, C., Xu, A., Qiu, B., Li, F., & Ding, W. (2022). Flav7 + DOX co-loaded separable microneedle for light-triggered chemo-thermal therapy of superficial tumors. *Chemical Engineering Journal*, *428*, 131913. https://doi.org/10.1016/j.cej.2021.131913

Wang, X., Gu, Y., Li, Q., Xu, Y., Shi, Y., Wang, Z., Xia, M., Li, J., & Wang, D. (2022). Synergistic chemo-photothermal cancer therapy of pH-responsive polymeric nanoparticles loaded IR825 and DTX with charge-reversal property. *Colloids and Surfaces B: Biointerfaces*, *209*, 112164. https://doi.org/10.1016/j.colsurfb.2021.112164 Received

Wang, Y., Wang, Y., Chen, G., Li, Y., Xu, W., & Gong, S. (2017). Quantum-dot-based theranostic micelles conjugated with an anti- EGFR nanobody for triple-negative breast cancer therapy. *Applied Materials & Interfaces*, *9*, 30297–30305. https://doi.org/10.1021/acsami.7b05654

Weber, P., Dzuricky, M., Min, J., Jenkins, I., & Chilkoti, A. (2021). Concentration-independent multivalent targeting of cancer cells by genetically encoded core-crosslinked elastin/resilin-like polypeptide micelles. *Biomacromolecules*, *22*, 4347–4356. https://doi.org/10.1021/acs.biomac.1c00897

Wilczewska, A. Z., Niemirowicz, K., Markiewicz, K. H., & Car, H. (2012). Nanoparticles as drug delivery systems. *Pharmacological Reports*, *64*(5), 1020–1037. https://doi.org/10.1016/S1734-1140(12)70901-5

Wu, H., Zhu, L., & Torchilin, V. P. (2013). pH-sensitive poly(histidine)-PEG/DSPE-PEG co-polymer micelles for cytosolic drug delivery. *Biomaterials*, *34*, 1213–1222. https://doi.org/10.1016/j.biomaterials.2012.08.072

Xiao, C.-D., Shen, X.-C., & Tao, L. (2013). Modified emulsion solvent evaporation

method for fabricating core–shell microspheres. *International Journal of Pharmaceutics*, *452*, 227–232. https://doi.org/10.1016/j.ijpharm.2013.05.020

Xie, X., Chen, Y., Chen, Z., Feng, Y., Wang, J., Li, T., Li, S., Qin, X., Wu, C., Zheng, C., Zhu, J., You, F., Liu, Y., & Yang, H. (2019). Polymeric hybrid nanomicelles for cancer theranostics: an efficient and precise anticancer strategy for the codelivery of doxorubicin/ miR-34a and magnetic resonance imaging. *ACS Applied Materials and Interfaces*, *11*, 43865–43878. https://doi.org/10.1021/acsami.9b14908

Xiong, W., Peng, L., Chen, H., & Li, Q. (2015). Surface modification of MPEG-b-PCL-based nanoparticles via oxidative self-polymerization of dopamine for malignant melanoma therapy. *International Journal of Nanomedicine*, *10*, 2985–2996. https://doi.org/10.2147/IJN.S79605

Xu, J., Zheng, Q., Cheng, X., Hu, S., Zhang, C., Zhou, X., Sun, P., Wang, W., Su, Z., Zou, T., Song, Z., Xia, Y., Yi, X., & Gao, Y. (2021). Chemo-photodynamic therapy with light-triggered disassembly of theranostic nanoplatform in combination with checkpoint blockade for immunotherapy of hepatocellular carcinoma. *Journal of Nanobiotechnology*, *19*, 355. https://doi.org/10.1186/s12951-021-01101-1

Yadav, K., Bhargava, P., Bansal, S., Singh, M., Gupta, S., Sandhu, G., Kumar, S., Sreekanth, V., & Bajaj, A. (2015). Nature of the charged head group dictates the anticancer potential of lithocholic acid-tamoxifen conjugates for breast cancer therapy. *MedChemComm*, *6*(5), 778–787. https://doi.org/10.1039/c4md00289j

Yang, W., Soares, J., Greninger, P., Edelman, E. J., Lightfoot, H., Forbes, S., Bindal, N., Beare, D., Smith, J. A., Thompson, I. R., Ramaswamy, S., Futreal, P. A., Haber, D. A., Stratton, M. R., Benes, C., McDermott, U., & Garnett, M. J. (2013). Genomics of Drug Sensitivity in Cancer (GDSC): A resource for therapeutic biomarker discovery in cancer cells. *Nucleic Acids Research*, *41*(D1), 955–961. https://doi.org/10.1093/nar/gks1111

Yao, Q., Kou, L., Tu, Y., & Zhu, L. (2018). MMP-responsive 'smart' drug delivery and tumor targeting. *Trends in Pharmacological Sciences*, *39*(8), 766–781. https://doi.org/10.1016/j.tips.2018.06.003

Ye, W. L., Zhao, Y. P., Li, H. Q., Na, R., Li, F., Mei, Q. B., Zhao, M. G., & Zhou, S. Y. (2015). Doxorubicin-poly (ethylene glycol)-alendronate self-assembled micelles for targeted therapy of bone metastatic cancer. *Scientific Reports*, *5*, 14614. https://doi.org/10.1038/srep14614

Zeng, Y., Ma, J., Zhan, Y., Xu, X., Zeng, Q., Liang, J., & Chen, X. (2018). Hypoxia-activated prodrugs and redox-responsive nanocarriers. *International Journal of Nanomedicine*, *13*, 6551–6574. https://doi.org/10.2147/IJN.S173431

Zhang, L., Xiao, H., Li, J., Cheng, D., & Shuai, X. (2016). Co-delivery of doxorubicin and arsenite with reduction and pH dual-sensitive vesicle for synergistic cancer therapy. *Nanoscale*, *8*(25), 12608–12617. https://doi.org/10.1039/c5nr07868g

Zhang, Y.-C., Zeng, P.-Y., Ma, Z.-Q., Xu, Z.-Y., Wang, Z.-K., Guo, B., Yang, F., & Li, Z.-T. (2022). A pH-responsive complex based on supramolecular organic

framework for drug- resistant breast cancer therapy. *Drug Delivery*, *29*(1), 1–9. https://doi.org/10.1080/10717544.2021.2010839

Zhang, Y., Huang, Y., & Li, S. (2014). Polymeric Micelles: Nanocarriers for Cancer-Targeted Drug Delivery. *AAPS PharmSciTech*, *15*(4), 862–871. https://doi.org/10.1208/s12249-014-0113-z

Zhao, X., Zou, X., & Ye, L. (2017). Controlled pH- and glucose-responsive drug release behavior of cationic chitosan based nano-composite hydrogels by using graphene oxide as drug nanocarrier. *Journal of Industrial and Engineering Chemistry*, *49*, 36–45. https://doi.org/10.1016/j.jiec.2016.12.023

Zhou, M., Li, L., Li, L., Lin, X., Wang, F., Li, Q., & Huang, Y. (2019). Overcoming chemotherapy resistance via simultaneous drug-efflux circumvention and mitochondrial targeting. *Acta Pharmaceutica Sinica B*, *9*(3), 615–625. https://doi.org/10.1016/j.apsb.2018.11.005

Zhu, W. T., Liu, S. Y., Wu, L., Xu, H. L., Wang, J., Ni, G. X., & Zeng, Q. B. (2017). Delivery of curcumin by directed self-assembled micelles enhances therapeutic treatment of non-small-cell lung cancer. *International Journal of Nanomedicine*, *12*, 2621–2634. https://doi.org/10.2147/IJN.S128921

APPENDICES

A. Calibration Study of Glycine in Sodium Bicarbonate Buffer (pH 8.5)

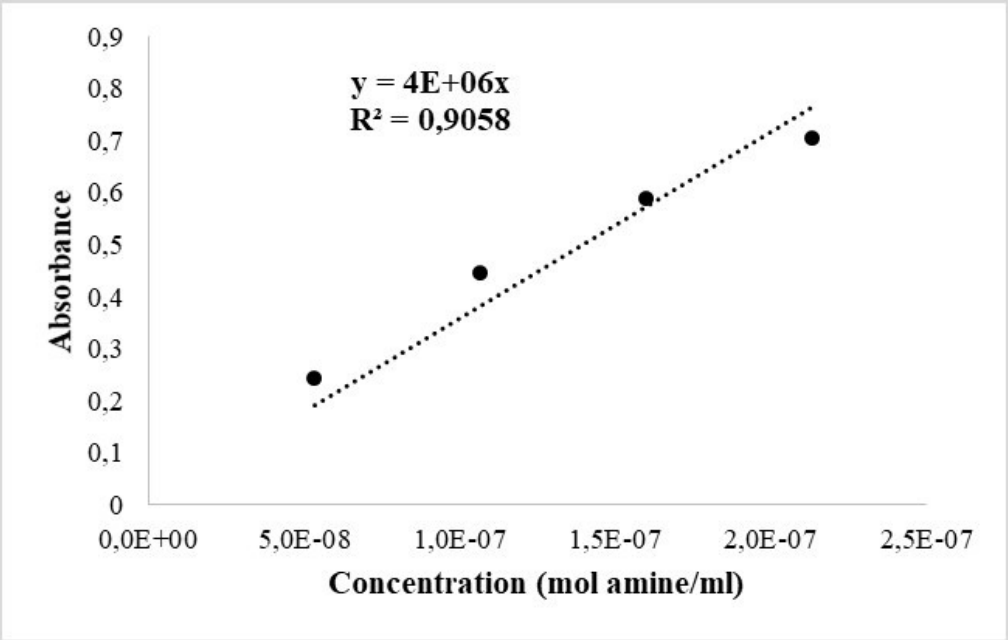

Appendix A1 Figure 1. Calibration curve constructed with different concentrations of glycine in 0.1 M sodium bicarbonate buffer (pH 8.5) for determining the primary amine amount in the mPEG-b-PCL-CO-NH-NH_2 polymer.

B. Calibration Study of DOX in Chloroform:Methanol (1:1, v/v)

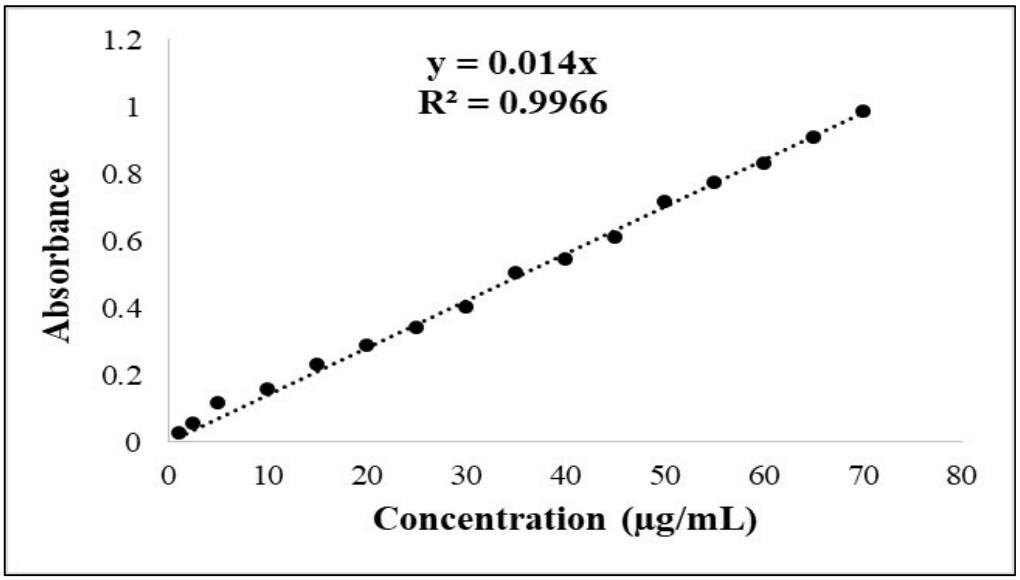

Appendix B1 Figure 1. Calibration curve constructed for DOX in chloroform:methanol (1:1, v/v) to determine the conjugation efficiency of DOX to the copolymer. Blank solution was chloroform:methanol (1:1, v/v).

C. Calibration Study of DOX in HCl (0.1 M)

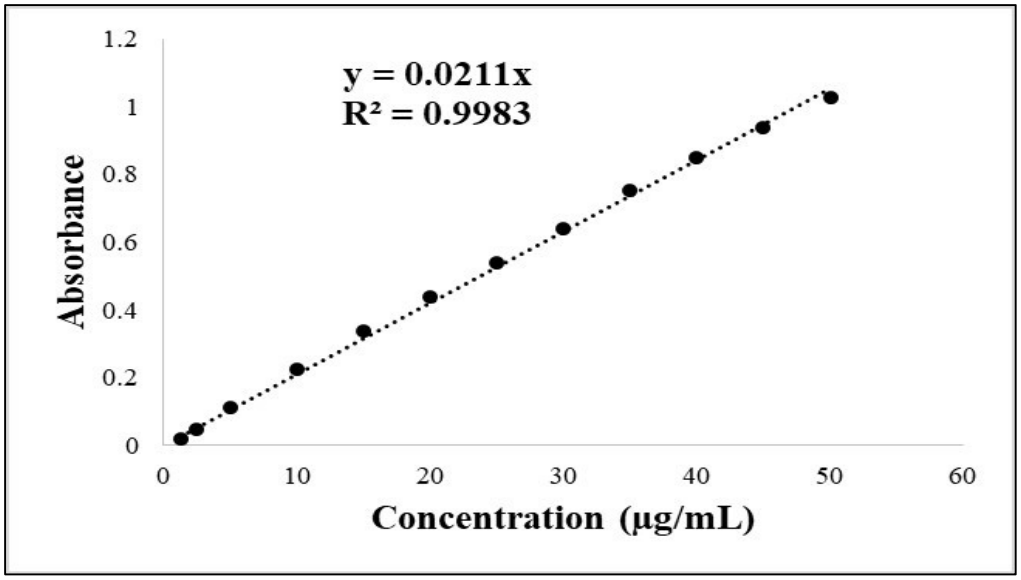

Appendix C1 Figure 1. Calibration curve constructed with different concentrations of DOX in hydrochloric acid (0.1 M HCl). Blank solution was 0.1 M HCl.

D. Calibration Study of DOX in HCl (12 M)

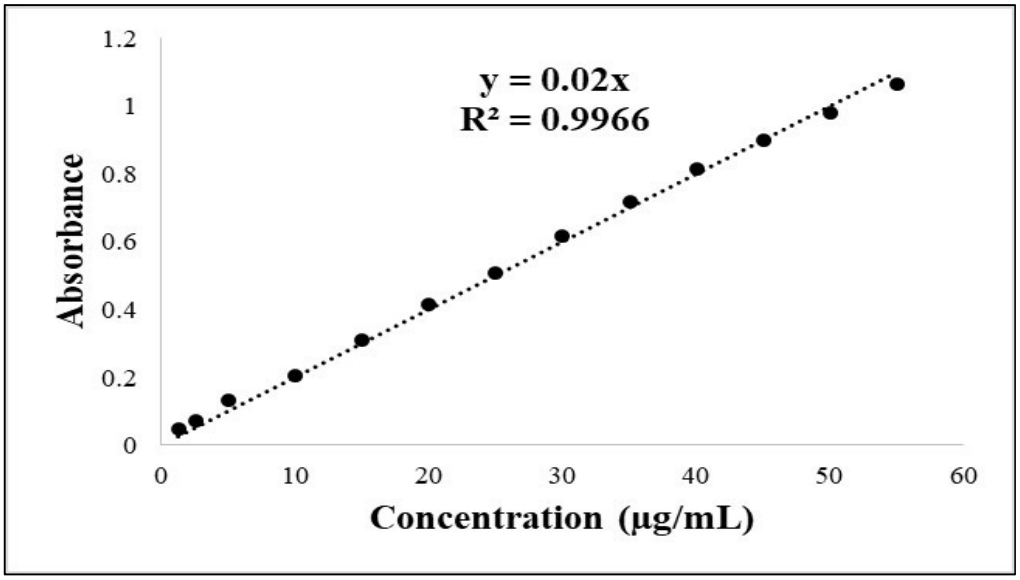

Appendix D1 Figure 1. Calibration curve constructed with different concentrations of DOX in concentrated hydrochloric acid (12 M HCl). Blank solution was concentrated hydrochloric acid.

E. Calibration Study of DOX in H_2SO_4 (18.3 M)

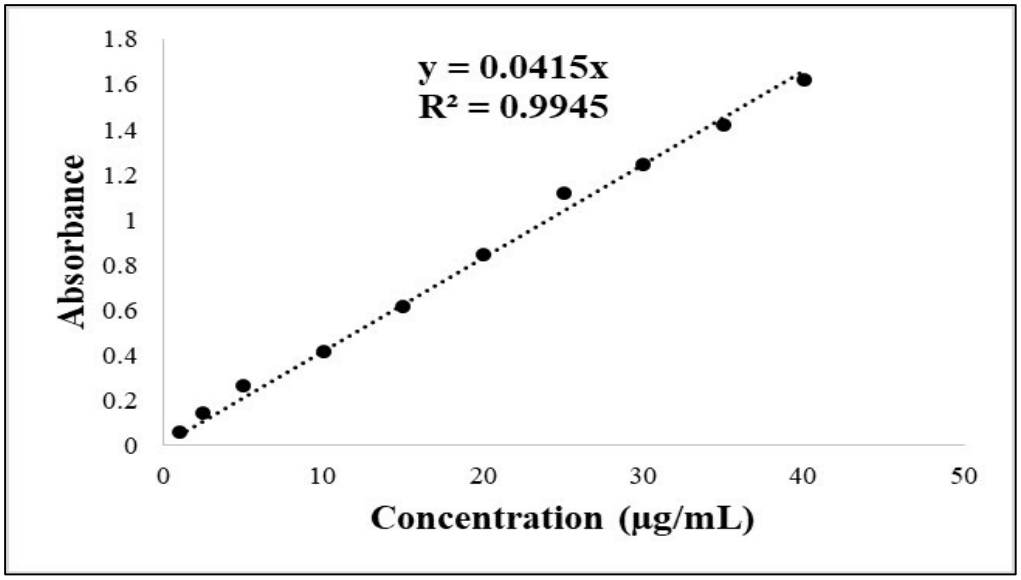

Appendix E1 Figure 1. Calibration curve constructed with different concentrations of DOX in concentrated sulfuric acid (18.3 M). Blank solution was concentrated sulfuric acid.

F. Calibration Study of LCA in H_2SO_4 (18.3 M)

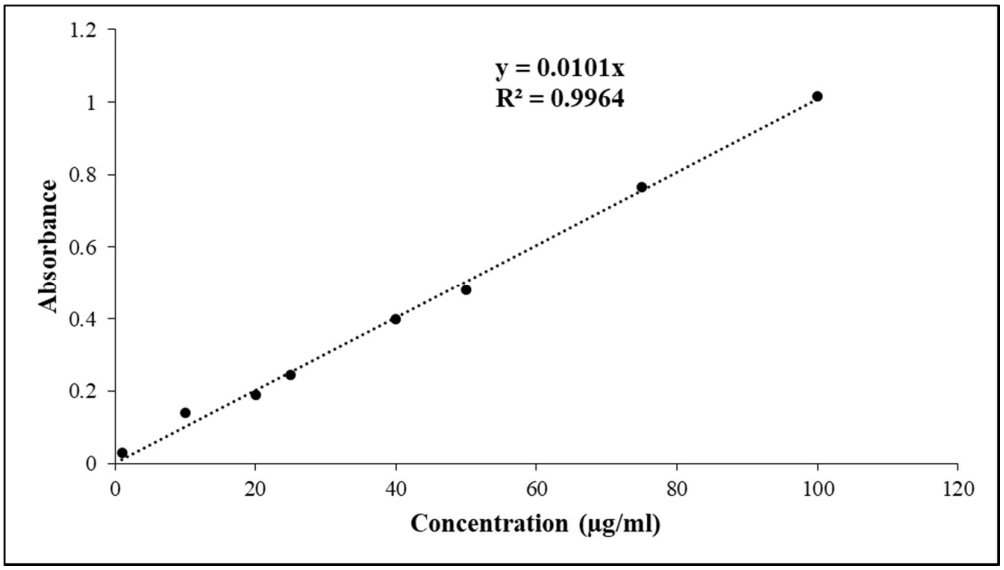

Appendix F1 Figure 1. Calibration curve constructed with different concentrations of LCA in concentrated sulfuric acid.

G. Calibration Study of LCA in Ethanol

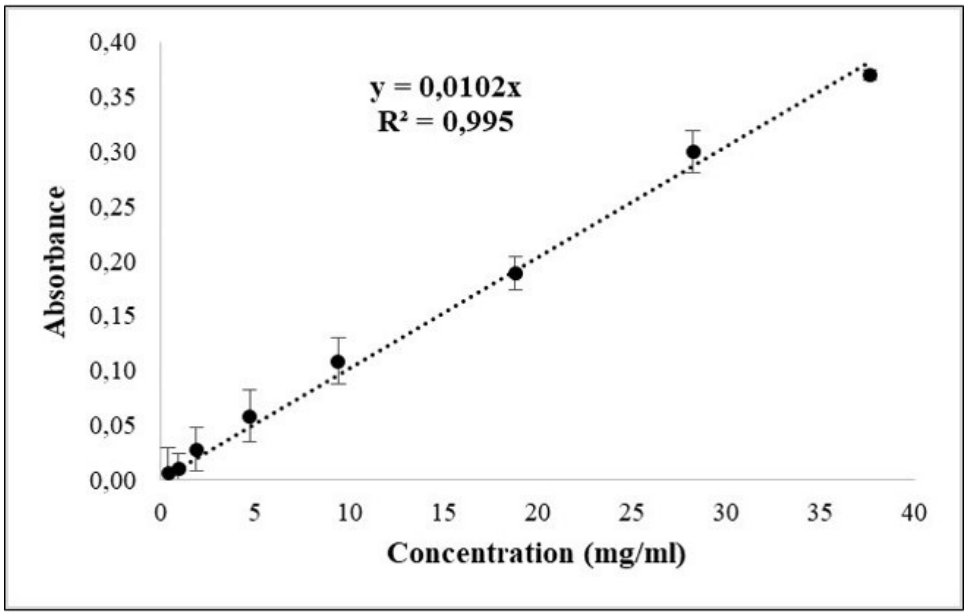

Appendix G1 Figure 1. Calibration curve constructed with different concentrations of LCA in ethanol (n=3).

H. Calibration Study of DOX in Ethanol

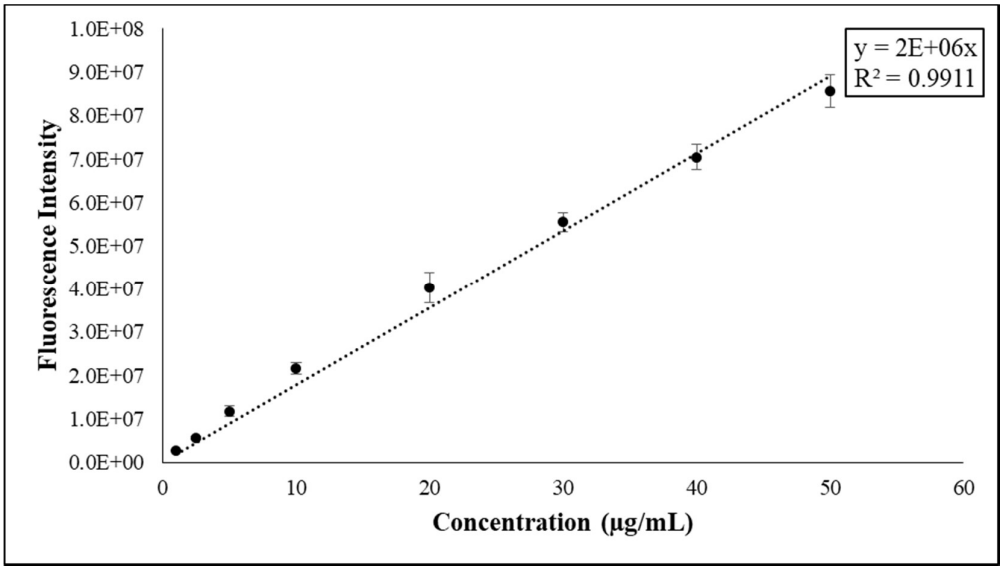

Appendix H1 Figure 1. Calibration curve constructed with different concentrations of DOX in ethanol (n=3).

I. Determination of IC_{50} of LCA on MDA-MB-231, A549, and SK-MEL-30 Cells with Old MTT Method

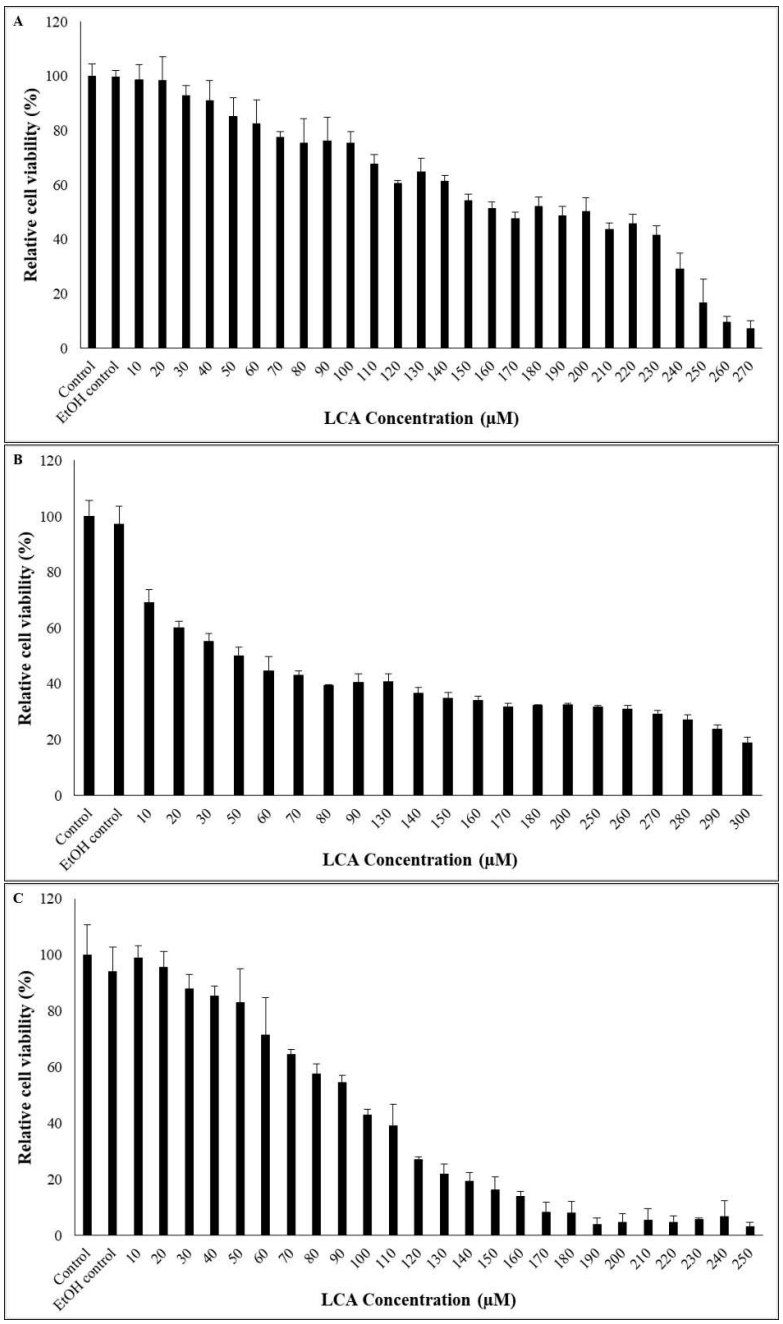

Appendix H1 Figure 1. Cytotoxic effect of different concentrations of free LCA on A) MDA-MB-231, B) A549, and C) SK-MEL-30 (n=4).

J. GraphPad Results for IC_{50} Determination of LCA on MDA-MB-231, A549, and SK-MEL-30 Cells with Old MTT Method

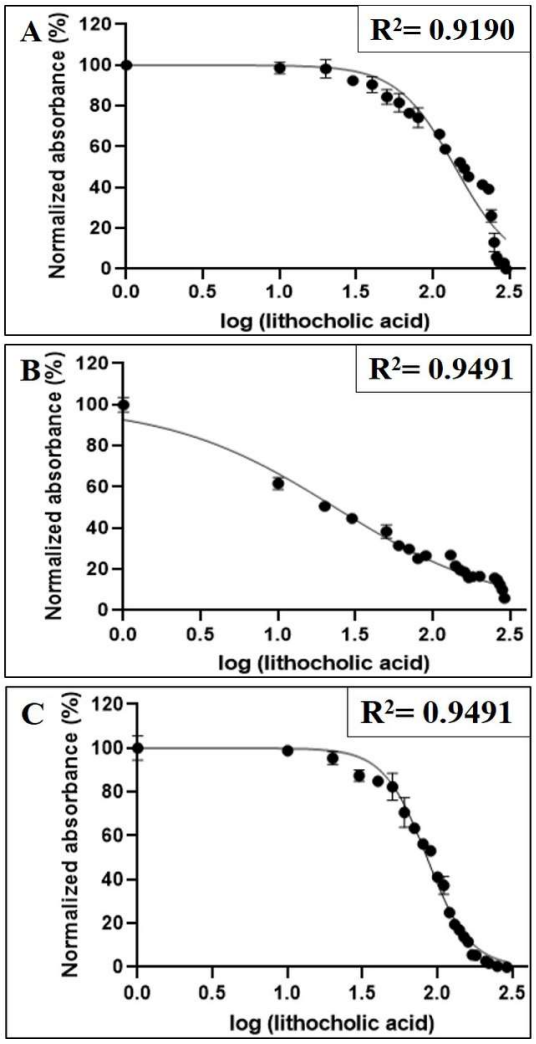

Appendix I1 Figure 1. Normalized absorbance against LCA concentration graphs of A) MDA-MB-231, B) A549 and C) SK-MEL-30 cells obtained using GraphPad Prism 8 software (n=4).

K. Determination of IC_{50} of LCA on A549, and SK-MEL-30 Cells with New MTT Method

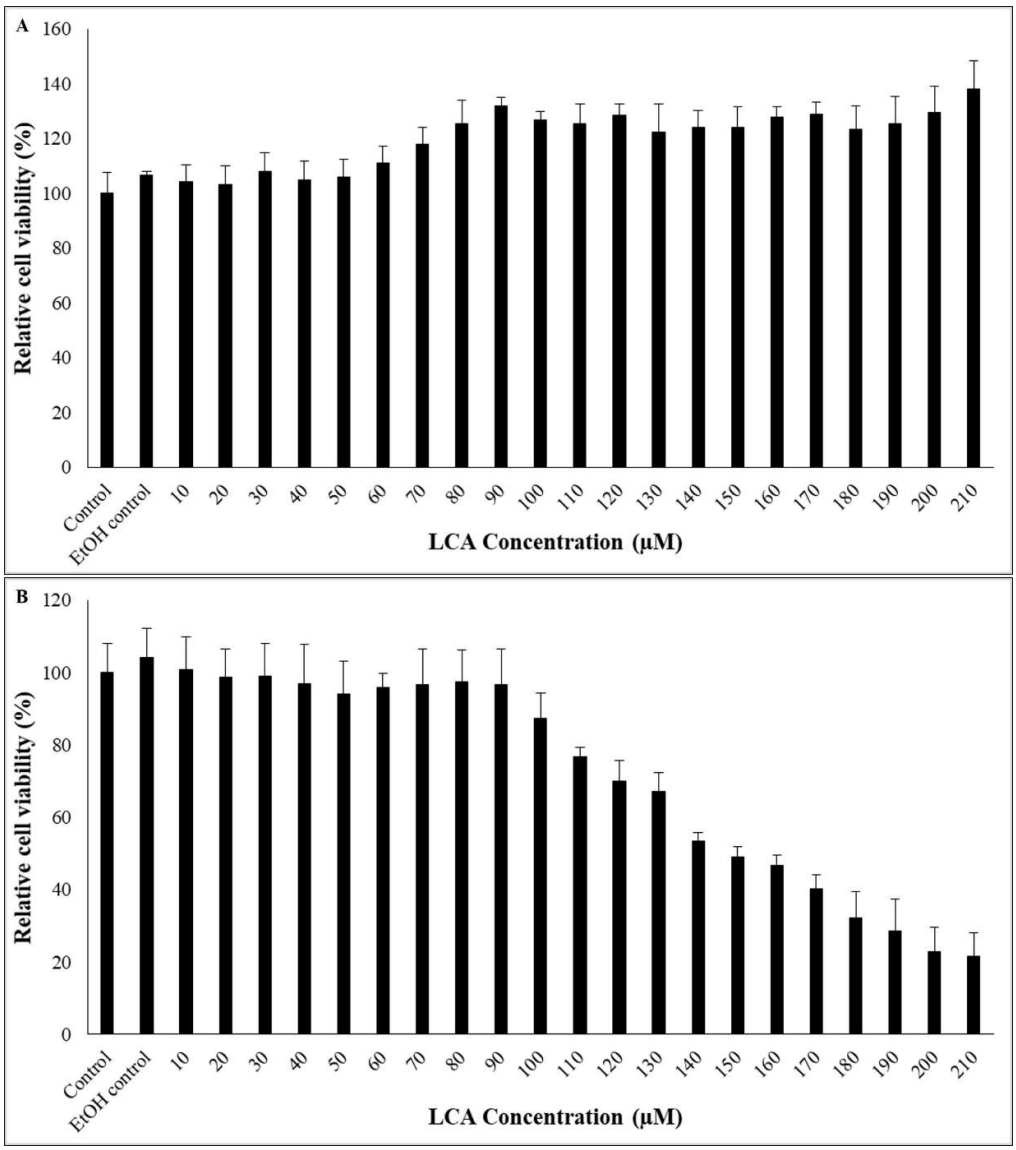

Appendix J1 Figure 1. Cell viability results of A) A549 and B) SK-MEL-30 cells after 48 hours incubation with different LCA concentrations (n=4). Positive control is the cells not incubated with LCA or ethanol.

L. GraphPad Results for IC_{50} Determination of LCA on A549, and SK-MEL-30 Cells with New MTT Method

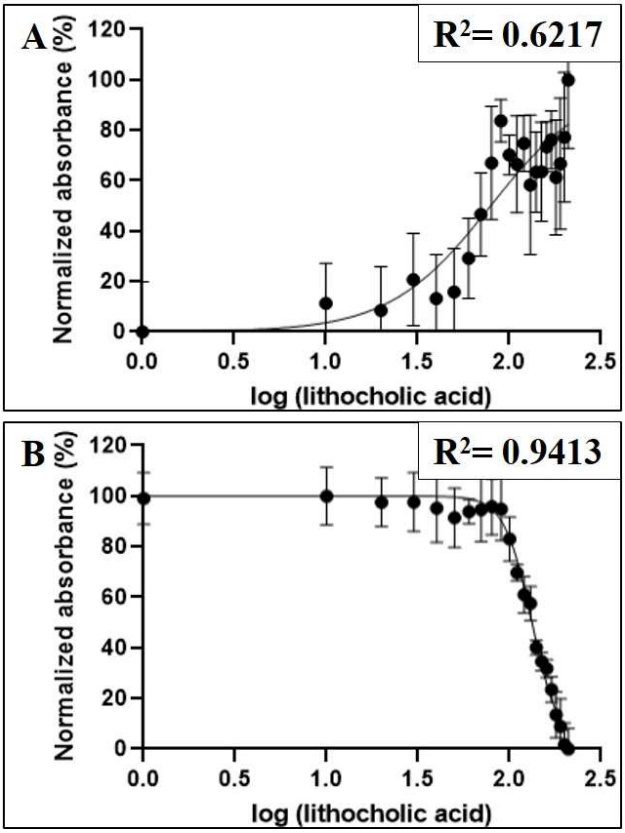

Appendix K1 Figure 1. Normalized absorbance against the LCA concentration plots of A) A549 and B) SK-MEL-30 cells obtained using GraphPad Prism 8 software after modifying the MTT method (n=4).

M. Morphology of A549 Cells After Treatment with LCA

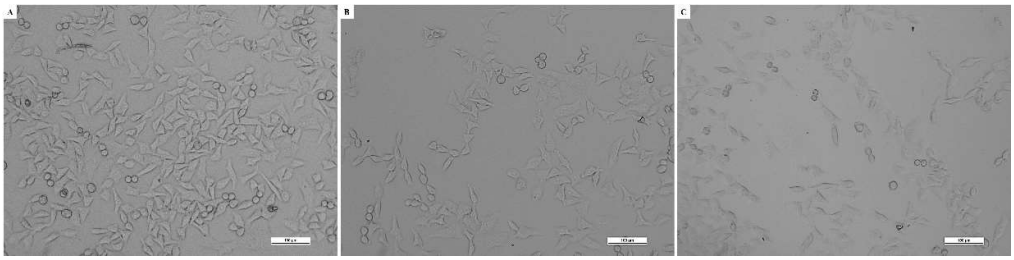

Appendix L1 Figure 1. Morphology of A549 cells after 48 hours incubation with A) 0 μM (control), B) 40 μM, and C) 80 μM LCA. Scale bars are 100 μm.

N. Morphology of SK-MEL-30 Cells After Treatment with LCA

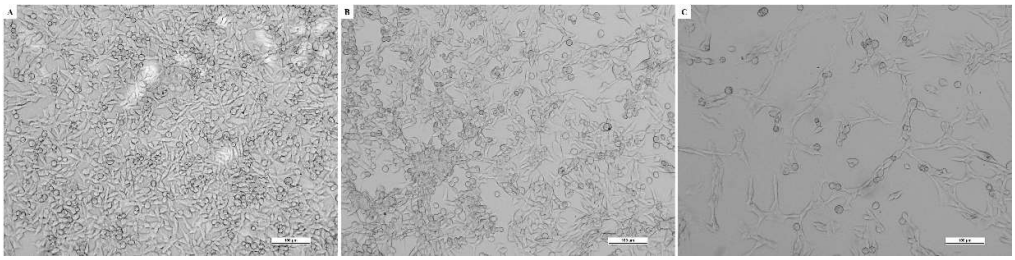

Appendix M1 Figure 1. Morphology of SK-MEL-30 cells after 48 hours incubation with A) 0 μM (control), B) 60 μM, and C) 133 μM LCA. Scale bars are 100 μm.

O. Determination of IC_{50} of DOX on A549, and SK-MEL-30 Cells with New MTT Method

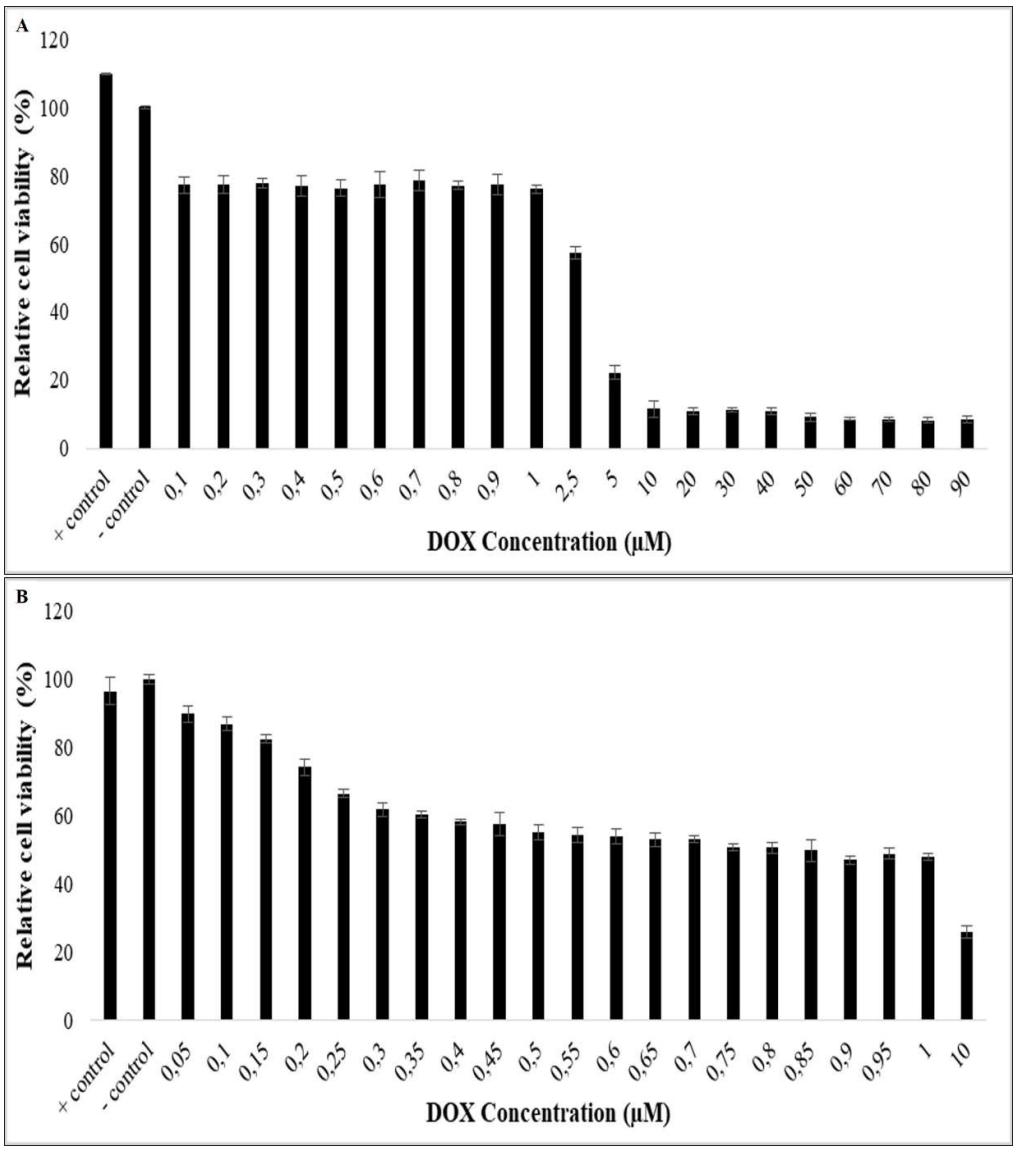

Appendix N1 Figure 1. Cell viability results of A) A549 cells and B) SK-MEL-30 cells after treatment with different concentrations of DOX (n=4).

P. GraphPad Results for IC_{50} Determination of DOX on A549, and SK-MEL-30 Cells with New MTT Method

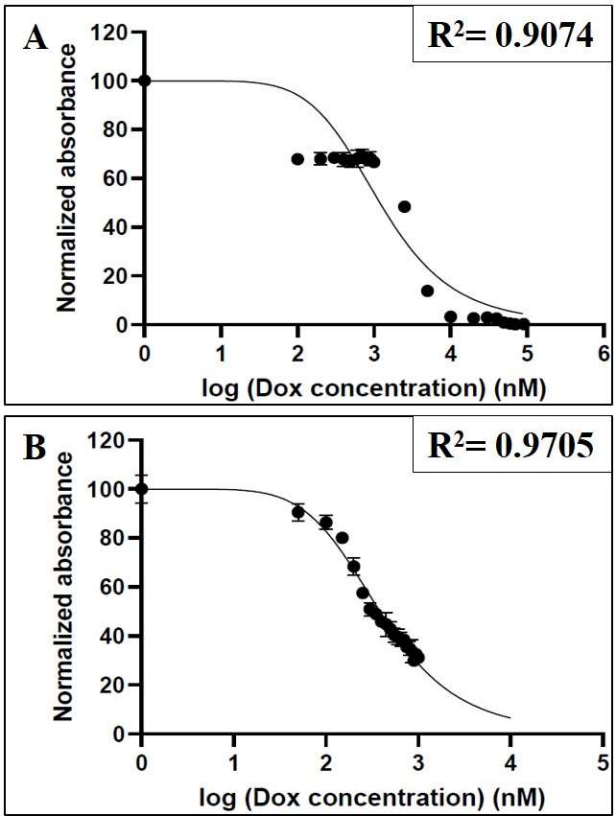

Appendix O1 Figure 1. Normalized absorbance vs. DOX concentration charts of A) A549, and B) SK-MEL-30 cells after data fitting using GraphPad Prism 8 software.

Q. Determination of Cytotoxicity of LCA60**M and M on MDA-MB-231, A549, and SK-MEL-30 Cells with Old MTT Method

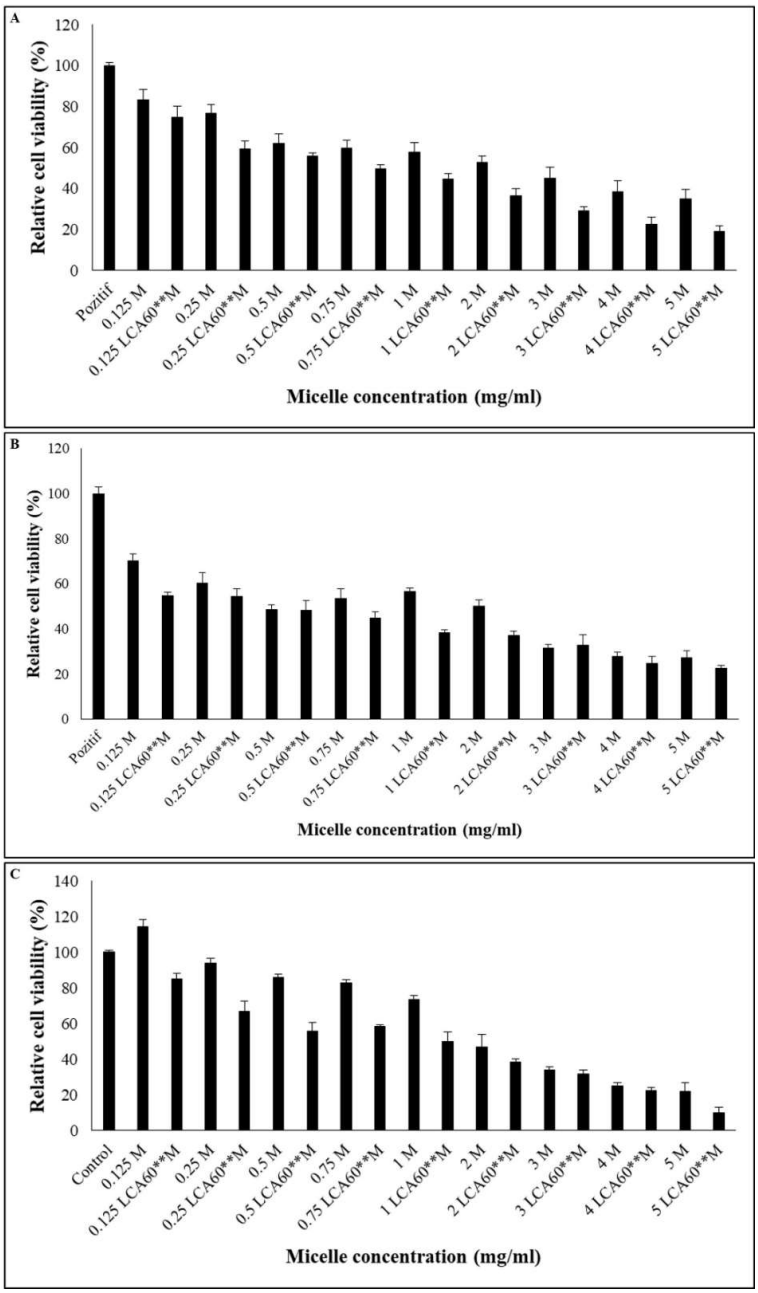

Appendix P1 Figure 1. Cytotoxic effect of different concentrations of LCA_{60}**M compared to M on A) MDA-MB-231, B) A549, and C) SK- MEL-30 (n=4).

R. Determination of Cytotoxicity of M on A549, and SK-MEL-30 Cells with Old New Method

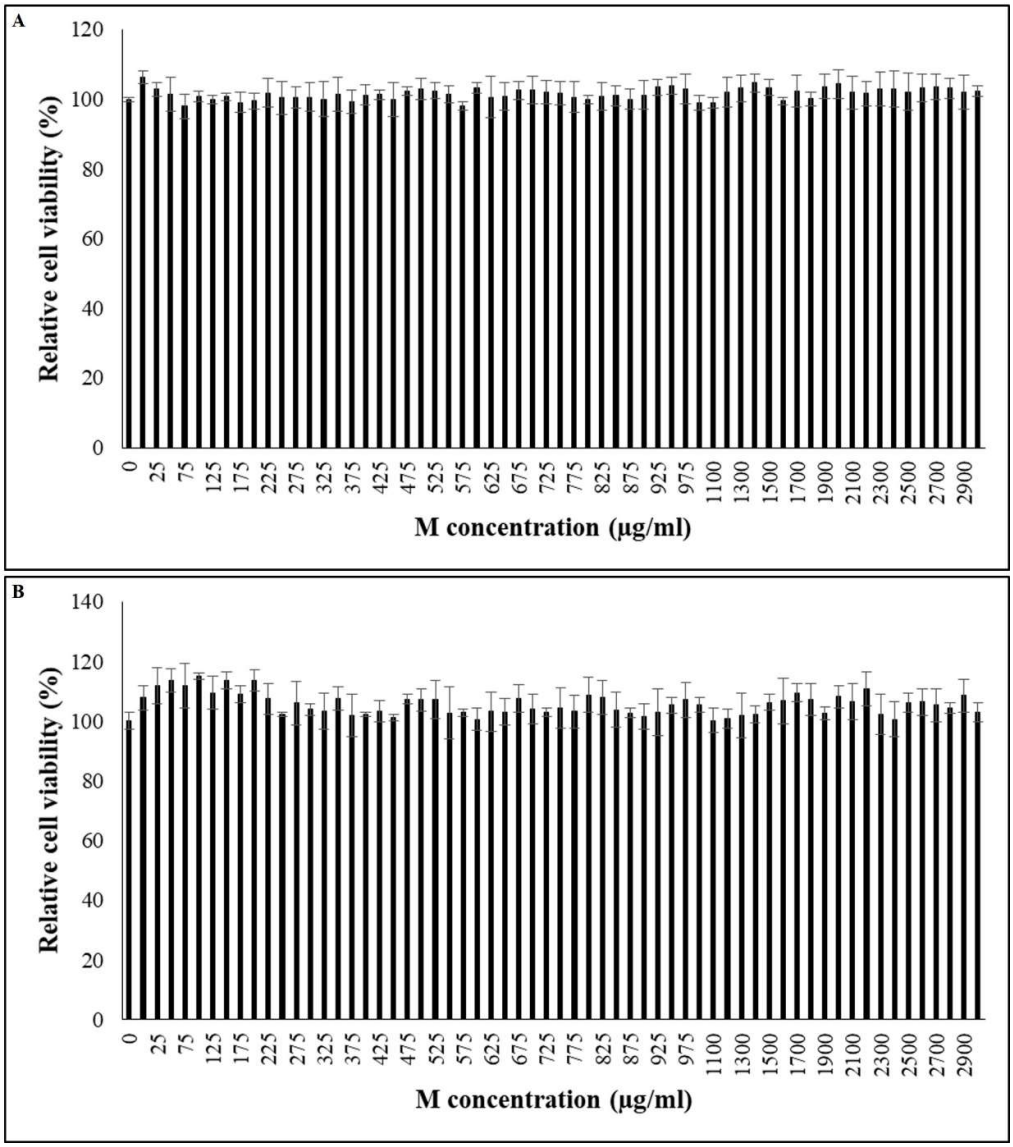

Appendix Q1 Figure 1. The cytotoxic effect of different concentrations of M on A) A549 and B) SK-MEL-30 cells (n=4).

S. Determination of Cytotoxicity of LCA60**M on A549, and SK-MEL-30 Cells with Old MTT Method

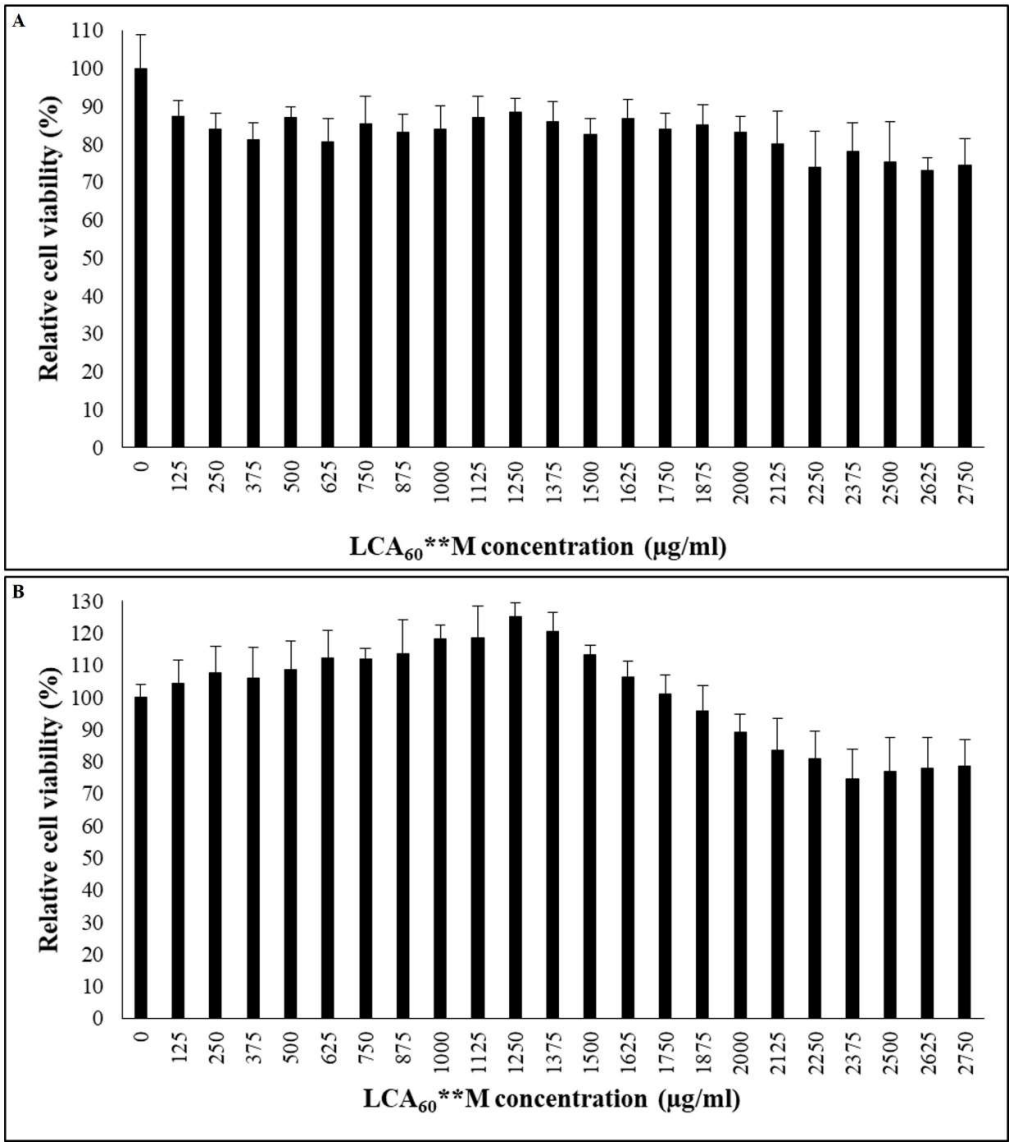

Appendix R1 Figure 1. Cytotoxic effect of different concentrations of LCA_{60}**M on A) A549, and B) SK- MEL-30 (n=4).

CURRICULUM VITAE

PERSONAL INFORMATION

Surname, Name: Işık, Gülhan

EDUCATION

Degree	Institution	Year of Graduation
BS	Ege University Department of Bioengineering	2014
High School	Dr. Binnaz Ege-Dr. Rıdvan Ege Anadolu High School, Ankara	2009

WORK EXPERIENCE

Year	Place	Enrollment
2020-Present	Virtual Trutrends Ltd. Şti.	Production and R&D Responsible
2019-2020	Turk İlaç and Serum Sanayi A.Ş.	Asst. Quality Assurance Specialist
2013 July-August	Ministry of Agriculture and Forestry, Institute of Foot and Mouth Disease	Intern Eng. Student
2012 June-August	Ege University Bioenginnering Department Research Laboratories	Intern Eng. Student

FOREIGN LANGUAGES

Advanced English, Basic German, Basic Italian, Basic Korean

PUBLICATIONS

1. Isik, G., Tezcaner, A., Hasirci, N., & Kiziltay, A. (2021). Determination of doxorubicin amount conjugated to mPEG-b-PCL copolymer via pH sensitive

hydrazone bond. Turkish Bulletin of Hygiene and Experimental Biology. https://doi.org/10.5505/TurkHijyen.2022.04317

2. Alshemary, A. Z., Bilgin, S., Isik, G., Motameni, A., Tezcaner, A., & Evis, Z. (2021). Biomechanical evaluation of an injectable alginate / dicalcium phosphate cement composites for bone tissue engineering. Journal of the Mechanical Behavior of Biomedical Materials, 118, 104439. https://doi.org/10.1016/j.jmbbm.2021.104439

3. Isik, G., Hasirci, N., Tezcaner, A., & Kiziltay, A. (2020). Multifunctional periodontal membrane for treatment and regeneration purposes. Journal of Bioactive and Compatible Polymers, 35(2), 117–138. https://doi.org/10.1177/0883911520911659